

Archive ouverte UNIGE

https://archive-ouverte.unige.ch

Thèse 2025

Open Access

This version of the publication is provided by the author(s) and made available in accordance with the copyright holder(s).

Selective activation of interleukin-2/interleukin-15 signaling in tumor microenvironment using paired bispecific antibodies

Montorfani, Julien

How to cite

MONTORFANI, Julien. Selective activation of interleukin-2/interleukin-15 signaling in tumor microenvironment using paired bispecific antibodies. Doctoral Thesis, 2025. doi: 10.13097/archive-ouverte/unige:185299

This publication URL: https://archive-ouverte.unige.ch/unige:185299

Publication DOI: <u>10.13097/archive-ouverte/unige:185299</u>

© This document is protected by copyright. Please refer to copyright holder(s) for terms of use.

,	,	
		/⊏
UNIVERSITÉ	DE GENEV	
• – • –		_

FACULTÉ DE MÉDECINE

Département de Pathologie et Immunologie

Professeur C. Jandus

Light Chain Bioscience – NovImmune SA

Dr. L. Shang

Activation sélective de la signalisation interleukine-2/interleukine-15 dans le microenvironnement tumoral par des paires d'anticorps bispécifiques

THÈSE

présentée aux Facultés de médecine et des sciences de l'Université de Genève pour obtenir le grade de Docteur ès sciences en sciences de la vie, mention Sciences biomédicales

par

Julien Montorfani

de

Lugano (Ticino)

Thèse Nº 334

GENÈVE

Nom de l'Atelier d'Impression

2025

Département de Pathologie et Immunologie

Professeur C. Jandus

Light Chain Bioscience - NovImmune SA

Dr. L. Shang

SELECTIVE ACTIVATION OF INTERLEUKIN-2/INTERLEUKIN-15 SIGNALING IN TUMOR MICROENVIRONMENT USING PAIRED BISPECIFIC ANTIBODIES

THESIS

présentée aux Facultés de médecine et des sciences de l'Université de Genève pour obtenir le grade de Docteur ès sciences en sciences de la vie, mention Sciences biomédicales

par

Julien Montorfani

de

Lugano (Ticino)

Thèse Nº 334

GENÈVE

Nom de l'Atelier d'Impression

2025



DOCTORAT ÈS SCIENCES EN SCIENCES DE LA VIE DES FACULTÉS DE MÉDECINE ET DES SCIENCES MENTION SCIENCES BIOMÉDICALES

Thèse de M. Julien Montorfani

intitulée :

« Selective activation of interleukin-2/interleukin-15 receptor signaling in tumor microenvironment using paired bispecific antibodies »

Les Facultés de médecine et des sciences, sur le préavis de Madame Camilla JANDUS, Professeure assistante et directrice de thèse (Département de Pathologie et Immunologie), Monsieur Limin SHANG, Post-doctorant et co-directeur de thèse (Directeur de Pharmacologie à Light Chain Bioscience), Monsieur Simone BECATTINI, Professeur assistant (Département de Pathologie et Immunologie), Monsieur Pedro ROMERO, Professeur (Département d'oncologie, UNIL, CHUV, Lausanne, Suisse) autorisent l'impression de la présente thèse, sans exprimer d'opinion sur les propositions qui y sont énoncées.

Genève, le 10 mars 2025

Thèse - 334 -

Le Doyen Faculté de médecine La Doyenne Faculté des sciences

N.B. - La thèse doit porter la déclaration précédente et remplir les conditions énumérées dans les "Informations relatives aux thèses de doctorat à l'Université de Genève".



Acknowledgments

I want to express my appreciation to my thesis director, Prof. Camilla Jandus, and my thesis co-director, Dr. Limin Shang. I want to thank Camilla for welcoming me to her laboratory and making me feel welcome and an integral part of the team. Her knowledge, advice, kindness, and enthusiasm have not only helped the project but also imparted her passion and helped me immensely. I want to thank Limin for welcoming me under his wing at Light Chain Bioscience. His helpfulness, advice, and extensive knowledge of immunology and immunotherapies have guided my path from day one and helped me adapt. His support and bright ideas have brought the project to life. I feel extremely fortunate to have found two great scientists and role models who inspire me to cultivate my passion for science.

I wish to thank the members of the jury, Prof. Simone Becattini and Prof. Pedro Romero. They participated in my TAC Meeting in 2022 and have devoted their time again to reviewing this manuscript and discussing my work.

I am very thankful to the leadership team at Light Chain Bioscience. I want to thank Nicolas for giving me the chance to bring his idea to light with this project. I want to thank Walter for his scientific advice. You have both my deepest gratitude for all the time you dedicated to the project and for your kindness. The enjoyable and productive work environment at Light Chain Bioscience reflects your leadership. I want to extend my gratitude to Krzystzof for his precious scientific advice and the time he devoted to the project. Gracias Jose, for your kindness and for sharing your passion for clinical development during very enriching discussions. Thank you, Valérie, for your precious help regarding everything that doesn't involve pipets and lab coats. I also wish to thank Oliver Eckelmann and the board of directors for the chance of doing my thesis at Light Chain Bioscience.

I want to thank Éric for his mentorship and scientific passion, which have helped me tremendously throughout this journey. I deeply value all our discussions and want to thank him on a personal level as well. His kindness and friendship have been very enriching, and working alongside him has been one of the highlights of my thesis.

I want to extend my appreciation to Vanessa, Xavier and Sara for the helpful discussions and advice. Your knowledge, kindness, and critical eye have genuinely helped me during these 4 years.

I am grateful to my colleagues at Light Chain Bioscience. I want to thank all the pharmacology members. You have welcomed and made me feel at home during these 4 years. Your advice and knowledge have been crucial; this project would not have been possible without it. I want to thank Laurence for her vital contribution to the project. Her expertise has been paramount to what has been achieved. I want to thank Laura for her critical help. I want to thank Bruno and Adeline for their. Your help, expertise, and your time have made this project possible. Thank you also to Valery for your kindness and precious advice.

I thank the protein engineering team for their vital contribution to the project and guidance. In particular, I want to express my appreciation to Pauline for her invaluable help and kindness. I also want to express my gratitude to the bioprocessing team. Thank you to Christophe, Guillemette, and Tereza for their advice, help, and kindness. I am also thankful to the phage display team. I wish to thank Ulla and Sébastien for their advice and precious contribution to the project. On a more personal note, I want to thank Diogo for all the enriching discussions and your friendship. Thank you Santiago for your kindness and friendship. I want to extend my gratitude to Alizée, Pauline, Mathieu, Mei and Lola. While some of you have also worked on the project, I wanted to thank you together for your kindness and our friendship. You have made these years even more enjoyable. While I could not mention everyone, I want to thank you all not only for the scientific exchange that helped me grow and made this project possible but also for your kindness and for having welcomed me so warmly. The productive and enjoyable work environment that you have created is truly special.

I also want to take the time to thank my current and former PhD student colleagues at Light Chain Bioscience. Thank you, Lise. You were present from the beginning of my journey, and I value your advice and our discussions deeply. Thank you for all your help with the project and for your friendship. I want to express my gratitude to my old desk neighbor; Elise S. I still hold close to my heart all our discussions. I want to thank Elise P. for her kindness and advice. I am grateful to Lucie for the enriching discussions and her kindness. I am also extremely grateful to Elise L. for your kindness; our discussions have helped me

tremendously. You have made this journey much more enjoyable, and I deeply value your friendship.

I am grateful to my current and past colleagues in the Jandus' laboratory. Thank you, Sara, Alejandra, Mara, Benedetta, Danae, Anthony, Hajar, Georgia, Daniela, Ziyang, Maryline, Margaux and Tania. Thank you for all the enriching discussions, the advice, and the fun times spent together.

I also want to thank the members of my previous laboratory, particularly my previous mentors, Stéphanie and Laure. I have extremely positive memories of my time in the laboratory, and what you have taught me has been invaluable during these last 4 years.

I want to thank the PhD school for its help and availability during my thesis and for reviewing this manuscript.

I want to express my appreciation to Cécile, Lan, and Gregory of the FACS facility of the University of Geneva for their help and advice.

I want to thank Luca. I am incredibly grateful for everything we have shared during this journey, and I am sure we will share much more in the future.

Thank you to Pablo, Anthony, and Maxime. I really appreciate our time together and deeply value your friendship. I also want to thank my sicilian friends Fra, Gabriele, Alberto, Crisitan, Zauddo, Zaudda, Vinz, Alessia, Ciccio, Alessia. Even though I have been away for a while, I want to thank Elia, Giulio, Andrea, Paolo, and Marco. Your friendship is still dear to my heart, and I know that we can count on each other.

Tengo molto a ringraziare la mia famiglia. Grazie ai miei genitori, Sergio e Yvette, per avermi supportato in tutte le scelte che mi hanno portato fino a qui. Vi voglio un mondo di bene e senza il vostro aiuto non sarei qui. Grazie mille a Elisa e a Yannick. Il tempo che passiamo insieme é preziosissimo e so di poter contare su di voi per qualsiasi cosa. E nautralmente ringrazio anche JD e Manuela. Voglio ringraziare anche il resto della mia amata famiglia per il supporto. Je tiens aussi à remercier le reste de ma famille bien-aimée pour leur soutien. Merci aussi à Guy, Nathalie et Carla. Vous m'avez fait me sentir comme chez moi depuis le début.

Lastly, I want to thank the person I intentionally left out in previous sections. Thank you Coline for all you have done throughout these years. You have been my rock and you have made this journey nicer than I could have imagined.

Table of contents

1	Summa	ry	11
2	Résumé	<u> </u>	12
3	List of p	ublications	14
4	List of A	bbreviations	15
5	Introduc	tion	18
	5.1 Ca	ncer	18
	5.2 lmr	mune system	19
	5.2.1	The major histocompatibility complex (MHC) I/II	20
	5.2.2	Cytokines	21
	5.2.2	.1 IL-2/IL-15 cytokine and receptor expression	22
	5.2.2.	.2 IL-2/IL-15 signaling	24
	5.2.3	Immune cells	27
	5.2.3	.1 NK cells	27
	5.2.3.	2 Dendritic cells	29
	5.2.3		
	5.2	.3.3.1 T cell receptor (TCR)	
	_	.3.3.2 T cell activation	
		.3.3.3 CD4 T cells	
	_	.3.3.4 CD8 T cells	
		.3.3.5 Memory T cells	
		.3.3.6 Dysfunctional T cells	
	5.2.3.		
		.3.4.1 Antibodies	
	5.2.4	Immunosurveillance	
	5.2.5	Tumor immunology	
	5.2.6	Cancer immunotherapies	
	5.2.7	Therapeutic Antibodies	
	5.2.7	•	
	5.2.7		
	5.2.8	IL-2 targeted therapies and limitations	
	5.2.9	IL-15 targeted therapies and limitations	
6			
7			
8		ion	
9	Conclus	ion	126

10	References	127
11	Appendices	170
11.1	Appendix 1:	170
11.2	P Appendix 2:	172
11.3	B Appendix 3:	191

1 Summary

The progress in immunotherapies has transformed the landscape of cancer therapies and greatly improved patient prognosis across many types of cancers. Although being one of the first immunotherapies approved in cancer treatment, the clinical application of high-dose recombinant interleukin-2 (IL-2) therapy has been impeded by associated severe systemic toxicities. This study introduced a novel strategy to harness the anti-tumor potential of IL-2/15 signaling while avoiding the liabilities, by using a pair of bispecific antibodies, where the first antibody binds to the IL-2/15 receptor subunit β (CD122) and a tumor-associated antigen, and the second antibody binds to the IL-2/15 receptor subunit γ (CD132) and the same or a different tumor-associated antigen. The bispecific antibody pair only activates IL-2/15 signaling in the presence of the tumor associated antigen(s) and thus restricts signaling to the tumor microenvironment.

This work combined in vitro and in vivo techniques to demonstrate the tumor-selective activity of this strategy. We showed, with reporter cells and primary cells, that activation of IL-2 signaling through the bispecific antibody pairs relied on the presence of tumorassociated antigens. In contrast to recombinant IL-2, the bispecific antibody pairs did not preferentially activate regulatory T cells expressing the high-affinity IL-2 receptor alpha chain (CD25). In vitro data showed that the bispecific antibody pairs alone did not kill tumor cells but could amplify the tumoricidal activity of T and natural killer (NK) cells induced by T cell engagers or monoclonal antibodies. In a transgenic hCD122/hCD132 mouse model, the bispecific antibody pairs induced the expansion of tumor infiltrating memory CD8+ T cells and NK cells, while being well-tolerated and not inducing any systemic release of inflammatory cytokines. Further, in vivo, combination of the bispecific antibody pair with an immune checkpoint inhibitor suppressed tumor growth more strikingly than the immune checkpoint inhibitor alone. Analysis of the tumor microenvironment demonstrated that the combination treatment induced the expansion of memory CD8+ T cells, NK cells and increased their expression of cytotoxic molecules like granzyme B. Additionally, this study demonstrated the possibility of using a bispecific antibody pair targeting two distinct tumorassociated antigens to further reduce the possibility of off-tumor immune cell activation.

Overall, this study describes a novel immunotherapeutic approach demonstrating tumor-specific IL-2/15 activation and favorable safety profile, thus having the potential to overcome the limitations of high-dose recombinant IL-2 therapy. This approach could be expanded to therapeutically harness the untapped potential of many other signaling pathways in cancer and beyond.

2 Résumé

Les progrès réalisés dans les immunothérapies ont étendu les possibilités de traitement de nombreux cancers et ont considérablement amélioré l'espérance de vie des patients. Bien que l'interleukine-2 (IL-2) recombinante à haute dose ait été l'une des premières immunothérapies approuvées pour le traitement du cancer, son application clinique a été limitée par la toxicité qu'elle induit.

Cette étude présente une stratégie innovante permettant d'exploiter le potentiel anti-tumoral des voies de signalisation des interleukines-2 et 15 tout en évitant ses effets indésirables, cela en utilisant une paire d'anticorps bispécifiques. Le premier anticorps se lie à la sous-unité β (CD122) du récepteur de l'interleukine-2/15 et à un antigène tumoral, alors que le second anticorps se lie à la sous-unité γ (CD132) du récepteur de l'interleukine-2/15 et au même antigène tumoral ou à un antigène tumoral différent. Cette paire d'anticorps bispécifiques active la signalisation interleukine-2/15 uniquement en présence des antigènes tumoraux, restreignant ainsi cette activité à l'environnement tumoral.

Ce travail a combiné des expériences in vitro et in vivo pour étudier l'activité sélective et intra-tumorale de cette approche. Nous avons pu démontrer, à l'aide d'un système de gène reporter ainsi que de cellules primaires, que l'activation de la signalisation de l'IL-2 par les paires d'anticorps bispécifiques dépendait strictement de la présence d'antigènes tumoraux. Contrairement à l'IL-2 recombinante, les paires d'anticorps bispécifiques n'activent pas de manière préférentielle les cellules T régulatrices qui expriment la chaîne alpha du récepteur de l'IL-2 (CD25). Les résultats in vitro ont montré que l'activité des paires d'anticorps bispécifiques à elle seule ne permet pas aux lymphocytes T et aux cellules NK de détruire les cellules tumorales, mais permet d'amplifier leur activité tumoricide induite par des anticorps bispécifiques capables de rediriger des lymphocytes T vers les cellules tumorales ou par des anticorps monoclonaux. Dans un modèle murin transgénique exprimant hCD122 et hCD132, les paires d'anticorps bispécifiques induisent l'accumulation au sein de la tumeur de cellules T CD8+ mémoire centrale et de cellules NK, tout en étant bien tolérées, sans libération systémique de cytokines inflammatoires. De plus, dans un modèle murin de cancer, la combinaison de la paire d'anticorps bispécifiques avec un inhibiteur de point de contrôle du système immunitaire a réduit la croissance tumorale de manière plus marquée que l'administration de l'inhibiteur de point de contrôle du système immunitaire seul. L'analyse des tumeurs a montré que le traitement combiné induisait l'expansion des cellules T CD8+ mémoire centrale, des cellules NK et augmentait l'expression de molécules cytotoxiques telles que la granzyme B. En outre, cette étude a

exploré la possibilité d'utiliser une paire d'anticorps bispécifiques ciblant deux antigènes tumoraux distincts permettant de réduire davantage la possibilité d'activation des cellules immunitaires hors du microenvironnement tumoral.

Dans l'ensemble, cette étude décrit une nouvelle approche immunothérapeutique permettant une activation des voies de signalisations des interleukine-2/15 spécifiquement dans les tumeurs et sans induire d'effets toxiques. Cette approche a ainsi le potentiel de surmonter les limitations de l'administration de haute dose d'IL-2 recombinante. Cette approche pourrait être étendue pour exploiter thérapeutiquement de nombreuses autres voies de signalisation de cytokines pour le traitement de cancers mais également dans le contexte d'autres maladies. (OpenAI. ChatGPT disponible sur : https://chatgpt.com/ a été utilisé pour traduire ce texte que j'ai écrit initialement en anglais. La traduction a été revue par moi-même et Dr. Nicolas Fischer).

3 List of publications

- Julien Montorfani, Eric Hatterer, Laurence Chatel, Adeline Lesnier, Alizee Viandier, Bruno Daubeuf, Lise Nouveau, Pauline Malinge, Sebastien Calloud, Krzysztof Masternak, Walter Ferlin, Nicolas Fischer, Camilla Jandus and Limin Shang. Selective activation of interleukin-2/interleukin-15 receptor signaling in tumor microenvironment using paired bispecific antibodies. In revision in Journal for ImmunoTherapy of Cancer (JITC).
- Mengzhu Sun, Laure Garnier, Romane Chevalier, Martin Roumain, Chen Wang, Julien Angelillo, Julien Montorfani, Robert Pick, Dale Brighouse, Nadine Fournier, David Tarussio, Stéphanie Tissot, Jean-Marc Lobaccaro, Tatiana V. Petrova, Camilla Jandus, Daniel E. Speiser, Manfred Kopf, Caroline Pot, Christoph Scheiermann, Krisztian Homicsko, Giulio G. Muccioli, Abhishek D. Garg & Stéphanie Hugues. Lymphatic-derived oxysterols promote anti-tumor immunity and response to immunotherapy in melanoma. Nature Communications 16, 1217 (2025).
- Nicolas Fischer, Julien Montorfani, Limin Shang, Eric Hatterer. Composition and methods for the selective activation of cytokine signaling pathways. World Intellectual Property. PCT/EP2023/051721 (2023).
- Laure Garnier, Robert Pick, Julien Montorfani, Mengzhu Sun, Dale Brighouse, Nicolas Liaudet, Thomas Kammertoens, Thomas Blankenstein, Nicolas Page, Jeremiah Bernier-Latamani, Ngoc Lan Tran, Tatiana V Petrova, Doron Merkler, Christoph Scheiermann, Stéphanie Hugues. IFN-γ-dependent tumor-antigen cross-presentation by lymphatic endothelial cells promotes their killing by T cells and inhibits metastasis. Sci. Adv. 8, eabl5162 (2022).

4 List of Abbreviations

ACT Adoptive Cell Transfer

ADA Anti-Drug Antibody

ADC Antibody-Drug Conjugates

ADCC Antibody-Dependent Cellular Cytotoxicity

Al Artificial Intelligence

AID Activation-Induced cytidine Deaminase

AP-1 Activator Protein 1

APC Antigen-Presenting Cell

BCG Bacillus Calmette-Guérin

BCR B Cell Receptor

bsAb Bispecific Antibody

C Constant region

CAR Chimer Antigenic Receptor

CD122 IL-2/15 receptor β

CD132 IL-2/15 receptor y or common y receptor

CD215 IL-15 receptor α

CD25 IL-2 receptor α

cDC Conventional Dendritic Cells

CDR Complementarity Determining Regions

CEA Carcinoembryonic antigen

CHO Chinese Hamster Ovary

CSF Colony Stimulating Factor

cTEC cortical Thymic Epithelial Cells

D Diversity

DAMP Damage-Associated Molecular Pattern

DC Dendritic Cell

EGFR Epidermal Growth Factor Receptor

EGR1 Early Growth Response Protein 1

ELF1 E74-like factor 1

ERK Extracellular Signal-Regulated Kinases

FADD Fas-Associated Death Domain

FasL Fas Ligand

FcR Fc Receptor

FcRN Neonatal fragment crystallizable Receptor

FOXP3 Forkhead Binding Protein

GABP GA-Binding Protein

gnzm Granzyme

HER2 Human Epidermal Growth Factor Receptor 2

HLA Human Leukocyte Antigen

HMG-I(Y) High Mobility Binding Protein

i.p. Intraperitoneal

i.v. Intravenous

ICI Immune Checkpoint Inhibitor

IFN Interferon

Ig Immunoglobulin

IL Interleukin

ILC Innate Lymphoid Cells
IRF-4 IFN regulatory factor 4

J Joining region
JAK Janus Kinase

KD Rate constant of dissociation at equilibrium

KIH Knob-into-Hole

KIR Killer immunoglobulin-like receptor

KO Knock-Out

KOFF Rate constant of dissociation

KON Rate constant of association

MAPK Mitogen-Activated Protein Kinase

MHC Major Histocompatibility Complex

MM Metastatic Melanoma

mo-DC Monocyte-derived Dendritic Cells

MSLN Mesothelin

mTEC medullary Thymic Epithelial cell

NFAT Nuclear factor of activated T cells

NF-κB Nuclear Factor-κB

NK Natural Killer

PAMP Pathogen-Associated Molecular Pattern

PBMC Peripheral Blood Mononuclear Cells

PBS Phosphate Buffered Saline

pDC Plasmacytoid Dendritic Cells

PEG Polyethylene Glycol

PI3K Phosphatidylinositol 3-Kinase

PIP2 Phosphatidylinositol-4,5-Bisphosphate

PIP3 Phosphatidylinositol-4,5-Trisphosphate

PK Pharmacokinetic

pSTAT phosphorylated Signal Transducer and Activator of Transcription

OCT1 Octamer-Binding Protein

RAG Recombination Activating Gene

RCC Renal Cell Carcinoma

SOCS Suppressor of Cytokine Signaling

SP1 Specific Protein 1

TAA Tumor-Associated Antigen

TCE T Cell Engager

TCM Central Memory T cell

TCR T Cell Receptor

Tdt Terminal deoxynucleotidyl transferase

TEM Effector Memory T cell

Tfh T follicular helper

Tg Transgenic

TGF- β Transforming growth factor β

Th T helper cell

TME Tumor Microenvironment

TNF Tumor necrosis factor

TRAIL TNF-related apoptosis-inducing ligand

Tregs regulatory T cells

TRM tissue-Resident Memory T cell

TSCM Stem Cell like Memory T cell

V Variable region

VLS Vascular Leak Syndrome

κ Kappa (referred to antibody and DNA locus)

λ Lambda (referred to antibody and DNA locus)

5 Introduction

5.1 Cancer

With rising life expectancy and shifts in lifestyle, cancer has cemented its place as one of the most prominent causes of death. The International Agency for Research on Cancer estimated close to 20 million cancer cases in 2022 and expects the number to rise by 76.6% by 2050.1 Fortunately, cancer deaths have not risen with the same speed. The National Cancer Institute reported data showing that survival rates in the United States have significantly improved rising from around 50% in 1975 to over 70 % in 2016 (Fig. 1A).² The improvement in cancer survival directly results from the growing scientific interest in cancer (Fig. 1B).³ Scientific efforts have significantly developed our understanding of cancer biology. In 2000, D. Hannan and R.A. Weinberg published the seminal list of six hallmarks acquired by cells during cancer development,4 which was updated in 2011 and again in 2022 to reflect the growing understanding in this field (Fig. 1C).^{5,6} Cancer cells develop from healthy cells that progressively become more dysfunctional. These cells can accumulate mutations during mitosis with a normal mutation rate of 10⁻⁷ to 10⁻⁸ per nucleotide per cell division. Many internal or external factors can significantly increase the speed at which mutations are accumulated. The cumulation of these mutations leads to dysregulated cell growth and ultimately cancer.⁴⁻⁶ Until the last decade of the 20th century, oncologists relied exclusively on surgery, radiotherapy, chemotherapy, or a combination of them. ⁷ Since then, our comprehension of cancer led to molecularly targeted therapies and immunotherapies.8 These "new pillars" of cancer therapy would not have been possible without a fundamental understanding of cancer and the immune system. In my thesis, I will present a novel cancer immunotherapy approach. Hence, the rest of the introduction will focus on the relevant components of the immune system, cancer, and related cancer therapies.

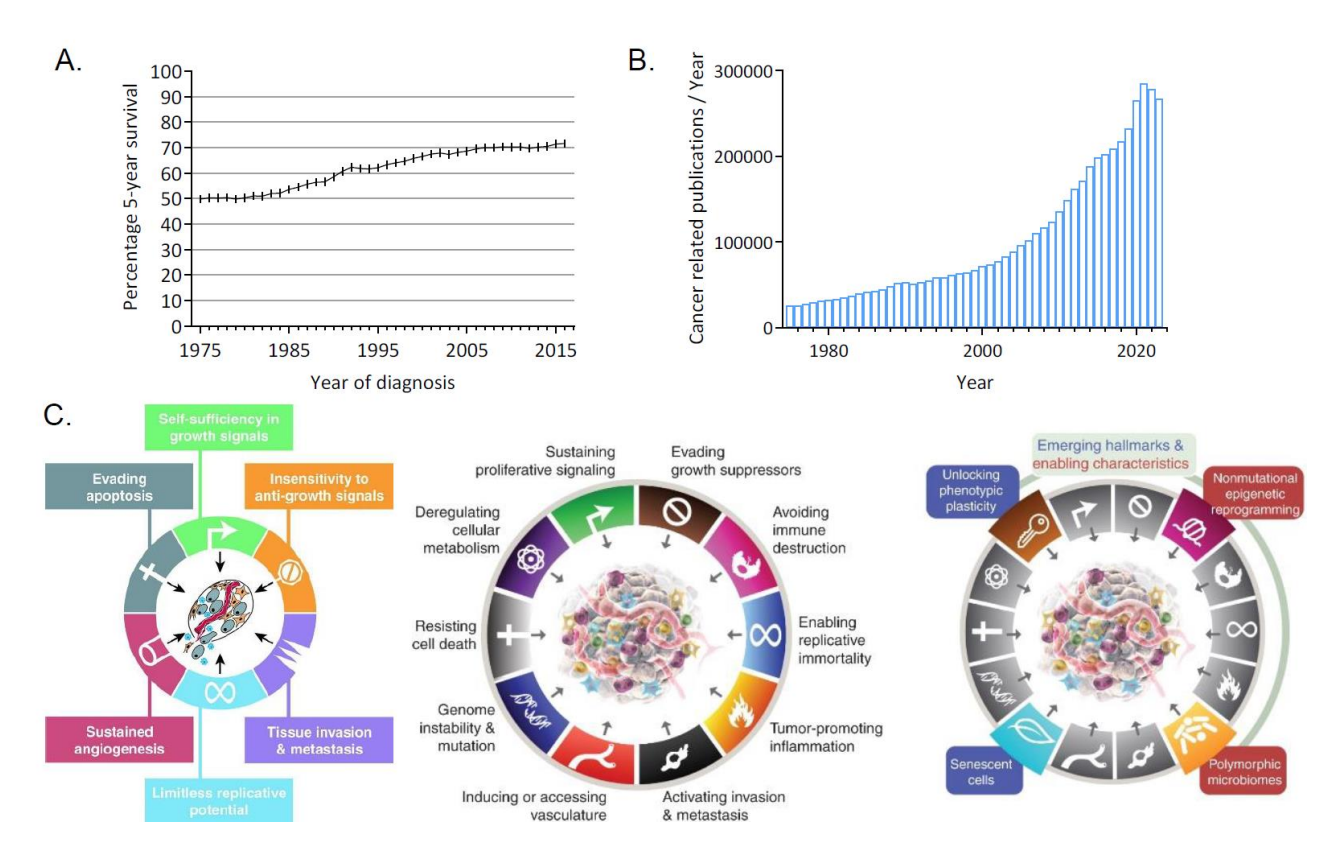


Figure 1 (A)The evolution of patient survival from 1975 to 2016. Graph created with data from the SEER Registries. (B) The amount of Pubmed entries mentioning "cancer" by year from 1975 until 2023. Graph created with data from pubmed.ncbi.nlm.nih.gov. (C) The Hallmarks of cancer across the years. Six were identified in the year 2000 (left), ten in the year 2011 (middle) and 14 in the year 2022 (right). Adapted from Hanahan D. et al., 2000 and Hanahan D. et al., 2022. ^{5,3,2,6}

5.2 Immune system

The immune system is a complex network of cells, soluble factors, and tissues that collaborate to maintain the body's homeostasis. The immune system is responsible for defending the body against external infections and dysregulated host cells. The individual's health is compromised whenever the immune system fails to fulfill any of these roles. The fight against external infections shares many similarities with the response to dysregulated cells but won't be further discussed here. The immune system can be divided into two main components: the innate and the adaptive immune systems. The innate immune system prevents or warns off most threats with a quick but non-specific response. It is composed of protective barriers, soluble components, and innate immune cells. Due to their relevance to this work, NK cells, dendritic cells, and soluble components such as cytokines will be introduced in dedicated sections. The adaptive immune system constitutes a second

line of defense that is slower but can develop a specific defense against its target. It comprises immune cells and soluble proteins released by some of these cells. 11 Due to their relevance to this work, T cells and antibodies will be introduced in dedicated sections. In this introduction, I will present some comparisons between the human and the mouse immune systems as syngeneic mouse models are used in this research.

5.2.1 The major histocompatibility complex (MHC) I/II

The MHC molecules play a central role in innate and adaptive immunity; hence, introducing them here will ease understanding the different cell populations. The MHC molecules are a group of proteins encoded by genes in the human leukocyte Antigen (HLA) region. These proteins are expressed at the surface of cells and allow the presentation of peptides to T cells. The high polymorphism of these genes results in populations capable of presenting a wider range of peptides and responding to most pathogens. MHC molecules can be distinguished between MHC class I and MHC class II.

MHC class I molecules are constitutively expressed on all healthy nucleated cells and are encoded by HLA-A, HLA-B, and HLA-C genes. HMC I are dimeric molecules composed of an α chain (composed of α 1, α 2, and α 3 extracellular domains, a transmembrane domain and a C-terminal cytoplasmic tail) bound to a β 2-microglobulin. The polymorphism of the MHC I is linked to variations in the peptide binding groove found between domains α 1 and α 2. MHC I molecules primarily load peptides of 8-10 amino acids. The β 2-microglobulin does not interact directly with the loaded peptides but is essential for the formation and the stability of the peptide binding groove of the α chain. Some peptides of extracellular origin can be loaded on MHC I through cross-presentation, but most are of intracellular origin. MHC I molecules are vital for the inhibition of NK cells and the development and activation of CD8+T cells.

MHC II molecules are composed of an α and a β chain.²⁰ α 1 and β 1 domains are highly polymorphic and are involved in the interaction with the loaded peptides, while the rest of the chains are involved in the interaction with CD4.^{20,21} These molecules are encoded by HLA-DP, HLA-DQ, and HLA-DR genes.¹⁴ Different from MHC class I molecules, MHC class II molecules are not ubiquitously expressed. They are expressed by antigen-presenting cells (APCs) such as dendritic cells (DCs), macrophages, B cells, and medullary thymic epithelial cells (mTECs).²² mTECs are cells involved in T cell development, and their function will be briefly discussed later. The other APCs can engulf and process extracellular antigens into

13-25 amino acid peptides that can be loaded on MHC II molecules. ^{17,23} The recognition of these complexes is essential for the development and activation of CD4⁺ T cells.

5.2.2 Cytokines

Cytokines are small secreted proteins produced by immune and non-immune cells that can affect many biological processes and are particularly important in the crosstalk between immune cells. They have been described to regulate cell growth, differentiation, migration, survival, inflammation, tissue repair, and immune responses.²⁴ Cytokines are classified into families based on structure and function: Transcription growth factor (TGF-β), Chemokines, Tumor necrosis factor (TNF) superfamily, Colony stimulating factors (CSFs), Interferons and interleukins. TGF-β promotes tissue growth and repair and is known to favor tumor progression.²⁵ Chemokines are a cytokine family that regulates cell migration through chemotactic gradients. The chemotactic gradient is sensed by cells expressing the appropriate receptor and guides cells to tissues where they can impact immune responses, inflammation, and angiogenesis.²⁶ Several chemokine receptor antagonists are being explored in the clinic as they could reduce tumor microenvironment (TME) infiltration by immunosuppressive cells.²⁷ TNF superfamily consists of ligands and receptors with some common structural motifs that regulate apoptosis, proliferation, survival, and differentiation. Anti-TNF antibodies are used for autoimmune diseases and no molecule has been approved for cancer treatment.²⁸ CSFs are a family of cytokines that is critical during hematopoiesis. CSF-targeting drugs are used to treat neutropenia in cancer patients undergoing chemotherapy. Interferons are a family of cytokines divided into type I, II, and III interferons based on the receptor that transduces its signaling. A wide range of cells produces type I and type III interferons in response to pathogen-associated molecular patterns (PAMPs) or damage-associated molecular patterns (DAMPs).^{29,30} Type I interferons are known to induce a strong systemic antiviral response. The strong anti-cancer response induced by type I interferons has resulted in the FDA approval of a few molecules to treat some cancer indications.³¹ The response to type III interferons induces similar intracellular signaling to type I interferons but results in a more controlled reaction focused on epithelial barriers.³² Interferon y (IFN-y) is the only type II interferon and is expressed by NK cells, T cells, and B cells during immune responses. Its receptor is widely expressed, and studies have shown both pro-tumorigenic effects and anti-tumor activity.33,34 There is still extensive research on the cytokine, but no drugs targeting this pathway have been approved in oncology.³⁵ Finally, interleukins are divided into families based on their

receptors and structural similarity, which is not always reflected in similar biological activities. Because the research presented later revolves around IL-2 and IL-15 signaling, these cytokines will be described in dedicated sections and the rest of the introduction. Both cytokines are members of the IL-2 family, a group of cytokines transducing their signal through receptor complexes involving CD132 (also called common γ receptor). This family of cytokines also includes IL-4, IL-7, IL-9, and IL-21. Despite some commonalities, these cytokines fulfill very different roles in the immune system.³⁶

5.2.2.1 IL-2/IL-15 cytokine and receptor expression

IL-2 and IL-15, in addition to binding the same CD132 subunit, share also the β subunit of their receptor (CD122, Fig. 2A).³⁷ Both the receptor for IL-2 and the one for IL-15 have an additional subunit that lacks an intracellular signaling domain but helps the receptor bind to its ligand with higher affinity. IL-2R α (CD25) binds the cytokine in cis (meaning on the same cell) and increases the receptor's affinity by around 100 times (Fig. 2A).³⁸ IL-15R α (also called CD215) is most often expressed by a different cell and captures IL-15.³⁹ The captured IL-15 is then presented to cells expressing CD122 and CD132.⁴⁰ Both cytokines can transduce signaling without their α subunit, but the downstream effects of the engagement are different.

Studies have shown that the IL-2 gene expression is controlled by many transcription factors with binding sites in IL-2 promoter. Nuclear factor of activated T cells (NFAT), activator protein 1 (AP-1), nuclear factor-κB (NF-κB), octamer-binding protein (OCT1 also called POU2F1), high mobility group protein HMG-I/HMG-Y (HMG-I(Y) also called HMGA1) and forkhead binding protein (FOXP3) are some of the most important regulators.^{41–45} The control of IL-15 is not comprehensively understood, but it is known to be induced by IRF-1 and NF-κB (Fig. 2B).⁴⁶

Some studies have been performed on the expression of the subunits composing the IL-2 and IL-15 receptors. Binding sites for ETS1, GA-binding protein (GABP), specific protein 1 (SP1), early growth protein 1 (EGR1), and EWS-WT1 are found in the promoter of CD122.^{47–49}

More interestingly, phosphorylated Signal transducer and activator of transcription 5 (pSTAT5) binding sites were also found, suggesting a positive feedback loop.^{50–52}

The studies regarding the CD132 promoter are more limited, but it is known that it contains multiple ETS binding sites.⁵³ CD25 expression was studied more extensively. Binding sequences for pSTAT5, pSTAT3, NFAT, NF-κB, AP-1, SP1, EGR1 and E74-like factor 1 (ELF1) have been identified in the promoter of CD25.^{54–57} It is worth noting that expression

studies and the numerous binding sites for pSTAT5 in the promoter show that IL-2 is an important inducer of CD25 expression (Fig. 2B).^{50,51} CD215 has been studied less extensively, and the information regarding its expression is more limited. A study has identified NF-κB and IFN regulatory factor 4 (IRF-4) as regulators of CD215 expression.⁵⁸ Sections dedicated to NK cells, DCs, T cells, and B cells will discuss the specific expression of IL-2 and IL-15 receptor subunits and specific signaling effects related to these cells. Endothelial cells, NKT cells, mast cells, macrophages, Innate lymphoid cells (ILCs, divided into ILC1, ILC2, and ILC3), and eosinophils can produce or respond to IL-2 and/or IL-15 signaling but won't be discussed at length here.

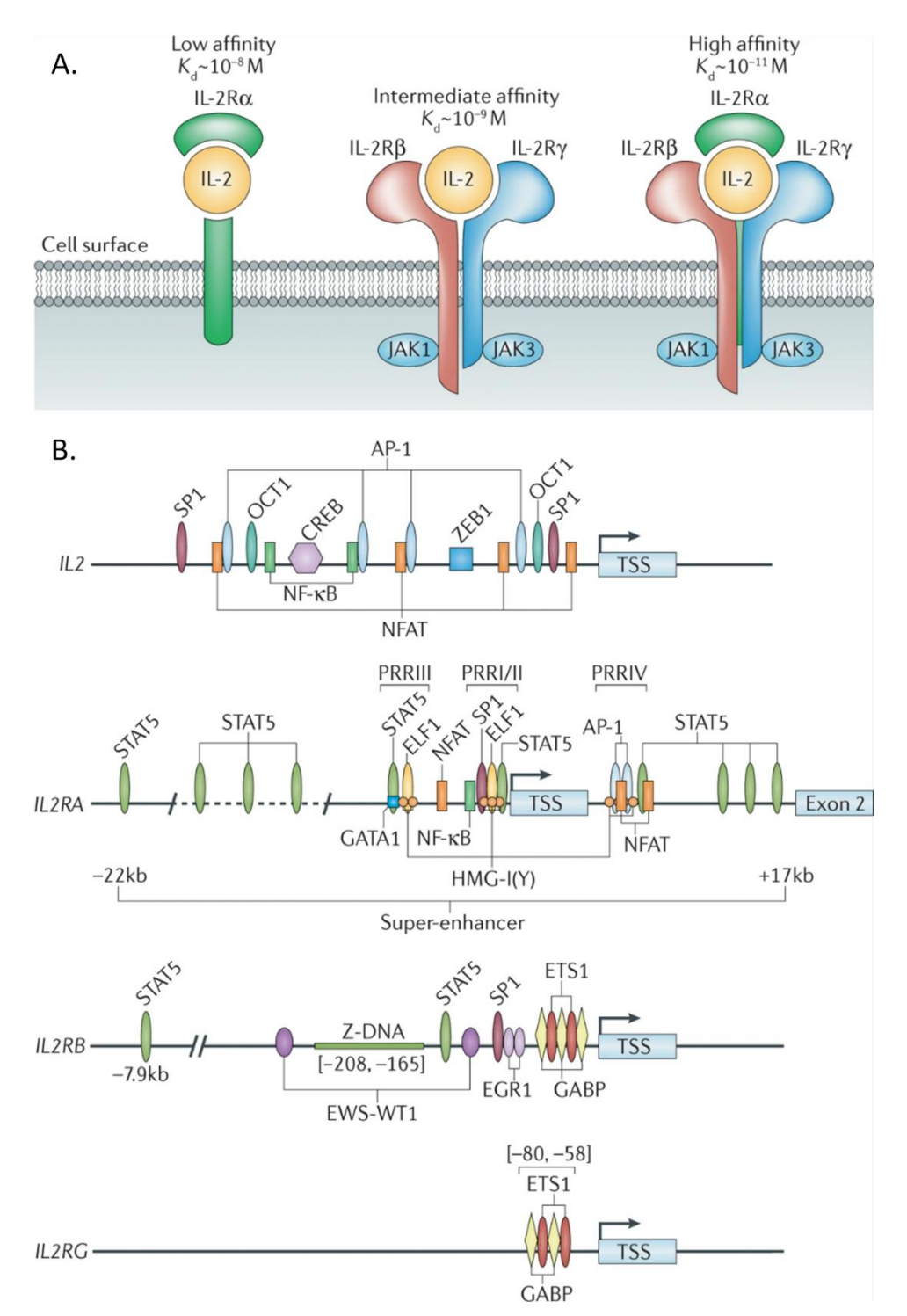


Figure 2 (A) IL-2 can bind to different forms of its receptor. CD25 binds IL-2 with low affinity (left), the dimeric CD122/CD132 has an intermediate affinity (middle) and the trimeric CD122/CD132/CD25 has a high affinity (right). (B) In order from top to bottom the figure depicts a schematic representation of the promoter of IL-2, CD25, CD122 and CD132. Adapted from Spolski et al.⁵⁹

5.2.2.2 IL-2/IL-15 signaling

Since the two cytokines share both receptor subunits with an intracellular signal transducing domain, their downstream signaling is inherently similar. IL-2/IL-15 can initiate three intracellular signaling cascades: (i) the Janus kinase (JAK)/ STATs, (ii) the

phosphatidylinositol 3-kinase (PI3K)/Protein kinase B (AKT or PKB) and (iii) the mitogenactivated protein kinase (MAPK)/extracellular signal-regulated kinases (ERK) pathways (Fig. 3). (i) Once IL-2 or IL-15 (complexed with CD215 or not) engage on the receptor, the CD122 associated JAK1 interacts with the CD132 associated JAK3.60,61 The interacting JAKs will then recruit and phosphorylate STAT molecules downstream. The activity of JAKs can be inhibited by negative regulators such as proteins in the suppressor of cytokine signaling (SOCS) family. STAT5 is the primary transcription factor recruited, but STAT3 and STAT1 can also be phosphorylated. The pSTAT forms homodimers and, in the case of STAT5, also tetramers, which can translocate to the nucleus and induce transcriptional changes.^{62–64} The engagement of IL-2 or IL-15 on the receptor, in addition to the recruitment of STATs, leads to the recruitment of adaptor proteins and other kinases to the receptor complex. (ii) In the activation of the PI3K/Akt pathway, PI3K is recruited to the receptor and initiates the activation of the downstream cascade by phosphorylating phosphatidylinositol-4,5-bisphosphate (PIP2) into phosphatidylinositol-4,5-trisphosphate (PIP3). PIP3 activates Akt and leads to the activation of mTOR.65-67 (iii) In the activation of the MAPK/ERK pathway, the recruitment of adaptor proteins leads to the activation of Raf through the GTPase activity of Ras. Raf phosphorylates MAPK/Erk, which can enter the nucleus to phosphorylate transcription factors.^{68–71} These three pathways downstream of the IL-2/IL-15 receptors have some distinct biological outcomes but are mostly linked to stimulatory/activating effects. (i) The JAK/STAT pathway is known to induce proliferation and cytokine production, favoring survival and effector function of T and NK cells.⁷²⁻⁷⁵ pSTAT5 binding sites are found in numerous genes, some of which have already been listed and are involved in IL-2/IL-15 signaling. (ii) The PI3K/Akt signaling pathway affects cell survival and metabolism. Notably, activating mTOR downstream of this cascade is a key controller of cellular metabolism. 76-78 (iii) The MAPK/ERK pathway is involved in cell differentiation and was shown to induce proliferation, reduce apoptosis and increase production of cytokines in immune cells.^{79,80}

IL-2 and IL-15, despite signaling through similar pathways downstream of their receptors, have some non-overlapping biological functions, which can be explained by the biological differences surrounding the two cytokines. First, while both cytokines initiate signaling through the same intracellular cascades, the contribution of each individual cascade and the importance of some downstream components differ. For example, IL-15 induces the proliferation of T cells through FKBP12 and a strong activation of mTOR in NK cells, while IL-2 relies on FKBP12.6 and does not activate mTOR to the same level.⁸¹ Additionally, these

cytokines can be produced and released by different cells that can respond to various stimuli and can be localized in different tissues. 82–84 The expression of the receptor subunits and the downstream components can fluctuate between cells and contribute to the differences in the responses to IL-2 and IL-15. Lastly, the cis-signaling of the soluble IL-2 compared to the trans-presentation of CD215-bound IL-15 to neighboring cells can also contribute to the observed responses and functions. 85–89 Altogether, IL-2 and IL-15 are potent stimulatory cytokines that rely on similar intracellular signaling pathways but have some distinct biological functions because of more complex biological reasons.

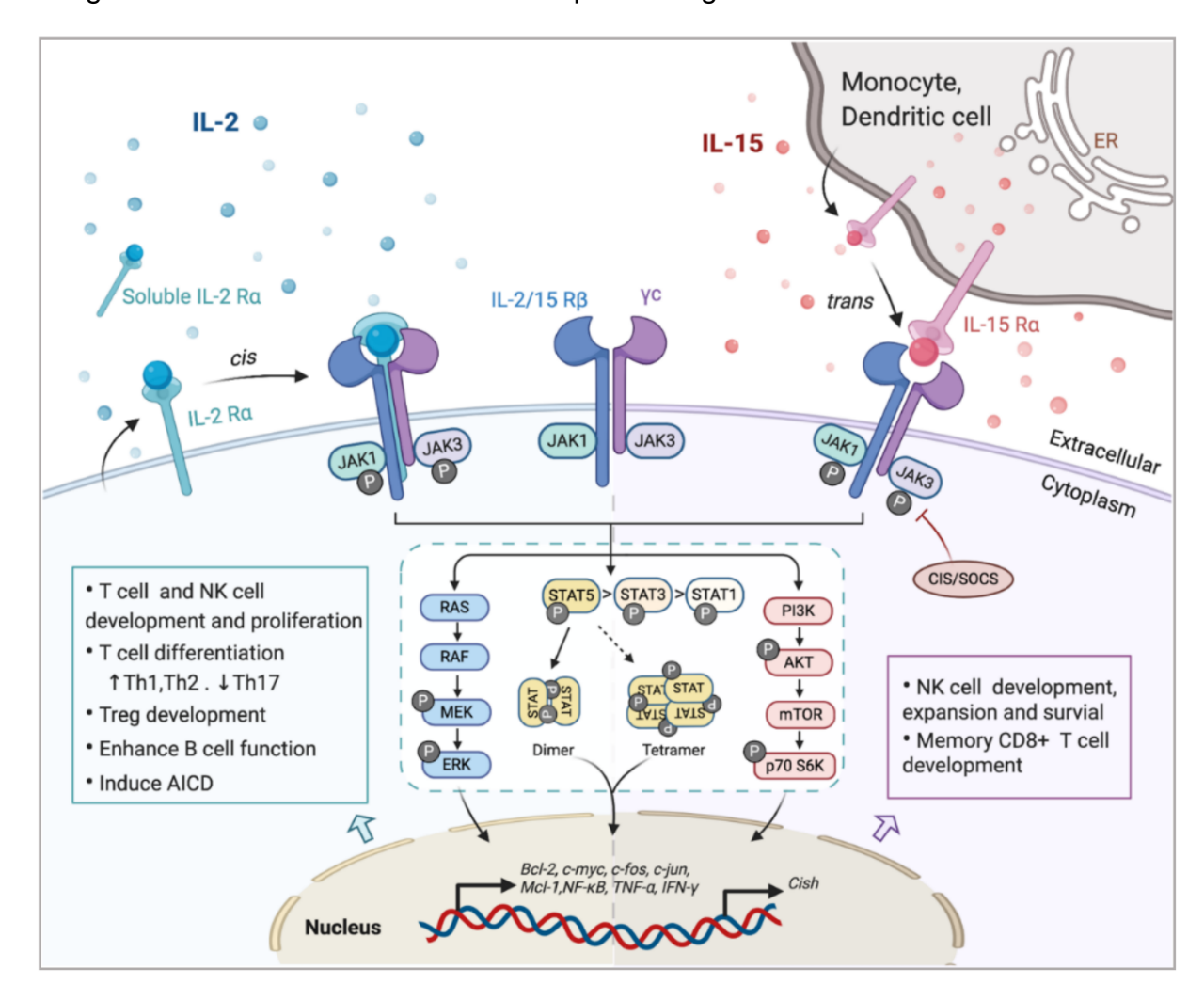


Figure 3 IL-2 and IL-15 share the same signal transducing receptor subunits (CD122/CD132). They have an additional distinct subunit that increases the affinity of the receptor. CD25 engages IL-2 and is expressed by the same cell expressing CD122/CD132. CD215 binds and present IL-15 to different cells. Both cytokines transduce their signal through the same 3 pathways: (i)MAPK/ERK, (ii)JAK/STAT and (iii)PI3K/Akt. Adapted from Yang and Lunqvist.⁹⁰

5.2.3 Immune cells

As mentioned, in addition to physical barriers and soluble factors, the immune system involves a complex network of immune cells communicating and interacting to defend the host. Some of these cells will be discussed here, emphasizing IL-2 and IL-15 signaling.

5.2.3.1 NK cells

NK cells are a subset of innate immune cells of lymphoid origin. These cells exist in humans and mice, but markers are not conserved between species. Human NK cells are commonly identified as CD3- and CD56+ and can be differentiated between CD56dim and CD56bright.91 CD56^{dim} cells are more abundant in the blood and have potent cytotoxic functions.⁹² CD56^{bright} cells are potent cytokine producers with less cytotoxic functions.^{92,93} CD56^{bright} was considered less mature, and a precursor to CD56^{dim}, but new studies suggest a less linear development.⁹⁴ Mouse NK cells are identified as CD3⁻ and NK1.1⁺ (in C57BL/6 mice). NKp46 is a cytotoxic receptor shared by humans and mice that is also used to identify NK cells. Similarly to other immune cells, NK cells display activating and inhibitory receptors. 95 Unlike T cells, NK cell activating receptors do not adapt to their target and mostly recognize some common or shared motifs in pathogens or stress induced molecules (Fig. 4C). A different example is CD16, which binds to the Fc portion of antibodies to carry out antibodydependent cellular cytotoxicity (ADCC).96 Killer immunoglobulin-like receptors (KIR) are inhibitory receptors that bind to MHC I and suppress the cytotoxic function of NK cells (Fig. 4A).97 Tumorigenic or virally infected cells might downregulate MHC I expression, which favors their elimination by NK cells (Fig. 4B).98 Activated NK cells can kill their target through two mechanisms. In the first, NK cells release perforin and granzymes (gnzm) through granules. Perforin will create pores in the target cell's membrane, and gnzm will induce apoptosis. In this process, the NK cells can recognize some molecules expressed at the cells' surface directly or indirectly through the Fc portion of the antibodies. 99 Alternatively, NK cells express Fas ligand (FasL) and Tumor necrosis factor (TNF)-related apoptosisinducing ligand (TRAIL) that can induce apoptosis in cells expressing their cognate receptors. 100 Activated NK cells can also produce cytokines that can directly affect target cells or shape the response of other immune cells.¹⁰¹

Studies have identified many signaling pathways involved in the survival and differentiation of NK cells from hematopoietic stem cells. Importantly for this work, IL-2 and IL-15 are important for NK cell differentiation and homeostasis and inducing their activation and proliferation. Naïve NK cells express CD122 and CD132 but not CD25. Upon activation, they can upregulate the expression of CD25, increasing their sensitivity to IL-

2.104 IL-2 is not necessary for the development of mature NK cells but is involved in their activation and their development of cytotoxic functions. 105 IL-2 was shown to increase the expression of cytotoxic molecules such as perforin and gnzm-B and to increase their cytolytic functions altogether. 106 Activating receptors such as NKG2D and NKp44 were also shown to be increased by IL-2 signaling. 107,108 IL-2 was also shown to amplify the response to IL-12 through up-regulation of STAT4 and the IL-12 receptor. 106,109 In addition to the classic proliferative signals resulting from the JAK/STAT pathway, IL-2 has been shown to reduce apoptosis through PI3K dependent reduction of ceramide in NK cells. 110 IL-15 is central to NK cell biology as it is essential for developing mature NK cells and their maintenance and function. Mice lacking IL-15 or IL-15R are almost entirely devoid of NK cells and fail to support the survival of transferred WT NK cells. 111,112 The induction of Bcl-2 and MCL1, two anti-apoptotic molecules downstream of the IL-15 receptor, is likely involved in the maintenance of survival of these cells. 113,114 IL-15 can increase the levels of perforin, gnzm-B and IFN-y, and activating receptors, all important molecules for NK cell function. 115,116 NK cells cannot produce IL-15 or IL-2 and rely on production from neighboring cells. IL-15 is often presented to NK cells by APCs bound to IL-15Rα at their surface, explaining the inability of IL-15Rα knock-out (KO) mice to support the survival of WT NK cells. 111,117

To summarize, NK cells are innate immune cells that can recognize and kill target cells. The balance between activating, inhibitory, and other signals controls the overall NK cell activation (Fig. 4). Many signaling pathways are involved in their development and regulation. Still, crucially for this work, IL-2 and IL-15 have been shown to promote their proliferation and functions, with IL-15 also being essential for their maturation and survival.

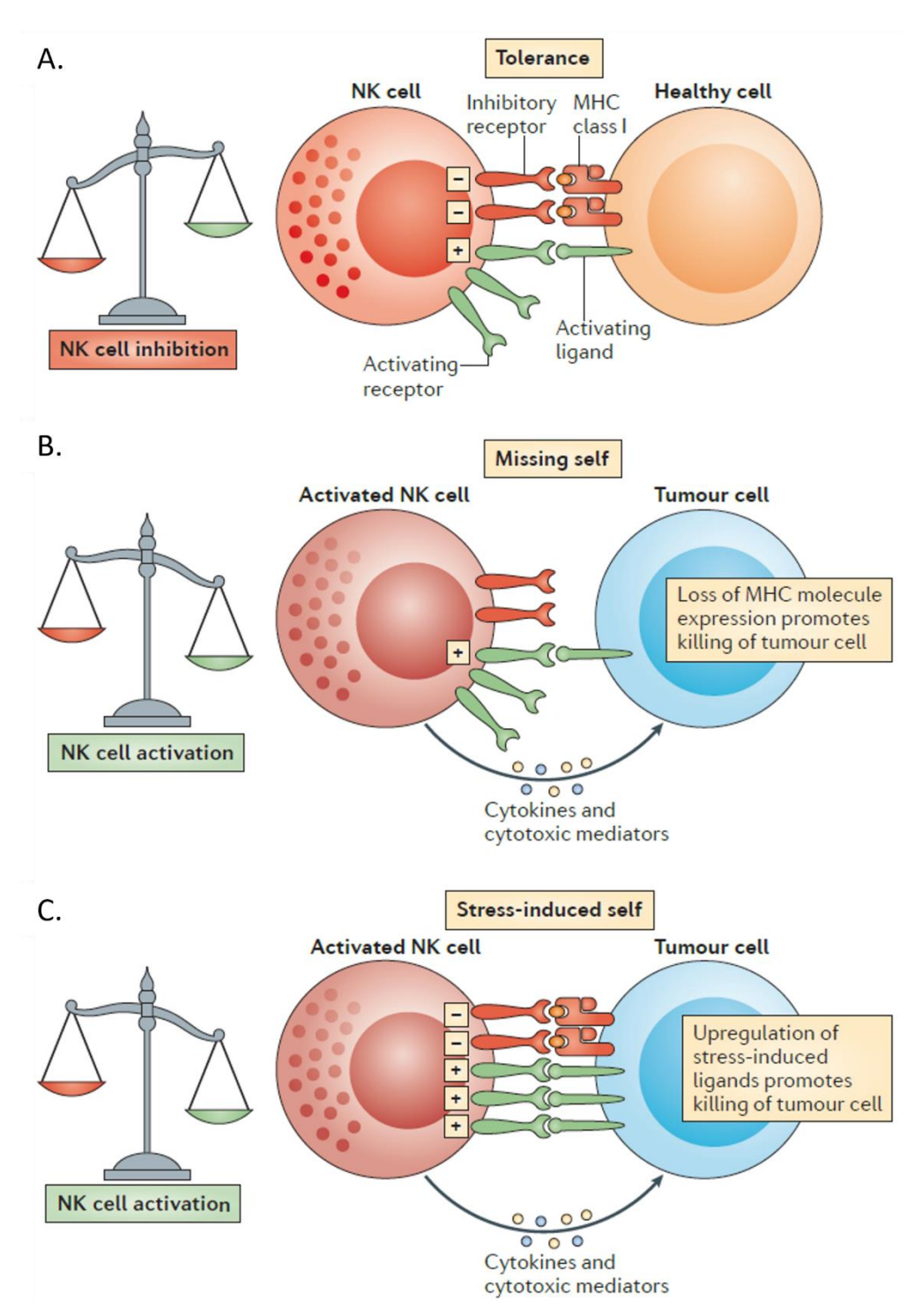


Figure 4 NK cell activation depends on the balance between activating and inhibitory signals. (A) MHC I will inhibit NK cells and prevent killing of healthy cells. (B) Tumor cells that downregulate MHC I lack inhibitory signals and activate NK cells. (C) Tumor cells increasing other stress signals recognized by NK cells, overshadowing the inhibitory signals provided by MHC I. Adapted from Vivier et al.¹¹⁸

5.2.3.2 Dendritic cells

DCs are a subset of APC at the crossroads between adaptive and innate immunity. DCs express various activating receptors that result in the phagocytosis of their targets. ¹¹⁹ Once internalized, DCs can process proteins into peptides and present them on MHC II or MHC I

through cross-presentation.¹²⁰ Upon capturing antigens, DCs will upregulate migratory molecules, such as CCR7, and migrate to lymphoid organs, where they can activate T cells to initiate the adaptive immune response.¹²¹ Several different types of dendritic cells have been identified, such as plasmacytoid DC (pDC), myeloid/conventional DC1 (cDC1), myeloid/conventional DC2 (cDC2), dendritic cells 3 (DC3) and monocyte-derived DC (mo-DC). These types of DCs are present both in humans and mice, and while not all the markers are conserved between the two species, their function is largely conserved (Fig. 5A).¹²²

pDCs are cells involved in the response to viral infections. These cells recognize viral nucleic acids through TLR7 and TLR9 and produce type I interferon following activation. 123 cDC1 can prime CD4+ T cells but are predominantly recognized as the primary crosspresenting APCs. Therefore, this DC subset is largely responsible for CD8⁺ T cell priming and activation. 124 cDC1 can also secrete type III interferon in response to viruses and activate CD4+ T helper 1 cells (Th1) through IL-12.125 cDC2 cells can also prime CD8+ T cells but are predominantly responsible for T_h1, T_h2, and T_h17 cells priming. (Fig. 5B)¹²⁶ Once activated, cDC2s secrete cytokines that will also contribute to the initiation and guide the adaptive immune response. 127 DC3 are intratumoral dendritic cells that likely develop from both cDC1 and cDC2 upon activation that are described in different cancer types across species. 128,129 DC3 are characterized by important transcriptional changes and the higher levels of immunoregulatory molecules, LAMP3, and CCR7 without migrating to lymphoid tissues. 129,130 Mo-DCs differentiate from monocytes during inflammation. 131 Once activated, mo-DCs can prime CD4+ and CD8+ T cells and secrete IL-12 and IL-23.131,132 While DCs do not produce IL-2, DC-derived IL-15 is essential for some immune cells. 133 In addition to IL-15, cDC1 and cDC2 also express IL-15Ra, allowing them to trans-present IL-15/IL-15Rα complexes to other cells. 111,117 T cells can be activated through transpresentation, but as mentioned in the previous chapter, this mechanism is crucial for the maintenance and function of NK cells. 134 pDC are not known to be directly involved in the trans-presentation of IL-15 but promote trans-presentation from other DCs indirectly through IFNs. 135 mo-DCs can produce IL-15 but have lower expression levels of IL-15Rα and are not considered the main trans-presenting DCs. 136 As mentioned, DCs do not produce IL-2 but are sensitive to both cytokines. 137 IL-2 favors the maturation and the function of conventional DCs. Studies have shown that IL-2 can increase MHC and co-stimulatory molecule expression. 138 IL-15 promotes the activation of both conventional DCs and moDCs.^{139,140} IL-15 signaling favors the production of type I IFN by pDC during viral infections.¹⁴¹

In conclusion, several types of DCs exist. They are innate cells that initiate adaptive immune responses against intracellular and extracellular pathogens by presenting antigens to CD4⁺ and CD8⁺ T cells and by producing cytokines.

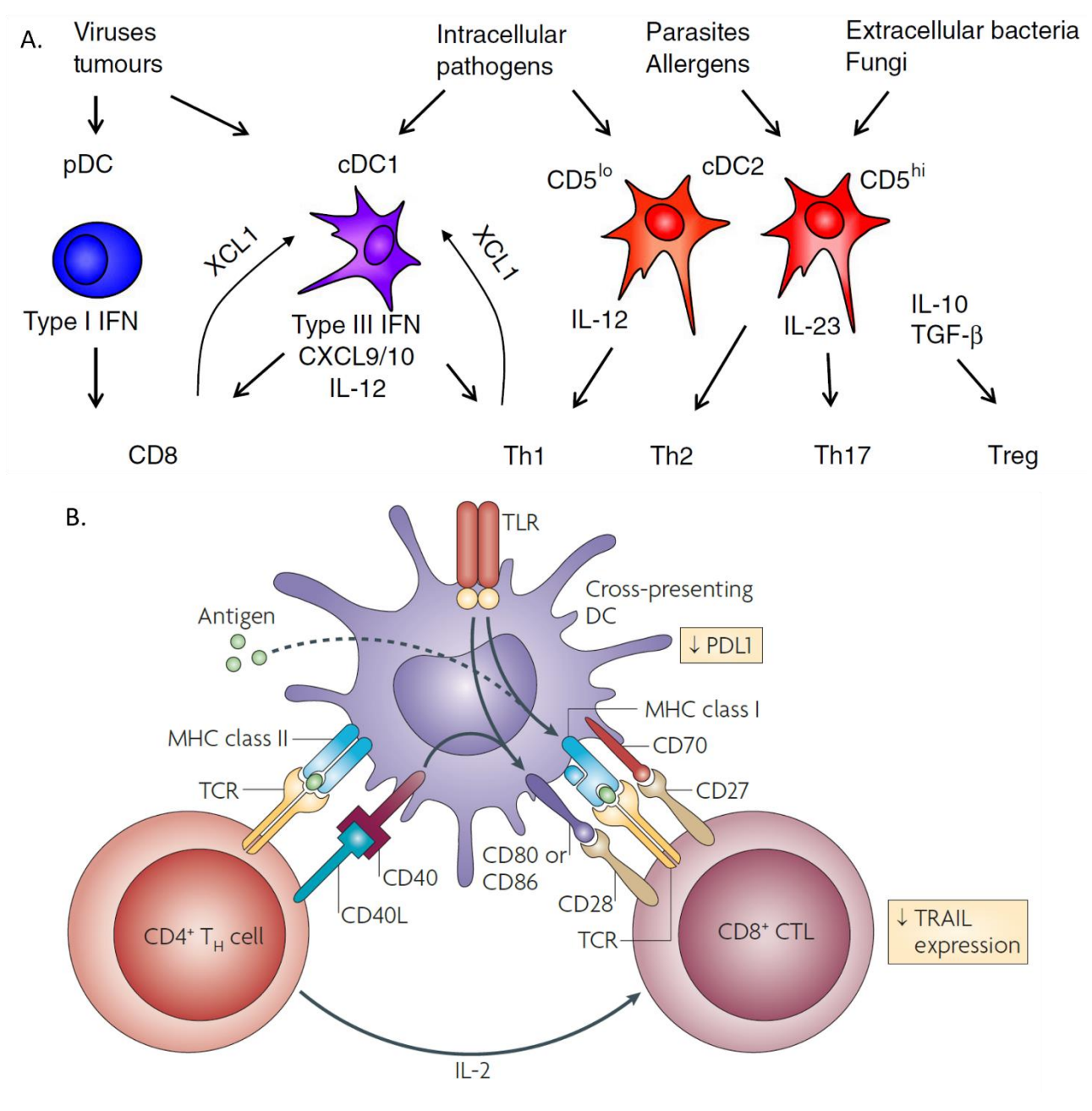


Figure 5 Dendritic cells can be differentiated between pDC, cDC1, cDC2 and mo-DC. (A) Each dendritic cell type responds to different pathogens/signal and interacts with different T cell populations. Adapted from Collin and Bigley¹²². (B) Dendritic cells can express both MHC I and MHC II to prime both CD4+ and CD8+ T cells. Dendritic cells express costimulatory molecules that are important for T cell activation. Adapted from Kurts et al. ¹²⁰

5.2.3.3 T cells

T cells are a major subset of adaptive immune cells and can be divided between CD4⁺ $\alpha\beta$, CD8⁺ $\alpha\beta$ and $\gamma\delta$ T cells. CD4⁺ T cells are a very diverse subset of cells that historically was mostly linked with a supporting role to other immune cells. It is now clear that their role is not limited to aiding other cells, but some have direct immunosuppressive or cytotoxic functions. CD8⁺ T cells are key cytotoxic cells involved in the defense against intracellular pathogens and tumors. $\gamma\delta$ T are less abundant compared to the other T cells but are enriched in some tissues like the lungs, intestines, and skin, where they are involved in immune responses, tissue repair, and maintenance.¹⁴²

5.2.3.3.1 T cell receptor (TCR)

T cells are one of the leading adaptive immune cell subset that develop from common lymphoid progenitor cells in the thymus. 143 The hematopoietic progenitors migrate to the thymus, where they start as double negative cells (meaning CD4⁻ and CD8⁻ cells) and start rearranging first their TCRβ and, later, TCRα. γδ TCRs also exist but won't be discussed in depth here. Once entirely rearranged, these two TCR chains will combine into the receptors responsible for recognizing specific antigens. The TCRα gene locus is composed of the variable (V), joining (J), and constant (C) regions. The TCRβ comprises the V, diversity (D), J, and C regions. During TCR rearrangements, enzymes called recombination activating gene 1 (RAG1) and RAG2 will induce double-strand breaks at different sites to rearrange the different regions of the TCRs and generate diversity by creating different combinations.¹⁴⁴ First, the TCRβ rearranges its segments in the following order: (i) Dβ with Jβ to form the DJβ complex, (ii) Vβ with DJβ to form VDJβ. This rearranged VDJβ segment is transcribed with the C segments and the introns between them. These introns and all but one C segment are removed during splicing to produce functional TCR receptors.¹⁴⁶ Cells also create diversity thanks to specific enzymes that add or delete nucleotides in the junctions between the different segments during rearrangements. 147 This process leads to great diversity and primarily affects the complementarity determining regions (CDR) of the TCR, and, more specifically, the CDR3, which is pivotal in recognizing antigens. 148 Once cells have selected their TCRβ chain, they become CD4+ and CD8+ (the so-called double-positive cells) and start selecting their TCRα chain. The process is similar to that of the TCRβ but limited to rearrangements between Vα and Jα segments. 149 After the rearrangements of the α chain, the TCR α/β complex is expressed by double-positive cells that, in the cortex of the thymus, will undergo positive selection. During positive selection, cells will be exposed to self-peptides loaded on MHC I and MHC II and expressed

by cortical thymic epithelial cells (cTECs). ¹⁵⁰ Cells recognizing MHC I or MHC II complexes will commit to CD8+ or CD4+, respectively, while cells failing to recognize any will not receive survival signals and die. ¹⁵¹ In the medulla of the thymus, the single positive cells are exposed to a wide range of self-peptides expressed by specialized cells called mTECs and presented by mTEC or dendritic cells on MHC I and MHC II. ¹⁵² CD4+ and CD8+ cells that recognize complexes with strong affinity are eliminated through apoptosis. Some self-reactive cells are kept alive but differentiate into regulatory CD4+ T cells with immunosuppressive roles. ^{150,152} Negative selection is important to prevent auto-immune diseases by eliminating T cells targeting self-peptides with strong affinity. The cells surviving this step are considered mature and can leave the thymus. ¹⁵¹ Altogether, T cells develop in the thymus through a process that results in cells with a unique TCR that will allow the recognition of a wide range of exogenous peptides. Depending on the MHC specificity, the differentiation results in CD4+ or CD8+ T cells. This process will result in CD4+ and CD8+ T cells expressing TCR receptors that will recognize their cognate antigens loaded on MHC II and MHC I, respectively.

5.2.3.3.2 T cell activation

Naïve T cells leaving primary lymphoid tissues have mature TCR but require additional signals to differentiate further and exert their functions. Binding of their TCR to their specific antigen-MHC complex is also called signal 1, providing a strong stimulatory signal to the T cell. 153 CD3 is an essential protein for the stabilization and function of the TCR during T cell development and in mature T cells. CD3 also has a signal-transducing moiety essential for activating antigen-specific cells and is considered part of signal 1.154 Studies have shown that in the absence of signal 2 and/or signal 3, signal 1 can lead to T cell apoptosis and anergy, which is a state of unresponsiveness. 155,156 Signal 2 is also called co-stimulation, which could be provided by different signaling pathways, with the most extensively studied being the CD28-CD80/CD86 pathway. CD28 is expressed by T cells, and its ligands are expressed by APCs, allowing them to initiate strong adaptive immune responses and sway the differentiation of the T cell. 157 Another example of signal 2 is 4-1BB-4-1BBL. 158 In addition to these two primary signals, the fate and activation of T cells also rely on a plethora of complementary signals from cytokines. In the following sections, the importance of some of the cytokines for the differentiation and function of T cells will be touched on. Naïve and non-activated T cells express CD122 and CD132 constitutively at varying levels. 159,160 In resting conditions, only a subset of CD4 T cells expresses CD25, but it can be induced in all T cells upon activation. 161 Among others, TCR signaling and IL-2 signaling lead to CD25

upregulation.¹⁶² CD215, as explained previously, is usually not expressed by T cells but by other cells that cross-present IL-15. Both cytokines generally lead to T cell proliferation and increase cell function, but the response can vary depending on the T cell population exposed to the cytokines. Additionally, T cells express inhibitory receptors at their surface upon activation. These inhibitory pathways, also known as checkpoints, are important to prevent immune cells' excessive activation and autoimmunity. Two of the first described inhibitory receptors on activated T cells are CTLA-4 and PD-1. CTLA-4 binds to CD80/CD86 with higher affinity than that of CD28 to CD80/CD86. This receptor dampens T cell activation by outcompeting CD28 and diminishing CD28 co-stimulation.¹⁶³ PD-1 binds to PD-L1 and PD-L2. PD-L1 is expressed by some immune and non-immune cells but is also exploited by cancerous cells to evade the immune system. PD-L2 is mainly expressed by APCs. The engagement of PD-1 on their ligands starts a signaling cascade that reduces T cell effector functions.^{164,165} Similarly to NK cells, T cells' outcome and activation state depend on the balance between all these inhibitory and stimulating signals.

5.2.3.3.3 CD4 T cells

After leaving the thymus, CD4⁺ T cells are considered naïve cells but can undergo further differentiation upon activation. Naïve cells encountering their cognate antigen will generally start clonal expansion. CD4⁺ T cells do not recognize antigens directly on target cells but rely on presentation from APCs. Depending on the strength and duration of the TCR signaling, co-stimulation, and other environmental signals, the proliferating activated cells will differentiate into different sub-populations (Fig. 6).¹⁶⁶ The main subpopulations of CD4⁺ T cells that have been described are the following:

- (i) Th1 are important in the response to intracellular pathogens and in cancer. ¹⁶⁷ The differentiation into Th1 cells is controlled by the transcription factor T-bet, induced by IL-12, and promoted by strong TCR signaling and IFN-γ. Once activated, Th1 can produce several cytokines like IFN-γ, IL-2 and TNF-α. ^{168,169} Thus, Th1 cells can promote their own differentiation and activate neighboring cells such as other CD4+ T cells, CD8+ T cells, macrophages, dendritic cells, and NK cells. Additionally, Th1 cells express CXCL9, CXCL10, and CXCL11, promoting the recruitment of immune cells such as CD8+ T cells to inflamed tissues. ¹⁷⁰
- (ii) Th2 differentiation is controlled by Gata3 and requires IL-4 signaling.¹⁷¹ Th2 cells are involved in the responses to extracellular parasites and in allergies.¹⁷² Activated Th2 cells produce cytokines such as IL-4, IL-5, and IL-13, promoting their own differentiation and other cells involved in the immune reaction to

- parasites and allergies. Their activation promotes IgE production, eosinophils, and mast cell activation. 173
- (iii) Th9 differentiation is favored by the combined IL-4 and TGF-β stimulation.¹⁷⁴ Th9, similarly to Th2, produce IL-9 and are involved in the response to parasites and allergies. These cells have not been studied as extensively as other populations, but they are known to activate mast cells and eosinophils.¹⁷⁵
- (iv) Th17 are key cells in the response to extracellular pathogens.¹⁷⁶ A strong TCR stimulation combined with IL-6 and TGF-β favors the differentiation and maintenance of Th17 cells for which the transcription factor RORγT is key.^{177,178} Th17, in response to extracellular pathogens, can activate neutrophils through IL-17A and IL-17F, while their release of IL-22 promotes epithelial repair and the production of antimicrobial peptides.¹⁷⁹
- (v) Th22, like Th17, promotes the repair of epithelial barriers and the production of antimicrobial peptides through the release of IL-22.¹⁸⁰ Their differentiation is favored by TCR signaling accompanied by IL-6 and TNF-α.¹⁸¹ They do not produce IL-17 and express CCR6, CCR4, and CCR10, which are important in guiding Th22 to the skin.^{182,183}
- (vi) T follicular helper cells (Tfh) are important in assisting B cells in producing antibodies in germinal centers. Differentiation of Tfh is controlled by the transcription factor Bcl-6 and is favored by prolonged TCR engagement on MHC II-antigen complexes presented by mature dendritic cells accompanied by IL-6 and IL-21 stimulation. 184–186 Thanks to their expression of CXCR5, Tfh are guided to B cell follicles in secondary and tertiary lymphoid structures, where dendritic cells guide them through the expression of CXCL13. 186 These germinal centers assist B cells in the production of high-affinity antibodies and in the development and survival of memory B cells and long-lived plasma cells. Tfh can interact and stimulate directly with B cells through TCR-MHC II interaction and co-stimulate B cells thanks to their expression of CD40L that binds to CD40 on B cells. 187 Tfh effect on B cells is mediated by direct cell-cell interaction and the release of IL-4, IL-6 and IL-21. 187–189
- (vii) Treg cells are immunosuppressive cells that help maintain self-tolerance and prevent excessive immune responses to avoid tissue damage. Tregs can be divided between thymic Tregs (tTregs) and peripheral Tregs (pTregs). 190,191 tTregs develop after recognizing self-antigens in the thymus and will suppress

self-reactive T cells that managed to leave the thymus, thus preventing autoimmunity. tTregs development and function is controlled by the transcription factor FoxP3 and express high levels of CD25. 192 pTregs are differentiated from mature CD4⁺ T cells outside of primary lymphoid tissues. Their differentiation is promoted by TGF-β signaling in the absence of strong co-stimulation. 193 pTregs are important in ensuring tolerance towards external antigens like those expressed by the commensal microbiota. 194 These peripherally differentiated Tregs can be further classified depending on different transcription factors and different markers expressed at their surface, but they all have high levels of CD25 and dampen immune responses. Once activated, Tregs can release immunosuppressive cytokines such as IL-10 and TGF-β to favor their own differentiation and reduce T cell responses. 195-197 Tregs function is not limited to the release of cytokines and can affect other cell populations through inhibitory membrane-bound proteins like CTLA-4.¹⁹⁸ Additionally, high expression of CD25 by Tregs under resting conditions makes them more sensitive to IL-2 compared to the other immune cells. In these conditions, the basal levels of IL-2 are captured mainly by Tregs and contribute to low immune activation without strong inflammatory stimuli. 199 This subset of CD4+ T cells also responds very differently to TCR signaling than other subsets. FoxP3 interacts with several transcription factors downstream of the TCR, altering the response to the recognition of antigens. An important signaling cascade downstream of the TCR results in NFAT activation. In non-Treg CD4⁺ T cells, NFAT increases IL-2 production. In Tregs, the interaction of FoxP3 with NFAT decreases IL-2 expression and increases expression of CD25 and CTLA-4.200 Similarly, FoxP3 binds to the transcription factor Runx1, forming a complex further decreasing IL-2 production.²⁰¹

(viii) Cytotoxic CD4⁺ T cells are thought to be defined by the transcription factors T-bet and Eomes. Reports supporting the cytotoxic functions of CD4⁺ T cells were already published at the end of the 1970s but their study has been neglected compared to cytotoxic CD8 T cells.²⁰² Some cytotoxic CD4⁺ T cell markers, like NKG2D, have been proposed, but a clear consensus is missing.²⁰³ Cytotoxic CD4⁺ T cells have increased levels of cytotoxic molecules, like gnzms and perforin, and are thought to be involved in chronic infections and cancer.^{204,205}

Activated CD4+ T cells generally differentiate into different subsets with different effector functions. Most activated cells will undergo apoptosis when the antigen is cleared, and other

stimulatory signals are decreased. Still, some will survive as memory CD4⁺ T cells to provide better and quicker responses in the future. Importantly for this work, the basal levels of IL-2 produced at homeostasis are mainly produced by the CD4⁺ T helper cells described here.²⁰⁶ Under inflammatory conditions, all the CD4⁺ T cells except regulatory T cells increase their production of IL-2, leading to much higher levels.²⁰¹

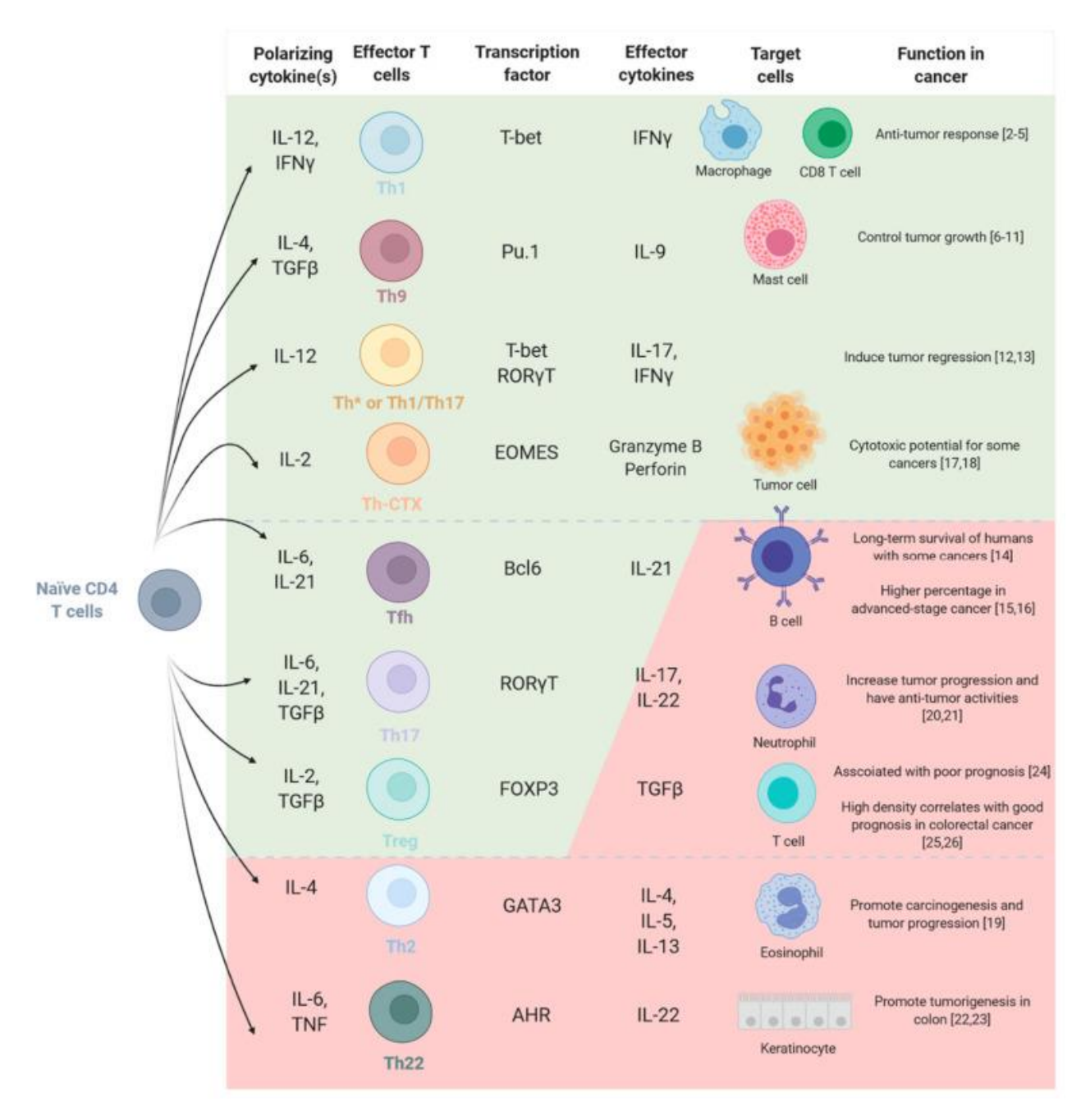


Figure 6 Naive CD4⁺ T cells can differentiate into many different subpopulations. The outcome is influenced by their environment and by the cytokines they are exposed to during their differentiation. The different CD4⁺ subpopulations exert different roles and produce different cytokines themselves. Adapted from Saillard M. et al. ²⁰⁷

5.2.3.3.4 CD8 T cells

The primary role of CD8+ T cells is to recognize and eliminate cancerous cells and cells infected by intracellular pathogens. Mature naïve CD8+ T cells that leave the thymus will circulate between secondary lymphoid organs and peripheral tissues. CD8+ T cells can bind their cognate antigen on DCs or directly on target cells. DCs also express high levels of CD80/CD86 and stimulatory cytokines, resulting in potent co-stimulation of CD8+ T cells through CD28 and activation through cytokine receptors (Fig. 7). 157 The stimulation of Naïve T cells by DCs happens mostly in secondary lymphoid organs where CD8+ T cells are guided by their high expression of CCR7 and CD62L.^{208,209} This stimulation of CD8⁺ T cells results in clonal expansion and differentiation into effector CD8+ T cells. Effector CD8+ T cells have increased levels of cytotoxic molecules and cytokines and are primed to recognize and eliminate target cells. Effector CD8+ T cells also have lower levels of CCR7 and CD62L, promoting their egress from secondary lymphoid organs. ^{208,209} They also have increased levels of other migratory molecules like CCR5 and CXCR3, facilitating their migration towards inflamed tissues.²¹⁰ When CD8⁺ T cells encounter their cognate antigen on target cells, the co-stimulatory signals provided by DCs are usually missing. However, CD8+ T cells already primed by DCs can exert their cytotoxic functions and clear the target cell. The primary mechanism through which CD8+T cells kill target cells is by releasing cytotoxic molecules towards the membrane of target cells. In this process, antigenexperienced CD8+ T cells recognize target cells through their TCR and form an immunological synapse by reorganizing their cytoskeleton.²¹¹ This synapse is directed towards the target cell, allowing the precise release of granules and sparing neighboring cells. The cytotoxic granules released in the synapse by CD8+T cells contain mainly perforin and gnzms.²¹² Perforin creates holes in the membrane of target cells, and gnzms induce apoptosis. CD8+ T cells can also kill target cells through a different mechanism. These cells express FasL and TRAIL, both known to cause apoptosis in target cells upon binding their receptors.²¹³ The binding of these death ligands to their receptors causes receptor trimerization. It initiates a signaling cascade leading to the activation of caspase-8 by the Fas-associated death domain (FADD) that results in apoptosis.²¹⁴ Additionally, activated CD8+ T cells can produce cytokines like IFN-γ, TNF-α, and IL-2.215 IL-2 is a paracrine and autocrine factor and induces CD8⁺ T cell proliferation, survival, and effector function.^{216,217} IL-2 has been shown to boost clonal expansion and the expression of antiapoptotic molecules like Bcl-2.218 Gnzm B and perforin are also increased downstream of this receptor.²¹⁹ IL-15 is not produced by CD8⁺ T cells but can also induce their proliferation.

But, unlike IL-2, IL-15 is less associated with increased effector functions and favors the differentiation into memory cells (Fig. 8A).²²⁰ Inhibitory molecules like PD-1 prevent indiscriminate and excessive killing by CD8+ T cells. (Fig. 7). Like NK cells, the balance between activating and inhibitory signals will guide the activation state of CD8+ T cells and decide whether target cells are killed. However, this mechanism can be exploited by tumor cells to avoid killing by CD8+ T cells.

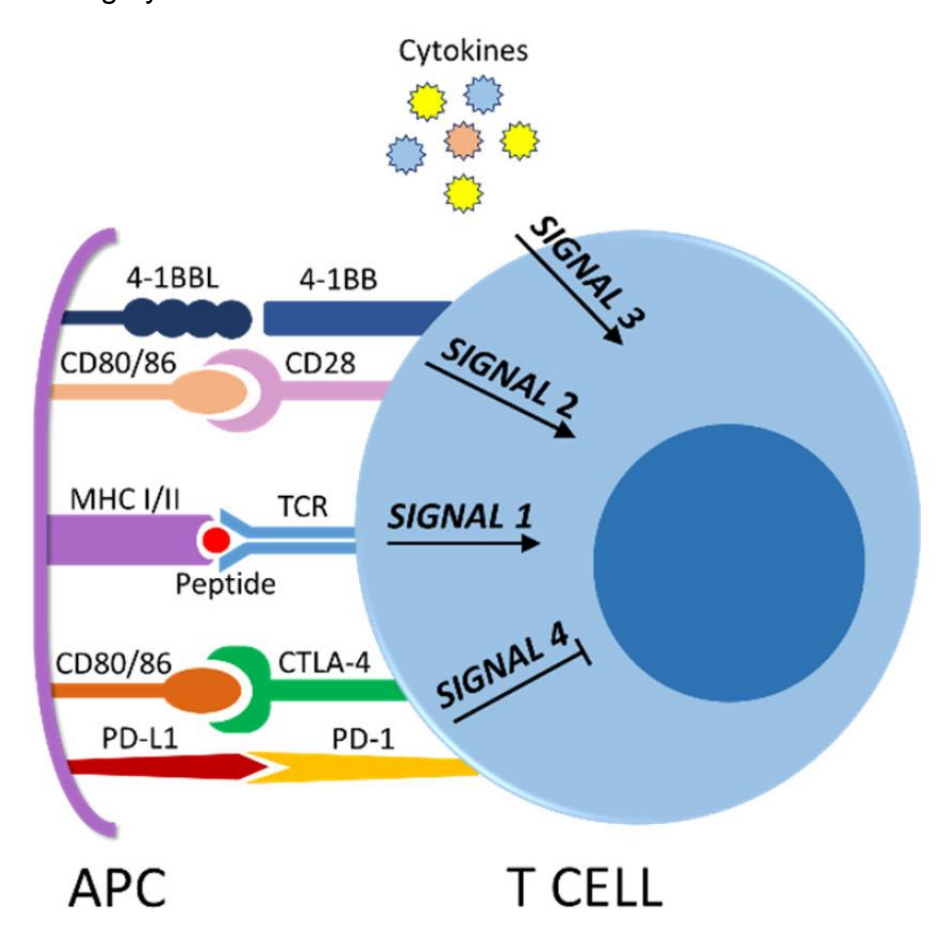


Figure 7 Priming of T cells by APCs is done through a combination of signals. TCR/CD3 binding to their cognate antigen provides signal 1. Signal 2 is given by co-stimulatory receptors like CD28 and 4-1BB. Signal 3 is given by cytokines. Signal 4 inhibits T cells and is given through inhibitory receptors like CTLA-4 and PD-1.Adapted from Montironi et al. ²²¹

5.2.3.3.5 Memory T cells

CD4⁺ T helper cells and CD8⁺ T cells exhibit increased effector function when exposed to their cognate antigen. Most of the time, their activity results in the successful clearance of the antigen. The immune system can learn from these encounters and build a long-lasting memory that allows it to respond quicker in the future (Fig. 8B). During immune responses, a portion of CD4⁺ and CD8⁺ T cells can differentiate into different subsets of memory cells. A short stimulation of cells favors the differentiation of these cells, while strong and very prolonged activation favors a dysfunctional phenotype (Fig. 8B-C).²²² IL-2 and IL-15 are

also involved in this differentiation step. Strong IL-2 stimulation has been shown to promote effector functions but is not as efficient as IL-15 at promoting the differentiation and survival of memory cells.^{223,224} IL-2 signaling without engaging the CD25 subunit of the receptor favors memory T cells similarly to IL-15.²²⁵ Stem cell like memory T cells (T_{SCM}) share many surface markers with naïve T cells but co-express memory markers, like CD95, CXCR3, IL-2Rβ, CD58 and CD11a.^{226,227} T_{SCM} are a subset of minimally differentiated T cells with selfrenewal capacity that can differentiate into most T cell subsets, like CM, EM and RM T cells. Central memory (CM) CD4⁺ and CD8⁺ T cells express high levels of CCR7 and CD62L, which allow them to home to lymphoid organs where they can rapidly expand and differentiate into effector cells upon future antigen exposures.²²⁸ Interestingly, IL-15 has been shown to be a potent inducer of T_{SCM} self-renewal.²²⁹ Effector memory (EM) T cells maintain some expression of effector molecules and do not home into secondary lymphoid organs. These cells remain in circulation and tissues to respond quicker during future exposures. Most tissue-resident memory (RM) T cells differentiate from CD8+ T cells and express molecules like CD69, CD103, and CXCR6 that keep them in tissues like the skin and mucosal barriers where they can rapidly respond.²³⁰ While not lasting indefinitely, all these memory cells can survive and are ready to respond quickly for many years.

5.2.3.3.6 Dysfunctional T cells

CD4+ and CD8+ T cells can differentiate into dysfunctional cells with reduced effector function. Anergy and exhaustion are two forms of dysfunction that result in reduced immune responses in cancer. In T cells, anergy is favored and was initially described as the state resulting from the engagement of MHC-antigen complex in the absence of co-stimulation.²³¹ Other signals such as the inhibition of mTOR can lead to anergy.²³² This situation results in an incomplete activation downstream of the TCR, leading to reduced proliferation, reduced cytokine production, reduced effector function, and increased expression of inhibitory molecules.²³² Anergy is important to prevent autoimmunity and tolerate commensal microbiota and food but is exploited in pathologies like cancer. T cell exhaustion is promoted by strong and prolonged antigen stimulation of cells (Fig. 8C). While moderate IL-2 activation reduces exhaustion, persistent and strong IL-2R activation can favor it.233 Immunosuppressive cytokines, like TGF-β and IL-10 or T cell inhibitory receptor ligands, contribute to an immunosuppressive phenotype that also favors T cell exhaustion (Fig. 8A). 234,235 Additionally, increasing evidence shows that metabolic changes are involved in this mechanism.²³⁶ A progressive loss of function characterizes exhaustion and happens commonly during chronic infections and cancer. During this progression, cells will increase their expression of inhibitory receptors, reduce their expression of effector molecules, and lose their ability to proliferate. Among others, the array of inhibitory receptors expressed by cells evolves during this progression and can be used to characterize cells.²³⁷ Exhaustion is a primary resistance mechanism used by tumors, and modulating its progression can reinvigorate anti-tumor responses.

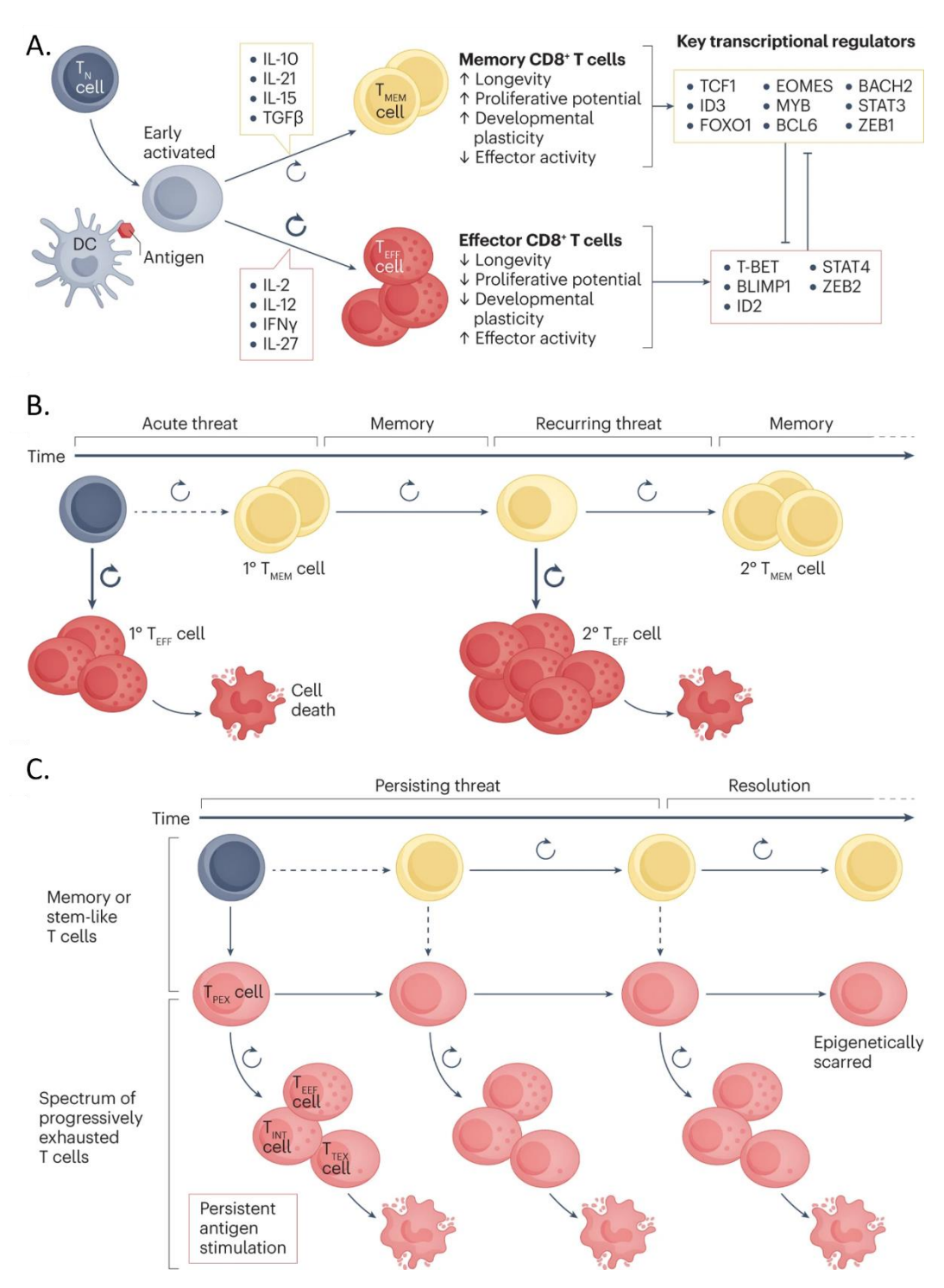


Figure 8 (A) Naive T cels are primed by APCs and become activated. Activated cells can acquire a memory or effector phenotype that are associated with different activities and characteristics. Cytokines can influence their outcome. (B) During acute infections a portion

of the activated T cells differentiate into effector cells and the rest will become memory T cells. Effector cells eliminate the antigen and differentiate or die by apoptosis. Memory cells will survive and produce new effector cells in future exposures to the antigen. (C) During chronic/longer exposures, effector cells will become dysfunctional/exhausted and their responsiveness will be decreased. Adapted from Gebhardt et al. ²³⁸

5.2.3.4 B cells

B cells are the second major adaptive immune system cell population and originate from the same lymphoid progenitor as T cells. Some evidence suggests they could develop from common myeloid progenitor cells as well.²³⁹ B cells are responsible for producing antibodies and diversify their B cell receptor (BCR) similar to how T cells diversify their TCR. In contrast to TCRs, BCRs bind to their cognate antigens directly without help from MHC molecules. The BCR comprises chains encoded by three genes with a structure similar to the TCR. The gene for the heavy chain is composed of V, D, and J segments and a constant region. The light chains are encoded by the kappa (κ) locus and the lambda locus (λ) and are composed of V and J segments associated with C regions. In the bone marrow, cells recombine their heavy chain's D and J segments.²⁴⁰ RAG1 and RAG2 induce recombination with the same mechanism observed in T cells and some diversity is introduced at junctions by Terminal deoxynucleotidyl transferase (Tdt).²⁴¹ The D-J segment is recombined with the V segment. Cells that successfully rearranged their heavy chains start expressing a precursor-BCR with surrogate light chains. Next, cells will recombine their light chain's V and J segments. Cells express their complete BCR as IgM at their surface and undergo negative selection to eliminate self-reactive cells. During this process, strongly self-reactive cells are eliminated by apoptosis, but in some cases, they undergo further light chain V-J rearrangements to attempt to create a new non-self-reactive BCR.242 After negative selection, cells leave the bone marrow and home to peripheral lymphoid organs, where they undergo further selection and become mature B cells expressing IgM and IgD at their surface. When naïve B cells encounter their cognate antigen, they will undergo further differentiation into short or long-lived plasma cells or memory B cells. Short-lived plasma cells secrete large quantities of antibodies, while long-lived plasma cells home to the bone marrow and provide a sustained production.²⁴³ Memory B cells do not secrete antibodies but, similarly to memory T cells, will respond quickly to future exposures. When naïve B cells are exposed to their cognate antigen in germinal centers, Tfh cells can interact with MHCII-antigen complexes on B cells through their TCR.²⁴⁴ Tfh provides B cells with costimulatory signals such as CD40L and cytokines, which are important for somatic hypermutation and class switch recombination.^{245,246} During somatic hypermutation,

activation-induced cytidine deaminase (AID) induces point mutations to the variable region of the BCR.²⁴⁷ B cells expressing BCRs with a higher affinity for the antigen are then selected. A class switch allows the B cells to produce other types of antibodies like Immunoglobulin G (IgG), IgA, and IgE by switching the constant region of their BCR.²⁴⁸

5.2.3.4.1 Antibodies

Antibodies are produced by activated B cells and plasma cells during immune responses, which have the same antigen binding domain as the BCR on the cells from which they are secreted. Each antibody monomer is composed of two identical heavy chains and two identical light chains.²⁴⁹ The heavy chains bind to each other, and the light chains pair each with a different heavy chain through disulfide bonds.²⁵⁰ Both the heavy and light chains contain a constant and a variable domain.²⁵¹ The variable domains contain three loops that, like in the TCR, are called CDR and are responsible for the binding and specificity to their target antigen.²⁵² The loops involved in the interaction are also called paratopes, and the target domain they recognize is called an epitope. Like in the TCR, the CDR3 is often the most critical loop in the paratope and corresponds to the region at the junction between V-D and J segments, where additional random modifications are introduced during recombination.²⁵³ The constant domain of the light chains is shorter than that of the heavy chain, functions as a scaffold, and stabilizes the pairing with the heavy chains. The constant domain of the heavy chain is more variable, and antibodies are divided into five classes, IgA, IgD, IgE, IgG and IgM, based on differences in this domain. This constant domain is composed of CH1, CH2, and CH3 for IgA, IgD, and IgG and of CH1, CH2, CH3, and CH4 for IgM and IgE (Fig. 9). 247,254 The constant domain of the heavy chains is important for the role of the antibody and determines whether multiple antibodies associate together to form multimers. The constant region also contains a binding domain for different Fc receptors that cells can express.²⁵⁵ The Fc receptor binding domain is crucial as several characteristics and functions of antibodies, such as activating NK cells, phagocytic cells and the complement system, rely on binding to Fc receptors through this portion.²⁵⁶ Among the five classes of antibodies, IgD is primarily expressed as a receptor by naïve cells and has limited functions apart from activating B cells. IgM are pentameric antibodies that are produced first during immune responses. IgM are very potent activators of the complement system.²⁵⁷ IgA, circulating in the serum mainly as a monomer, is often secreted at mucosal surfaces as a dimer, which is important in the defense against external pathogens. IgGs, including four subclasses (IgG1, IgG2, IgG3 and IgG4) based on differences in heavy chain constant regions, are the most abundant antibodies in the bloodstream and extracellular

fluid.²⁵⁷ The different subclasses are all monomers and have different hinges and disulfide bonds that affect their flexibility, with IgG2 being the most rigid and IgG3 being the most flexible. IgG1 is the most abundant and binds with high affinity to FcγR. IgG2 has a lower affinity for FcγR compared to IgG1. IgG3 has a longer hinge and is a potent activator of the complement system. IgG4 binds very weakly to FcγR.²⁵⁸ IgEs are mostly found as monomers and bind to FcεR, expressed by immune cells involved in allergic reactions.

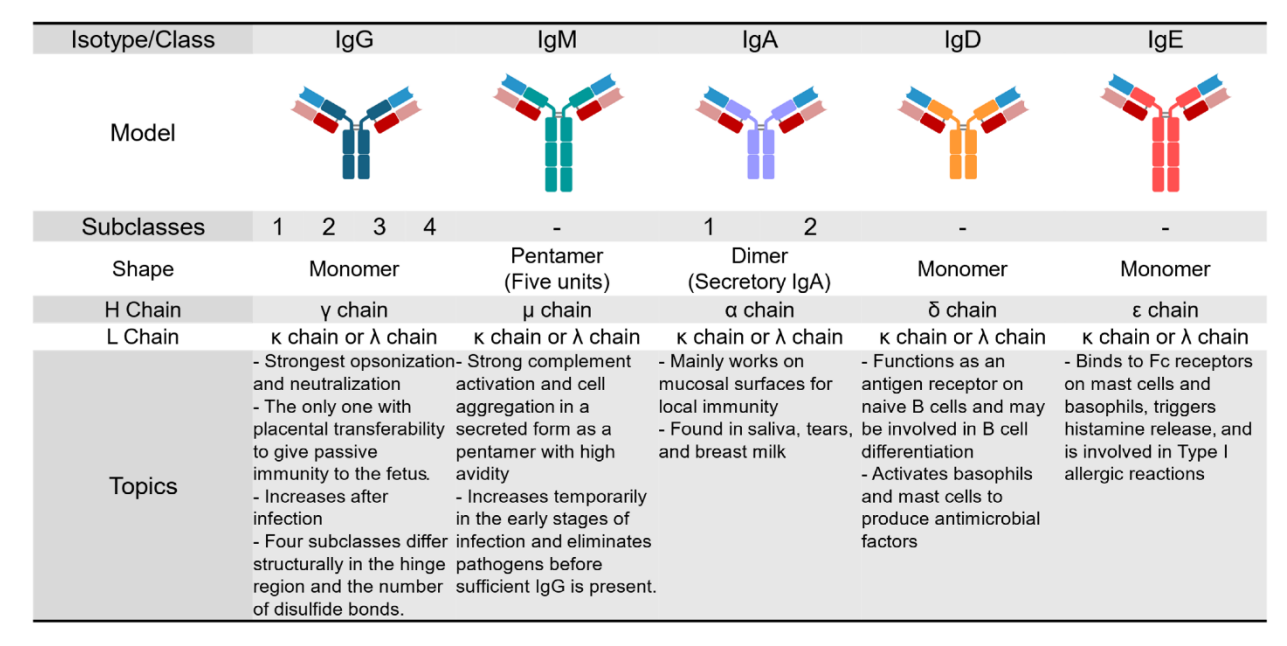


Figure 9 Class switch allows B cells to express 5 different classes of antibodies: IgG, IgM, IgA, IgD and IgE. These classes of antibodies have different constant regions that differentiate them. They have different structures and different roles in the body. Adapted from Araki and Maeda.²⁵⁴

5.2.4 Immunosurveillance

All the immune system components collaborate to keep the body safe from external pathogens and dysregulated self-cells. The concept of immunosurveillance posits that these dysregulated cells interact with the immune system and can be eliminated, at equilibrium or escape (Fig. 10). In the first case, the immune system will actively eliminate the dysregulated cells. In the second case, it will fail to eliminate all cells but prevent their spreading and disease progression. In the last case, the immune cells fail, and the disease progresses.²⁵⁹ Immunotherapies are treatments that aim to tilt the balance of this interaction towards the elimination of the dysregulated cells by favoring the antitumoral activity of immune cells.

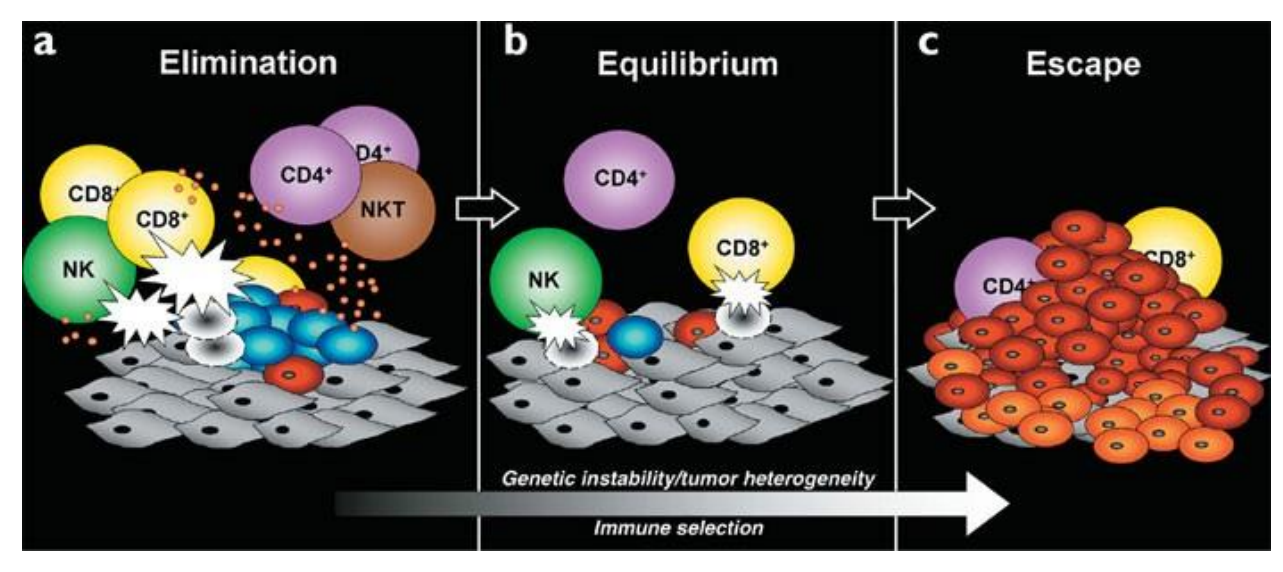


Figure 10 The concept of Immunosurveillance or the 3 "Es". Elimination: the immune system eliminates the tumor. Equilibrium: the immune system controls the tumor without eliminating it. Escape: the immune system fails to control the tumor. Adapted from Alexander and Yang.²⁶⁰

5.2.5 Tumor immunology

Innate and adaptive immune systems are important and complementary in anti-tumor immunity. As explained above, cancerous cells develop from healthy cells through the successive accumulation of mutations. These mutations can have different results: (i) Mutations leading to reduced protein expression. (ii) Mutations leading to increased expression of a protein. (iii) Mutations leading to mutated proteins.²⁶¹ (i) A reduced protein expression can lead to different advantages for tumor cells. Decreasing the expression of proteins involved in controlling cell divisions or ensuring the correct DNA replication during mitosis can increase the growth rate and the genomic instability of dysfunctional cells, which can also be advantageous. MHC I, as anticipated before, is also often downregulated. The reduced expression of MHC I results in reduced recognition and killing by CD8+ T cells, but it can also activate NK cells.^{262,263} (ii) The increase in protein expression that is usually not expressed or expressed at lower levels allows dysregulated cells to acquire advantages over healthy cells. Some cancer cells increase the expression of proteins such as Epidermal growth factor receptor (EGFR) and/or Human epidermal growth factor receptor 2 (HER2) that can promote their own growth and survival.^{264,265} HER2, EGFR and other membrane proteins expressed at levels higher than typically observed are called Tumor-associated antigens (TAAs). These Cancer cells can also express molecules that suppress immune responses or modulate their immune environment, such as PD-L1, CCL22, and IL-10.²⁶⁶⁻ ²⁶⁸ (iii) Another possible outcome of mutations is the creation of new proteins due to point mutations, deletions, or insertions. These new and mutated proteins can either lose or

acquire functions. Both cases can lead to advantages for dysregulated cells over healthy cells. The proteins generated in this last case are new, not encoded in the genome of the other healthy cells, and are called neoantigens. The adaptive immune system can target the TAAs and the neoantigens that arise from mutations. Both T cells and B cells can target these antigens. APCs can uptake these antigens and stimulate antitumoral immune responses that sometimes control or eliminate the mutated cells. However, as these proteins or similar proteins are natively encoded in the host genome, the negative selection steps usually eliminate immune cells expressing high-affinity receptors for these antigens, limiting responses.^{269,270} Neoantigens with major mutations have been targeted more successfully.²⁷¹ While immune responses can control or eliminate dysregulated cells and stop cancer progression, mutations can lead to situations where the abnormal cells escape their control and cancer develops. To summarize, dysregulate cells use a combination of strategies, including the downregulation of MHCI, direct inhibitory chemoattractants, immunosuppressive cytokines, and modifications to their extracellular space to limit immune cell activation, immune infiltration and make their environment immunosuppressive.

5.2.6 Cancer immunotherapies

Since their addition to oncologists' toolkit, immunotherapies have dramatically improved the prognosis for several cancers.²⁷² These treatments exploit the human immune system to target and eliminate cancer cells. While some earlier immunotherapies were already pioneered at the end of the 19th century, a recombinant form of hIL-2 became the first FDAapproved immunotherapy in 1992.²⁷³ As our understanding of the immune system and its interaction with cancer cells widened, immune checkpoint inhibitors (ICI), cancer vaccines, and adoptive cell therapy (ACT) joined cytokine therapies in the clinic. Cancer vaccines aim to elicit immune responses against TAAs, neoantigens, or viral proteins in the case of virusinduced cancers. In the case of HPV-related cancers, the vaccine is prophylactic, but others are used after the disease has developed.²⁷⁴ Cancer vaccines rely on the ability of the adaptive immune system to initiate an immune response against the desired antigen expressed by cancer cells. Initial vaccines encountered significant hurdles in clinical trials, but several approaches have made it to the clinic.^{275,276} ACT consists of the extraction of immune cells and the injection of these cells back into patients following ex vivo expansion or modification. Several strategies have been developed, including T-cell therapy, TCR therapy, chimeric antigenic receptor-T (CAR-T) cell therapy, NK cell therapy, and CAR-NK

cell therapy (Fig. 11). 277,278 T cell therapy and NK cell therapy consist of extracting cells from patients or donors, expanding, stimulating, and sometimes genetically modifying them before injecting them into patients. TCR therapy is similar but involves changing the TCR of extracted T cells to recognize specific antigens before injecting them back into patients. CAR-T and CAR-NK cell therapy introduce chimeric receptors that recognize specific antigens without being loaded on MHC molecules. Binding to target antigens is sufficient to initiate the killing of the target cell and is not dependent on other signals.²⁷⁹ ACT is used today in the clinic, but it is limited by several factors like toxicity and cost that newer approaches try to solve.²⁸⁰ Checkpoint inhibitors target inhibitory pathways of immune cells, aiming to reinvigorate immune responses against tumor cells. The prolonged exposure to antigens and the expression of inhibitory receptors such as PD-L1 and CTLA-4 by cancer or immunoregulatory cells can reduce immune activation and/or lead to exhausted immune cells. Extensive research and clinical data have shown that blocking these inhibitory pathways can remove the brake holding down immune responses and lead to long-lasting patient responses.^{281–285} Ipilimumab, an anti-CTLA4 antibody blocking its interaction with CD80/CD86, became the first ICI approved in 2011. It showed a response rate of 10-15%, and the responding patients would often have long-lasting responses.²⁸⁶ Soon after, other blocking anti-PD-1 and anti-PDL-1 antibodies were adopted in the clinic and demonstrated convincing clinical benefits in a sub-group of cancer patients.^{287,288} Today, drugs blocking the interaction of inhibitory receptors with their ligands have become the first-line treatment for several types of cancer. 289,290 While some clinical studies have recently been stopped, the research in this field is still investigating other inhibitory receptors like TIGIT or TIM-3. Other groups are focusing on biomarkers or predictive models that can predict the response to each treatment more accurately.^{291–294} Despite being the earliest type of immunotherapy adopted in the clinic, cytokine therapies are still being studied extensively. A few more recombinant cytokines have been approved. However, their number is still quite limited compared to the number that entered clinical trials because of severe side effects. Much of the research and trials in this field now focus on exploiting these powerful signaling pathways but limiting their side effects by making them more specific and targeted. Because of their relevance to this work, IL-2 and IL-15 targeting therapies and their limitations will be discussed in a dedicated section.

Approaches for cancer immunotherapy

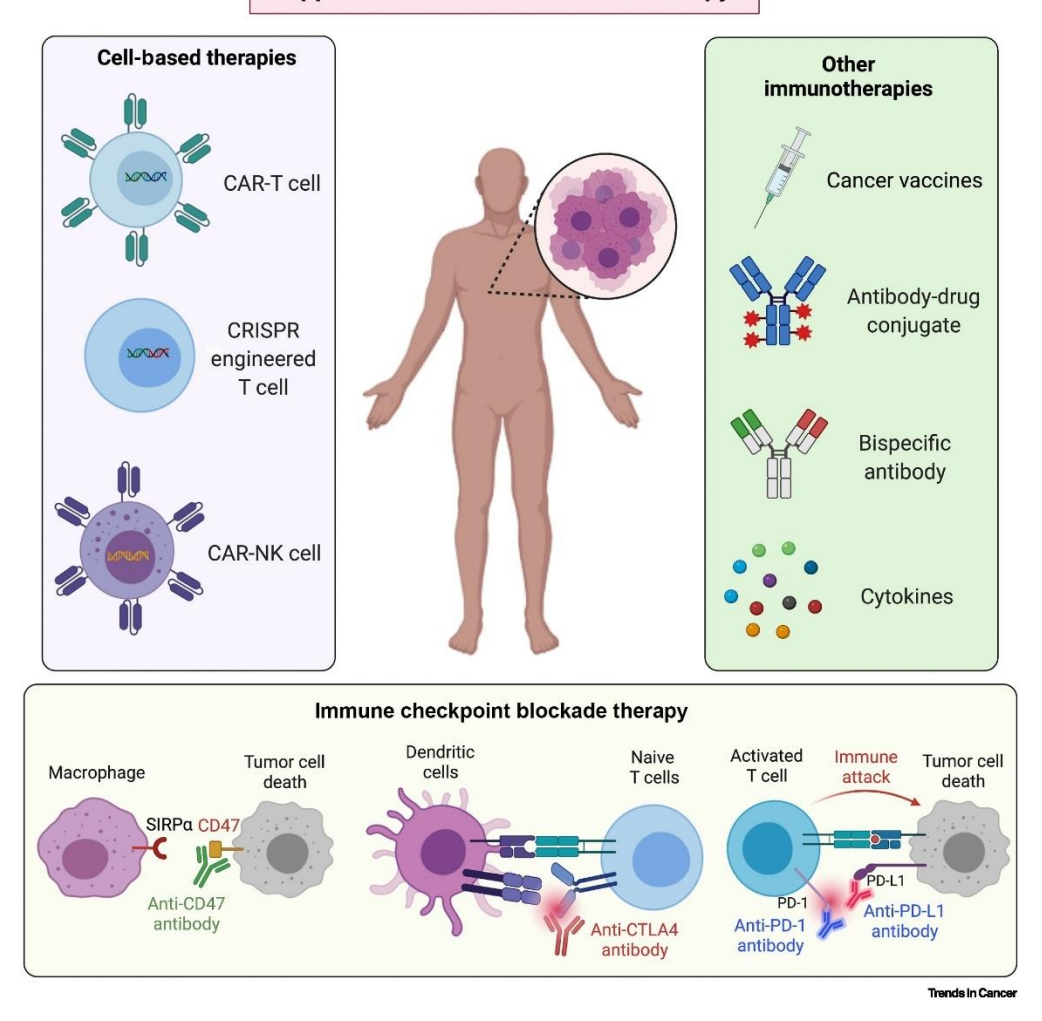


Figure 11 Advances have allowed the development of many cancer immunotherapies. Adoptive cell transfer, immune checkpoint inhibitors, bispecific antibodies and ADCs are notable examples. Gupta et al.²⁹⁵

5.2.7 Therapeutic Antibodies

Antibodies have many characteristics that make their structure appealing for the design of drugs. Among others, antibodies are stable proteins with a relatively long half-life and a well-defined structure with a constant scaffold and CDRs that can bind their target epitope with high affinity and specificity. The earliest forms of therapeutic antibodies were produced in animals exposed to antigens, such as serum obtained from horses exposed to diphtheria toxins, in a method that awarded Emi von Behring the first Nobel Prize for Medicine and Physiology in 1901.²⁹⁶ Sera extracted from animals contains a cocktail of antibodies produced by different B cell clones called polyclonal antibodies. These cocktails were a breakthrough for treating various conditions but have some limitations. The antibodies produced by animals differ from human antibodies and can elicit undesired immune responses. The polyclonal nature of the serum means there is little control over the epitope

and antigen targeted by antibodies in the serum, leading to considerable variability between batches and possible off-target binding and toxicity. Antibody technology has gradually advanced and transitioned to monoclonal antibodies that now dominate the market. A monoclonal antibody is an engineered antibody with desired specificity produced by a single cell clone. It has favorable inter-batch consistency and less off-target toxicity comparing to the polyclonal antibody drugs. Monoclonal antibodies were initially produced through hybridoma cells obtained by fusing a B cell with an immortalized myeloma cell.^{297–299} Initially, the technology was developed with mouse monoclonal antibodies that could cause undesired immune reactions in human.³⁰⁰ This technology was refined to make the proteins less immunogenic by replacing the constant region with human sequences, creating chimeric antibodies, and later by replacing all but CDRs with human sequences, creating humanized antibodies. 301,302 George P. Smith and Gregory Winter were awarded the Nobel Prize in 2018 for their pioneering work that led to the development of phage display. 301,303,304 This technology allows for the selection of fully human antibody sequences in vitro. This technique fuses large libraries of diversified antibody fragments to coat proteins of bacteriophages. This produces large libraries of bacteriophages that express diverse antibody fragments at their surface. Bacteriophages with high-affinity sequences for the antigen can be selected over multiple rounds by incubating them with immobilized target antigens. The selected sequences can then be reformatted into full-length human antibodies or other formats. If the affinity obtained is unsatisfactory, sequences can be further optimized using secondary libraries introducing variations to selected binders.³⁰⁵ The sequences produced through phage display technology are then engineered into vectors under the control of strong promoters. These vectors are often transfected in Chinese hamster ovary (CHO) cells.306 The best clones of transfected CHO cells are selected to create stable cell lines and frozen master cell banks for stable and consistent antibody production. These cells can produce large quantities of antibodies in bioreactors that can be purified through chromatography and filtration.³⁰⁷ The purified antibodies produced by this process have revolutionized the treatment of many diseases, including cancer. The technology led to the development of Humira, the first fully human monoclonal therapeutic antibody approved by the FDA for treating rheumatoid arthritis, in 2002. Since then, other technologies like yeast display, mammalian display and humanized mice have been developed, but phage display remains the most used approach to generating monoclonal antibodies. 308 Since its advent, many sequences identified through phage display have been approved. 309,310 While some exceptions exist, most of the research and the molecules that

entered the market are reformatted in fully human IgG backbones. The high stability, long half-life, ease of production, and well-established effector functions of IgG over other classes of antibodies are why they have been the first choice of most laboratories.

Recent advances in artificial intelligence (AI) have allowed the development of computational models that can guide and assist in identifying antibody sequences. In the future, AI models could replace phage displays, but now, they are primarily used in addition to experimental approaches.³¹¹

5.2.7.1 Mechanism of action of therapeutic monoclonal antibodies

When engineering a monoclonal antibody, its backbone, targeted epitope, and affinity are generally the most important characteristics that will influence its mechanism of action. As previously mentioned, monoclonal antibodies are often built on an IgG backbone, but the subclass of choice will depend on desired features. IgG1 is the most used backbone, and it is chosen for its long half-life and/or the affinity of its Fc portion for FcyR. IgG1 antibodies are usually potent activators of NK cells, phagocytosis, and the complement system. 312,313 IgG2 is rarely chosen, but its rigid structure and limited activation of the immune system make it an appealing option in some specific cases.314 IgG3 are potent activators of the complement system, but their long and flexible structure makes them relatively unstable and limits their applications.³¹⁵ IgG4 has a long half-life without binding FcγR and activating the immune system. It is the second most used IgG backbone and limits inflammation compared to IgG1.316 The targeted epitope is the second characteristic that will guide the mechanism of action of antibodies. The engineered antibodies can be used to block or activate signaling pathways. A common strategy to block a pathway is to engineer an antibody binding with high affinity to a receptor or a ligand near their binding domain to block their function. 317,318 This is the primary mechanism of action of checkpoint inhibitors such as Ipilimumab, Pembrolizumab, Nivolumab, and Atezolizumab. These molecules engage inhibitory receptors (CTLA-4 for Ipilimumab and PD-1 for Pembrolizumab and Nivolumab) or their ligand (PD-L1 for Atezolizumab) to prevent their interaction and reinvigorate immune responses in cancer.^{281–288} Monoclonal antibodies can be tuned to activate pathways on the opposite side of the spectrum. Induced clustering of target receptors through cross-linking and stabilizing receptors in their active state are some of the possible mechanisms. For example, Urelumab targets and induces clustering of the co-stimulatory receptor 4-1BB, leading to increased proliferation, survival, and effector functions of CD8+ T cells.319 The affinity of antibodies is a key feature of antibodies, and for many years, the tendency was to achieve the highest possible affinity for any target. While this approach might still be valid for blocking antibodies targeting molecules not expressed by healthy cells, the decision regarding the ideal affinity for agonistic antibodies is very likely more complex.³²⁰ Depending on the mechanism of action, aiming for more moderate affinities could prove advantageous in some cases. Therapeutic monoclonal antibodies are highly versatile structures that can be tuned and modified for different purposes.

5.2.7.2 Evolution of monoclonal antibodies

After the revolution brought about by monoclonal antibodies, the technology has been developed further. Some notable advances in the field have been the development of antibodies with modified Fc portions, antibody-drug conjugates (ADCs), and bispecific antibodies (bsAbs) (Fig. 11).³²¹

As already illustrated, the Fc portion is a key part of antibodies, and engaging the Fc receptors expressed by different cells can drive some of its functions. While the choice of IgG subclass offers some variety regarding the Fc receptor, further research into the interaction with immune cells allows us to modify this segment to fit the needs of a project.³²² Today, we can either increase the affinity for specific Fc receptors or abrogate the binding without compromising the structural integrity of antibodies.³²³ Many IgG1 today are built using specific mutations to their Fc portion to abrogate their binding to FcyR and avoid immune activation while benefitting from other advantages of the subclass.³²⁴ ADC is a class of molecules where two technologies join hands to benefit from each other's strengths. Antibodies can be engineered to have very high affinity and specificity for surface protein, but while some induce signaling directly, most rely on the immune system to clear their target. On the other hand, small molecule drugs can be highly efficacious due to their high cytotoxicity on cancer cells but highly toxic due to their non-selective effects on healthy cells.³²⁵ ADCs deliver these powerful cytotoxic molecules to their target cells by conjugating them with highly specific antibodies.³²⁶ An example is Trastuzumab emtansine (Kadcyla) where the already FDA-approved anti-HER2 Trastuzumab in conjugated with Mertansine. The FDA approved this combination in 2013 as it offered survival benefits to patients resistant to Trastuzumab alone. 327 BsAbs are another important development in monoclonal antibody technology. A portion of bsAbs in the human body assemble naturally in the extracellular space from IgG4 antibodies because of the weak interaction between their heavy chains.328 Several strategies have been adopted to produce bsAbs with higher efficiency compared to what would be possible by relying on natural assembling. Here, I will present the concept and evolution of CrossmAb technology and κλ-technology, the two strategies used in this project, but many other strategies exist. In 1983, the quadroma

technology was the first method to produce bsAbs.³²⁹ In this method, two hybridomas that produce different antibodies are fused. The fused cell would produce two heavy chains and two light chains that would randomly combine. This method was inefficient; on average, only 1/16 of the antibodies produced would be the desired bsAb. In 1996, Genentech developed Knob-into-hole (KIH). 330 This technology applies small modifications to monoclonal antibody sequences to produce bsAbs more efficiently than before. Vectors transfected into cells to produce traditional monoclonal antibodies contain the sequences for one heavy chain and one light chain that will be paired by themselves. KIH uses tetracistronic vectors (vectors designed for four genes). The innovation comes from the introduction of a bulky amino acid in the CH3 domain of one heavy chain (knob) and a few small amino acids in the CH3 domain of the other heavy chain (hole) that will favor the heterodimerization of these chains. The vector also encodes for the light chains that will pair randomly to the heavy chain, bringing the efficiency to around 25% of the antibodies produced, which is the desired bsAb. Other mutations taking advantage of the attractive forces between positively and negatively charged amino acids have also been studied.³³¹ CrossMab is a technology developed by Roche in 2010 and is an evolution of the KIH technology.³³² CrossmAb combines the mutations in the CH3 region with other asymmetric mutations that will favor the correct pairing of light chains. This is achieved by introducing paired mutations in the CH1 domain of one heavy chain and complementary mutations in the constant region of the partner light chain that will increase their affinity for each other. On the other side, the CH1 domain of the heavy chain will be replaced with the constant region of the light chain and vice versa. At the interface between the constant and variable regions, "Elbow sequences" are flexible segments added to allow more freedom for the swapped domains to fold properly and maintain the binding specificity. The yield of CrossMab is much higher than that of older methods and can reach upwards of 90%. One of the downsides of Cross-mAbs is that, while they allow for higher yields, the mutations introduced lead to sequences not naturally found in human antibodies and increase the risk of immunogenicity. κλ-bodies, the other bsAb technology used in this project, uses a different approach to increase the yield without introducing mutations to minimize immunogenicity.333 This approach uses tricistronic vectors encoding one fixed heavy chain, one κ light chain, and a second λ light chain. The heavy chain is common to both arms in this format, and the light chains drive the specificity. Once transfected with these vectors, cells produce monoclonal antibodies and about 50% of κλ-bodies. These antibodies can be purified through resins specific to the different light

chains. Both these technologies have specific advantages, and bsAbs were successfully produced and purified using both technologies in this project.

The possibility of bsAbs to engage two different epitopes has opened the doors for new opportunities and mechanisms. BsAbs against multiple antigens on target cells are used to reduce off-tumor effects. BsAbs targeting surface proteins on different cells can redirect immune cell activity. T cell engagers (TCE) bind to an antigen on target cells and a surface protein on T cells (often CD3 or CD28). This approach is promising and the FDA has approved some TCE for cancer. Bringing together different molecules allows for activating new pathways or inhibiting multiple ones concomitantly. Companies have developed monoclonal antibodies even further and merged it with other strategies or created molecules with a different structure, some of which can engage even more epitopes. 337,338

5.2.8 IL-2 targeted therapies and limitations

Despite its early approval, Proleukin has a few downsides that limit its applications in the clinic. Proleukin's antitumoral activity's primary mechanism of action is the expansion and activation of immune cells such as CD8+ T cells and NK cells. 339 The main limitations of Proleukin are linked to its toxicity and the relatively low percentages of responding patients, with objective response rates of 14% and 16% for renal cell carcinoma (RCC) and metastatic melanoma (MM), respectively. 340,341 Proleukin has a very short half-life and is given over two cycles of up to 14 doses at 600'000 IU/kg 3 times daily to treat both RCC and MM. This regimen is very inconvenient for patients, and the high doses injected lead to strong systemic activation, resulting in severe toxicities and, sometimes, death. 42 Patients undergoing Proleukin treatment can develop Vascular leak syndrome (VLS), hypotension, pulmonary edema, renal failure, diarrhea, and others. Another problem stems from the different sensitivity of different cell lines to the cytokine. Tregs, the only immune cell population expressing CD25 constitutively, are the most sensitive cells to IL-2. High doses can sometimes overcome the superior sensitivity, but in Treg-rich TMEs, it is not necessarily enough to tilt the balance.

Over the years, laboratories have designed different strategies to safely harness the potential of IL-2 activation in cancer and reduce activation of Tregs. This section is not an exhaustive compendium of all IL-2 targeting drugs developed but aims to showcase a few molecules from the diverse repertoire of strategies. IL-2 targeting molecules can be divided between (i) molecules that engage the native receptor similarly to IL2 (unbiased IL-2

strategies), (ii) molecules that decrease or abrogate binding to CD25 (not-alpha strategies), and (iii) molecules that modify the affinity to the other IL-2R subunits.

(i) Unbiased IL-2 strategies

Polyethylene glycol IL-2 (PEG-IL-2). Recombinant native IL-2 was conjugated to several PEG molecules to increase the half-life.³⁴³ This molecule has a half-life 10-20 times longer than Proleukin and showed promising results in mice. The molecule was evaluated in clinical trials but didn't go past phase I. One trial showed similar toxicity to high-dose IL-2. Another trial evaluated PEG-IL-2 in combination with IL-2 and did not show an improvement in antitumor activity compared to IL2 alone.³⁴⁴

APN-301 is obtained by fusing WT IL-2 at the C terminus of anti-GD2 antibodies. GD2 is present at the membrane of some tumor cells and is used to guide WT IL-2 to the tumors. Phase I and II clinical trials showed similar anti-tumor activity and toxicity to Proleukin and suspended development.^{345,346}

WTX-124 consists of a WT IL-2 fused through cleavable linkers to a domain that prevents IL-2 engagement on its receptor and a second domain that extends its half-life. The linkers used are cleaved by proteases that are preferentially expressed within tumors. In mouse models, the molecule showed significant anti-tumor activity that was not observed with uncleavable linkers. Preclinical data also suggested that WTX-124 has a larger therapeutic window compared to IL-2 and leads to a higher CD8+T cell/Treg ratio. WTX-124 is still undergoing phase I clinical trials as a monotherapy and in combination with pembrolizumab. Preliminary data from the WTX-124 trial as monotherapy suggests a favorable safety profile with signs of antitumoral activity. In the second domain that extends its preference in the work of the second domain that extends its preference in the second domain that extends its preference in the second domain that extends its preference in the work of the w

(ii) Not-alpha strategies

Bempegaldesleukin is a recombinant IL-2 conjugated with 6 PEG chains. The chains are strategically placed to block binding to CD25 and reduce activation of Tregs. Bempegaldesleukin is injected as a prodrug with reduced activity and becomes fully active over time when the PEG chains are released. Preclinical data was very promising, and preferential activation of NK cells and CD8⁺ T cells compared to Tregs was reported.³⁴⁹ Early clinical trials suggested a relatively safe profile and hopeful signs of activity when combined with checkpoint inhibitors.³⁵⁰ Controversially, in phase III clinical trials, Bempegaldesleukin did not meet satisfactory antitumor activity and safety profiles and was discontinued.³⁵¹

Nevamleukin is an engineered IL-2 fused with CD25 to block binding to trimeric IL-2 receptors on cells and extend the half-life. Nevamleukin was tolerated and showed encouraging antitumor activity in early trials. It is currently in a phase III trial in combination with Pembrolizumab and is being compared to chemotherapy in platinum-resistant ovarian cancer, making it the most clinically advanced IL-2 targeting cancer immunotherapy. Encouragingly, reports from several of these trials also showed the expansion of NK and CD8+ T cells in patients.

Roche has developed RO7284755 based on Cergutuzumab amunaleukin and Simlukafusp alfa, two older IL-2 targeting molecules from their portfolio. They used the same not-alpha IL-2 variant from these molecules and fused it with an anti-PD-1 blocking antibody. In preclinical data, they demonstrated superior antitumor activity compared to their previous molecules. Their data shows that the PD-1 antibody drives preferential activation of memory CD8+T cell subsets. This molecule is currently in phase I clinical trial as monotherapy and combined with Atezolizumab. The previous molecules amonotherapy and combined with Atezolizumab.

(iii) CD122/CD132 biased IL-2

MDNA11 is a mutated IL-2 with an increased affinity for CD122 and no engagement of CD25, and is fused to albumin to increase its half-life. Preclinical data showed superior CD8⁺ T cells and NK cell activation compared to IL-2.³⁵⁹ The molecule is being evaluated in a phase I/II clinical trial that is still recruiting.³⁶⁰

The strategies presented here use a variety of approaches to overcome the limitations of Proleukin. Most strategies manage to increase the limited half-life. To activate CD8+ T cells and NK cells while limiting the activation of the immunoregulatory Tregs, the most popular strategy adopted by laboratories is to modify the affinity of their drug for the subunits of the IL-2 receptor. Most drugs in this class have reduced binding affinity to CD25 as the subunit is constitutively expressed only by Tregs. MDNA11 adopted a different strategy and aims to promote antitumoral immune responses with an increased binding affinity to CD122, which is expressed at higher levels in CD8+ T cells. 159,160,361 A few strategies are also attempting to limit peripheral activation. Two examples are WTX-124 and RO7284755. While the cleavable linkers of WTX-124 are preferentially expressed within tumors, molecules with cleavable linkers that have entered the clinic are known to be partially cleaved in the serum. RO7284755 uses an anti-PD-1 antibody to preferentially direct the activity of its IL-2 variant to tumor-specific T cells. This strategy can potentially reduce

toxicity but cannot entirely avoid the activation of peripheral cells. The data presented regarding many IL-2 targeting drugs is very promising, but an approach with the potential to overcome all the limitations of Proleukin is still missing.

IL-2 is also being studied in combination with ACT, as its addition can extend the survival of the injected cells. Interestingly, pairs of mutated IL-2 and IL-2R (called orthogonal IL-2/IL-2R) that interact with each other but not with the WT cytokine and receptor have been developed. Studies evaluate the use of these orthogonal pairs as an alternative to supplementing WT cytokines to reduce toxicity. One of these pairs is being evaluated for non-renal systemic lupus erythematosus and lupus nephritis. 363

5.2.9 IL-15 targeted therapies and limitations

IL-15 has been an attractive cytokine for cancer immunotherapies for several reasons. Its importance for NK cells, CD8+T cells, and the memory compartment of T cells, combined with the lack of preferential activation of the immunoregulatory Tregs observed for IL-2, attracted interest from multiple laboratories. The development of IL-15 targeting therapies is complicated as the cytokine and signaling pathway have some limitations, the main one being its short half-life. In 2024, N-803 was evaluated in combination with Bacillus Calmette-Guérin (BCG) in bladder cancer and became the first approved IL-15 targeting drug. N-803 results from the fusion of an IL-15Rα sushi domain with the Fc domain of an IgG1 and an IL-15 mutein with increased binding to CD122. The IL-15Rα sushi domain mimics cross-presentation, and the Fc domain increases the half-life and allows dimerization. The superagonist is injected directly inside the bladder, which allows for avoiding toxicity.

Clinical trials of other IL-15-targeting drugs are ongoing, and some have already been discontinued. While IL-15 targeting strategies are less diverse, NKTR-255 is a recombinant IL-15 conjugated with PEG molecules that don't impair activity but extend the half-life. Preclinical data demonstrated superior antitumor activity compared to native recombinant IL-15.³⁶⁵ NKTR-255 is currently being studied in phase I and II clinical trials combined with checkpoint inhibitors and ACT.³⁶⁶

A few other molecules are currently being studied, but most rely on similar mechanisms as N-803, as the majority are fusion proteins or complexes with domains or proteins mimicking IL-15R α and extending the drug's half-life. Similarly to IL-2, IL-15 is also being used in combination with ACT, as IL-15 can extend the survival of the injected cells.³⁶⁷

Both IL-2 and IL-15 targeting drugs have demonstrated impressive activity in preclinical models. No IL-2 targeting therapy since the approval of Proleukin has managed to get FDA

approval for cancer. N-803, an IL-15 targeting superkine, was approved 2024 to treat bladder cancer. While both pathways have great potential to be applied to broader cancer applications, a method capable of harnessing their potential while overcoming their limitations is still missing.

6 Aims

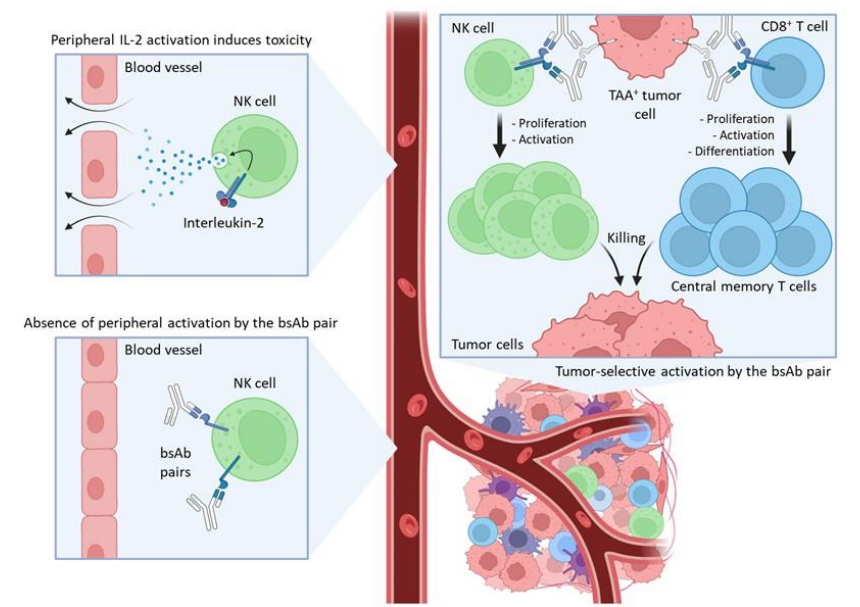
The goal of my thesis is to demonstrate that the IL-2/IL-15 pathway can be activated selectively within tumors through pairs of bsAbs. The thesis involves using a first bsAb that targets CD122 and a TAA, and a second bsAb that targets CD132 and the same or a different TAA. This broad goal can be divided into several more tangible aims:

- Engineer and produce the pairs of bsAbs: the aim is to produce pairs of bsAbs. Sequences of described antibodies are cloned into crossmAb backbones to create bispecific antibodies. Antibodies developed by phage display are combined into κλbodies. Antibodies are produced and purified, and their binding is verified.
- 2. **Demonstrate the selective activity of pairs of bsAbs:** the goal is to evaluate the TAA-dependent agonistic activity of pairs of bsAbs. This involves investigating the effect of pairs of bsAbs on IL-2/IL-15 signaling with or without TAA and their ability to favor the killing of TAA+ tumor cells.
- 3. **Evaluate the effect of bsAbs:** the thesis aims to establish a relevant mouse tumor model to analyze the effect of pairs of bsAbs on the tumor microenvironment and peripheral tissues with a focus on T and NK cells.
- 4. **Evaluate the safety profile of pairs of bsAbs:** the study aims to compare the safety profile of pairs of bsAbs with Proleukin in mice. The goal is to evaluate the tolerability of bsAbs through clinical signs and systemic signs of immune activation.
- 5. Evaluate antitumor activity of pairs of bsAbs with checkpoint inhibitors: the thesis aims to evaluate the effect of pairs of bsAbs combined with checkpoint inhibitors in mice. This includes following tumor growth and dissecting the tumor microenvironment.

7 Results

The original Manuscript for this thesis was submitted in September 2024 to the Journal for ImmunoTherapy of cancer (JITC). The current version of the manuscript included here was modified to meet the reviewers' expectations and was resubmitted to JITC in February 2025. This manuscript embodies the core of my PhD thesis. I was involved in all experiments presented in this manuscript and had a leading role in all experiments using HER2-targeting bsAb pairs. I analyzed the data, created the graphs of the *in vitro* section of the article and I was involved in the analysis and in the interpretation of the rest of the article. I performed experiments involving primary human NK cells and bsAb combinations targeting different TAAs that were asked during the revision of the manuscript. I wrote the initial manuscript draft with Eric Hatterer and Limin Shang, with whom I also collaborated to review the manuscript and to write the rebuttal letter to the reviewers.

Selective activation of interleukin-2/interleukin-15 receptor signaling in tumor microenvironment using paired bispecific antibodies



Authors

Julien Montorfani*, Eric Hatterer*, Laurence Chatel, Adeline Lesnier, Alizee Viandier, Bruno Daubeuf, Lise Nouveau, Pauline Malinge, Sebastien Calloud, Krzysztof Masternak, Walter Ferlin, Nicolas Fischer, Camilla Jandus and Limin Shang

*equal contribution

Correspondence

limin.shang@lightchainbio.com

In Brief

- bsAb pairs induce TAA-dependent activation and proliferation of NK, CD8* T, and central memory CD8* T cells
- bsAb pairs avoid peripheral activation and toxicities associated with systemic interleukin-2 activation
- bsAb pairs synergize with anti-mPD1, resulting in better tumor growth control

Selective activation of interleukin-2/interleukin-15 receptor signaling in tumor microenvironment using paired bispecific antibodies

Julien Montorfani^{1,2*}, Eric Hatterer^{1*}, Laurence Chatel¹, Adeline Lesnier¹, Alizee Viandier¹, Bruno Daubeuf¹, Lise Nouveau¹, Pauline Malinge¹, Sebastien Calloud¹, Krzysztof Masternak¹, Walter Ferlin¹, Nicolas Fischer¹, Camilla Jandus^{2, 3, 4, 5} and Limin Shang¹

¹Light Chain Bioscience - Novimmune S.A, Geneva, Switzerland

²Université de Genève – Département de Pathologie et Immunologie, Geneva, Switzerland

³Ludwig Institute for Cancer Research, Lausanne Branch, Lausanne, Switzerland

⁴Geneva Center for Inflammation Research (GCIR), Geneva, Switzerland

⁵Translational Research Centre in Onco-Hematology (CRTOH), Geneva, Switzerland

*Equal contribution

Correspondence to Dr. Limin Shang: limin.shang@lightchainbio.com

ABSTRACT

Background: Owing to their roles in promoting T cell and Natural Killer (NK) cell activation and proliferation, interleukins-2 (IL-2) and -15 (IL-15) have been pursued as promising pathways to target in cancer immunotherapy. Nonetheless, their wider therapeutic application has been hampered by severe dose-limiting toxicities including systemic cytokine release and organ edema for IL-2, and inconvenient intra-tumoral administration for IL-15. To address these safety issues, we generated IL-2R/IL-15RxTAA (Tumor associated antigen) bispecific antibody (bsAb) pairs to selectively activate IL-2R signaling in the tumor microenvironment.

Methods: Each bsAb pair is composed of one bsAb targeting CD122 and a TAA epitope, and the other bsAb targeting CD132 and the same or a different TAA epitope. *In vitro* assays were performed to characterize the IL-2R/IL-15R agonistic activity of the bsAb pairs, as well as their capacity to enhance T-cell mediated killing of TAA+ malignant cells. Using a syngeneic mouse tumor model, *in vivo* biological activity and systemic toxicity of the bsAb pairs were assessed in comparison with IL-2. The *in vivo* anti-tumor activity was assessed in combination with an anti-mPD-1 monoclonal antibody.

Results: We demonstrated with two different TAAs (human epidermal growth factor receptor 2 (HER2) and mesothelin (MSLN)) that the CD122xTAA/CD132xTAA bsAb pairs mediate effective activation of immune cells exclusively in the presence of TAA+ tumor cells. In syngeneic hMSLN-MC38 tumor-bearing mice, the CD122xMSLN-1/CD132xMSLN-2 bsAb pair promotes selective activation and expansion of NK cells and central memory CD8+ T cells inside the tumor without inducing organ edema or systemic cytokine release, two well-known manifestations of IL-2 associated toxicity. In combination with checkpoint inhibitor anti-mPD-1, the bsAb pair boosts the accumulation of CD8+ effector T cells and NK cells, leading to a favorable CD8+ T cell to CD4+ regulatory T cell (Treg) ratio for a more robust inhibition of tumor growth.

Conclusions: Overall, the findings suggest that this innovative therapeutic approach effectively leverages the anti-tumor activity of IL-2 and IL-15 pathways while minimizing their associated systemic toxicities. This dual bsAb format holds potential for broader application in other immune-activating pathways.

Key messages

What is already known on this topic – IL-2 and IL-15 agonists have been approved as cancer therapies. However, their clinical application has been impeded by systemic toxicities.

What this study adds — We demonstrated that IL-2/IL-15R signaling can be selectively activated within the tumor, thereby minimizing associated systemic toxicities, by utilizing a bsAb pair consisting of CD122xTAA and CD132xTAA bsAbs.

How this study might affect research, practice or policy – This strategy could pave the way for safer anti-tumor therapies targeting immune-activating cytokines.

INTRODUCTION

IL-2 and IL-15 are two closely related T cell- and NK cell-stimulating cytokines that share two signaling receptor subunits, IL-2/IL-15 receptor beta (IL-2Rβ, IL-15Rβ, also known as CD122) and IL-2/IL-15 receptor gamma (the common gamma chain or CD132). Each of the two cytokines has a specific receptor subunit (IL-2Rα/CD25 for IL-2, IL-15Rα/CD215 for IL-15), which enhances the binding affinity of the cytokines to the signal transduction receptor subunits [1]. Owing to their role in promoting T cell and NK cell activation and proliferation, IL-2 and IL-15 have been pursued as promising therapeutic targets in cancer immunotherapy [2]. High dose of recombinant human IL-2 (hIL-2/Proleukin) has been approved for the treatment of metastatic renal cell carcinoma and metastatic melanoma. However, severe toxic effects due to systemic activation, the most severe being vascular leaking syndrome (VLS), culminating in multi-organ edema and damage, have limited its clinical use [3,4]. Another complication with IL-2, which is not a concern for IL-15, is that high affinity trimeric IL-2R (comprising CD25, CD122 and CD132) is constitutively expressed on Tregs. A low dose of IL-2 preferentially stimulates Tregs and suppresses immune response. Thus, high dose of IL-2 is required to stimulate immune activation, which also increases the risk of toxicity.

Both direct activation of high affinity IL-2 trimeric receptor on endothelial cells and natural killer (NK) cell-mediated cytokine release have been shown to be involved in IL-2-induced systemic toxicity [5,6]. To mitigate endothelial cell-mediated toxicity and Treg activation, one approach is to

reduce IL-2 binding to IL-2Rα, which is expressed on endothelial cells and renders them highly sensitive to IL-2. This so-called "not-alpha" strategy can be achieved by different approaches [7-13]. However, a pegylated IL-2, NKTR-214, although achieving favorable CD8⁺ T cell/Treg ratio, showed comparable toxicity to non-modified IL-2 (Proleukin), which limited its dose escalation [3], suggesting that not-alpha strategy alone may not be enough to mitigate IL-2-associated toxicity in patients. As NK cells constitutively express only the intermediate-affinity IL-2 dimeric receptor composed of CD122 and CD132, efforts have been made to develop IL-2 variants with reduced binding to CD122 to mitigate NK-mediated toxicity. Unfortunately, one such molecule, BAY50-4798, showed similar toxicity profile to that of non-modified IL-2, suggesting that reducing NK cell activation may also not be sufficient to mitigate IL-2-associated toxicity [14].

Considering that reducing systemic activation of endothelial cells or NK cells appears insufficient to mitigate IL-2-associated toxicity, further avoidance of systemic IL-2 activation may be required to achieve this goal. Various approaches have been explored to guide IL-2 activation specifically in the tumor microenvironment (TME). A potential strategy involves engineering pro-IL-2 with an attached masking element to prevent systemic activation [15,16]. However, while cleavage of the mask occurs more in tumors, the cleavage has been observed in human serum, and cleaved IL-2 has been detected in the blood of treated mice [15,17]. IL-2-linked to a tumor targeting antibody is also used to guide IL-2 activation preferentially in the TME [18-20]. As the IL-2 part of the molecule is not masked, the molecule is still active systemically. A further development of this strategy is to split an IL-2-mimetic molecule into two separate fragments. Each fragment is linked to a separate anti-TAA antibody. Upon binding of the two IL-2-mimetic fragment-anti-TAA conjugates to TAA on tumor cells, the two fragments of the IL-2-mimetic will be brought into proximity and induce receptor activation [21]. However, the two fragments of the IL-2-mimetic could bind to each other in the absence of TAA and potentially cause systemic activation.

We present a novel strategy for selectively activating IL-2/IL-15 receptors within the TME using a pair of bsAbs. One bsAb has an arm that binds to CD122, while the other targets a TAA. The second bsAb binds to CD132 on one arm and either the same TAA-epitope or an alternate TAA-epitope (Figure 1A). In circulation, these bsAbs cannot activate the CD122/CD132 receptor because TAAs are not expressed outside the tumor. However, within the tumor, binding to the TAA brings the two bsAbs into proximity, allowing their CD122 and CD132 binding arms to engage receptors on tumor-infiltrating T cells or NK cells, triggering receptor activation. Our findings from mouse models highlight the TME-specific activity and improved safety profile of this innovative approach.

METHODS

Reagents and cell lines

The reagents and cell lines used in this study were listed in the online Supplemental Tables 1-2.

IL-2 reporter cell assay

Reporter cell assays were performed using HEK-Blue IL-2 and/or HEK-Blue CD122 / CD132 following the manufacturer's recommendation with bsAb combinations added onto 50000 reporter cells and 150000 TAA-coated streptavidin microspheres or 150'000 NCI-N87 cells. Absorbance at 640 nm was acquired using a SpectraMax-i3x (Molecular Devices).

Characterization of pSTAT5 induction

In 96-well plates, NK-92 cells, PBMCs or purified human NK cells were stained with Fixable Viability Dye eFluor 506, washed and incubated with Fc Block. NK-92 and primary human NK cells were stained with anti-CD45 antibody while PBMCs cells were stained with anti-CD3, -CD45, -CD4, -CD8, -CD14, -CD19, and-CD56 antibodies. Cells were incubated with Proleukin or with TAA-expressing tumor cells and bsAbs at 37°C for 30 min. Cells were fixed, washed and permeabilized.

NK-92 and primary human NK cells were stained with an anti-pStat5 antibody while PBMCs were stained with an anti-pStat5 and an anti-Foxp3 antibodies (antibodies are listed in Supplemental Table 3).

TDCC and ADCC assays

1.5 million PBMCs were incubated with 1.5 million target tumor cells and a suboptimal dose of H4G5-Trastuzumab for 72 h in 6-well plates. PBMCs were distributed in 96-well plates with fresh target tumor cells (effector:target ratio 10:1) and bsAbs or Proleukin for 72 h. 200'000 isolated NK cells were incubated with 10'000 NCI-N87 cells overnight at 37°C in presence of 30 nM CD122xMSLN-1/CD132xMSLN-2 bsAb pair in 96-well plates. A suboptimal dose of Trastuzumab is added and plates are incubated for 6 h at 37°C. After incubation, specific killing was measured with CellTiter-Glo® Luminescent Cell Viability Assay following manufacturer's recommendations (Specific lysis = 100-[(100xSample mean)/Effector&Target mean]).

Tumor Model in vivo

Female hCD122 / hCD132 KI mice (Biocytogen, 6-8 weeks old) with established hMSLN-MC38 tumors were treated in a Specific Pathogen-Free room of the animal facility with vehicle (PBS), Proleukin or CD122xMSLN-1/CD132xMSLN-2 bsAb pair. Proleukin was dosed intraperitoneally (i.p.) at 3 mg/kg daily for 5 consecutive days; bsAb combination was dosed intravenously (i.v.) at 10 mg/kg twice weekly for 1 week. All treated animals were included in analysis. To analyze the TME, tumors were harvested 5 days after treatment initiation for analysis by flow cytometry. Tumors, spleens and lungs were analyzed for immune cell infiltration and phenotype (antibodies listed in Supplemental Table 4). Separately, to evaluate tumor growth control, hMSLN-MC38 tumor bearing mice were treated intravenously twice weekly for 2 weeks with vehicle (PBS), anti-mPD-1 (5 mg/kg), CD122xMSLN-1/CD132xMSLN-2 bsAb pair (10 mg/kg) or

both anti-mPD-1 and bsAb combination. To analyze the TME, tumors were harvested 9 days after treatment started for analysis by flow cytometry. For both experiments, tumor sizes were measured 3x/week using a caliper (Tumor volume [mm³] = Length x Width² x 0.5 and % of Tumor growth inhibition (at time = t) = {1-[(mean Tumor volume (t)-mean initial tumor volume)/(mean control tumor volume (t)-mean initial control tumor volume)]x100). To compare the probability of survival between treatment groups, Kaplan-Meier survival curves were generated. Mice with tumors > 1500 mm³ were euthanized.

IL-2-induced Toxicity in vivo

hCD122 / hCD132 KI mice engrafted with hMSLN-MC38 tumors, received vehicle (PBS), Proleukin (5 mg/kg daily i.v. for 5 days) or bsAb combination (10 mg/kg biweekly i.v. for 1 week). Body weight was measured 3x/week. On sacrifice day, lungs and spleens were weighed and processed for immune profiling via flow cytometry. TNF- α and IFN- γ levels in the serum were determined using MSD kits following manufacturer's instruction.

Human whole blood cytokine release assay

Cytokine secretion was detected using fresh human whole blood collected from healthy individuals (with Heparin-Lithium). 20X concentrated test articles were added to each well of a sterile 96-well round bottom plate: Cetuximab (negative control, 300 nM), Proleukin (1000 nM), and CD122xMSLN-1/CD132xMSLN-2 bsAb pairs (300 nM each). Fresh human whole blood was incubated with test articles at 37°C overnight. Samples were centrifuged and plasma was transferred to a 96-well microplate and kept frozen (-80°C) until MSD analysis of TNF- α and IL-6 levels.

Tissues immune profiling via flow cytometry

Single cell suspensions were stained for viability, washed with staining buffer and incubated with purified rat anti-mouse CD16/CD32. Fluorescent-conjugated antibody mix (extracellular markers - Supplemental Table 4) was added to the cell suspension. For bsAb tissue distribution anti-human Fc were used (Supplemental Table 4). If no intracellular staining was needed, stained cells were washed and fixed. For intracellular staining, samples were stimulated with PMA/ionomycin for 4 h, washed with staining buffer, fixed and permeabilized (Supplemental Table 4). Cells were incubated first with rat anti-mouse CD16/CD32 and, later, with antibody mix (intracellular staining-Supplemental Table 4).

Statistics

Statistical analyses were performed using GraphPad Prism Software, version 10. Differences between multiple groups were determined using a one-way analysis of variance (ANOVA) with multiple comparison test. P values are the following * = P < 0.05; ** = P < 0.01; **** = P < 0.001. Statistical difference between survival curves was calculated using the log-rank (Mantel-Cox) test with the Bonferroni correction comparison.

RESULTS

CD122/CD132xTAA bsAb pairs induce IL-2/IL-15 signaling in reporter cells

We hypothesize that, in the presence of TAA-expressing cells, a bsAb pair of CD122xTAA and CD132xTAA could bring CD122 and CD132 into proximity on immune cells and induce CD122/CD132 dimeric receptor signaling by trans-engaging TAAs on tumor cells (Figure 1A). To this end, we generated bsAbs, with one arm targeting either human CD122 or human CD132 and the other arm targeting distinct epitopes on human HER2, referred to as HER2-1 and HER2-2 or MSLN, referred to as MSLN-1 and MSLN-2, using antibody arms pre-existing or generated *in house* with phage display (Supplemental Figure S1A-C). In the presence of HER2-coated microspheres to mimic HER2-

expressing cancer cells, CD122xHER2-1/CD132xHER2-2 bsAb pair, but not an individual bsAb, activated IL-2/IL-15 signaling in reporter cells to a level similar to that induced by recombinant human IL-2 (rhIL-2) (Figure 1B). Importantly, the activation is reliant on TAA as the bsAb pair did not activate cells when combined with irrelevant TAA-coated microspheres (Figure 1B). IL-2R agonistic activity was confirmed using HER2+ NCI-N87 cells instead of HER2-coated beads (Figure 1C). The approach is not limited to HER2 since the CD122xMSLN-1/CD132xMSLN-2 bsAb pair, but not an individual bsAb, also activated reporter cells in the presence of MSLN-coated microspheres (Figure 1D). When testing bsAb pairs targeting different MSLN epitopes, different reporter activation profiles were observed with bsAb pairs targeting different TAA epitope combinations (Figure 1E and Supplemental Figure S2A). The CD122xMSLN-1/CD132xMSLN-2 pair, with MSLN-1 arm targeting a membrane-proximal epitope and MSLN-2 arm targeting a membrane-distal one, showed the highest potential to induce reporter cell activation and thus was selected for further study. A similar epitope-dependent phenomenon was also observed with HER2-targeting bsAb pairs (Supplemental Figure S2B). We also evaluated bsAb pairs targeting the same TAA epitope and demonstrated that this approach can activate signaling for both MSLN- and HER2-targeting bsAbs. While there was some loss of potency when targeting the same epitope for MSLN, this reduction was not observed for HER2 (Figure 1F and Supplemental Figure S2C). Altogether, we demonstrated with two different TAAs that IL-2/IL-15 signaling can be activated through combinations of bsAbs that bring CD122 and CD132 into proximity in a TAA-dependent manner.

CD122/CD132xTAA bsAb pairs induce STAT5 phosphorylation in NK cell line and human peripheral blood mononuclear cells (PBMCs)

In a more physiologically relevant system, we tested the concept with the human NK cell line, NK-92 cells, in the presence of cancer cells expressing different levels of target TAAs. IL-2/IL-15 signaling was evaluated by measuring the level of phosphorylated STAT5 (pSTAT5), a transcription

factor downstream of the IL-2/IL-15 R signaling. The CD122/CD132xHER2 bsAb pair induced substantial increase of pSTAT5 in presence of NCI-N87 cells, the tested tumor cell line with ~400k HER2/cell, while it induced a lower level of pSTAT5 in presence of JIMT-1 cells, a cell line with ~69k HER2/cell. When incubated with MC38-hHER2, an engineered cell line with ~44k HER2/cell, we observed only marginal levels of pSTAT5 (Figure 2A, left panel, Supplemental Table 2). The TAA-density-dependent pSTAT5 increase was also observed with the MSLN-targeting bsAb pair, with the difference that the MSLN bsAb pair was more potent at inducing pSTAT5 towards cell lines expressing lower levels of MSLN compared to the HER2 counterparts (Figure 2A, Supplemental Table 2). As shown in Figure 2A, although JIMT-1 cells express a lower level of MSLN than HER2 (9k MSLN/cell vs 69k HER2/cell), HER2 bsAb pair and MSLN bsAb pair stimulated similar profiles of pSTAT5 in NK-92 when combined with this cell line.

As T cells play a pivotal role in IL-2-mediated anti-tumor activity [22], we tested whether the CD122/132xMSLN bsAb pair could stimulate primary T cells from human PBMCs in the presence of NCI-N87 cells. In contrast to rhIL-2, which stimulated IL-2Rα-positive Tregs at lower concentrations than those required to stimulate IL-2Rα-negative CD8⁺ T cells (Figure 2B, left panel), the CD122xMSLN-1/CD132xMSLN-2 combination led to very similar activation of Tregs and CD8⁺ T cells (Figure 2B, right panel), as expected for a not-alpha strategy of IL-2 activation.

CD122/CD132xTAA bsAb pairs induce TAA-dependent killing of cancer cells in vitro

IL-2/IL-15 signaling plays a supportive role in TCR-mediated antigen-specific target cell killing but are not expected to induce non-activated T cells to kill tumor cells alone. To assess the tumoricidal potential of our bsAb pairs, we preactivated human PBMCs for 3 days using NCI-N87 cells and H4G5xTrastuzumab, a T-cell engager that binds to CD3 and HER2. These preactivated PBMCs were then used to evaluate the specific killing of MSLN-expressing cancer cells, induced by the CD122xMSLN-1/CD132xMSLN-2 bsAb pair. As a positive control, Proleukin induced killing by

preactivated PBMCs of all tested cancer cell lines, including MSLN-negative MDA-MB-468 and SH-SY5Y cells (Figure 2C & Supplemental Figure S3A-D). In contrast, the CD122xMSLN-1/CD132xMSLN-2 bsAb pair only induced killing of the MSLN-positive cell lines, with significant killing of MSLN-high NCI-N87 cells (~20k MSLN/cell) as well as HPAC cells (~14k MSLN/cell), and detectable but not significant killing of MSLN-low JIMT-1 cells (~9k MSLN/cell) (Figure 2C & Supplemental Figure S3B-D). Killing of MSLN-negative cells, MDA-MB-468 and SH-SY5Y, was not induced by the bsAb pair. Complementary experiments were also conducted using human primary NK cells. The overnight incubation of NK cells with CD122xMSLN-1/CD132xMSLN-2 bsAb pair and NCI-N87 cells enhanced NK-mediated antibody-dependent cellular cytotoxicity (ADCC) of NCI-N87 cells induced by the Fcactive anti-HER2 antibody Trastuzumab (Figure 2D). The increased killing correlates with a detectable, although variable, increase in pSTAT5 in primary NK cells when co-cultured with MSLNpositive NCI-N87 cells in the presence of the CD122xMSLN-1/CD132xMSLN-2 bsAb pair (Supplemental Figure S3E). Altogether, we showed that our bsAbs induced killing of tumor cells by pre-activated T cells and NK cells in a TAA-dependent manner. The reliance on signal 1 prestimulation or the presence of Fc-active TAA antibody and TAA expression by target tumor cells supports the superior safety profile of this novel approach.

TAA-dependent tumor engagement of CD122/CD132xTAA bsAb pairs induces robust accumulation and activation of tumor-infiltrating CD8⁺ T cells and NK cells

To evaluate the *in vivo* activity of the CD122/CD132xTAA bsAb pairs, we tested the CD122xMSLN-1/CD132xMSLN-2 bsAb pair in a syngeneic and fully immunocompetent mouse model. As the targeting arms of the bsAb pair are not mouse cross-reactive (Supplemental Figure S1C), hCD122/hCD132 transgenic mice (Tg-mice) were engrafted subcutaneously with hMSLN-expressing MC38 colon cancer cells (Figure 3A). Tumor immunophenotyping by flow cytometry at day 5 post treatment initiation showed that the CD122/CD132xMSLN bsAb pair enhanced CD45⁺

leukocyte infiltration and significantly increased the number of infiltrating CD8+ tumor-infiltrating T lymphocytes (TILs) (Figure 3B, Supplemental Figure S4). A non-significant increase of CD8⁺ TILs was observed in Proleukin-treated mice (Figure 3B). The reported low expression of CD122/CD132 on CD4⁺ T cells [23] may account for the observed only marginal effect on CD4⁺ TILs as reported by other not-alpha strategies [24,25]. Importantly, while Proleukin had no effect, the bsAb pair drastically increased the proportion of central memory CD8+ TILs (CD44+ CD62L+) (Figure 3C) and enhanced significantly CD8+ TILs proliferation (measured by Ki67) (Figure 3D). However, Q-PCR analysis demonstrated that the bsAb pair did not increase intra-tumoral proinflammatory cytokines (IFN- γ , IL-6, and TNF- α) 5 days post treatment initiation (Supplemental Figure S5). The number, proliferation and cytotoxic potential of tumor-infiltrating NK cells were also significantly increased by the bsAb pair (Figure 3E). The CD122/CD132xMSLN bsAb pair did not alter the Treg population within the tumor or the spleen. In contrast, Proleukin decreased intra-tumoral Tregs, likely through their redistribution to the spleen (Supplemental Figure S6A). In another set of experiments, we compared two bsAb pairs with high or medium affinity for CD122 and CD132 (referred to CD122-H/CD132-H versus CD122-M/CD132-M, Supplemental Figure S1). In vitro tests revealed greater IL-2R agonistic potency for the high-affinity pair compared to the medium-affinity pair (Supplemental Figure S6B). Interestingly, the medium affinity CD122/CD132 arms increased the intra-tumoral NK cell infiltration more substantially compared to the higher affinity CD122/CD132 arms (Supplemental Figure S6C), likely due to less binding to CD122⁺ and/or CD132⁺ immune cells in circulation leading to better tumor infiltration by the medium affinity bsAb pair. The high and medium affinity bsAb pairs induced similar levels of central memory CD8⁺ T cells (Supplemental Figure S6D). As such, the next experiments were performed using the bsAb pair carrying the medium affinity CD122/CD132 binding arms.

To confirm that the CD122/CD132xMSLN bsAb pair-induced TME modulation is TAA-dependent, we compared it with a bsAb pair targeting an irrelevant TAA (CD122xirrel-1/CD132xirrel-2). Flow cytometry analysis demonstrated that the CD122/CD132xMSLN bsAbs accumulated on the cancer cell surface (gated as CD45⁻ cells) in hMSLN-expressing MC38 tumors of mice treated with CD122/CD132xMSLN bsAb pair, whereas no human antibody binding to the cancer cells was detected in tumors of mice treated with the CD122xirrel-1/CD132xirrel-2 bsAb pair (Figure 3F). As expected, CD122/CD132xMSLN bsAb pair but not CD122xirrel-1/CD132xirrel-2 bsAb pair increased infiltration of NK cells and T cell subpopulations into the TME (Figure 3G and Supplemental Figure S6E). In summary, these data demonstrate that combining CD122/CD132xTAA bsAbs increases the numbers of CD8⁺ TILs similarly to Proleukin. In contrast to Proleukin, the bsAb pair also increases the number of tumor-infiltrating central memory CD8⁺ T and NK cells as well as enhancing NK cell activation in a TAA-dependent manner.

Improved safety profile of the CD122/CD132xTAA bsAb pair relative to Proleukin

To test whether the targeted activation of immune cells with the CD122/CD132xTAA bsAb pairs could avoid the adverse effects associated with high-dose Proleukin, hMSLN-MC38 tumor-bearing Tg-mice were dosed with either Proleukin or the CD122xMSLN-1/CD132xMSLN-2 bsAb pair and mouse body weights were monitored. After 5 consecutive daily injections of Proleukin, significant body weight loss was observed and mice showed reduced activity as well as piloerection. In contrast, mice treated with CD122/CD132xMSLN bsAb pair did not lose body weight (Figure 4A, supplemental Figure S7A) nor display any clinical signs of toxicity. Monitoring body weight over an extended period in a separate experiment did not reveal any weight loss, further supporting the safety profile of the bsAb pair (Supplemental Figure S7B). Proleukin treatment also increased spleen and lung weights (Figures 4B-C), two common manifestations of IL-2-induced organ edema. In contrast, no change in spleen or lung weight was observed in mice treated with the

CD122/CD132xMSLN bsAb pair (Figures 4B-C). Furthermore, Proleukin induced a significant upregulation of serum TNF-α and IFN-y while the CD122/CD132xMSLN bsAb pair did not stimulate cytokine release in tumor-bearing mice (Figures 4D-E). In agreement with these observations, Proleukin injection resulted in increased numbers of CD45⁺, CD3⁺ and CD8⁺ T cells and effector CD8⁺ T cells (CD44+ CD62L-) in the lungs relative to vehicle group. Albeit to a lower level, the same cellular change was observed in the spleen as well. In contrast, most of these immune cell subpopulations were not altered by the CD122/CD132xMSLN bsAb pair treatment, with the exception of a significant increase of the NK cells in both lung and spleen (Supplemental Figures S8A-B), which may be attributed to immune cell recirculation from the tumor. The presence of soluble MSLN (sMSLN) detectable in the blood of tumor-engrafted mice (Supplemental Figure S9A) could be another factor driving the increase of NK cells in the spleen and lung of mice treated with the bsAb pair, as the bsAb pair mediated low level of IL-2R signaling in presence of similar sMSLN concentrations in an in vitro assay (Supplemental Figure S9B). Proleukin treatment reduced the number of circulating lymphocytes on day 5 post treatment initiation. The bsAb pair did not affect the number of circulating lymphocytes at either day 5 or day 9 post treatment initiation (Supplemental Figure S9C-D).

Additionally, we performed a human whole blood assay to assess potential cytokine release induction in the presence of CD122/CD132xTAA bsAb pairs. Results showed that in contrast to Proleukin, which significantly induced IFN- γ and IL-6 production in human blood as expected, the CD122/CD132xMSLN bsAb pair did not induce any cytokine production with levels of IFN- γ and IL-6 close to those obtained with a negative control antibody (Cetuximab) or PBS (Figures 4F-G). It is worth mentioning that even in the presence of a large amount of sMSLN (400 nM), the CD122/CD132xMSLN bsAb pair didn't upregulate any of the proinflammatory cytokines tested

(Supplemental Figures S9E-F). These data further corroborate our *in vivo* findings, where the bsAb pair didn't induce cytokine release even in the presence of circulating sMSLN (Figures 4D-E).

CD122/CD132xTAA bsAb pairs drive potent anti-tumor activity in combination with anti-PD-1

Preclinical evidence suggests that combining IL-2 pathway activation with PD-1 checkpoint blockade represents a promising immunotherapy strategy [20,25-27]. To address the potential benefit of combining the CD122/CD132xTAA bsAb pairs and PD-1 blockade, in vivo efficacy studies were performed. Treatments were initiated when tumors reached a volume of 100 - 150 mm³ (Figure 5A). As expected, anti-mPD-1 monotherapy resulted in only partial control of tumor growth. Although the CD122/CD132xMSLN bsAb pair alone didn't control tumor growth, combining the bsAb pair with anti-mPD-1 therapy resulted in a significantly stronger inhibition of tumor growth compared to anti-mPD-1 alone (at day 13, tumor growth inhibition (TGI) = 45% for anti-mPD-1 alone vs 75% for the combination), with 2/7 animals achieving nearly complete tumor clearance (Figure 5B and Supplemental Figure S10A). Combined treatment also led to an increased survival probability relative to the vehicle group (Figure 5C). Immunophenotyping of TILs at day 9 posttreatment initiation showed that in vivo efficacy correlates with immunophenotypic changes in the TME. Anti-mPD-1 monotherapy or combined to CD122/CD132xMSLN bsAb pair induced a significant increase in tumor infiltration of CD45⁺ and CD8⁺ T cells as well as cytotoxic GZB⁺ CD8⁺ T cells over vehicle-treated mice (Figures 5D-F). In contrast to anti-mPD-1 monotherapy, the combined treatment with anti-mPD-1 and the bsAb pair resulted in a significant increase of NK, proliferating NK and a more favorable CD8⁺ T cell/Treg ratio compared to the vehicle control (Figures 5G-I, Supplemental Figures S10B-D). The treatments did not change the proportion of tumor specific CD8⁺ T cells in circulation or in the tumor, however, the absolute number showed a trend of increase in the tumor of mice from the anti-PD-1 and the combination treatment groups (Supplemental Figure S11). The results suggest that the combination therapy enhances tumor clearance by increasing the presence of cytotoxic T cells and NK cells relative to Tregs. In summary, anti-mPD-1/bsAb pair combination therapy integrates immunological outcomes observed with anti-mPD-1 monotherapy, characterized by an increase in effector and cytotoxic T cells, with those observed with CD122/CD132xMSLN bsAb pair therapy, which promotes expansion of NK cells and central memory CD8⁺ T cells, resulting in a favorable TME for better tumor control.

Distinct TAAs can be combined to further improve specificity

TAA expression on normal cells is a common cause of toxicity in TAA targeted therapies. Targeting two distinct TAAs simultaneously may further restrict the beneficial effects to tumor cells co-expressing the two TAAs while sparing normal cells expressing only one TAA. We thus tested whether the bsAb pair strategy also works by combining bsAbs targeting two different TAAs (HER2 and MSLN). First, we tested the concept with CD122xHER2-1/CD132xMSLN-2 bsAb pair using HEK Blue CD122/CD132 reporter cell line and microspheres co-coated with various levels of MSLN and HER2. Results demonstrated that reporter cells were activated by the combination of CD122xHER2-1/CD132xMSLN-2 in a TAA density-dependent manner (Figure 6A). It was interesting to observe that higher TAA densities were required to support the bsAb pair targeting two distinct TAAs than those targeting a single TAA (Figure 6A, Supplemental Figure S12A). Next, we sought to repeat this compelling observation using cancer cells expressing both TAAs (NCI-N87 cells) and immune cells expressing the dimeric receptor (NK-92 cells). Our data showed that the bsAb pair targeting both HER2 and MSLN induced an increase of pSTAT5 level, although to a level slightly lower than those induced by bsAb pairs targeting a single TAA (Figure 6B). We also tested the concept with a cell line expressing lower levers of both TAAs (JIMT-1) than NCI-N87. With this cell line, the bsAb pair targeting both TAAs also induced detectable pSTAT5 in NK-92 cells, which was substantially lower than that induced by the bsAb pairs targeting a single TAA (Supplemental Figure S12B). As expected, no activation was observed when using TAA-negative cancer cells (Supplemental Figure S12C).

DISCUSSION

In this study, we described a strategy to restrict IL-2/IL-15 activation to TME by using a pair of bsAbs, with one bsAb targeting CD122 and a TAA, the other bsAb targeting CD132 and the same TAA or a different TAA expressed on the same tumor cell. This approach allows a broad T-cell activation regardless of their TCR specificity by stimulating tumor-specific and bystander infiltrating T cells, both of which may contribute to tumor cell killing when combining the bsAb pair with a T cell engager bsAb. We demonstrated with HER2 and MSLN that this strategy activates IL-2/IL-15 signaling in a TAA-dependent manner. In contrast to Proleukin, the bsAb pair did not induce cytokine release in human blood nor lung edema in mouse models, confirming it as a safe strategy to harness IL-2/IL-15 activation inside the tumor. The strategy is likely to be expandable to other TAAs.

The bsAb pair does not induce IL-2R signaling without the presence of TAA, as the two bsAbs are unable to bring the IL-2R subunits together in the absence of TAA-expressing cells. This is different from the immunocytokine strategy where an active IL-2 molecule is ligated to a tumor targeting antibody [18,19], which still induces systemic IL-2R activation although with preferred tumor accumulation. As antibodies have a much longer half-life than IL-2, the strategy also addresses the inconvenient dosing schedule issues facing the high-dose IL-2 therapy. In addition, the two bsAbs do not naturally associate with each other in the absence of TAA-expressing cells, they thus can be administered simultaneously in a clinical setting, which may not be possible for the split IL-2 strategy [21].

When pairing bsAbs targeting different epitopes on the same TAA, bsAbs targeting certain epitope combinations showed higher potency than targeting other combinations. It has been reported that targeting a membrane proximal TAA epitope by a bsAb bridging immune cells and

tumor cells induced higher levels of immune cell activation than targeting a membrane distal epitope [28-30]. Although the activity of the bsAb pair is also affected by the TAA epitope, we did not see a clear correlation with the membrane proximity of the TAA epitopes, suggesting that CD45-exclusion may not be the underlying mechanism here. As binding by CD122xCD132 bsAbs induces alternative dimeric receptor geometries compared to IL-2 [13], it is of interest to investigate whether targeting different TAAs or different TAA epitopes by our strategy also induces different geometries of the CD122/CD132 dimer, which is out of scope of this study. The affinity of the different TAA binding arms could be another factor in addition to epitope position affecting the activity of the bsAb pairs.

Treatment with CD122/CD132xMSLN bsAb pair, but not Proleukin, induced significant increase of central memory CD8⁺ T cells and NK cells in TME of an engineered mouse tumor model. One possible explanation to the observed difference in central memory T cells is that the weaker signaling induced by the bsAb pair favors memory T cell proliferation as reported previously [13,31]. Alternatively, the in vivo biological effects of the CD122/CD132xMSLN bsAb pair could mimic those of IL-15, which is well-established for a role in promoting memory T cell and NK cell proliferation [2]. IL-15 is usually [25,27,32] trans-presented to CD122/CD132 dimer-expressing immune cells by IL-15Rα-expressing cells while IL-2 engages its receptor subunits through cis-binding [2]. As such, the trans-presentation of IL-15 could be geometrically similar to the trans-presentation of the CD122/CD132xTAA bsAb pair by TAA-expressing tumor cells to CD122/CD132 dimer-expressing immune cells. This geometrical similarity may be one factor underlying the similar biological effects of the CD122/CD132xTAA bsAb pair and IL-15. Upon IL-2-induced activation, CD122 and CD132 are known to be internalized as a negative feedback mechanism to down-regulate signaling [33]. The trans-presentation mechanism may decrease the rate of CD122/CD132 internalization by ligating them to another cell and thus prolong signal activation induced by IL-15 and the bsAb pair, in contrast to IL-2. It could be interesting to assess whether the receptor dynamics and downstream signaling kinetics induced by the bsAb pair are similar to those induced by IL-15 instead of IL-2 in a separate study. Due to technical limitations, IL-2 signaling *in vivo* was not measured directly with pSTAT5, but with surrogate readouts such as T cell and NK cell activation/proliferation in this study, following a common practice in the field [21,25]. Further technical innovation allowing in vivo pSTAT5 tracking in real time will provide more insights to this field. Cis-binding to IL-2Ra, or other engineered strategies to guide IL-2 signaling to antigen-specific T cells have been demonstrated important to the *in vivo* efficacy of IL-2 targeting strategies [25,27,32], which, together with the clinical failure of bempegaldesleukin [34], casts doubts on the validity of the non-targeted not-alpha IL-2 strategy. However, the clinical success and subsequent approval by FDA of N803 [35,36], an IL-15 superagonist, suggests that mimicking IL-15 biological effects locally in the tumor, although being not-alpha by nature, could be a valid anti-tumor therapeutic strategy. Similar to other not-alpha strategies, the bsAb pair also avoids preferential activation of Tregs vs CD8⁺ T cells, in contrast to IL-2.

In addition to inducing immune activation in TME, treatment with the CD122/CD132xMSLN bsAb pair also showed some signs of immune activation in mouse spleens and lungs. This could be due to recirculation of activated immune cells from the tumor to the circulation, or be mediated by sMSLN in circulation, which is reported in sera of patients with MSLN-expressing cancers [37], and detected in sera of the tumor-bearing mice from this study. Nonetheless, the combination of sMSLN up to 400 nM (more than 20-fold higher than the levels detected in the tumor model) with the CD122/CD132xMSLN bsAb pair does not induce cytokine release in human whole blood samples from healthy donors. In agreement, the CD122/CD132xMSLN bsAb pair does not induce systemic cytokine release and does not induce lung edema in the tested mouse tumor model, in contrast to

Proleukin. The results suggest that CD122/CD132xTAA bsAb pairs are safe even with soluble TAA in circulation.

We demonstrated that the bsAb strategy synergizes with checkpoint inhibitors in a mouse model, potentially by combining the immunological effects of anti-mPD-1 monotherapy, which increases effector and cytotoxic T cells, with the effects of the CD122/CD132xMSLN bsAb pair therapy, which promotes the expansion of NK cells and memory CD8⁺ T cells. Our data showed that bsAb combination can control tumor growth only when combined with PD-1 blockade. While our CD122/CD132 x TAA bsAb pair activates IL2R signaling, it is less potent than WT IL-2 possibly due to its not-alpha nature and may be insufficient to control tumor growth on its own. The addition of PD-1 blockade likely enhances this effect by synergistically promoting T cell activation and functionality within the TME. Several other published not-alpha IL-2 variants have also shown only modest or no efficacy in directly controlling tumor growth, but efficacy was achieved when combined with additional treatment modalities [25,38]. Due to observed effects on memory T cells and NK cells, the strategy may also be combined with other T- and NK cell-mediated immunotherapies such as T/NK cell engagers, CAR T cells and anti-tumor mAbs. Combination with immune-stimulating strategies may be required to treat cold tumors lacking immune infiltration. The absence of mouse cross-reactivity of our targeting bsAbs and the usage of hCD122/hCD132 transgenic mice are a limitation of our study. Additional safety studies will be necessary before advancing to clinical trials.

Importantly, this strategy also proved effective when each bsAb in the pair targeted a different TAA. Since many TAAs are also expressed on healthy cells, albeit at lower levels, targeting two distinct TAAs with the bsAb pair could further restrict IL-2 activation to tumors co-expressing both TAAs, while sparing healthy cells that express only one. Looking ahead, this dual-targeting

approach holds significant potential to enhance the specificity and safety of IL-2-based immunotherapies, offering a more precise way to target tumors while minimizing off-target effects on healthy tissues.

With both bsAb pairs targeting a single TAA and those targeting two distinct TAAs, we noticed that lower TAA densities on tumor cells than that on TAA-coated beads were required to activate IL-2R signaling. This could be explained by the better TAA mobility on cell membranes than on TAA-coated beads. In addition, we noticed that the bsAb pairs targeting two TAAs required higher TAA density than those targeting a single TAA, which could be due to the potential clustering of a single TAA to increase its local density and the possibility of engaging both bsAbs with a single TAA molecule. On top of TAA density, other factors, such as the membrane distribution and targeted geometry of TAAs on cancer cell surface, may also influence the overall agonistic activity of our CD122/CD132 x TAA bsAb combination strategy. Addressing these pertinent questions would require additional specific experiments that fall outside the scope of the present study. We recognize the regulatory challenges of developing a combination of two bsAbs but believe that the potential clinical benefits justify pursuing this approach.

Acknowledgements: The authors thank Valery Moine, Coline Burnet-Merlin, Laura Cons, Pauline Lloveras, Christophe Guillamo, Guillemette Pontini, Theresa Batuzova and Mélanie Cettour-Cavé for experimental support. The authors thank Diogo Tavares and Ulla Ravn for insightful scientific discussions. The authors thank Te Guo at Biocytogen Co., Ltd. for his valuable support related to hCD122/hCD132 Tg mice.

Contributors: Planning and supervising: LS, EH, CJ, NF, WF and KM. Experimenting: JM, LC, AV, AL, BD, LN, PM and SC. Writing: JM, EH and LS. Guarantor: LS.

Funding: This work was supported by Light chain Biosciences - Novimmune S.A.

Competing interests: JM, EH, LC, AV, AL, BD, SC, PM, KM, WF, NF and LS are employees of Light chain Biosciences - Novimmune S.A. Patent application number WO 322145-2988, with relevance to this work, has been filed by Light Chain Biosciences - Novimmune S.A.

Patient consent for publication Not applicable

Ethics approval *In vivo* experiments were performed in accordance with the Swiss Federal Veterinary Office guidelines and approved by the Cantonal Veterinary Office (protocol: #GE319).

Availability of data and material: The data analyzed and presented in this study are available upon request to the corresponding author.

REFERENCES

- 1 Wang X, Rickert M, Garcia KC. Structure of the Quaternary Complex of Interleukin-2 with Its a, b, and gc Receptors. 2005;310.
- Yang Y, Lundqvist A. Immunomodulatory Effects of IL-2 and IL-15; Implications for Cancer Immunotherapy. Cancers. 2020;12:3586. doi: 10.3390/cancers12123586
- 3 Sznol M, Rizvi N. Teaching an old dog new tricks: re-engineering IL-2 for immuno-oncology applications. J Immunother Cancer. 2023;11:e006346. doi: 10.1136/jitc-2022-006346
- 4 Sprent J, Boyman O. Optimising IL-2 for Cancer Immunotherapy. Immune Netw. 2024;24:e5. doi: 10.4110/in.2024.24.e5
- 5 Krieg C, Létourneau S, Pantaleo G, et al. Improved IL-2 immunotherapy by selective stimulation of IL-2 receptors on lymphocytes and endothelial cells. Proc Natl Acad Sci. 2010;107:11906–11. doi: 10.1073/pnas.1002569107

- Peace DJ, Cheever MA. Toxicity and therapeutic efficacy of high-dose interleukin 2. In vivo infusion of antibody to NK-1.1 attenuates toxicity without compromising efficacy against murine leukemia. J Exp Med. 1989;169:161–73. doi: 10.1084/jem.169.1.161
- Arenas-Ramirez N, Zou C, Popp S, et al. Improved cancer immunotherapy by a CD25-mimobody conferring selectivity to human interleukin-2. Sci Transl Med. 2016;8. doi: 10.1126/scitranslmed.aag3187
- Joerger M, Calvo E, Laubli H, et al. Phase 1 first-in-human dose-escalation study of ANV419 in patients with relapsed/refractory advanced solid tumors. J Immunother Cancer. 2023;11:e007784. doi: 10.1136/jitc-2023-007784
- Lopes JE, Fisher JL, Flick HL, et al. ALKS 4230: a novel engineered IL-2 fusion protein with an improved cellular selectivity profile for cancer immunotherapy. J Immunother Cancer. 2020;8:e000673. doi: 10.1136/jitc-2020-000673
- Merchant R, Galligan C, Munegowda MA, et al. Fine-tuned long-acting interleukin-2 superkine potentiates durable immune responses in mice and non-human primate. J Immunother Cancer. 2022;10:e003155. doi: 10.1136/jitc-2021-003155
- 11 Silva D-A, Yu S, Ulge UY, et al. De novo design of potent and selective mimics of IL-2 and IL-15. Nature. 2019;565:186–91. doi: 10.1038/s41586-018-0830-7
- Harris KE, Lorentsen KJ, Malik-Chaudhry HK, et al. A bispecific antibody agonist of the IL-2 heterodimeric receptor preferentially promotes in vivo expansion of CD8 and NK cells. Sci Rep. 2021;11:10592. doi: 10.1038/s41598-021-90096-8
- 13 Yen M, Ren J, Liu Q, et al. Facile discovery of surrogate cytokine agonists. Cell. 2022;185:1414-1430.e19. doi: 10.1016/j.cell.2022.02.025

- Margolin K, Atkins MB, Dutcher JP, et al. Phase I Trial of BAY 50-4798, an Interleukin-2–
 Specific Agonist in Advanced Melanoma and Renal Cancer. Clin Cancer Res. 2007;13:3312–9.
 doi: 10.1158/1078-0432.CCR-06-1341
- Nirschl CJ, Brodkin HR, Hicklin DJ, et al. Discovery of a Conditionally Activated IL-2 that Promotes Antitumor Immunity and Induces Tumor Regression. Cancer Immunol Res. 2022;10:581–96. doi: 10.1158/2326-6066.CIR-21-0831
- Guzman W, Bialucha UC, Madala HR, et al. 841 XTX202, a tumor-selective protein-engineered IL-2, exhibited enhanced anti-tumor activity in combination with checkpoint inhibition in mice. Regular and Young Investigator Award Abstracts. BMJ Publishing Group Ltd 2022:A877–A877.
- Shi W, Liu N, Liu Z, et al. Next-generation anti-PD-L1/IL-15 immunocytokine elicits superior antitumor immunity in cold tumors with minimal toxicity. Cell Rep Med. 2024;101531. doi: 10.1016/j.xcrm.2024.101531
- 18 Klein C, Waldhauer I, Nicolini VG, et al. Cergutuzumab amunaleukin (CEA-IL2v), a CEA-targeted IL-2 variant-based immunocytokine for combination cancer immunotherapy:

 Overcoming limitations of aldesleukin and conventional IL-2-based immunocytokines.

 Oncolmmunology. 2017;6:e1277306. doi: 10.1080/2162402X.2016.1277306
- Ongaro T, Gouyou B, Stringhini M, et al. A novel format for recombinant antibody-interleukin-2 fusion proteins exhibits superior tumor-targeting properties in vivo.

 Oncotarget. 2020;11:3698–711. doi: 10.18632/oncotarget.27726
- Waldhauer I, Gonzalez-Nicolini V, Freimoser-Grundschober A, et al. Simlukafusp alfa (FAP-IL2v) immunocytokine is a versatile combination partner for cancer immunotherapy. mAbs. 2021;13:1913791. doi: 10.1080/19420862.2021.1913791

- Quijano-Rubio A, Bhuiyan AM, Yang H, et al. A split, conditionally active mimetic of IL-2 reduces the toxicity of systemic cytokine therapy. Nat Biotechnol. 2023;41:532–40. doi: 10.1038/s41587-022-01510-z
- Overwijk WW, Tagliaferri MA, Zalevsky J. Engineering IL-2 to Give New Life to T Cell Immunotherapy. Annu Rev Med. 2021;72:281–311. doi: 10.1146/annurev-med-073118-011031
- 23 Smith GA, Taunton J, Weiss A. IL-2Rβ abundance differentially tunes IL-2 signaling dynamics in CD4+ and CD8+ T cells. Sci Signal. 2017;10:eaan4931. doi: 10.1126/scisignal.aan4931
- 24 Carmenate T, Montalvo G, Lozada SL, et al. The antitumor effect induced by an IL-2 'noalpha' mutein depends on changes in the CD8+ T lymphocyte/Treg cell balance. Front Immunol. 2022;13. doi: 10.3389/fimmu.2022.974188
- 25 Codarri Deak L, Nicolini V, Hashimoto M, et al. PD-1-cis IL-2R agonism yields better effectors from stem-like CD8+ T cells. Nature. 2022;610:161–72. doi: 10.1038/s41586-022-05192-0
- Piper M, Hoen M, Darragh LB, et al. Simultaneous targeting of PD-1 and IL-2Rβγ with radiation therapy inhibits pancreatic cancer growth and metastasis. Cancer Cell. 2023;S1535610823001174. doi: 10.1016/j.ccell.2023.04.001
- 27 Hashimoto M, Araki K, Cardenas MA, et al. PD-1 combination therapy with IL-2 modifies

 CD8+ T cell exhaustion program. Nature. 2022;610:173–81. doi: 10.1038/s41586-022-05257-0
- 28 Li J, Stagg NJ, Johnston J, et al. Membrane-Proximal Epitope Facilitates Efficient T Cell Synapse Formation by Anti-FcRH5/CD3 and Is a Requirement for Myeloma Cell Killing. Cancer Cell. 2017;31:383–95. doi: 10.1016/j.ccell.2017.02.001

- 29 Qi J, Li X, Peng H, et al. Potent and selective antitumor activity of a T cell-engaging bispecific antibody targeting a membrane-proximal epitope of ROR1. Proc Natl Acad Sci. 2018;115. doi: 10.1073/pnas.1719905115
- 30 Hatterer E, Chauchet X, Richard F, et al. Targeting a membrane-proximal epitope on mesothelin increases the tumoricidal activity of a bispecific antibody blocking CD47 on mesothelin-positive tumors. mAbs. 2020;12:1739408. doi: 10.1080/19420862.2020.1739408
- 31 Ortiz-Miranda Y, Masid M, Jiménez-Luna C, et al. Transcriptional reprogramming by IL-2 variant generates metabolically active stem-like T cells. 2023.
- Andreata F, Moynihan KD, Fumagalli V, et al. CD8 cis-targeted IL-2 drives potent antiviral activity against hepatitis B virus. Sci Transl Med. 2024;16:eadi1572. doi: 10.1126/scitranslmed.adi1572
- Dautry-Varsat A. Endocytosis of Interleukin 2 Receptors in Human T Lymphocytes: Distinct Intracellular Localization and Fate of the Receptor a,/3, and -yChains. 1995.
- Diab A, Gogas H, Sandhu S, et al. Bempegaldesleukin Plus Nivolumab in Untreated Advanced
 Melanoma: The Open-Label, Phase III PIVOT IO 001 Trial Results. J Clin Oncol. 2023;41:4756–
 67. doi: 10.1200/JCO.23.00172
- Chamie K, Chang SS, Rosser CJ, et al. N-803 Plus BCG Treatment for BCG-Naïve or Unresponsive Non-Muscle Invasive Bladder Cancer: A Plain Language Review. Future Oncol.
 2024;1–11. doi: 10.1080/14796694.2024.2363744
- Chamie K, Chang SS, Kramolowsky E, et al. IL-15 Superagonist NAI in BCG-Unresponsive Non–Muscle-Invasive Bladder Cancer. NEJM Evid. 2023;2. doi: 10.1056/EVIDoa2200167
- 37 Hassan R, Ho M. Mesothelin targeted cancer immunotherapy. Eur J Cancer. 2008;44:46–53. doi: 10.1016/j.ejca.2007.08.028

Rosen DB, Kvarnhammar AM, Laufer B, et al. TransCon IL-2 β/γ : a novel long-acting prodrug with sustained release of an IL-2R β/γ -selective IL-2 variant with improved pharmacokinetics and potent activation of cytotoxic immune cells for the treatment of cancer. J Immunother Cancer. 2022;10:e004991. doi: 10.1136/jitc-2022-004991

FIGURE LEGENDS

Figure 1: CD122xTAA/CD132xTAA bsAb pairs induce IL-2/IL-15 signaling in reporter cells. (A) Schematic representation showing the combination of CD122xTAA/CD132xTAA bsAbs selectively activating IL-2/IL-15 signaling on immune cells in the presence of TAA-expressing tumor cells by targeting different TAA epitopes (panel 3) or the same TAA epitope (panel 4). (B-F) In vitro biological activity of CD122xTAA/CD132xTAA bsAb pairs was explored using HEK Blue CD122/CD132 reporter cells and TAA-coated microspheres (B, D-F) or NCI-N87 tumor cells (C). rhIL-2 and hIgG1 were used as positive and negative controls. (B) Reporter activity induced by a dose range of the CD122xHER2-1/CD132xHER2-2 bsAb pair or individual bsAbs in presence of HER2-coated microspheres. (C) Reporter activity induced by a dose range of the CD122xHER2-1/CD132xHER2-2 bsAb pair in presence of HER2-expressing NCI-N87 cells. (D) Reporter activity induced by a dose range of the CD122xMSLN-1/CD132xMSLN-2 bsAb pair or individual bsAbs tested at the maximal concentration in presence of MSLN-coated microspheres. (E) Reporter activity induced by a dose range of CD122xMSLN-1 bsAb paired with CD132xMSLN bsAbs targeting three different MSLN epitopes (MSLN-2, MSLN-3 and MSLN-4). (F) Reporter activity induced by a dose range of IL-2RxMSLN bsAb pairs targeting either two different MSLN epitopes (CD122xMSLN-1/CD132xMSLN-2) or the same MSLN epitope (CD122xMSLN-1/CD132xMSLN-1 or CD122xMSLN-2/CD132xMSLN-2) with MSLN coated microspheres. Graphs show Mean ± SEM.

Figure 2: CD122xTAA/CD132xTAA bsAb pairs induce STAT5 phosphorylation (pSTAT5) in human NK cells and T cells and enhance T cell dependent cytotoxicity (TDCC) of tumor cells as well as NKmediated antibody-dependent cell-mediated cytotoxicity (ADCC) in a TAA-dependent manner. (A) Dose-dependent induction of pSTAT5 in NK-92 cells by CD122xHER2-1/CD132xHER2-2 (left panel) or CD122xMSLN-1/CD132xMSLN-2 (right panel) following incubation with cancer cells expressing different levels of the corresponding TAA. (B) Dose-dependent induction of pSTAT5 in human CD8⁺ T cells and Tregs by Proleukin (left panel) or CD122xMSLN-1/CD132xMSLN-2 in the presence of NCI-N87 cells (right panel). (C) TDCC of cancer cell lines expressing different levels of MSLN induced by a hlgG1 isotype control, CD122xMSLN-1/CD132xMSLN-2 or Proleukin. Specific killing was calculated by subtracting unspecific killing measured in control wells with PBMCs (n=4/5) and cancer cell lines only. Graphs show Mean ± SEM and statistical significance between groups was measured using one-way ANOVA for each cancer cell line independently. (D) NK cell-mediated ADCC of NCI-N87 cancer cells induced by overnight incubation with CD122xMSLN-1/CD132xMSLN-2 followed by 6 h incubation with Trastuzumab. Specific killing was calculated by subtracting unspecific killing measured in control wells with NK cells and cancer cell lines only. Graphs show Mean ± SEM and statistical significance between groups was measured using paired t test.

Figure 3: Treatment with CD122/CD132xMSLN bsAb pairs induce MSLN-dependent expansion and activation of intra-tumoral CD8 $^+$ T cells and NK cells. *In vivo* biological activity was explored in hCD122/hCD132 transgenic mice engrafted with hMSLN-expressing MC38 colon cancer cells. (A-E) Mice were treated with vehicle control (n = 5), Proleukin (*i.p.* 3 mg/kg for 5 consecutive days, n = 6) or CD122xMSLN-1/CD132xMSLN-2 bsAb pair (*i.v.* 10 mg/kg, twice (d0 and d3), n = 7). Tumor-infiltrating immune cells were assessed 5 days post treatment initiation. Shown are (B) absolute counts of CD45 $^+$ leukocytes, CD4 $^+$ or CD8 $^+$ T cells, (C) proportion of central memory T cells among CD8 $^+$ T cells, (D) Ki67 mean fluorescence intensity (MFI) of CD8 $^+$ T cells and proportion of

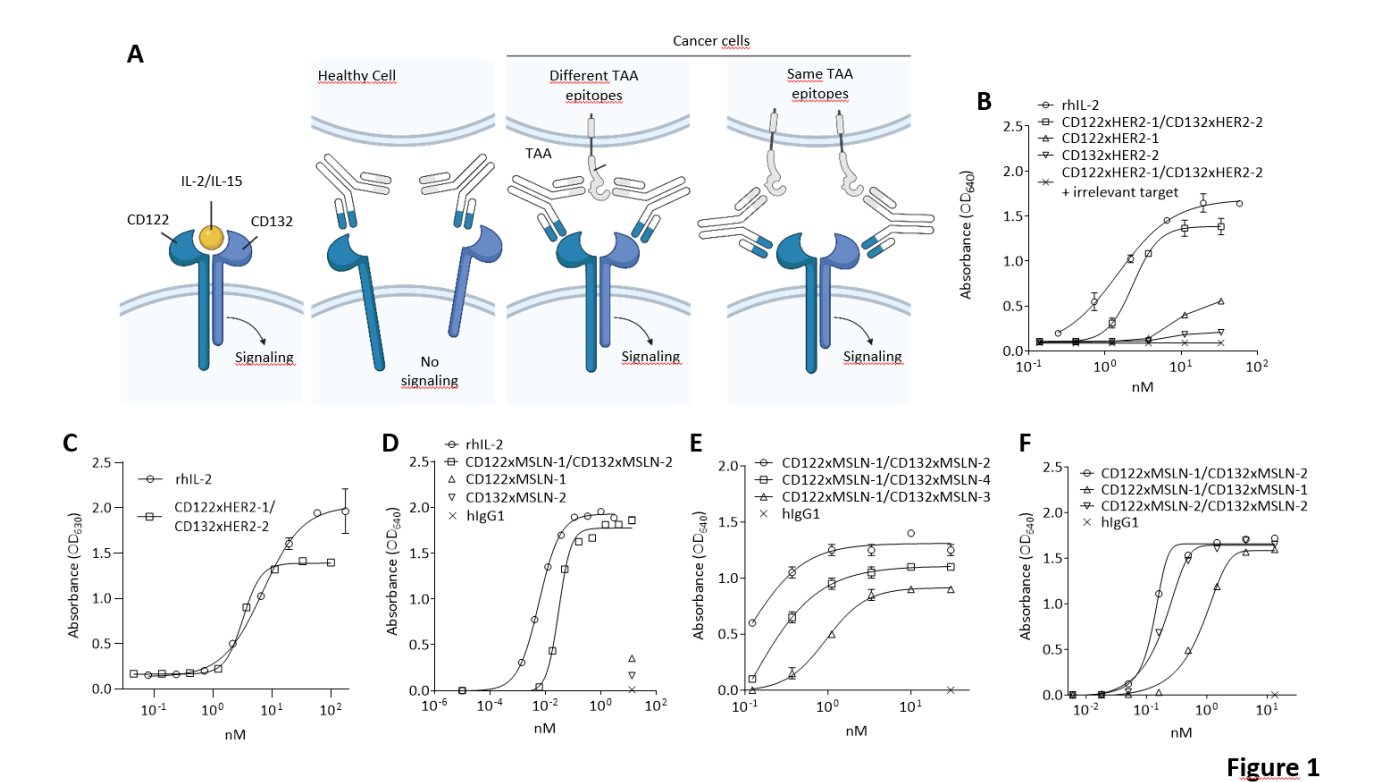
GZB⁺ cells among CD8⁺ T cells, (E) absolute count of NK cells, Ki67 MFI of NK cells and proportion of GZB⁺ cells among NK cells. (F-G) Mice were treated with vehicle control (n = 7), CD122-MxMSLN-1/CD132-MxMSLN-2 (n = 7) or bsAb pair targeting an irrelevant TAA (CD122xirrel-1/CD132xirrel-2 (n = 6)), twice (d0 and d3) at 10 mg/kg (i.v.) and tumors were analyzed 5 days post treatment initiation. Shown in the panels are (F) specific detection of human antibodies binding to MSLN-positive tumor cells, (G) absolute numbers of intra-tumoral NK cells. Graphs show mean values \pm SEM and statistical significance were determined using a one-way ANOVA with multiple comparison test.

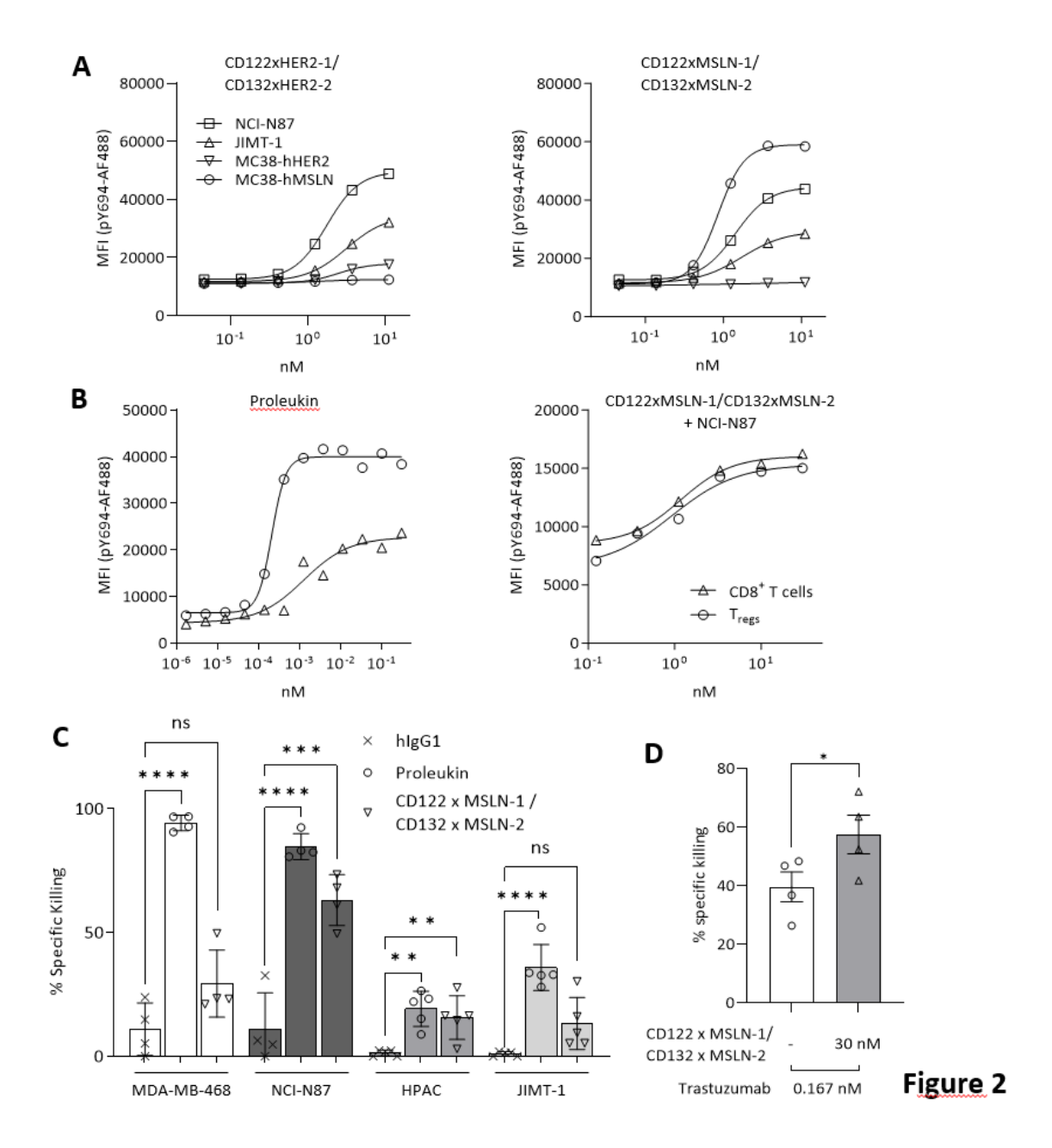
Figure 4: Improved safety profile of CD122/CD132xMSLN bsAb pairs in comparison to Proleukin. (A to E) hCD122/hCD132 transgenic mice were engrafted with hMSLN-expressing MC38 colon cancer cells. Mice were treated with vehicle (PBS) (n = 7), Proleukin (n = 6) or CD122 x MSLN-1/CD132 x MSLN-2 bsAbs (n = 7). Mice were euthanized 5 days post treatment initiation. Shown in the panels are body weight (A), spleen weight (B), lung weight (C), serum TNF- α (D) and serum IFN- γ (E) of the treated mice. (F-G) Induction of IFN- γ (F) and IL-6 (G) release in human whole blood (10 healthy donors) by Cetuximab, Proleukin or CD122/CD132xMSLN bsAb pair. Graphs show mean values \pm SEM and statistical significance between treatment groups was determined using a one-way ANOVA with multiple comparison test.

Figure 5: CD122/CD132xMSLN bsAb pair potently inhibits tumor growth in combination with anti-PD1. Therapeutic efficacy was tested in hCD122/hCD132 transgenic mice engrafted with hMSLN-expressing MC38 cancer cells. (A-C) Mice were treated with vehicle (PBS) (n = 8), CD122xMSLN-1/CD132xMSLN-2 bsAb pair, anti-mPD-1 (n = 7) or both anti-mPD-1 (n = 6) and bsAb combination (n = 8). Shown are average tumor volume (B) and Kaplan-Meier survival curves (C). Arrows indicate dosing of antibodies. Statistical analysis was performed using the log-rank (Mantel-Cox) test with

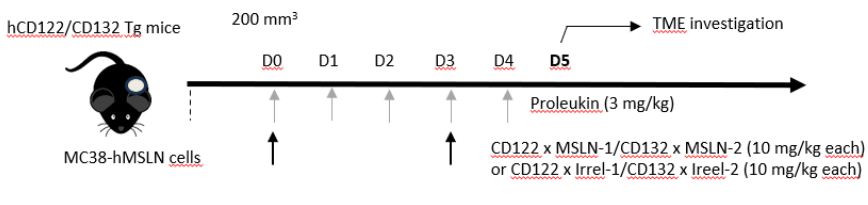
Bonferroni correction comparison (*p<0.0125). (D-I) Analysis of tumor-infiltrating immune cells 9 days post treatment initiation. Shown in the panels are absolute counts of CD45⁺ immune cells (D), CD8⁺ T cells (E), proportion of GZB⁺ cells among CD8⁺ T cells (F), CD8⁺ T cells / Tregs ratio (G), Ki67 MFI within NK cells (H) and absolute counts of NK cells (I) in tumors of treated mice. Data are represented as Mean ± SEM. Statistical analysis was performed using a one-way ANOVA.

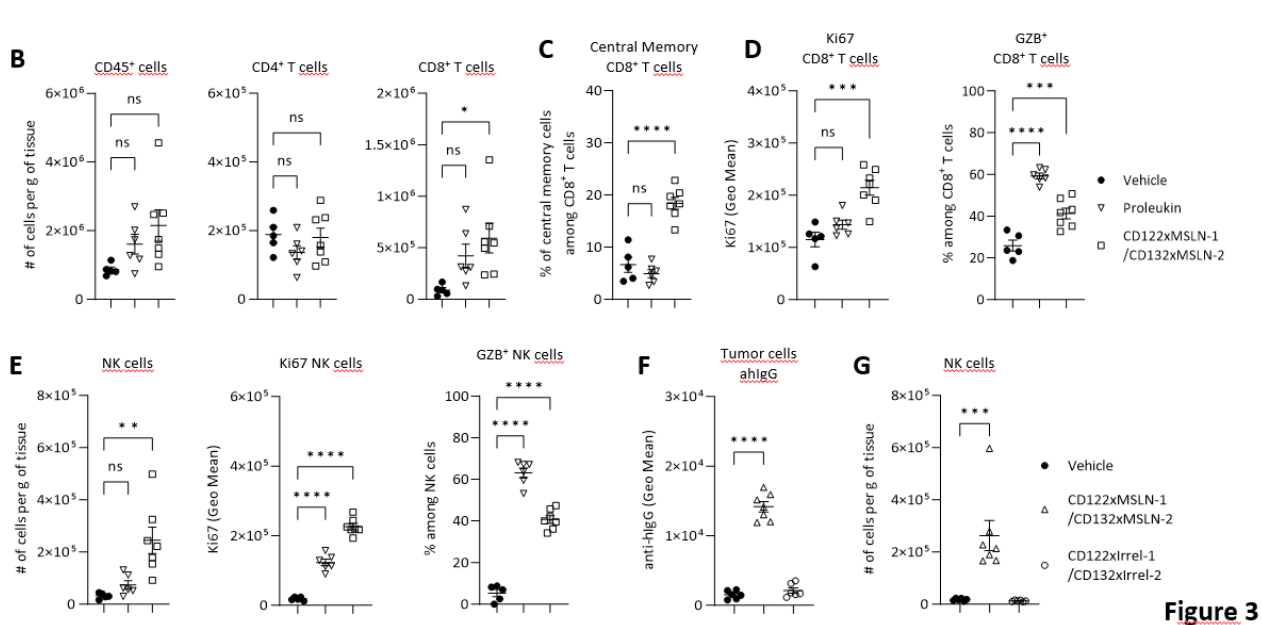
Figure 6: BsAbs targeting different TAAs can be combined to further improve specificity. (A) Induction of reporter activity of HEK Blue CD122/CD132 reporter cells by a dose range of CD122xHER2-1/CD132xMSLN-2 bsAb pair in presence of microspheres coated with different quantities of both MSLN and HER2. (B) Dose-dependent induction of pSTAT5 in NK-92 cells by CD122xHER2-1/CD132xHER2-2, CD122xMSLN-1/CD132xMSLN-2 or CD122xHER2-1/CD132xMSLN-2 bsAb pairs following incubation with HER2 and MSLN expressing NCI-N87 cells.











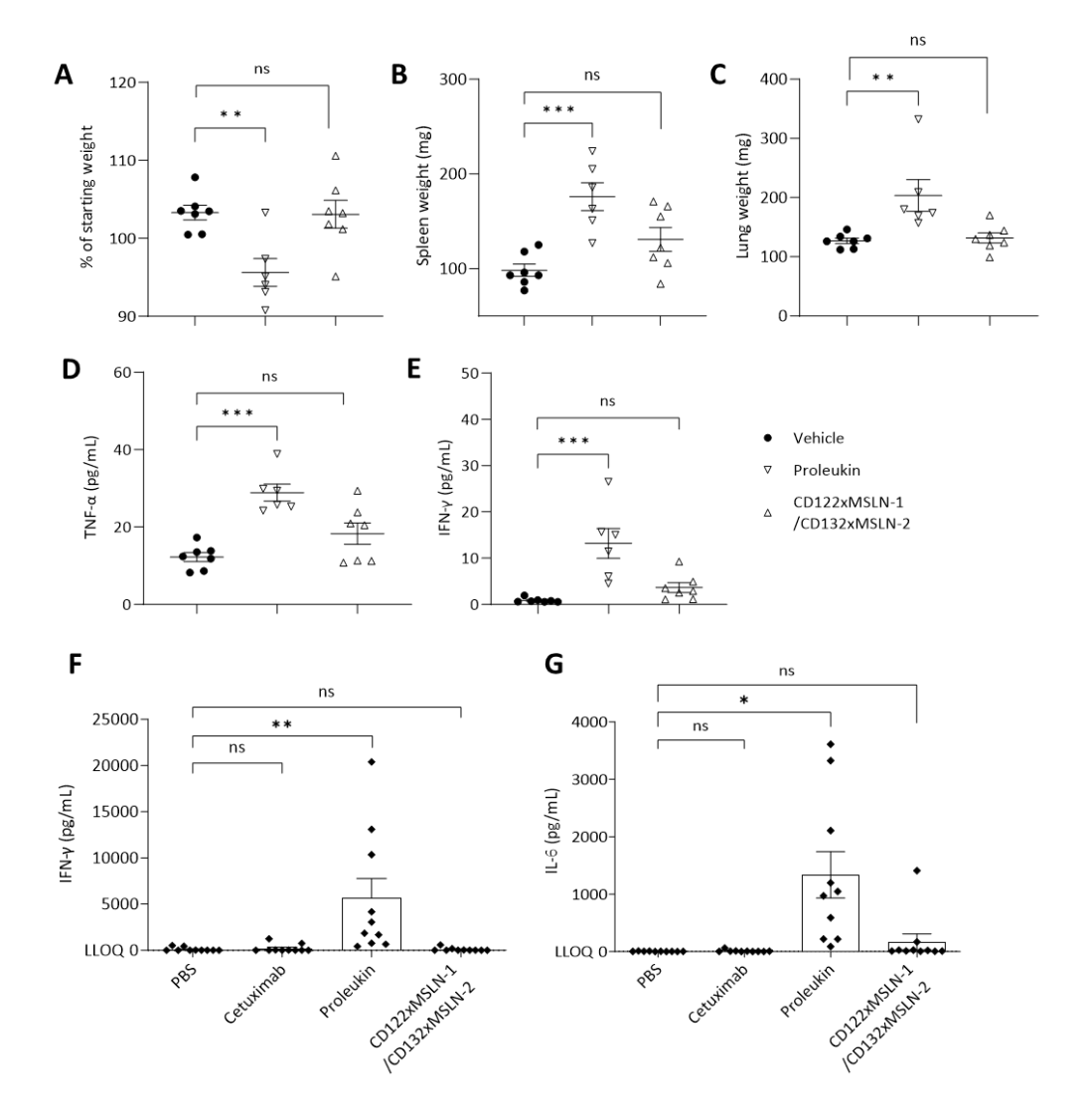
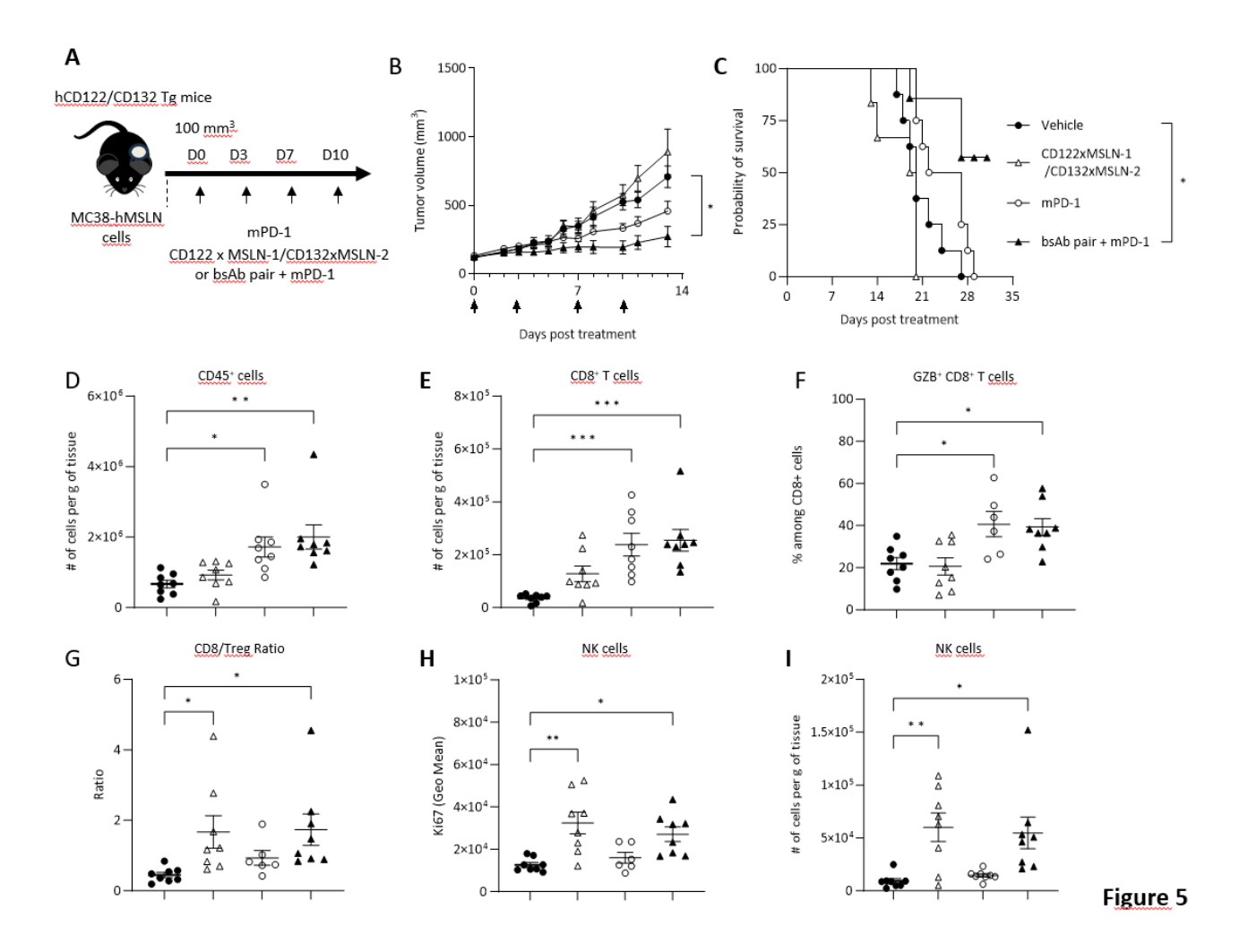
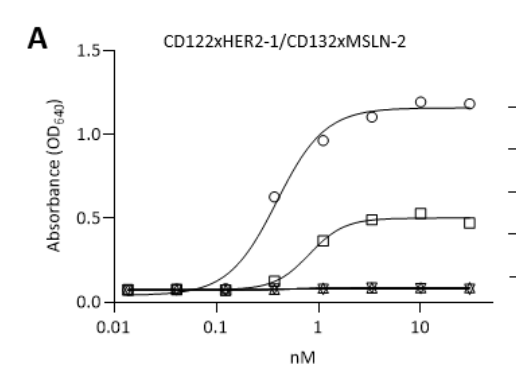
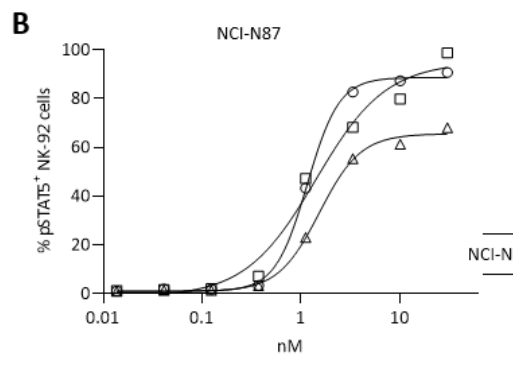


Figure 4





	SABC		TAA/μm²	
	HER2	hMSLN	HER2	hMSLN
-	390'170	355'300	3568	3249
-	175'868	146'772	1608	1342
	71'206	54'389	651	497
-∀-	24'234	12'774	222	117



-O- CD122xHER2-1/CD132xHER2-2

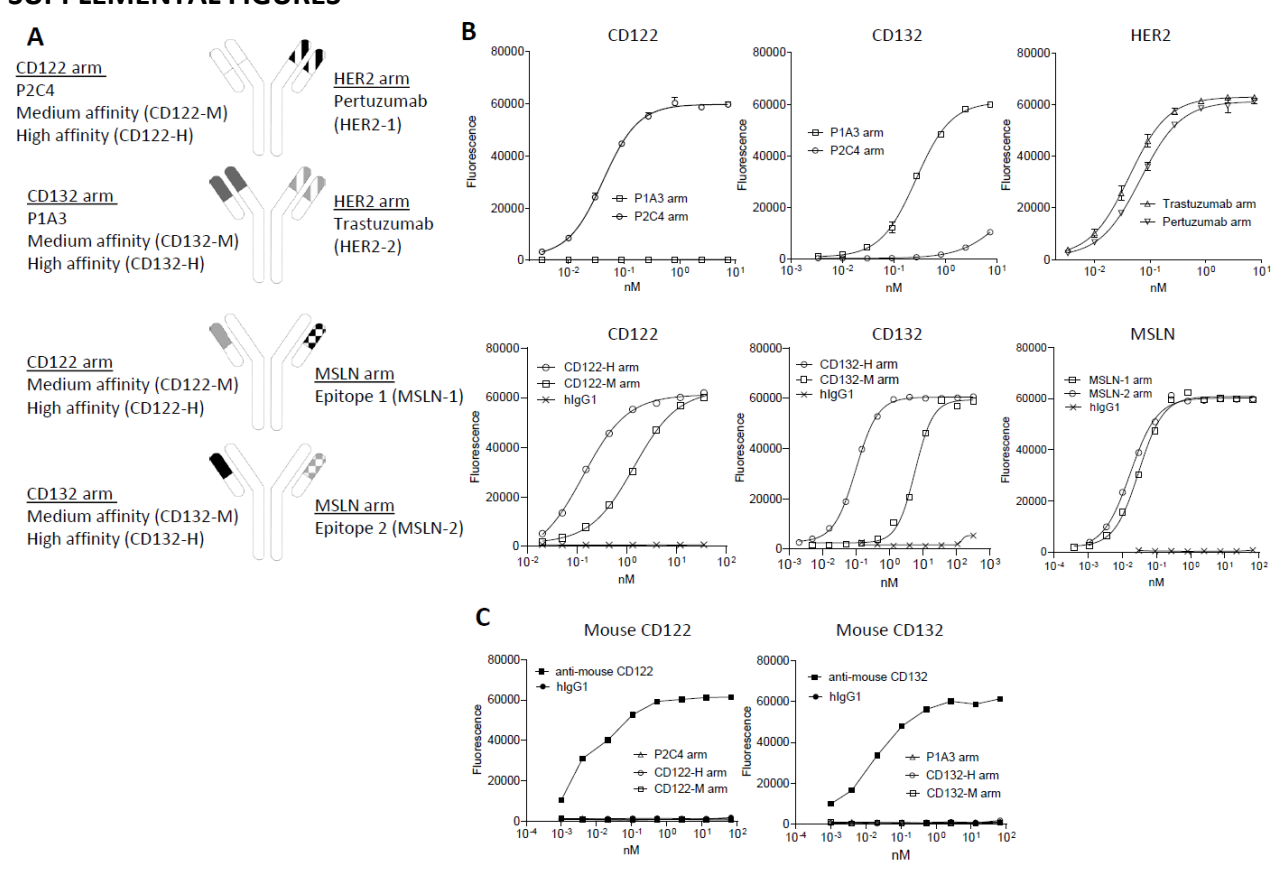
CD122xMSLN-1/CD132xMSLN-2

—— CD122xHER2-1/CD132xMSLN-2

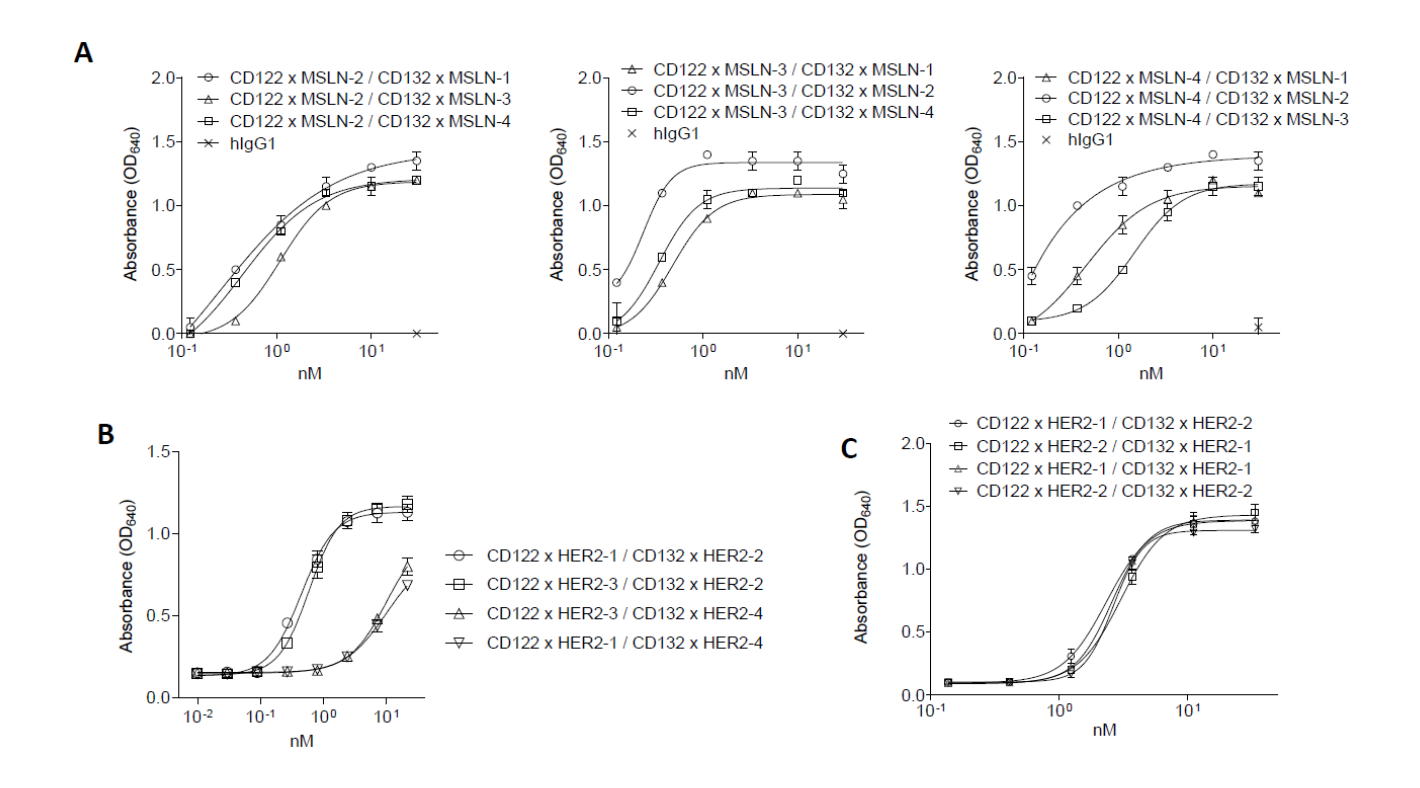
	SABC		TAA/μm²		
	HER2	hMSLN	HER2	hMSLN	
187	401'376	20'103	701	35	

Figure 6

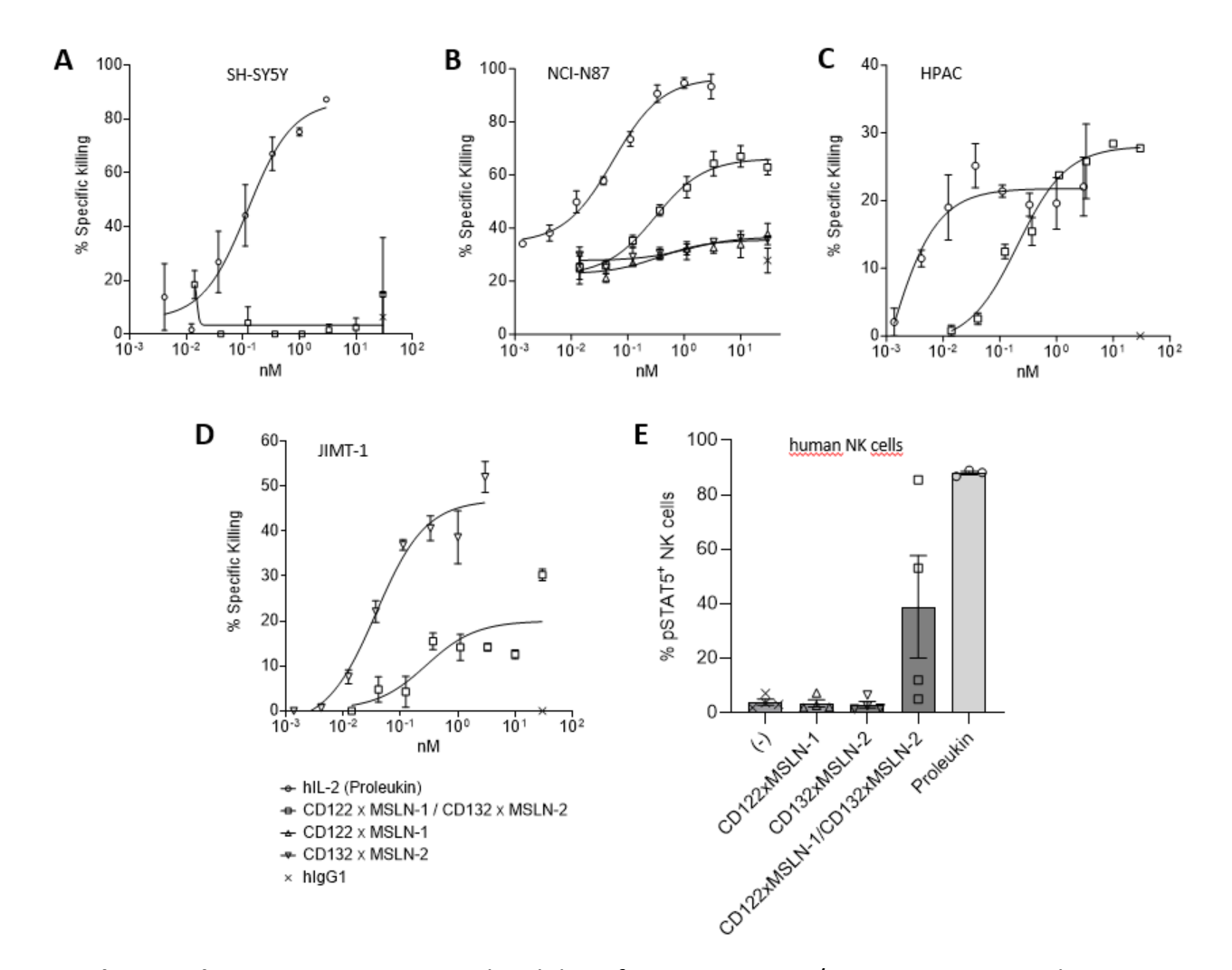
SUPPLEMENTAL MATERIAL SUPPLEMENTAL FIGURES



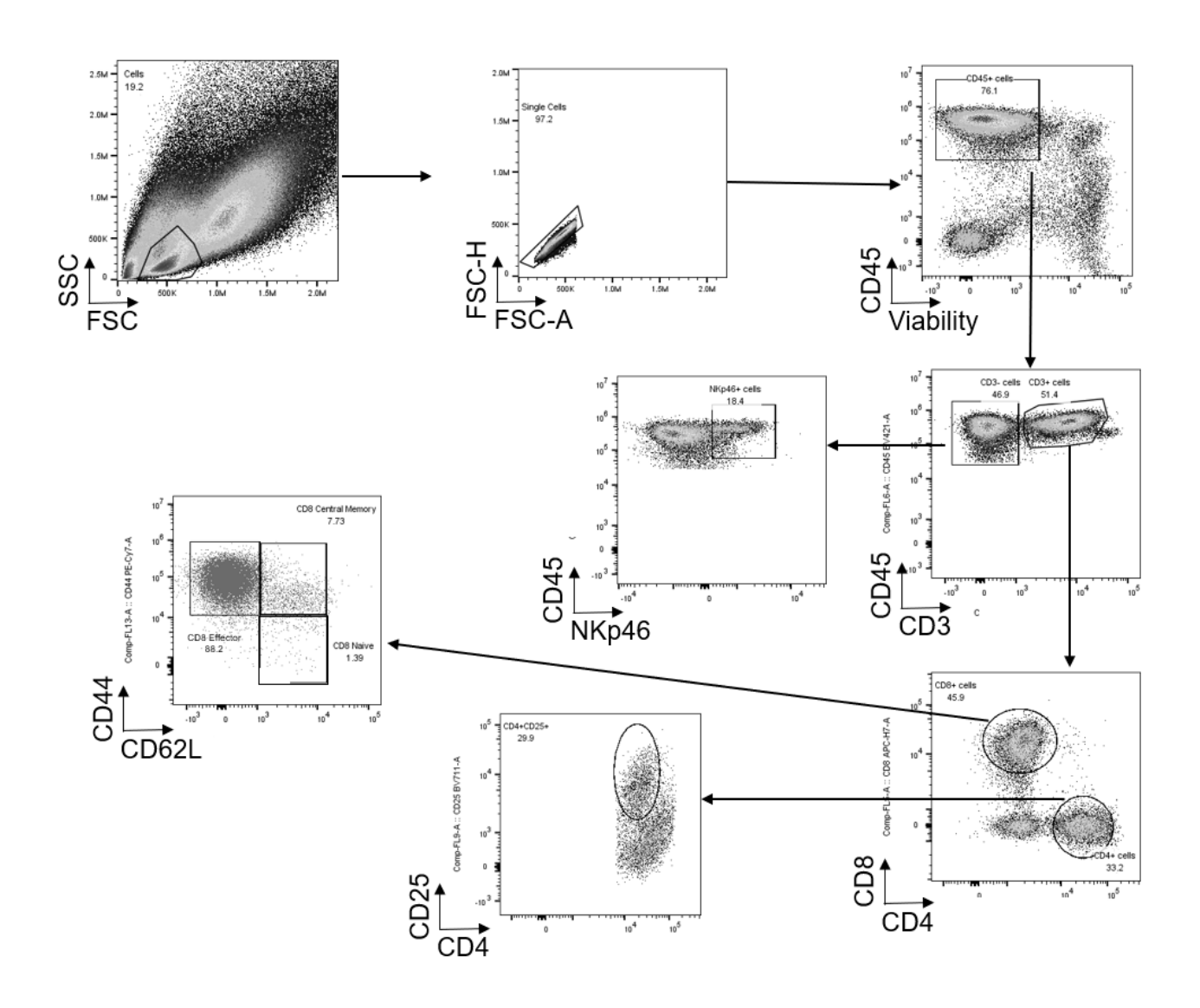
Supplemental Figure S1. (A) Schematic representation of the bispecific antibodies targeting CD122 or CD132 on one arm and HER2 or MSLN with the other arm. (B) Binding of the bsAbs was tested by direct ELISA using biotynilated CD122 (left), CD132 (middle), HER2 (top right) and hMSLN (bottom right). (C) Binding of the bsAbs on recombinant mouse CD122 (left), and mouse CD132 (right). Binding is measured through fluorescence with Amplex Red and secondary antibodies conjugated with hydrogen peroxydase. Graphs show mean ± SD.



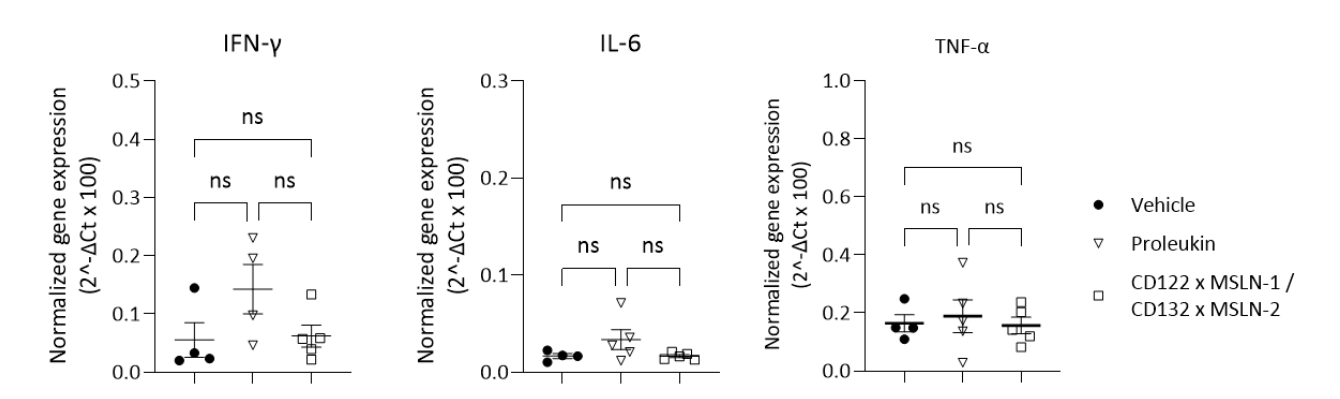
Supplemental Figure S2 Activity was explored using HEK Blue CD122/CD132 reporter cells and measured by colorimetry. (A) Activity was measured with hMSLN coated microspheres and the combination of CD122xMSLN-2 with bsAbs targeting CD132 and different epitopes of MSLN (MSLN-1, MSLN-3 and MSLN-4, left panel), CD122xMSLN-3 with bsAbs targeting CD132 and different epitopes of MSLN (MSLN-1, MSLN-2 and MSLN-4, middle panel) or CD122xMSLN-4 with bsAbs targeting CD132 and different epitopes of MSLN (MSLN-1, MSLN-2 and MSLN-3, right panel). (B) The effect of targeting different TAA epitopes was explored using HER2 targeting bsAbs. CD122 arm was combined with HER2-1 and HER2-3 arms into bsAbs and CD132 arm was combined with HER2-2 and HER-4 arms into bsAbs. These bsAbs were combined to compare the agonistic activity of the different possible combinations. (C) Activity was compared between combinations of bsAbs targeting different HER2 epitopes (CD122xHER-1/CD132xHER2-2 and CD122xHER-2/CD132xHER2-1) or the same HER2 epitope (CD122xHER2-1 /CD132xHER2-1 and CD122xHER2-2/CD132xHER2-2) with HER2 coated microspheres. Graphs show Mean ± SD.



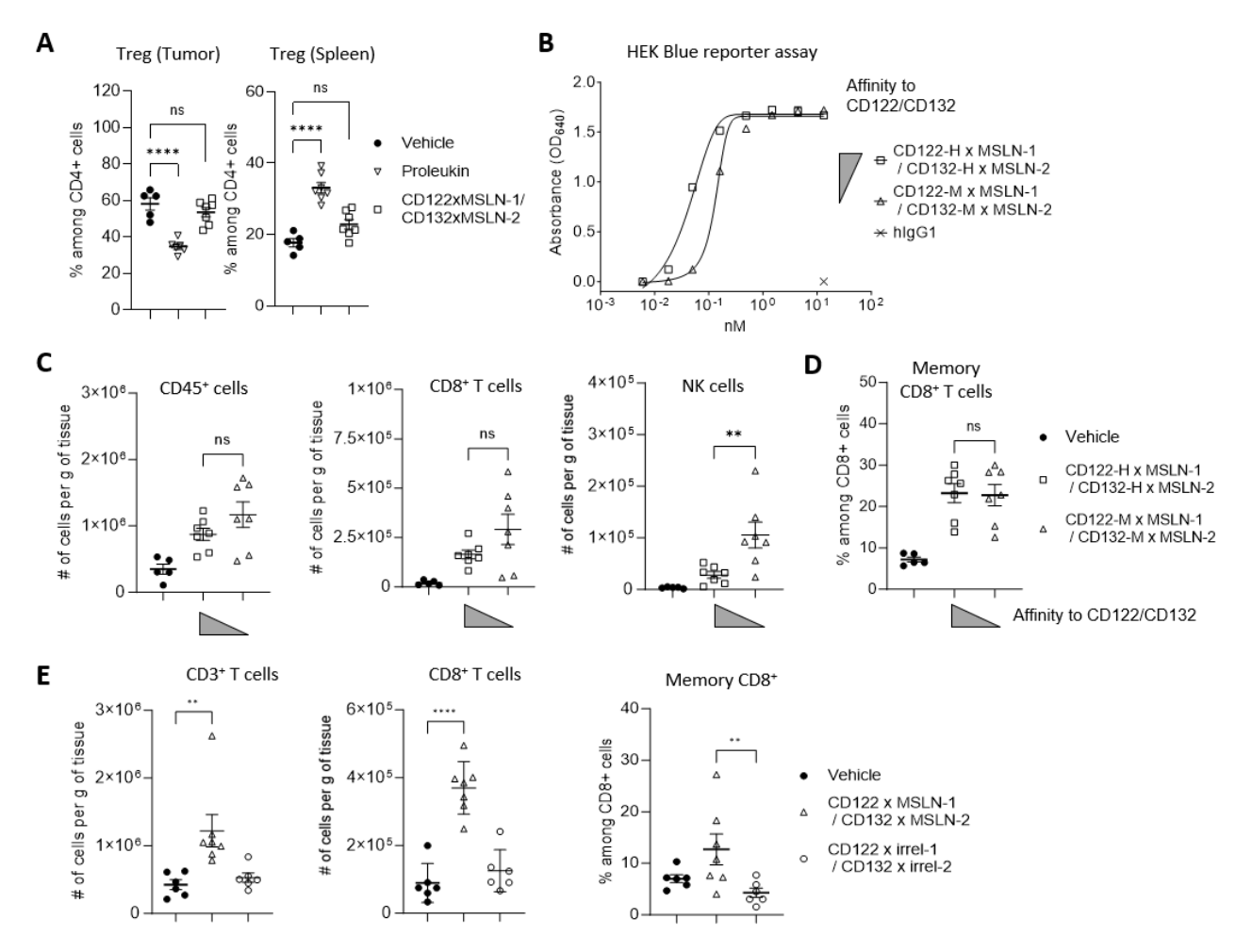
Supplemental Figure S3 To compare the ability of CD122xMSLN-1/CD132xMSLN-2 with an isotype control and proleukin to induce specific killing of tumor cells, T cell dependent cytotoxicity (TDCC) assays were performed. (A-D) Pre-activated human peripheral blood mononuclear cells (PBMCs) were incubated with SH-SY5Y (A), NCI-N87 (B), HPAC (C), and JIMT-1 (D) and under different test conditions. Specific killing was calculated by subtracting unspecific killing measured in control wells with PBMCs and cancer cell lines only. Graphs show Mean ± SD. (E) Induction of pSTAT5 in isolated human NK cells incubated with NCI-N87 cancer cells and CD122xMSLN-1, CD132xMSLN-2, CD122xMSLN-1/CD132xMSLN-2 pair and Proleukin. Data are represented as Geomean ± SEM.



Supplemental Figure S4 Gating strategy for flow cytometry *ex vivo* tissue analysis of tumor-bearing hCD122/hCD132 transgenic mice. Example of a gating approach to phenotype the main tumor infiltrating lymphocytes and NK cells. Panel of antibodies used are listed in supplementary Table 4.

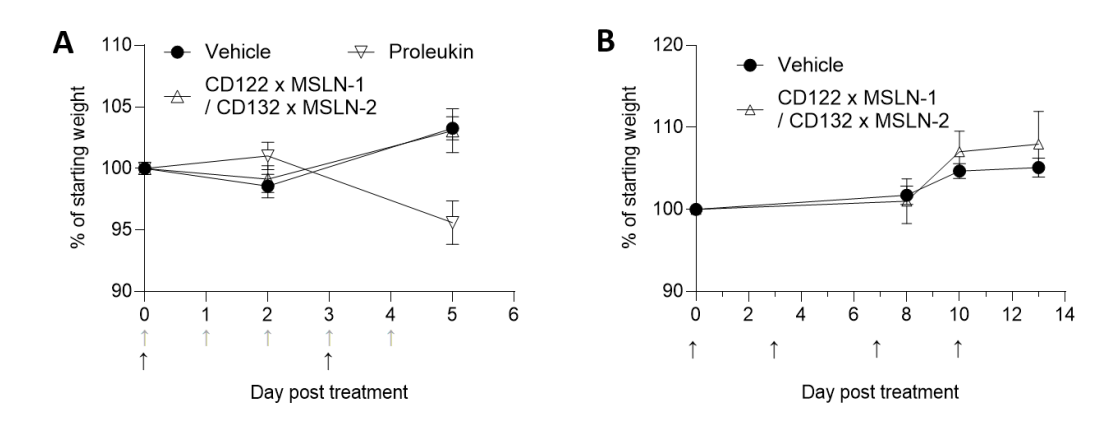


Supplemental Figure S5. Cytokine profile in the tumor post-treatment. hCD122/hCD132 transgenic mice were engrafted with hMSLN-expressing MC38 colon cancer cells. Mice were treated with vehicle control (n = 4), Proleukin (*i.p.* 3 mg/kg for 5 consecutive days, n = 5) or CD122xMSLN-1/CD132xMSLN-2 bsAb pair (*i.v.* 10 mg/kg, twice (d0 and d3), n = 5). mRNA were extracted from each tumor at day 5 post-treatment initiation. IFN- γ , IL6 and TNF- α mRNA cytokines levels were measured by Q-PCR and compared between treatment groups. Data are represented as mean \pm SEM.

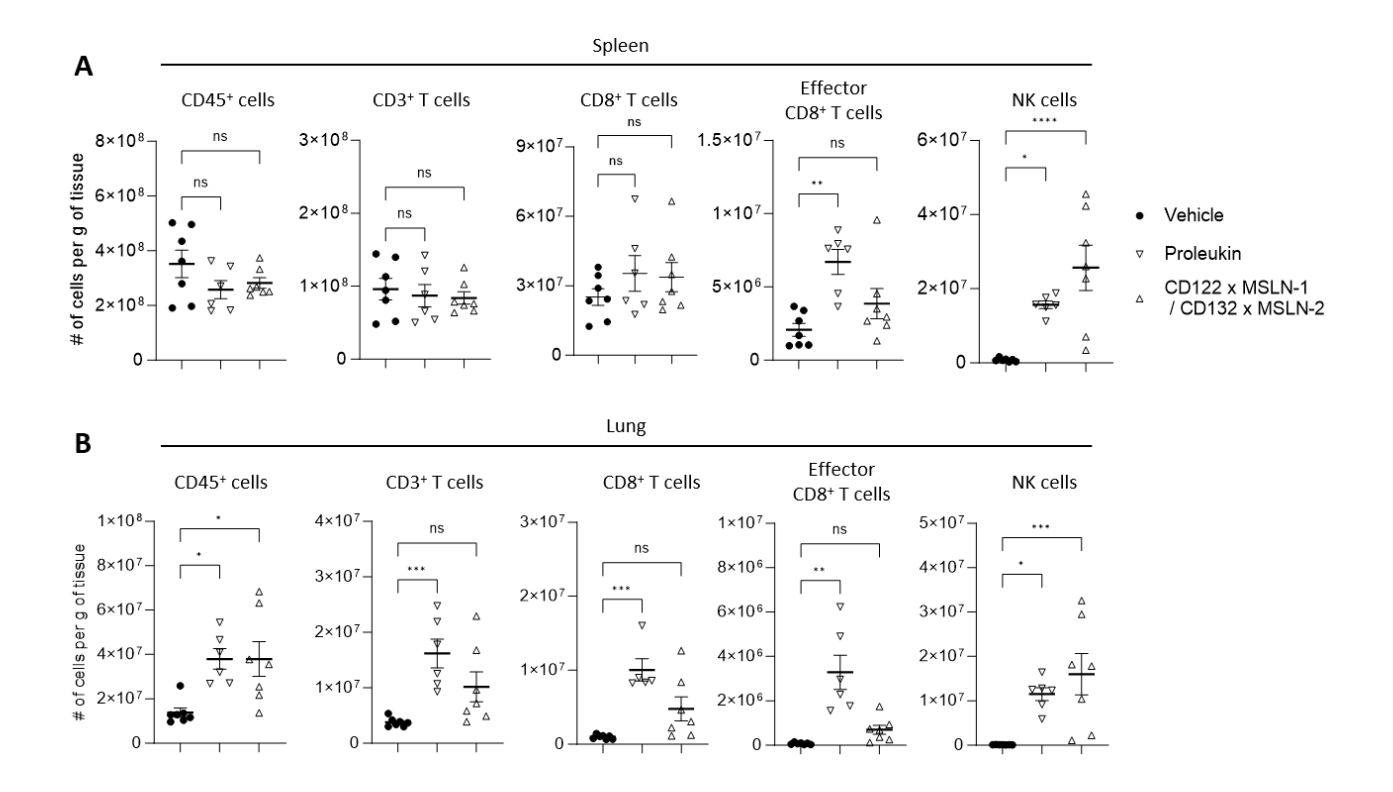


Supplemental Figure S6 (A) Proportion of CD25⁺FoxP3⁺CD4⁺ Tregs in the tumor (left) and the spleen (right) was measured 5 days after the start of treatment with Proleukin (i.p. dose of 3 mg/kg for 5 consecutive days, 6 mice) or combined CD122xMSLN-1/CD132xMSLN-2 bsAbs (i.v. dose of 10 mg/kg each at day 0-3 post-treatment initiation, 7 mice). (B) IL2/IL-15 in vitro reporter activity comparing pairs of bsAbs carrying the high or the medium affinity CD122/CD132 binding arms. Assay was done by co-incubating MSLN-coated beads as a provider of the target and IL-2 reporter cell line as effector cells (C-D) Immune profiling of tumor infiltrating immune cells in hCD122/hCD132 transgenic mice engrafted with hMSLN-expressing MC38 colon cancer cells. Tumors were analyzed at day 9 post-treatment with the combined CD122-HxMSLN-1/CD132-HxMSLN-2 versus CD122-MxMSLN-1/CD132-MxMSLN-2 bsAbs (i.v. dose of 10 mg/kg each at day 0 and 3 post-treatment initiation, 7 mice). Shown are (C) absolute counts of CD45⁺, CD8⁺ and NK cells, (D) proportion of central memory CD8+ T cells (CD44+/CD62L+). (E) *In vivo* activity comparison between MSLN- versus irrelevant-targeted bsAb pairs (respectively, CD122xMSLN-1/CD132xMSLN-2 and CD122xirrel-1/CD132xirrel-2). Shown are absolute counts of CD3⁺, CD8⁺ and proportion of central memory CD8+ T cells

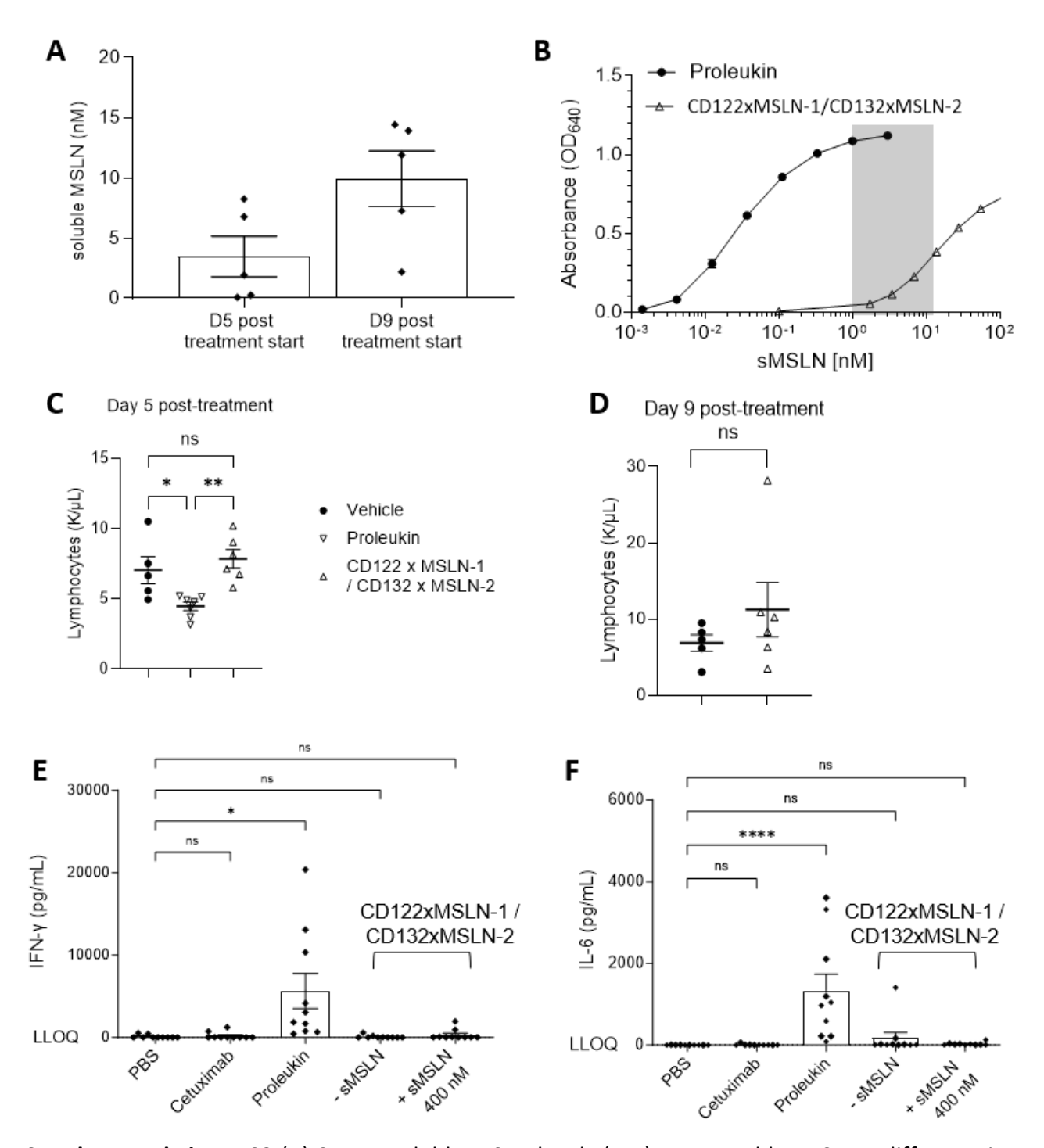
(CD44 $^+$ /CD62L $^+$). Data are represented as mean \pm SEM. Statistical analysis performed using a one-way ANOVA with multiple comparison test.



Supplemental Figure S7. Body weight post-treatment initiation of hCD122/hCD132 transgenic mice engrafted with hMSLN-expressing MC38 colon cancer cells. (A) Mean body weight post-Vehicle (i.v. dose of PBS at day 0-3 post treatment initiation, 7 mice), Proleukin (i.p dose of 3 mg/kg for 5 consecutive days, grey arrows, 6 mice) or combined CD122xMSLN-1/CD132xMSLN-2 bsAbs (i.v. dose of 10 mg/kg each at day 0-3 post-treatment initiation, Black arrows, 7 mice) until day 5 post treatment initiation. (B) Mean body weight post-Vehicle or combined CD122xMSLN-1/CD132xMSLN-2 bsAbs (i.v. at day 0-3-7-10 post-treatment initiation). Data are represented as mean ± SEM.

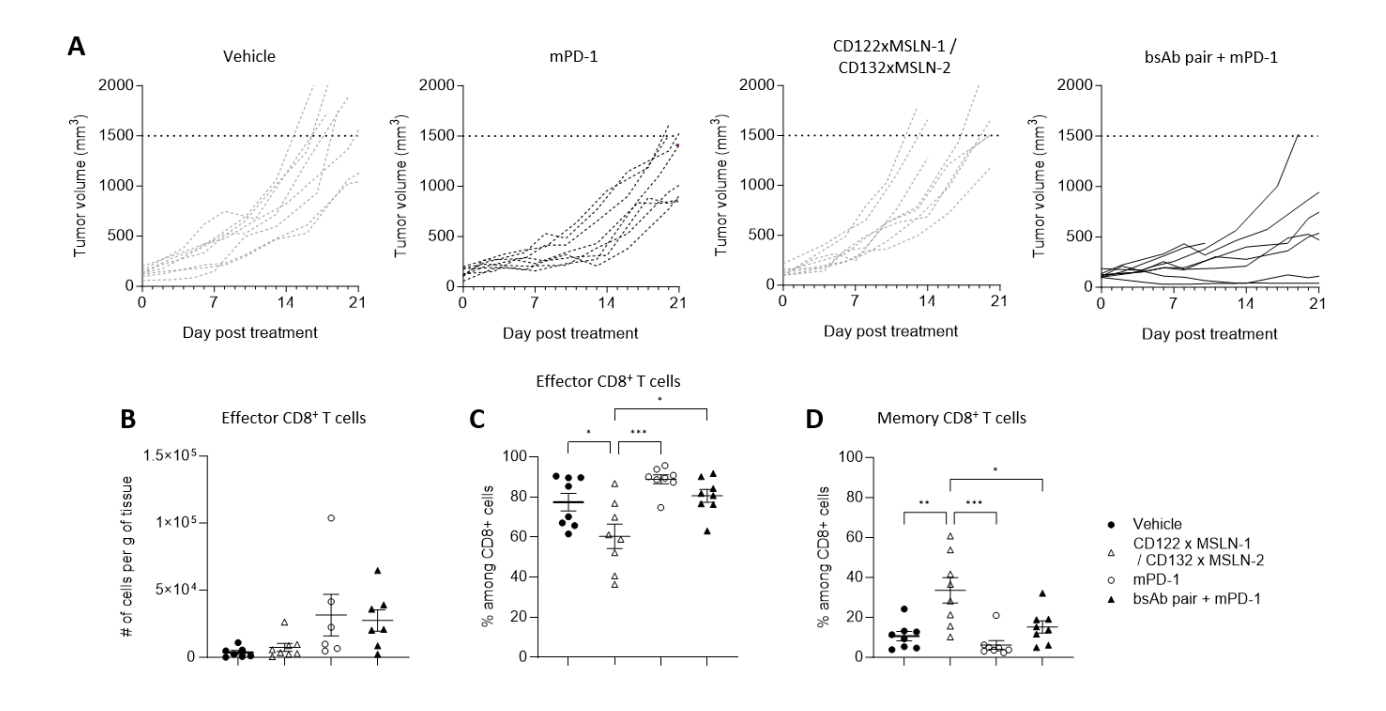


Supplemental Figure S8 Immune profiling of infiltrating immune cells in (A) the spleen and (B) the lung of hCD122/hCD132 transgenic mice engrafted with hMSLN-expressing MC38 colon cancer cells. Tissue samples were analyzed by flow cytometry at day 5 post-treatment with Proleukin (i.p. dose of 5 mg/kg for 5 consecutive days, 6 mice) or combined CD122xMSLN-1/CD132xMSLN bsAbs (i.v. dose of 10 mg/kg each at day 0 and 3 post-treatment initiation, 7 mice) relative to vehicle control group (7 mice). For each tissue sample (spleen or lung), shown are the absolute counts of CD45⁺, CD3⁺, CD8⁺ T cells, effector CD8⁺ T cells (CD44⁺/CD62L⁻) and NK cells. Data are represented as mean ± SEM. Statistical analysis performed using a one-way ANOVA with multiple comparison test.

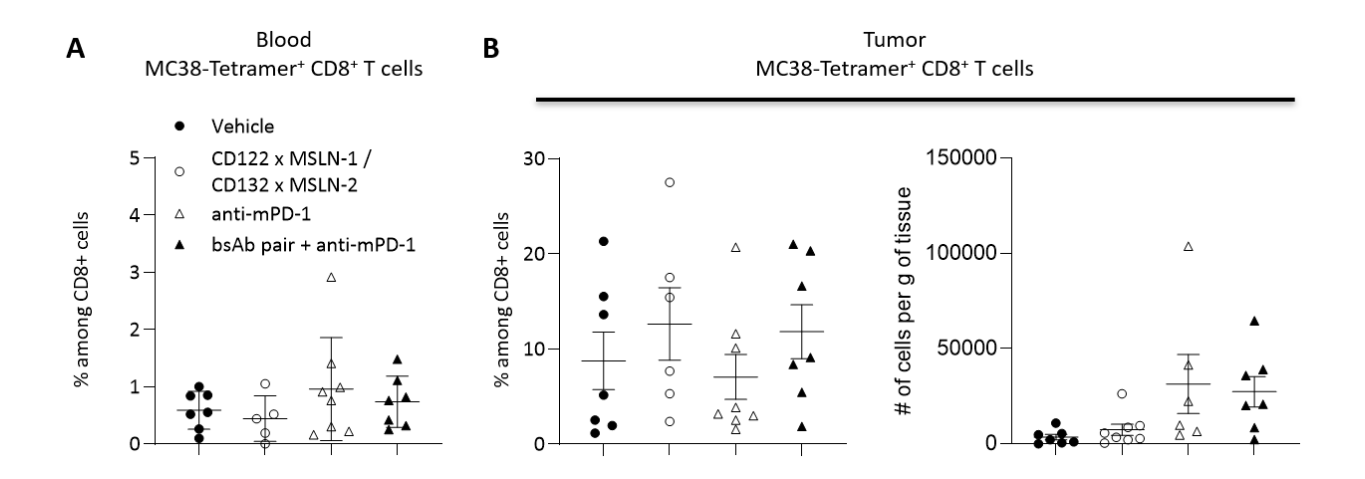


Supplemental Figure S9 (A) Serum soluble MSLN levels (nM) measured by MSD at different time points (day 5 and 9 post treatment initiation with vehicle control, 5 mice each) in hCD122/hCD132 transgenic mice engrafted with hMSLN-expressing MC38 colon cancer cells. sMSLN was measured using a customized MSD sandwich format that utilizes two MSLN-specific monoclonal antibodies as described in supplementary material and methods. (B). HEK Blue IL2R reporter cell line were incubate with a dose range of sMSLN and a fixed dose of CD122/CD132xMSLN bsAbs (17.4 ug/mL). The grey area represents the concentration of sMSLN found in the sera of hCD122/hCD132

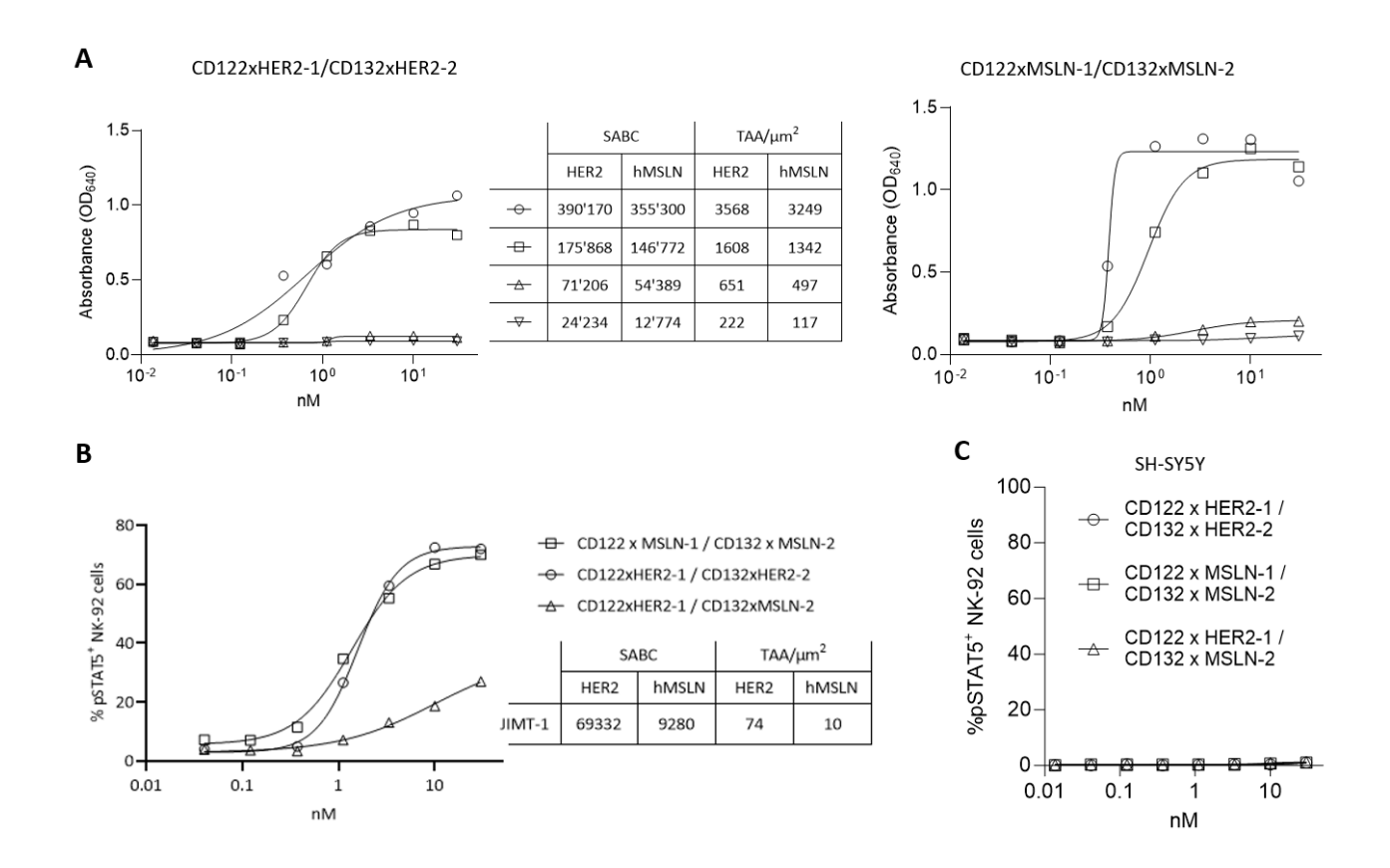
transgenic mice engrafted with hMSLN-expressing MC38 colon cancer cells at day 5 and day 9 post treatment initiation. (C-D) hCD122/hCD132 transgenic mice were engrafted with hMSLN-expressing MC38 colon cancer cells. Mice were treated with vehicle control (n = 5), Proleukin (*i.p.* 3 mg/kg for 5 consecutive days, n = 6) or CD122xMSLN-1/CD132xMSLN-2 bsAb pair (*i.v.* 10 mg/kg, twice on d0 and d3 post-treatment initiation, n = 6). On (C) day 5 and (D) 9 post-treatment initiation, peripheral blood was analyzed using the ProCyte Hematology Analyzer. (E-F) Fresh human whole blood (10 healthy individual donors), was incubated overnight with fixed doses of Cetuximab, Proleukin, combined CD122/CD132xMSLN bsAbs in absence or presence of soluble human MSLN added at 400 nM final concentration. Plasma samples were analyzed to measure levels of (E) IFN- γ and (F) IL-6. Graphs show mean values \pm SEM and statistical significance between treatment groups were determined using a one-way ANOVA with multiple comparison test.



Supplemental Figure S10 (A) Individual tumor growth curves post treatment initiation of hCD122/hCD132 transgenic mice engrafted with hMSLN-expressing MC38 colon cancer cells. (B-D) Flow cytometry analysis of TILs including (B) the absolute counts of effector CD8+ T cells (CD44+/CD62L-), (C) the percentage of effector CD8+ T cells among total CD8+ T cells and (D) proportion of central memory CD8+ T cells (CD44+/CD62L+). Data are represented as mean ± SEM. Statistical analysis performed using a one-way ANOVA with multiple comparison test.



Supplemental Figure S11. (A) Percentage of circulating MC38-tetramer-specific (KSPWFTTL tetramer) CD8⁺ T cells in blood, (B) percentage and absolute counts of tumor infiltrating MC38-tetramer⁺ intra-tumoral CD8⁺ T cells in hCD122/hCD132 transgenic mice engrafted with hMSLN-expressing MC38 colon cancer cells at day 9 post treatment initiation. Data are represented as mean ± SEM.



Supplemental Figure S12 (A) HEK Blue CD122/CD132 reporter cells were incubated with CD122xHER2-1/CD132xHER2-2 (top panel) and CD122xMSLN-1/CD132xMSLN-2 (bottom panel) and microspheres coated with different quantities of MSLN, HER2 and an irrelevant protein. (B) Dosedependent induction of pSTAT5 in NK-92 cells by CD122xHER2-1/CD132xHER2-2, CD122xMSLN-1/CD132xMSLN-2 or CD122xHER2-1/CD132xMSLN-2 bsAb pairs following incubation with HER2 and MSLN expressing JIMT-1 cells. (C) pSTAT5 levels in NK-92 cells after incubation with TAA- SH-5YSY cells (Supplemental table 2) and CD122xHER1/CD132xHER2-2, CD122 MSLN-1/CD132xMSLN-2 and CD122xHER2-1/CD132xMSLN-2.

SUPPLEMENTAL TABLES

Supplemental Table 1 – List of recombinant proteins and reagents used in the current study

Recombinant cytokines or Reagents	Vendor	Cat No.	Usage	
Recombinant human IL-2	Peprotech	200-02	In vitro	
Recombinant human IL-15	Peprotech	200-15	In vitro	
Proleukin (Aldesleukin)	Farmamondo	100009320	In vivo, in vitro	
Anti-mPD-1 (clone RMP1- 14)	BioXCell	BE0146	In vivo	
Streptavidin-coated beads	Polysciences	24158-5	In vitro	
Biotinylated-hHER2	Acrobiosystems	HE2-H82E2	In vitro	
Biotinylated-hMSLN	Produced in house	?	In vitro	
Biotinylateu-mvistiv	Acrobiosystems	MSN-H82E9-200ug	In vitro	
Quanti Blue™ Solution	Invivogen	rep-qbs	In vitro	
BD Phosflow Fix Buffer I	BD Biosciences	557870	In vitro Flow cytometry	
BD Phosflow Perm Buffer III	BD Biosciences	558050	In vitro Flow cytometry	
Qifikit	Agilent Technologies	K007811-8	In vitro Flow cytometry	
H4G5-Trastuzumab	Produced in house	•	In vitro killing assay	
CD3 Monoclonal Antibody (OKT3)	ThermoFisher Scientific	16-0037-85	In vitro killing assay coating	
EasySep Human NK Cell Isolation Kit	StemCell	17955	In vitro ADCC	
CellTiter-Glo® Luminescent Cell Viability Assay	Promega AG	G9242	In vitro killing assay	
Tumor dissociation kit, mouse	Miltenyi Biotec	130-096-730	Ex vivo for Flow cytometry	
Phorbol 12-myristate 13-acetate	Sigma-Aldrich	P8139-1MG	Ex vivo Flow cytometry	
Ionomycin	Sigma-Aldrich	19657-1MG	Ex vivo Flow cytometry	
GolgiStop Protein transport inhibitor	BD Biosciences	554724	Ex vivo Flow cytometry	
MSD U-PLEX Biomarker	MSD	C0065-2	Ex vivo & plasma	
Lympholyte-M	Cedarlane	CL5035	Ex vivo Flow cytometry	
Collagenase, Type IV	Gibco	17104019	Ex vivo Flow Cytometry	

Bovine pancreas Deoxyribonuclease I (DNAse I)	Sigma-Aldrich	DN25-1G	Ex vivo Flow Cytometry
FoxP3 Transcription Factor staining Buffer Set	ThermoFisher Scientific	00-5523-00	Ex vivo Flow cytometry
Cetuximab	Eli Lilly and Company	LY2939777	Ex vivo Whole Blood

Supplemental Table 2 – List of effector and cancer cell lines used in the current study

Cell line (Vendor, cat No.)	Origin	Type of cells	Human MSLN density (SABC)	Human HER2 density (SABC)	Culture Medium
NK 92 (DSMZ, ACC488)	NK lymphoma	Effecto r cells	N/A	N/A	MEM alpha medium supplemented with 12.5 % heat-inactivated fetal calf serum (FCS HI), 12.5 % heat-inactivated horse serum (HI), 2 mM L-glutamine and 5 ng/mL hIL-2
HEK-Blue IL-2 (Invivogen, hkb- il2)	IL2R Reporter cells	Effecto r cells	N/A	N/A	DMEM with 4.5 g/L glucose, 2 mM L-glutamine, 10% FCS HI, 25 μg/ml
HEK-Blue CD122/CD132 (Invivogen, hkb- il2bg)	IL2R Reporter cells	Effecto r cells	N/A	N/A	gentamycin and 100 μg/mL normocin and 1 μg/mL puromycin and 1xCLR selection
NCI-N87 (ATCC, CRL-5822)	gastric carcinoma	Cancer cells	20′103	401'376	RPMI 1640 medium with 10 % FCS HI and 2 mM L-glutamine
JIMT-1 (ATCC, ACC589)	breast carcinoma	Cancer cells	9'280	69'332	DMEM (High Glucose) medium containing 10% FCS HI
SH-SY5Y (ECACC, 94030304)	Neuro- blastoma	Cancer cells	0	0	Ham's F12 and EMEM (EBSS) (1:1) supplemented with 2 mM L-glutamine, 1 % non-essential amino acids (NEAA), and 15 % fetal bovine serum (FBS)
MDA-MB-468 (ATCC, ACC738)	Breast carcinoma	Cancer cells	0	0	L-15 Medium with 10 % FCS HI and 2 mM L-glutamine
HPAC (ATCC, CRL-2119)	pancreas carcinoma	Cancer cells	14'000	4'000	DMEM F12-HAM medium supplemented with 5 % FCS HI, 2 mM L-glutamine, 15 mM HEPES, 0.5 mM sodium pyruvate, Insulin-Transferrin-Selenium-Ethanolamine 1X, 40 ng/mL hydrocortisone, and 10 ng/mL

					mouse epidermal growth factor (mEGF)
MC38-hMSLN (Biocytogen, ZHY20121216)	Mouse colon carcinoma expressing hMSLN	Cancer cells	100'00	0	DMEM (High Glucose) +10 % FCS HI + 2 mM L-Glutamine +1mM pyruvate + 10mM HEPES + 1X NEAA
MC38-hHER2 (Biocytogen, ZJY20230115)	Mouse colon carcinoma expressing hHER2	Cancer cells	0	44'000	DMEM (High Glucose) +10 % FCS HI + 2 mM L-Glutamine +1mM pyruvate + 10mM HEPES + 1X NEAA

N/A: not applicable, SABC: specific antibody binding capacity

Supplemental Table 3 – List of antibodies used in the current study to characterize pSTAT5

induction via flow cytometry.

Antibody	Fluorochrom e	Vendor	Cat No.	Clone	Final dilution	Localization
live dead	Near-IR	ThermoFishe r Scientific	L34976	N/A	1:1000	intracellular
Fixable Viability Dye	eFluor 506	ThermoFishe r Scientific	65-0866-18	N/A	1/1000	intracellular
Human BD Fc Block	N/A	BD Biosciences	564220	Fc1	3 μL/test	extracellular
CD45	V500	BD Biosciences	560777	HI30	1:100	extracellular
CD45	PE-Cy7	BD Biosciences	557748	HI30	1:100	extracellular
CD3	AF594	Biolegend	300446	UCHT1	1:100	extracellular
CD4	BV421	BD Biosciences	562424	RPA-T4	1:100	extracellular
CD8	APC-Cy7	BD Biosciences	557834	SK1	1:100	extracellular
CD14	efluor 506	ThermoFishe r Scientific	69-0149-42	61D3	1:100	extracellular
CD19	efluor 506	ThermoFishe r Scientific	69-0199-42	HIB19	1:100	extracellular
CD56	efluor 506	ThermoFishe r Scientific	69-0566-42	TULY56	1:100	extracellular
pStat5 (pY694)	AF488	BD Biosciences	562075	47	4 μL/test	intracellular

Foxp3	AF647	BD Biosciences	560045	259D/C7	10 μL/test	intracellular	
		biosciences			μι/ ιεςι		

Supplemental Table 4 – List of reagents and antibodies used in the current study for ex vivo immune profiling via flow cytometry

Antibody	Fluorochrom e	Vendor	Cat No.	Clone	Final dilution	Localization
Fixable Viability Dye	eFluor506	eBioscience	65-0866-18	N/A	1:1000	intracellular
Rat anti- mouse CD16/CD32 (mouse Fc Block)	N/A	BD Biosciences	553142	2.4G2	1:50	extracellular
CD45	BV421	BD Biosciences	563890	30-F11	1:100	extracellular
CD3	AF594	BioLegend	100240	17A2	1:100	extracellular
CD4	PerCP-Cy5.5	BioLegend	100434	GK1.5	1:100	extracellular
CD8a	АРС-Н7	BD Biosciences	560182	53-6.7	1:100	extracellular
NK1.1	PE	eBioscience	12.5941-83	PK136	1:100	extracellular
NKp46	AF700	eBioscience	56-3351-82	29A1.4	1:100	extracellular
CD44	PE-Cy7	eBioscience	25-0441-82	IM7	1:100	extracellular
CD62L	AF647	BioLegend	104421	MEL-14	1:100	extracellular
Foxp3	PE-Cy7	eBioscience	25-5773-82	FJK-16s	1:100	intracellular
GZB	AF647	BioLegend	515406	GB11	1:100	intracellular
Ki67	AF488	eBioscience	53-5698-82	SolA15	1:100	intracellular
CD25	BV711	eBioscience	407-0251-82	PC61.5	1:100	extracellular
CD4	PerCP- eFluor710	eBioscience	46-0041-82	GK1.5	1:100	extracellular
CD8a	FITC	ThermoFisher Scientific	MA5-16759	KT15	1:100	extracellular
H-2Kb ß- Gal tetramer- DAPIYTNV	APC	MBL	TB-M501-2	N/A	1:25	extracellular

H-2Kb						
MuLV-p15E	APC	NADI	TB-M507-2	N/A	1:25	extracellular
Tetramer-	APC	MBL	10-101307-2	IN/A	1.23	extracellular
KSPWFTTL						
Goat anti-		ThermoFisher				
human IgG	AF647	Scientific	A21445	N/A	1:200	extracellular
H+L		Scientific				

SUPPLEMENTAL METHODS

Reagents and cell lines

The reagents used in this study are included in Supplementary Table 1 and the list of detection antibodies are listed in Supplementary Table 3. All effector and target cell lines were cultured at 37°C 5% CO₂ in their appropriate cell culture medium and are listed Supplementary Table 2.TAA expression at the surface of cancer cell lines was measured using Quantitative Analysis kits (QIFIKIT), following manufacturer's recommendation (see Supplementary Table 2 for quantification data).

PBMCs and NK cells isolation

Buffy coats purchased from the "Centre de transfusion sanguine de Genève (CTS)". PBMCs are isolated from buffy coats with SepMate™ PBMC isolation Tubes according to manufacturer's recommendations. NK cells were isolated using EasySep™ Human NK Cell Isolation Kit from isolated PBMCs.

CD132xTAA and CD132xTAA bispecific antibody (bsAb) engineering

All bsAbs carried an inactive human IgG1 Fc (LALA PA mutations: L234A/L235A/P329A). We used two distinct technologies to generate the bsAbs: Firstly, we used phage display to produce unique full-length IgG in which the specificity is driven by a diversified light chain that is coupled to an invariant dummy heavy chain. We generated κ antibodies against CD122 and CD132 and λ antibodies against hMSLN and hHER2. The light chains of κ and λ antibodies were combined with the heavy dummy chain in proprietary tri-cistronic vectors. We transfected CHO or Expi293 cells to generate bsAbs without the need of additional mutations or linkers. The antibodies are purified through a 3-step process described by Fischer and colleagues. (Fischer N et al, 2015). Secondly, CDR sequences of anti-CD132 (P1A3), anti-CD122 (P2C4) and anti-hHER2 (Pertuzumab and Trastuzumab) were obtained from published sequences (WO 2017/021540 Al and US 2006/0275305 A1 respectively). The CDR sequences were synthesized by Eurofins and combined in proprietary tetracistronic vectors using the Knob-into-Hole (KiH), CrossMAb technologies (US 2017/0129962 A1). Anti-HER2 were inserted into the knob arm and anti-CD122/CD132 were inserted into the hole arm. Lastly, we combined the CDR of some of our κ and λ antibodies targeting CD122 and CD132 with the anti-HER2 arms (Trastuzumab and Pertuzumab) into CrossMab antibodies. We transfected CHO cells and purified KiH through a two-step process. KiH were purified using CaptureSelect™ FcXL Affinity Matrix and CaptureSelect™ IgG-CH1 Affinity Matrix successively and were eluted using glycine pH 3.0 buffer and desalted against 25 mM Histidine/125 mM NaCl pH 6.0 buffer in 50 kDa Amicon Ultra Centrifugal filter units. The quality of κλ-bodies and KiH was verified by SEC-HPLC, electrophoresis in denaturing conditions, IsoElectric Focusing gel and by Agilent 2100 Bioanalyzer with the Protein 80 kit. Aggregates levels above 5 % were removed by size exclusion chromatography.

Measurement of bsAbs binding to their respective targets by ELISA

Binding specificity of all bsAbs was evaluated by direct ELISA. Streptavidin-coated 96-well plates were coated with 50 μ L/well of 1 μ g/mL biotinylated CD122, CD132, hHER2, hMSLN and an irrelevant protein. Binding of bsAbs to coated proteins was measured using HRP-linked goat antihuman IgG-Fc γ and Ample χ TM UltraRed Reagent. Data were acquired using a Synergy HT (Biotek) at the following wavelengths: excitation: 530/25, emission: 590/35.

Streptavidin microspheres coating

Streptavidin-coated beads were incubated with biotinylated proteins. Biotinylated-hHER2, biotinylated-hMSLN and an irrelevant biotinylated protein were incubated separately, to obtain hHER2-, hMSLN- and irrelevantly coated microspheres, or together in different ratios, to produce hHER2/hMSLN/irrelevant protein-coated microspheres with variable target densities.

Flow cytometry acquisition and analysis

All flow cytometry data acquired during this study was acquired on a CytoFLEX S V4-B2-Y4-R3 Flow cytometer and data was analyzed using FlowJo 10.8.1 software.

Detection of hMSLN & hHER2 protein copy number on cell lines and microspheres

Selected human cancer cell lines (NCI-N87, HPAC, JIMT-1, HPAC, MDA-MB-468, SH-SY5Y cells) and coated streptavidin microspheres were incubated with an isotype control (#0102-01) anti-human MSLN (#MAB32653) or anti-human HER2 antibodies (#MAB9896) and with the secondary FITC-conjugated antibody provided with the kit. The standard beads from QIFIKIT were also stained with the same secondary antibody. Samples were analyzed on a CytoFLEX S V4-B2-Y4-R3 Flow cytometer and data were analyzed using FlowJo software. The MFI of standard beads was used to generate a standard curve. The MFI of stained cells and coated streptavidin microspheres were used to calculate the hMSLN or hHER2 copy number on cells using the standard curve and following manufacturer's instruction. Values are provided as SABC (specific antigen binding capacity.

Mouse model

hCD122/hCD132 KI mice were purchased from Biocytogen Co., Ltd. (all on a C57BL/6 background). In these mice, the exons 2-8 of mouse CD122 gene that encodes the extracellular domain were replaced by human CD122 exons 2-8. The exons 1-8 of mouse CD132 gene that encodes the full-coding region sequences were replaced by human CD132 exons 1-8. Phenotypic analysis of mice

showed that, in contrast to mCD122/mCD132, hCD122/hCD132 were detectable in all mouse T cells and NK cells. Furthermore, the humanization of these genes does not change the overall development, differentiation or distribution of immune cell types in spleen, blood and lymph node (Biocytogen's data). Mice were 8–9 weeks old at the start of studies. Experiments were performed in accordance with the Swiss Federal Veterinary Office guidelines and approved by the Cantonal Veterinary Office (approved protocol: #GE319). Upon reception, mice underwent a 1-week acclimatation period in the laboratory environment to reduce stress and variability, particularly, important given that transgenic mice were important from Biocytogen Co., Ltd, and needed time to adjust to their new surroundings. Mice were housed in cages with soft bedding and environmental enrichment was provided through the inclusion of cardboard rolls to promote natural behaviors. Randomization was used to allocate mice to groups and based on tumor volume (tumor volume mean per group not statistically different). The number of animals used in each group of experiments was selected based on statistical power calculations to ensure sufficient sample size for reliable and valid results while minimizing animal use in line with ethical considerations. A preliminary conducted to evaluate the amplitude of tumor growth in hCD122/hCD132 Tg mice, which allowed for efficient assessment of tumor growth variability informing the sample size calculations for the main study. Animal were excluded a priori if they displayed pre-existing health conditions or abnormal behavioral criteria. Mice were also excluded if tumor sizes (measured using a caliper) were not within the predetermined range following randomization to ensure balanced distribution of tumor sizes across experimental groups. No mice met exclusion criteria, and therefore all animals were included in the final analysis. To minimize potential confounders, treatment groups were mixed within mice cages, ensuring that environmental factors such as cage location or handling did not influence the experimental outcomes. Score sheets were filled 3 times per week to monitor animal welfare and to implement intervention to reduce pain, suffering and distress (Refine and Humane endpoints). Finally, the researchers conducting the treatments and data collection were blinded to the group allocation, while only the study coordinator had access to the randomized sequence to prevent bias. A protocol (including the research question, key design features, and analysis plan) was not prepared before the study.

Measurement of human soluble MSLN in the sera of hCD122/hCD132 Tg mice engrafted with hMSLN-expressing MC38 colon cancer cells

The assay is a validated biomarker MSD-based assay designed in a sequential format capable of detecting free human sMSLN. After the minimum required dilution, samples were added to a

streptavidin MSD plate previously coated with the biotinylated capture antibody. Then, Sulfo-TAGTM-conjugated detection antibody was added, and electrochemiluminescence (ECL) was measured on the MSD platform following manufacturer's recommendations.

Ex vivo single cell suspension preparation for flow cytometry analysis

For flow cytometry single cell suspensions from tissues were prepared. Single-cell suspension from spleen was prepared by mechanical digestion with the gentleMACSTM Dissociator, followed by red blood cell lysis using ACK buffer (Ammonium-Chloride-Potassium). Lungs were enzymatically digested in collagenase IV (Gibco) and DNase I (Sigma-Aldrich) for 30 min at 37°C, followed by mechanical digestion with the gentleMACSTM Dissociator. Tumors were processed into single-cell suspensions using the mouse tumor dissociation kit from Miltenyi Biotec according to the manufacturer's instructions. Erythrocytes, majority of dead cells and debris were then removed from tumor-cell suspensions using a density separation medium (Lympholyte®-M, Cedarlane). Tissue-cell suspensions were filtered through a 70 μm Nylon filter (BD Falcon) and counted using a cell viability analyzer (Vi-CELL).

Ex vivo flow cytometry analysis of tumor specific T cells.

Single cell suspensions were stained for viability, washed with staining buffer and incubated with purified rat anti-mouse CD16/CD32. Fluorescent-conjugated antibody mix and MC38-specific tetramers (extracellular markers - Supplemental Table 4) were added to the cell suspension. Stained cells were washed and fixed.

Ex vivo qPCR analysis of tumor tissue.

Total RNA from tumor was extracted with the RNeasy Mini Kit (Qiagen) according to the manufacturer's instructions. Reverse transcription was performed by using High-Capacity cDNA Reverse Transcription kit (Applied Biosystems). Quantitative PCR (Q-PCR) was performed in triplicates using SYBR Green Master Mix (Applied Biosystems). Data were acquired and analyzed with LightCycler® 480 Real-Time PCR System (Roche). Sequences primers are: β-actin, forward: AGCCTTCCTTCTTGGGTATGG and reverse: CAACGTCACACTTCATGATGGAAT; GAPDH, forward: CATGGCCTTCCGTGTTCCTA and reverse: TGTCATCATACTTGGCAGGTTTCT; IFNγ, forward: CAACAGCAAGGCGAAAAAGG and reverse: CCTGTGGGTTGTTGACCTCAA; IL-6: forward, TCGGAGGCTTAATTACACATGTTC and reverse: TGCCATTGCACAACTCTTTTCT; TNF α , forward: GCCACCACGCTCTTCTGTCT and reverse: GGTCTGGGCCATAGAACTGATG. The relative expression levels were calculated as 2^(Ct gene-Ct HKG) x 100 with β-actin and GAPDH RNA as the housekeeping gene endogenous control.

8 Discussion

Cancer has cemented itself as one of the primary challenges in advancing public health. The increasing scientific interest in cancer therapies and the progress in our understanding of cancer immunology have led to the development of cancer immunotherapies and better patient prognosis.² Among immunotherapies, ICI have made the most significant impact and are now used as first-line treatments for several cancer indications.^{289,290} While being the first to enter the clinic, cytokine therapies have seen limited use in cancer.²⁷³ IL-2 and IL-15 signaling are desirable targets in immunotherapies for their described effects on NK and CD8+ T cells. Despite its approval by the FDA, the clinical use of Proleukin, a human recombinant IL-2, is limited by its shortcomings including severe toxicity, short half-life, and preferential engagement of Tregs due to their constitutive expression of CD25. N-803, an engineered IL-15 targeting superkine recently approved in combination with BCG for treating bladder cancer,⁴⁰² bypasses the effect of systemic cytokine administration through topical intravesical administration. This local administration strategy does not apply to many other cancer indications, and harnessing IL-2/IL-15 effectively while avoiding its side effects remains challenging.

In this study, we presented a novel approach that uses bsAb pairs to harness IL-2/IL-15 signaling, avoiding limitations associated with recombinant IL-2 and IL-15. The first antibody targets CD122 and a TAA, and the second antibody targets CD132 and the same or a different TAA. We used in vitro and in vivo models to show TAA-dependent IL-2/IL-15 activation and antitumoral activity. The TAA-dependent feature of our bsAb pairs restricts IL-2/IL-15 activation inside the tumor and thus does not induce systemic toxicity, a hallmark of traditional IL-2/IL-15 therapies, which is mainly linked to the peripheral activation of immune cells and the release of inflammatory cytokines in the circulation. Molecules like WTX-214 and RO7284755 use clever strategies to focus their activity on the TME but can't entirely avoid peripheral activation. 358,382 The strategy closest to ours in the literature is split-Neoleukin-2/15,³⁸⁸ which is based on Neuleukin-2/15, a not-alpha synthetic IL-2/15 mimetic investigated in phase I clinical trial but discontinued in 2023 for "strategic reasons". split-Neoleukin-2/15 divides Neoleukin-2/15 into two inactive parts that are fused separately to DARPins (small molecules engineered to bind specific targets) and can activate IL-2/15 signaling when combined. The approach was tested in vivo, but the two parts were injected separately in distinct injection sites, suggesting they can combine and become active without binding through their DARPins. This differentiates our approach as our two bsAbs

do not interact with each other directly and become active only in the presence of the TAAexpressing cell.

Our bsAbs were constructed using cross-mAb and κλ-body technology. Both backbones are very close to natural human proteins and are well-tolerated in humans. We introduced mutations in the Fc portion of our bsAbs to abrogate their binding to FcyR and complement receptors but maintain neonatal Fc receptor (FcRn) binding. This strategy allowed us to take advantage of the long half-life of the IgG1 or IgG1-like backbones while avoiding the undesired activation of FcyR-expressing cells and the complement system, which may result in systemic immune activation. Maintaining FcRn binding is crucial to preserving their long half-life. FcRn receptors are expressed at the surface of various tissues and are crucial for the transfer and recycling of antibodies. They are involved in the transfer of antibodies from mother to offspring through epithelial barriers and in the clearance of IgG in the kidneys. 406,407 FcRn prevent the degradation of antibodies by binding internalized antibodies, which prevents their degradation and reroutes them to the surface. 408 Pharmacokinetic (PK) studies have been performed on other molecules with cross-mAb and κλ-body backbones, and we expect our molecules to align with those. 409,410 While we performed no PK studies, we showed a significant accumulation of intratumoral antibodies in the hCD122/hCD132 transgenic mouse model (Article Fig. 3E) 48h after the last i.v. injection, which is well beyond the half-life of recombinant IL-2 and IL-15. While this observation was encouraging, this model would not be ideal for PK or biodistribution studies. The first limitations are the potential immunogenicity and incompatibility of our human antibodies with syngeneic mouse models. Repeated injections of non-mouse antibodies often elicit mouse immune responses and the development of anti-drug antibodies (ADA), leading to toxicity and rapid drug clearance. Supporting this, we observed hunched posture and reduced mobility after injecting the 4th dose in our anti-mPD-1 + bsAbs experiment, which are typical symptoms of an immune response driven by ADA. It's also noteworthy that the binding affinity of human antibodies to murine FcRn is lower and would likely lead to underestimating the molecule's half-life. Another limitation is linked to the possible impact of the genetic mutations on the expression levels and biodistribution of the hIL-2 receptor. We could envisage engineering mouse surrogate antibodies to perform PK and biodistribution studies in tumor-bearing mice. To this end, we could use AB12 (a mMSLN expressing mouse mesothelioma cell line) engrafted BALB/c mice or TRAMP-C3 (a mMSLN expressing mouse prostate adenocarcinoma cell line) engrafted C57/BL6 mice. 411 However, the identification and production of murine antibodies would require significant efforts. A

better model to study PK and biodistribution would be the cynomolgus monkey. Cynomolgus monkeys' physiology and genetics are much closer to those of humans, making them a closer model for the human system. Human antibodies are closely homologous to cynomolgus monkey's antibodies and are less likely to lead to ADA in this system. In addition, all antibodies used in this project cross-react with cynomolgus proteins. Altogether, the antibodies presented in this study are expected to have a much longer half-life than Aldesleukin. While their half-life has not been measured, the dosing would probably align with the favorable schedule of other therapeutic antibodies.

The in vitro and in vivo data presented here also support this approach's superior safety. In vitro, the bsAb pairs induced IL-2/IL-15 signaling and killing of tumor cells exclusively in the presence of their cognate TAA. In our in vivo model, TAA dependent activation of IL-2/IL-15 signaling was observed inside the tumor. Although the bsAb pairs induced some signs of activity outside of tumors in the lungs, the bsAbs were well-tolerated by mice and didn't impact circulating inflammatory cytokines nor their body or organ weights, in contrast to the severe toxicity induced by Proleukin. The extra-tumoral activity we observed is unlikely to be linked to the engagement of the anti-CD122/CD132 arms without binding to the TAA arms as the bsAb pairs targeting an irrelevant protein instead of the TAA did not induce IL-2/IL-15 activation in the TME or in circulation (Article Fig. S5D). Rather, the impact of bsAb pairs on the immune infiltrates in the lung could be due to the recirculation of activated cells from the TME to the lung or a consequence of circulating soluble MSLN (Article Fig. S6B). Regardless, the presence of activated peripheral immune cells did not induce significant lung inflammation nor impact systemic levels of inflammatory cytokines. We could perform additional experiments to verify our hypotheses regarding the origin of the changes observed in the lungs. Multiple sheddases cleave MSLN and release it in the serum, which can be detected in most patients with mesothelioma. 412,413 To avoid the shedding of MSLN, two strategies can be tried. The first consists of knocking out multiple sheddases, which could have other repercussions, as sheddases are involved in signaling and cell adhesion and their disruption has been linked to inflammation and Alzheimer's disease.414 The second strategy is to make MSLN resistant to the sheddases. Sheddases seem to cleave MSLN in a small region close to the plasma membrane. 413 A mutated version of MSLN that is resistant to cleavage by the most predominant sheddase has been reported. 415 Other sheddases would still release some soluble MSLN with this MSLN variant. Engineering a version resistant to all sheddases could be feasible and could help understanding the involvement of sMSLN in peripheral activation but would require significant efforts.

Additionally, the mutations could impact the folding of MSLN and, consequently, the binding of our antibody pairs. We could also replace MSLN with a different TAA that is not shed at the same level. Since we already have bsAbs for HER2, we tried but could not establish an in vivo model due to insufficient HER2 expression on the available engineered human HER2 expressing MC38 mouse tumor cell line.

Using the transgenic hCD122 / hCD132 mouse model, we showed that our pairs of bsAbs induce proliferation and activation of memory CD8+ T cells and NK cells inside TAAexpressing tumors (Fig. 3 B, D). This is different from high doses of Proleukin, where treatment leads to the activation and proliferation of effector CD8⁺ T cells and NK cells.²¹⁹ Our observations are more aligned with not-alpha IL-2 strategies and IL-15 activation, which are less potent activators of IL-2 signaling and favor proliferation and activation of memory CD8+ T cells and NK cells.377 In consistent with the in vivo observations, we showed that our bsAb pairs induce lower levels of pSTAT5 in PBMCs than Proleukin (Fig. 2B). Interestingly, Roche's IL-2 receptor β- and y-chain (IL-2Rβy)-biased agonist fused to anti-PD-1 (RO7284755) induces the differentiation of PD-1+TCF-1+ stem-like CD8+ T cells, which they call better effector CD8+ T cells. 392,394 In future experiments, we could test whether the combination of our bsAbs with anti-mPD-1 leads to CD8+ T cells with a similar phenotype, which might be involved in the tumor growth inhibition we observed. IL-15 signaling favors the proliferation of memory T and NK cells.416 Our bsAb pairs engage CD122 and CD132 with one arm and a TAA with their other arm, which could mimic the trans-presentation of IL-15 by CD215-expressing cells. Presentation of CD215-bound IL-15 is usually accompanied by complementary signals, like DC-derived type III interferons or IL-12, that will be mostly missing with bsAbs binding to TAAs. Additionally, while transpresentation of CD215-IL-15 complexes is important, IL-15 can still engage dimeric CD122/CD132 receptors in cis, which our pairs of bsAbs can't do. It is unlikely that our bsAbs could replace IL-15 cross-presentation, but the effects on the TME are similar. The ability of our bsAbs to bind immune cells and tumor cells simultaneously also resembles the mechanism of TCE. While our approach does not mediate CD3/TCR signaling, our bsAb pairs could retain immune cells near TAA+ cells and favor their elimination. So far, in vitro, we have focused on reporter cells, pSTAT5 quantification, and killing of target cells as a proxy for IL-2/IL-15 signaling. To better understand the signaling induced by our bsAb pairs, we could measure the contribution of PI3K/AKT and MAPK/ERK. Several techniques could be used, but a phosphoproteomic approach would be well-adapted. 417 Knocking out specific downstream factors or kinome profiling that are known to be predominantly crucial for one

of the two cytokines would also be informative. Furthermore, future pSTAT5 experiments should take into account the signal duration and dynamics. When IL-2 binds to its receptor, the complex is internalized to avoid prolonged signaling in the absence of new IL-2.⁴¹⁸ It is possible that the simultaneous binding of the receptor and a protein on a different cell by our bsAb pairs modifies the rate of internalization of the IL-2 receptor and changes the signaling dynamics. We could compare pSTAT5 dynamics among our bsAb pairs, IL-2, and IL-15 in future experiments. Including bsAb pairs with a range of affinities both on the TAA and the CD122/CD132 arms could guide further development of this strategy.

Targeting membrane-proximal epitopes is advantageous for single bsAbs that trans-engage two individual cells.419 The trans-engagement of our bsAbs on target cells and IL-2R expressing cells suggests that the position of the targeted epitopes on the TAA or IL-2Rs may also affect the activity of the bsAb pairs. Our study demonstrated that the potency of the bsAb pairs varied depending on the epitopes targeted. However, we have not identified the general rules underlying these differences (Fig.1D). We observed that HER2-targeting BsAb pairs are more potent when CD122 is associated with a more membrane-proximal epitope of HER2 compared to that associated with CD132. The opposite is observed for the MSLN-targeting pairs. We hypothesize that the agonistic potential of the pairs may depend on geometrical factors, where distance and orientation could play a significant role. Some combinations may lead to incompatible distances or angles, making it hard for the two antibodies to co-engage. Other than the capacity to stimulate IL-2R signaling, specific biological properties of each TAA also need to be considered when choosing the target epitope on TAAs. As an example, HER2 is known to form homodimers and heterodimers, which stimulate the proliferation of tumor cells. Pertuzumab, but not Trastuzumab, was shown to block HER2:HER3 heterodimerization, which could provide the approach with an additional mechanism of action.⁴²⁰

While engineering our bsAbs, we developed arms targeting different epitopes for CD122, CD132 or the TAAs with different affinities. Our in vitro data guided us to choose two bsAb pairs among the possible IL-2RxMSLN combinations, with different affinities for CD122 and CD132, for further in vivo testing. In both pairs, the anti-CD122 arm was combined with an arm targeting a proximal MSLN epitope (dissociation constant=K_D=22 nM), and the anti-CD132 arm was combined with an arm targeting a distal MSLN epitope (K_D=0.48 nM). In initial in vivo experiments, we observed that the two pairs had similar effects on the TME. Therefore, we continued with the pair with a lower affinity for CD122 and CD132 for the remaining experiments. We hypothesized that using lower affinity sequences for CD122 and

CD132 would reduce the number of antibodies retained in the periphery by IL-2R expressing cells and favor intratumoral accumulation via the higher affinity anti-MSLN arms. Furthermore, having moderate affinities for CD122 and CD132 could be beneficial for activating IL-2/IL-15 signaling. Unlike blocking antibodies, where higher affinity is often associated with increased activity, evidence suggests that agonistic antibodies aimed at activating receptor signaling can benefit from lower affinities. 421 As the ideal affinity is likely to change depending on the targeted epitope, we could engineer variants of our sequences with different affinities to compare head to head. A structure-guided mutational approach could be used to make sure the target epitope does not change. Alternatively, optimization and de-optimization campaigns could be performed starting from one of our initial sequences, followed by molecular modeling to ensure the target epitope remains unaltered. The K_D, i.e., the off-rate constant (K_{OFF}) divided by the on-rate constant (K_{ON}), quantifies the speed of dissociation and association of a complex and is most often used as the quantification parameter for the affinity of antibodies. We hypothesize that both Koff and Kon are important for molecules aimed at modulating signaling activity and considering them separately from each other could further inform insightful decisions in antibody engineering. For example, a sequence with slow association and slow dissociation could have the same K_D as a different sequence with faster association and dissociation. Despite having the same K_D, we think the two antibodies could have significantly different effects on signaling activation and dynamics.

This study demonstrated that this novel approach could activate IL-2/IL-15 signaling by bringing them together through two different TAAs, HER2 and MSLN. In initial experiments, we targeted CD122, CD132, and HER2 for various reasons. IL-2 and IL-15 are well known to activate cells involved in antitumor immune responses, and harnessing IL-2 signaling safely has been a major challenge for many years. Many tools like reporter cells and recombinant proteins are available. Additionally, antibody sequences had been published for CD122, CD132, and several HER2 epitopes and could be combined through CrossmAb technology. This approach allowed us to validate the concept quickly and extend it to κλ-bodies and MSLN. Many signaling pathways initiate signaling cascades after their receptor subunits form a multimer. We think that our approach may not be limited to CD122 and CD132 combinations with HER2 and MSLN but can be applied to many others. The safety and TAA selectivity we demonstrated make bsAb pairs well-versed in targeting pathways limited by their toxicity. For example, IL-12 has been an attractive target in cancer immunotherapies, but no FDA-approved IL-12 targeting immunotherapy exists due to

severe systemic toxicities associated with T and NK cell activation. 422 As IL-12 receptor (IL-12R) comprises two subunits, IL-12R β 1 and IL-12R β 2, it could potentially also be targeted and activated in a TAA-dependent manner through bsAb pairs. Another development of our approach that has not been investigated so far is using bsAb pairs that target subunits of different receptors. A study has demonstrated using bispecific antibodies composed of small antibody domains targeting two receptor subunits of different receptors that non-natural heterodimeric receptors, like IL-2R β -IL-10R β , can transduce signaling in target cells. 423 This possibility opens up even more possible strategies for bsAb pairs.

We demonstrated the agonistic potential of bsAb pairs where the first antibody targets HER2 and the second targets MSLN (Fig. 6, S9). In this case, signaling is activated only with target cells expressing both TAAs. Targeting multiple TAAs can further improve the specificity of our bsAb pairs. Some TAAs are marginally expressed by healthy cells, but it is unlikely that healthy cells will express more than one. The two-TAA bsAb pairs thus selectively target tumor cells co-expressing both TAAs while sparing healthy cells expressing only one of them. A different possible development of this approach could be to target a cytokine receptor, and a protein co-expressed on the same cell (in cis). This approach would likely increase peripheral activation but offers an alternative in projects where peripheral activation is less concerning. Similarly to RO7284755, anti-PD-1 blocking arms could be combined with IL-2R targeting arms to favor the activation of antigen-experienced immune cells.⁴²⁴

Finally, the great success of ICI and increasing evidence that IL-2 activation synergizes with anti-PD-1 treatment convinced us to combine our bsAb pairs with anti-mPD-1 antibody administration. We could show that the reduction in tumor burden in mice treated with the combination is associated with an immune infiltration profile different from that associated with either the bsAb pair or the anti-mPD-1 alone. For example, we observed a CD8+/Treg ratio similar to the bsAb pair alone, but the percentage of gnzmB+ CD8+ T cells was closer to what we observed with anti-mPD-1 alone (Fig. 5 E-F). In addition to ICI, we believe our approach could also be partnered successfully with other therapeutic approaches, such as cancer vaccines and ACT. Cancer vaccines have been shown to remodel the TME and increase immune cell infiltration. A study has shown that Ad-carcinoembryonic antigen (Ad-CEA), a vaccine targeting CEA, fails to control tumor growth alone but induces significant changes in the TME, including an increase of the infiltration of CD8+, gnzmB+ CD8+ T cells and higher CD8+/Treg ratios. 425 Considering that we observed similar results with our bsAb pairs and that vaccines inherently boost the pool of antigen-specific T cells, we believe that

combining the two strategies could be beneficial. ACT comprises T cell therapy, NK cell therapy, CAR T cell therapy, and CAR NK cell therapy. As we demonstrated significant effects both on CD8+ and NK cells and ACT is often combined with injections of IL-2 and IL-15 to support the maintenance of the injected cells, we believe the two strategies would be natural partners. 427

9 Conclusion

In this thesis, we have developed a novel immunotherapeutic strategy. By demonstrating the tumor-selective IL-2/IL-15 activation of immune cells and the favorable safety profile of pairs of bsAbs, this thesis illustrates an approach that overcomes the limitations of cytokine therapies. Importantly, we did not observe any worrying clinical signs of toxicity and circulating inflammatory cytokines remained unchanged after bsAb treatment of mice. We believe that the reduction in tumor growth accompanied by the proliferation and activation of memory CD8+ T and NK cells supports the applicability of the approach and warrants further studies. Altogether, this thesis demonstrates a new approach to activate IL-2/IL-15 signaling that could serve as an example for a new generation of cytokine-targeting therapies capable of circumventing toxicity and improving patients' quality of life.

10 References

- 1. Cancer Tomorrow. https://gco.iarc.who.int/today/.
- Registry Groupings in SEER Data and Statistics SEER Registries. SEER
 https://seer.cancer.gov/registries/terms.html.
- 3. Pubmed entries wih 'cancer'. https://pubmed.ncbi.nlm.nih.gov/?term=cancer (2024).
- 4. Hanahan, D. & Weinberg, R. A. The Hallmarks of Cancer. Cell 100, 57–70 (2000).
- 5. Hanahan, D. Hallmarks of Cancer: New Dimensions. *Cancer Discov.* **12**, 31–46 (2022).
- 6. Hanahan, D. & Weinberg, R. A. Hallmarks of Cancer: The Next Generation. *Cell* **144**, 646–674 (2011).
- 7. Gianfaldoni, S. *et al.* An Overview on Radiotherapy: From Its History to Its Current Applications in Dermatology. *Open Access Maced. J. Med. Sci.* **5**, 521–525 (2017).
- 8. AACR Cancer Progress Report 2024. cancerprogressreport.org.
- 9. Chaplin, D. D. Overview of the immune response. J. Allergy Clin. Immunol. 125, S3-23 (2010).
- Marshall, J. S., Warrington, R., Watson, W. & Kim, H. L. An introduction to immunology and immunopathology. *Allergy Asthma Clin. Immunol. Off. J. Can. Soc. Allergy Clin. Immunol.* 14, 49 (2018).
- 11. Netea, M. G., Schlitzer, A., Placek, K., Joosten, L. A. B. & Schultze, J. L. Innate and Adaptive Immune Memory: an Evolutionary Continuum in the Host's Response to Pathogens. *Cell Host Microbe* **25**, 13–26 (2019).
- 12. Mungall, A. J. *et al.* The DNA sequence and analysis of human chromosome 6. *Nature* **425**, 805–811 (2003).
- 13. Wieczorek, M. *et al.* Major Histocompatibility Complex (MHC) Class I and MHC Class II

 Proteins: Conformational Plasticity in Antigen Presentation. *Front. Immunol.* **8**, 292 (2017).

- 14. Trowsdale, J., Ragoussis, J. & Duncan Campbell, R. Map of the human MHC. *Immunol. Today* 12, 443–446 (1991).
- 15. Madden, D. R., Gorga, J. C., Strominger, J. L. & Wiley, D. C. The three-dimensional structure of HLA-B27 at 2.1 A resolution suggests a general mechanism for tight peptide binding to MHC. *Cell* **70**, 1035–1048 (1992).
- 16. Parham, P. Functional sites of human class I MHC molecules: Paradigms a dozen? *Immunol.**Res. 6, 153–178 (1987).
- 17. Chicz, R. M. *et al.* Predominant naturally processed peptides bound to HLA-DR1 are derived from MHC-related molecules and are heterogeneous in size. *Nature* **358**, 764–768 (1992).
- 18. Berko, D. *et al.* Membrane-Anchored β2-Microglobulin Stabilizes a Highly Receptive State of MHC Class I Molecules 1. *J. Immunol.* **174**, 2116–2123 (2005).
- 19. Jung, S. *et al.* In vivo depletion of CD11c+ dendritic cells abrogates priming of CD8+ T cells by exogenous cell-associated antigens. *Immunity* **17**, 211–220 (2002).
- 20. Brown, J. H. *et al.* Three-dimensional structure of the human class II histocompatibility antigen HLA-DR1. *Nature* **364**, 33–39 (1993).
- 21. Jones, E. Y., Fugger, L., Strominger, J. L. & Siebold, C. MHC class II proteins and disease: a structural perspective. *Nat. Rev. Immunol.* **6**, 271–282 (2006).
- 22. Jurewicz, M. M. & Stern, L. J. Class II MHC Antigen Processing in Immune Tolerance and Inflammation. *Immunogenetics* **71**, 171–187 (2019).
- 23. Rudensky, A., Preston-Hurlburt, P., Hong, S. C., Barlow, A. & Janeway, C. A. Sequence analysis of peptides bound to MHC class II molecules. *Nature* **353**, 622–627 (1991).
- 24. Foster, J. R. The functions of cytokines and their uses in toxicology. *Int. J. Exp. Pathol.* **82**, 171–192 (2001).

- 25. Siegel, P. M. & Massagué, J. Cytostatic and apoptotic actions of TGF-beta in homeostasis and cancer. *Nat. Rev. Cancer* **3**, 807–821 (2003).
- 26. Ozga, A. J., Chow, M. T. & Luster, A. D. Chemokines and the immune response to cancer. *Immunity* **54**, 859–874 (2021).
- Zamarin, D. et al. Mogamulizumab in Combination with Durvalumab or Tremelimumab in Patients with Advanced Solid Tumors: A Phase I Study. Clin. Cancer Res. Off. J. Am. Assoc.
 Cancer Res. 26, 4531–4541 (2020).
- 28. Bongartz, T. *et al.* Anti-TNF antibody therapy in rheumatoid arthritis and the risk of serious infections and malignancies: systematic review and meta-analysis of rare harmful effects in randomized controlled trials. *JAMA* **295**, 2275–2285 (2006).
- 29. Kotenko, S. V. *et al.* IFN-λs mediate antiviral protection through a distinct class II cytokine receptor complex. *Nat. Immunol.* **4**, 69–77 (2003).
- 30. Isaacs, A. & Lindenmann, J. Virus interference. I. The interferon. *Proc. R. Soc. Lond. B Biol. Sci.* **147**, 258–267 (1957).
- 31. Moschos, S. J. et al. Neoadjuvant treatment of regional stage IIIB melanoma with high-dose interferon alfa-2b induces objective tumor regression in association with modulation of tumor infiltrating host cellular immune responses. J. Clin. Oncol. Off. J. Am. Soc. Clin. Oncol. 24, 3164–3171 (2006).
- 32. Broggi, A., Tan, Y., Granucci, F. & Zanoni, I. IFN-λ suppresses intestinal inflammation by non-translational regulation of neutrophil function. *Nat. Immunol.* **18**, 1084–1093 (2017).
- Song, M. et al. Low-Dose IFNγ Induces Tumor Cell Stemness in Tumor Microenvironment of Non-Small Cell Lung Cancer. Cancer Res. 79, 3737–3748 (2019).
- 34. Nastala, C. L. *et al.* Recombinant IL-12 administration induces tumor regression in association with IFN-gamma production. *J. Immunol. Baltim. Md* 1950 **153**, 1697–1706 (1994).

- 35. Zibelman, M. *et al.* A phase 1 study of nivolumab in combination with interferon-gamma for patients with advanced solid tumors. *Nat. Commun.* **14**, 4513 (2023).
- 36. Lin, J.-X. & Leonard, W. J. The Common Cytokine Receptor γ Chain Family of Cytokines. *Cold Spring Harb. Perspect. Biol.* **10**, a028449 (2018).
- 37. Giri, J. G. *et al.* Utilization of the beta and gamma chains of the IL-2 receptor by the novel cytokine IL-15. *EMBO J.* **13**, 2822–2830 (1994).
- 38. Takeshita, T. *et al.* Cloning of the gamma chain of the human IL-2 receptor. *Science* **257**, 379–382 (1992).
- 39. Giri, J. G. *et al.* Identification and cloning of a novel IL-15 binding protein that is structurally related to the alpha chain of the IL-2 receptor. *EMBO J.* **14**, 3654–3663 (1995).
- 40. Dubois, S., Mariner, J., Waldmann, T. A. & Tagaya, Y. IL-15Rα Recycles and Presents IL-15 In trans to Neighboring Cells. *Immunity* **17**, 537–547 (2002).
- 41. Shapiro, V. S., Truitt, K. E., Imboden, J. B. & Weiss, A. CD28 mediates transcriptional upregulation of the interleukin-2 (IL-2) promoter through a composite element containing the CD28RE and NF-IL-2B AP-1 sites. *Mol. Cell. Biol.* 17, 4051–4058 (1997).
- 42. Rooney, J. W., Sun, Y. L., Glimcher, L. H. & Hoey, T. Novel NFAT sites that mediate activation of the interleukin-2 promoter in response to T-cell receptor stimulation. *Mol. Cell. Biol.* **15**, 6299–6310 (1995).
- 43. Kim, H. P., Imbert, J. & Leonard, W. J. Both integrated and differential regulation of components of the IL-2/IL-2 receptor system. *Cytokine Growth Factor Rev.* **17**, 349–366 (2006).
- 44. Himes, S. R., Coles, L. S., Reeves, R. & Shannon, M. F. High mobility group protein I(Y) is required for function and for c-Rel binding to CD28 response elements within the GM-CSF and IL-2 promoters. *Immunity* **5**, 479–489 (1996).

- 45. Müller, M. R. & Rao, A. NFAT, immunity and cancer: a transcription factor comes of age. *Nat. Rev. Immunol.* **10**, 645–656 (2010).
- 46. Azimi, N., Tagaya, Y., Mariner, J. & Waldmann, T. A. Viral Activation of Interleukin-15 (IL-15): Characterization of a Virus-Inducible Element in the IL-15 Promoter Region. *J. Virol.* **74**, 7338–7348 (2000).
- 47. Lin, J. X., Bhat, N. K., John, S., Queale, W. S. & Leonard, W. J. Characterization of the human interleukin-2 receptor beta-chain gene promoter: regulation of promoter activity by ets gene products. *Mol. Cell. Biol.* **13**, 6201–6210 (1993).
- 48. Lin, J. X. & Leonard, W. J. The immediate-early gene product Egr-1 regulates the human interleukin-2 receptor beta-chain promoter through noncanonical Egr and Sp1 binding sites.

 Mol. Cell. Biol. 17, 3714–3722 (1997).
- 49. Wong, J. Induction of the interleukin-2/15 receptor beta-chain by the EWS-WT1 translocation product. *Oncogene* (2002).
- 50. Lin, J.-X. *et al.* Critical Role of STAT5 transcription factor tetramerization for cytokine responses and normal immune function. *Immunity* **36**, 586–599 (2012).
- 51. Li, P. *et al.* STAT5-mediated chromatin interactions in superenhancers activate IL-2 highly inducible genes: Functional dissection of the Il2ra gene locus. *Proc. Natl. Acad. Sci. U. S. A.* **114**, 12111–12119 (2017).
- 52. Siegel, J. P., Sharon, M., Smith, P. L. & Leonard, W. J. The IL-2 receptor beta chain (p70): role in mediating signals for LAK, NK, and proliferative activities. *Science* **238**, 75–78 (1987).
- 53. Markiewicz, S. *et al.* Tissue-specific activity of the gammac chain gene promoter depends upon an Ets binding site and is regulated by GA-binding protein. *J. Biol. Chem.* **271**, 14849–14855 (1996).

- 54. Imada, K. *et al.* Stat5b is essential for natural killer cell-mediated proliferation and cytolytic activity. *J. Exp. Med.* **188**, 2067–2074 (1998).
- 55. Nakajima, H. *et al.* An indirect effect of Stat5a in IL-2-induced proliferation: a critical role for Stat5a in IL-2-mediated IL-2 receptor alpha chain induction. *Immunity* **7**, 691–701 (1997).
- 56. Schuh, K. *et al.* The interleukin 2 receptor alpha chain/CD25 promoter is a target for nuclear factor of activated T cells. *J. Exp. Med.* **188**, 1369–1373 (1998).
- 57. Kim, H. P., Imbert, J. & Leonard, W. J. Both integrated and differential regulation of components of the IL-2/IL-2 receptor system. *Cytokine Growth Factor Rev.* **17**, 349–366 (2006).
- 58. Mariner, J. M., Mamane, Y., Hiscott, J., Waldmann, T. A. & Azimi, N. IFN regulatory factor 4 participates in the human T cell lymphotropic virus type I-mediated activation of the IL-15 receptor alpha promoter. *J. Immunol. Baltim. Md* 1950 **168**, 5667–5674 (2002).
- 59. Spolski, R., Li, P. & Leonard, W. J. Biology and regulation of IL-2: from molecular mechanisms to human therapy. *Nat. Rev. Immunol.* **18**, 648–659 (2018).
- 60. Rodig, S. J. *et al.* Disruption of the Jak1 Gene Demonstrates Obligatory and Nonredundant Roles of the Jaks in Cytokine-Induced Biologic Responses. *Cell* **93**, 373–383 (1998).
- 61. Russell, S. M. *et al.* Interaction of IL-2R beta and gamma c chains with Jak1 and Jak3: implications for XSCID and XCID. *Science* **266**, 1042–1045 (1994).
- 62. Lin, J.-X. *et al.* Critical Role of STAT5 transcription factor tetramerization for cytokine responses and normal immune function. *Immunity* **36**, 586–599 (2012).
- 63. Lin, J.-X. *et al.* Critical functions for STAT5 tetramers in the maturation and survival of natural killer cells. *Nat. Commun.* **8**, 1320 (2017).
- 64. Friedmann, M. C., Migone, T. S., Russell, S. M. & Leonard, W. J. Different interleukin 2 receptor beta-chain tyrosines couple to at least two signaling pathways and synergistically

- mediate interleukin 2-induced proliferation. *Proc. Natl. Acad. Sci. U. S. A.* **93**, 2077–2082 (1996).
- 65. Ray, J. P. *et al.* The Interleukin-2-mTORc1 Kinase Axis Defines the Signaling, Differentiation, and Metabolism of T Helper 1 and Follicular B Helper T Cells. *Immunity* **43**, 690–702 (2015).
- 66. Marzec, M. *et al.* IL-2– and IL-15–induced activation of the rapamycin-sensitive mTORC1 pathway in malignant CD4+ T lymphocytes. *Blood* **111**, 2181–2189 (2008).
- 67. Nandagopal, N., Ali, A. K., Komal, A. K. & Lee, S.-H. The Critical Role of IL-15–PI3K–mTOR Pathway in Natural Killer Cell Effector Functions. *Front. Immunol.* **5**, (2014).
- 68. Fairhurst, R. M., Daeipour, M., Amaral, M. C. & Nel, A. E. Activation of mitogen-activated protein kinase/ERK-2 in phytohaemagglutin in blasts by recombinant interleukin-2: contrasting features with CD3 activation. *Immunology* **79**, 112–118 (1993).
- 69. Crawley, J. B. *et al.* T cell proliferation in response to interleukins 2 and 7 requires p38MAP kinase activation. *J. Biol. Chem.* **272**, 15023–15027 (1997).
- 70. Karnitz, L. M., Burns, L. A., Sutor, S. L., Blenis, J. & Abraham, R. T. Interleukin-2 triggers a novel phosphatidylinositol 3-kinase-dependent MEK activation pathway. *Mol. Cell. Biol.* **15**, 3049–3057 (1995).
- 71. Adunyah, S. E., Wheeler, B. J. & Cooper, R. S. Evidence for the involvement of LCK and MAP kinase (ERK-1) in the signal transduction mechanism of interleukin-15. *Biochem. Biophys.***Res. Commun. 232, 754–758 (1997).
- 72. Musso, T. *et al.* IL-2 induces IL-6 production in human monocytes. *J. Immunol. Baltim. Md* 1950 **148**, 795–800 (1992).
- 73. Zamorano, J. *et al.* Regulation of Cell Growth by IL-2: Role of STAT5 in Protection from Apoptosis But Not in Cell Cycle Progression1. *J. Immunol.* **160**, 3502–3512 (1998).

- 74. Moriggl, R. et al. Stat5 Is Required for IL-2-Induced Cell Cycle Progression of Peripheral T Cells. *Immunity* **10**, 249–259 (1999).
- 75. Tripathi, P. et al. STAT5 IS CRITICAL TO MAINTAIN EFFECTOR CD8+ T CELL RESPONSES. J. Immunol. Baltim. Md 1950 **185**, 2116–2124 (2010).
- 76. Mao, Y. et al. IL-15 activates mTOR and primes stress-activated gene expression leading to prolonged antitumor capacity of NK cells. *Blood* **128**, 1475–1489 (2016).
- 77. Kurebayashi, Y. *et al.* PI3K-Akt-mTORC1-S6K1/2 Axis Controls Th17 Differentiation by Regulating Gfi1 Expression and Nuclear Translocation of RORy. *Cell Rep.* **1**, 360–373 (2012).
- 78. Pompura, S. L. & Dominguez-Villar, M. The PI3K/AKT signaling pathway in regulatory T-cell development, stability, and function. *J. Leukoc. Biol.* **103**, 1065–1076 (2018).
- 79. Le Gallou, S. *et al.* IL-2 requirement for human plasma cell generation: coupling differentiation and proliferation by enhancing MAPK-ERK signaling. *J. Immunol. Baltim. Md* 1950 **189**, 161–173 (2012).
- 80. D'Souza, W. N., Chang, C.-F., Fischer, A. M., Li, M. & Hedrick, S. M. The Erk2 MAPK Regulates

 CD8 T Cell Proliferation and Survival. *J. Immunol. Baltim. Md* 1950 **181**, 7617–7629 (2008).
- 81. Dubois, S. *et al.* Distinct pathways involving the FK506-binding proteins 12 and 12.6 underlie IL-2-versus IL-15-mediated proliferation of T cells. *Proc. Natl. Acad. Sci. U. S. A.* **100**, 14169–14174 (2003).
- 82. Cui, G. et al. Characterization of the IL-15 niche in primary and secondary lymphoid organs in vivo. *Proc. Natl. Acad. Sci.* **111**, 1915–1920 (2014).
- 83. DiToro, D. *et al.* Differential IL-2 Expression Defines Developmental Fates of Follicular versus Non-follicular Helper T cells. *Science* **361**, eaao2933 (2018).

- 84. Park, J.-Y., Ligons, D. L. & Park, J.-H. Out-sourcing for Trans-presentation: Assessing T Cell Intrinsic and Extrinsic IL-15 Expression with Il15 Gene Reporter Mice. *Immune Netw.* **18**, (2018).
- 85. Mortier, E., Woo, T., Advincula, R., Gozalo, S. & Ma, A. IL-15Ralpha chaperones IL-15 to stable dendritic cell membrane complexes that activate NK cells via trans presentation. *J. Exp. Med.*205, 1213–1225 (2008).
- 86. Dubois, S., Mariner, J., Waldmann, T. A. & Tagaya, Y. IL-15Ralpha recycles and presents IL-15 In trans to neighboring cells. *Immunity* **17**, 537–547 (2002).
- 87. Schluns, K. S., Klonowski, K. D. & Lefrançois, L. Transregulation of memory CD8 T-cell proliferation by IL-15Ralpha+ bone marrow-derived cells. *Blood* **103**, 988–994 (2004).
- 88. Chirifu, M. *et al.* Crystal structure of the IL-15–IL-15Rα complex, a cytokine-receptor unit presented in trans. *Nat. Immunol.* **8**, 1001–1007 (2007).
- 89. Stauber, D. J., Debler, E. W., Horton, P. A., Smith, K. A. & Wilson, I. A. Crystal structure of the IL-2 signaling complex: Paradigm for a heterotrimeric cytokine receptor. *Proc. Natl. Acad. Sci. U. S. A.* **103**, 2788–2793 (2006).
- 90. Yang, Y. & Lundqvist, A. Immunomodulatory Effects of IL-2 and IL-15; Implications for Cancer Immunotherapy. *Cancers* **12**, 3586 (2020).
- 91. Freud, A. G., Mundy-Bosse, B. L., Yu, J. & Caligiuri, M. A. The broad spectrum of human natural killer cell diversity. *Immunity* **47**, 820–833 (2017).
- 92. Fehniger, T. A. *et al.* Differential Cytokine and Chemokine Gene Expression by Human NK Cells Following Activation with IL-18 or IL-15 in Combination with IL-12: Implications for the Innate Immune Response. *J. Immunol.* **162**, 4511–4520 (1999).
- 93. Mamessier, E. *et al.* Human breast cancer cells enhance self tolerance by promoting evasion from NK cell antitumor immunity. *J. Clin. Invest.* **121**, 3609–3622 (2011).

- 94. Cichocki, F., Grzywacz, B. & Miller, J. S. Human NK Cell Development: One Road or Many?

 Front. Immunol. 10, (2019).
- 95. Tomaz, D. *et al.* Nanoscale Colocalization of NK Cell Activating and Inhibitory Receptors Controls Signal Integration. *Front. Immunol.* **13**, (2022).
- 96. Park, J.-E. *et al.* Anti-tumor effects of NK cells and anti-PD-L1 antibody with antibody-dependent cellular cytotoxicity in PD-L1-positive cancer cell lines. *J. Immunother. Cancer* **8**, e000873 (2020).
- 97. Shang, Q.-N. *et al.* Functional Competence of NK Cells via the KIR/MHC Class I Interaction Correlates with DNAM-1 Expression. *J. Immunol.* **208**, 492–500 (2022).
- 98. Bern, M. D. *et al.* Inducible down-regulation of MHC class I results in natural killer cell tolerance. *J. Exp. Med.* **216**, 99–116 (2019).
- 99. Krzewski, K., Gil-Krzewska, A., Nguyen, V., Peruzzi, G. & Coligan, J. E. LAMP1/CD107a is required for efficient perforin delivery to lytic granules and NK-cell cytotoxicity. *Blood* **121**, 4672–4683 (2013).
- 100. Takeda, K. *et al.* Involvement of tumor necrosis factor-related apoptosis-inducing ligand in surveillance of tumor metastasis by liver natural killer cells. *Nat. Med.* **7**, 94–100 (2001).
- 101. Wang, R., Jaw, J. J., Stutzman, N. C., Zou, Z. & Sun, P. D. Natural killer cell-produced IFN-γ and TNF-α induce target cell cytolysis through up-regulation of ICAM-1. *J. Leukoc. Biol.* **91**, 299–309 (2012).
- 102. Sun, Y. *et al.* A Transcriptional Signature of IL-2 Expanded Natural Killer Cells Predicts More Favorable Prognosis in Bladder Cancer. *Front. Immunol.* **12**, (2021).
- 103. Huntington, N. D. *et al.* IL-15 trans-presentation promotes human NK cell development and differentiation in vivo. *J. Exp. Med.* **206**, 25–34 (2008).

- 104. Lee, S.-H., Fragoso, M. F. & Biron, C. A. Cutting edge: a novel mechanism bridging innate and adaptive immunity: IL-12 induction of CD25 to form high-affinity IL-2 receptors on NK cells. *J. Immunol. Baltim. Md* 1950 **189**, 2712–2716 (2012).
- 105. Wang, K. S., Frank, D. A. & Ritz, J. Interleukin-2 enhances the response of natural killer cells to interleukin-12 through up-regulation of the interleukin-12 receptor and STAT4. *Blood* **95**, 3183–3190 (2000).
- 106. DeBlaker-Hohe, D. F., Yamauchi, A., Yu, C. R., Horvath-Arcidiacono, J. A. & Bloom, E. T. IL-12 synergizes with IL-2 to induce lymphokine-activated cytotoxicity and perforin and granzyme gene expression in fresh human NK cells. *Cell. Immunol.* **165**, 33–43 (1995).
- 107. Cantoni, C. *et al.* NKp44, a triggering receptor involved in tumor cell lysis by activated human natural killer cells, is a novel member of the immunoglobulin superfamily. *J. Exp. Med.* **189**, 787–796 (1999).
- 108. Vuletić, A. *et al.* IL-2 And IL-15 Induced NKG2D, CD158a and CD158b Expression on T, NKT-like and NK Cell Lymphocyte Subsets from Regional Lymph Nodes of Melanoma Patients. *Pathol. Oncol. Res.* **26**, 223–231 (2020).
- 109. Wang, K. S., Ritz, J. & Frank, D. A. IL-2 Induces STAT4 Activation in Primary NK Cells and NK Cell Lines, But Not in T Cells1. *J. Immunol.* **162**, 299–304 (1999).
- 110. Taguchi, Y. et al. Interleukin-2-induced survival of natural killer (NK) cells involving phosphatidylinositol-3 kinase-dependent reduction of ceramide through acid sphingomyelinase, sphingomyelin synthase, and glucosylceramide synthase. Blood 104, 3285–3293 (2004).
- 111. Koka, R. *et al.* Interleukin (IL)-15R α -deficient Natural Killer Cells Survive in Normal but Not IL-15R α -deficient Mice. *J. Exp. Med.* **197**, 977–984 (2003).

- 112. Kennedy, M. K. *et al.* Reversible defects in natural killer and memory CD8 T cell lineages in interleukin 15-deficient mice. *J. Exp. Med.* **191**, 771–780 (2000).
- 113. Ranson, T. et al. IL-15 is an essential mediator of peripheral NK-cell homeostasis. Blood 101, 4887–4893 (2003).
- 114. Huntington, N. D. *et al.* Interleukin 15–mediated survival of natural killer cells is determined by interactions among Bim, Noxa and Mcl-1. *Nat. Immunol.* **8**, 856–863 (2007).
- 115. Vendrame, E., Fukuyama, J., Strauss-Albee, D. M., Holmes, S. & Blish, C. A. Mass cytometry analytical approaches reveal cytokine-induced changes in natural killer cells. *Cytometry B Clin. Cytom.* **92**, 57–67 (2017).
- 116. Zhang, C., Zhang, J., Niu, J., Zhang, J. & Tian, Z. Interleukin-15 improves cytotoxicity of natural killer cells via up-regulating NKG2D and cytotoxic effector molecule expression as well as STAT1 and ERK1/2 phosphorylation. *Cytokine* **42**, 128–136 (2008).
- 117. Lucas, M., Schachterle, W., Oberle, K., Aichele, P. & Diefenbach, A. Natural Killer Cell-Mediated Control of Infections Requires Production of Interleukin 15 by Type I IFN-Triggered Dendritic Cells. *Immunity* **26**, 503–517 (2007).
- 118. Vivier, E., Ugolini, S., Blaise, D., Chabannon, C. & Brossay, L. Targeting natural killer cells and natural killer T cells in cancer. *Nat. Rev. Immunol.* **12**, 239–252 (2012).
- 119. Nuriya, S., Yagita, H., Okumura, K. & Azuma, M. The differential role of CD86 and CD80 costimulatory molecules in the induction and the effector phases of contact hypersensitivity.

 Int. Immunol. 8, 917–926 (1996).
- 120. Kurts, C., Robinson, B. W. S. & Knolle, P. A. Cross-priming in health and disease. *Nat. Rev. Immunol.* **10**, 403–414 (2010).
- 121. Sallusto, F. et al. Rapid and coordinated switch in chemokine receptor expression during dendritic cell maturation. Eur. J. Immunol. 28, 2760–2769 (1998).

- 122. Collin, M. & Bigley, V. Human dendritic cell subsets: an update. *Immunology* **154**, 3–20 (2018).
- 123. Kader, M. *et al.* Blocking TLR7- and TLR9-mediated IFN-α Production by Plasmacytoid

 Dendritic Cells Does Not Diminish Immune Activation in Early SIV Infection. *PLOS Pathog.* **9**, e1003530 (2013).
- 124. den Haan, J. M., Lehar, S. M. & Bevan, M. J. CD8(+) but not CD8(-) dendritic cells cross-prime cytotoxic T cells in vivo. *J. Exp. Med.* **192**, 1685–1696 (2000).
- 125. Jongbloed, S. L. *et al.* Human CD141+ (BDCA-3)+ dendritic cells (DCs) represent a unique myeloid DC subset that cross-presents necrotic cell antigens. *J. Exp. Med.* **207**, 1247–1260 (2010).
- 126. Sittig, S. P. *et al.* A Comparative Study of the T Cell Stimulatory and Polarizing Capacity of Human Primary Blood Dendritic Cell Subsets. *Mediators Inflamm.* **2016**, 3605643 (2016).
- 127. Santegoets, S. J. *et al.* CD163+ cytokine-producing cDC2 stimulate intratumoral type 1 T cell responses in HPV16-induced oropharyngeal cancer. *J. Immunother. Cancer* **8**, e001053 (2020).
- 128. Gerhard, G. M., Bill, R., Messemaker, M., Klein, A. M. & Pittet, M. J. Tumor-infiltrating dendritic cell states are conserved across solid human cancers. *J. Exp. Med.* **218**, e20200264 (2021).
- 129. Zhang, Q. *et al.* Landscape and Dynamics of Single Immune Cells in Hepatocellular Carcinoma. *Cell* **179**, 829-845.e20 (2019).
- 130. Maier, B. *et al.* A conserved dendritic-cell regulatory program limits antitumour immunity.

 *Nature 580, 257–262 (2020).

- 131. León, B., López-Bravo, M. & Ardavín, C. Monocyte-Derived Dendritic Cells Formed at the Infection Site Control the Induction of Protective T Helper 1 Responses against Leishmania. Immunity 26, 519–531 (2007).
- 132. Segura, E. & Amigorena, S. Inflammatory dendritic cells in mice and humans. *Trends Immunol.* **34**, 440–445 (2013).
- 133. Avice, M.-N. *et al.* IL-15 Promotes IL-12 Production by Human Monocytes Via T Cell-Dependent Contact and May Contribute to IL-12-Mediated IFN-γ Secretion by CD4+ T Cells in the Absence of TCR Ligation1. *J. Immunol.* **161**, 3408–3415 (1998).
- 134. McGill, J., Van Rooijen, N. & Legge, K. L. IL-15 trans-presentation by pulmonary dendritic cells promotes effector CD8 T cell survival during influenza virus infection. *J. Exp. Med.* **207**, 521–534 (2010).
- 135. Colpitts, S. L. *et al.* Cutting Edge: The Role of IFN-α Receptor and MyD88 Signaling in Induction of IL-15 Expression In Vivo. *J. Immunol.* **188**, 2483–2487 (2012).
- 136. Bergh, J. V. den *et al.* Transpresentation of interleukin-15 by IL-15/IL-15Rα mRNA-engineered human dendritic cells boosts antitumoral natural killer cell activity. *Oncotarget* 6, 44123–44133 (2015).
- 137. Naranjo-Gómez, M. *et al.* Expression and function of the IL-2 receptor in activated human plasmacytoid dendritic cells. *Eur. J. Immunol.* **37**, 1764–1772 (2007).
- 138. Sanarico, N. *et al.* Human monocyte-derived dendritic cells differentiated in the presence of IL-2 produce proinflammatory cytokines and prime Th1 immune response. *J. Leukoc. Biol.* **80**, 555–562 (2006).
- 139. Saikh, K. U., Kissner, T. L., Nystrom, S., Ruthel, G. & Ulrich, R. G. Interleukin-15 Increases

 Vaccine Efficacy through a Mechanism Linked to Dendritic Cell Maturation and Enhanced

 Antibody Titers. *Clin. Vaccine Immunol.* **15**, 131–137 (2008).

- 140. Saikh, K. U., Khan, A. S., Kissner, T. & Ulrich, R. G. IL-15-induced conversion of monocytes to mature dendritic cells. *Clin. Exp. Immunol.* **126**, 447–455 (2001).
- 141. Gary-Gouy, H., Lebon, P. & Dalloul, A. H. Type I interferon production by plasmacytoid dendritic cells and monocytes is triggered by viruses, but the level of production is controlled by distinct cytokines. *J. Interferon Cytokine Res. Off. J. Int. Soc. Interferon Cytokine Res.* 22, 653–659 (2002).
- 142. Ribot, J. C., Lopes, N. & Silva-Santos, B. γδ T cells in tissue physiology and surveillance. *Nat. Rev. Immunol.* **21**, 221–232 (2021).
- 143. Scimone, M. L., Aifantis, I., Apostolou, I., von Boehmer, H. & von Andrian, U. H. A multistep adhesion cascade for lymphoid progenitor cell homing to the thymus. *Proc. Natl. Acad. Sci.* **103**, 7006–7011 (2006).
- 144. Oettinger, M. A., Schatz, D. G., Gorka, C. & Baltimore, D. RAG-1 and RAG-2, Adjacent Genes

 That Synergistically Activate V(D)J Recombination. *Science* **248**, 1517–1523 (1990).
- 145. Yannoutsos, N. *et al.* The Role of Recombination Activating Gene (RAG) Reinduction in Thymocyte Development in Vivo. *J. Exp. Med.* **194**, 471–480 (2001).
- 146. Qian, L. *et al.* T cell receptor-beta mRNA splicing: regulation of unusual splicing intermediates. *Mol. Cell. Biol.* **13**, 1686–1696 (1993).
- 147. Bassing, C. H., Swat, W. & Alt, F. W. The Mechanism and Regulation of Chromosomal V(D)J Recombination. *Cell* **109**, S45–S55 (2002).
- 148. Robins, H. S. *et al.* Comprehensive assessment of T-cell receptor β -chain diversity in $\alpha\beta$ T cells. *Blood* **114**, 4099–4107 (2009).
- 149. Capone, M. *et al.* TCR beta and TCR alpha gene enhancers confer tissue- and stage-specificity on V(D)J recombination events. *EMBO J.* **12**, 4335–4346 (1993).

- 150. Nakagawa, Y. *et al.* Thymic nurse cells provide microenvironment for secondary T cell receptor α rearrangement in cortical thymocytes. *Proc. Natl. Acad. Sci. U. S. A.* **109**, 20572–20577 (2012).
- 151. Klein, L., Kyewski, B., Allen, P. M. & Hogquist, K. A. Positive and negative selection of the T cell repertoire: what thymocytes see and don't see. *Nat. Rev. Immunol.* **14**, 377–391 (2014).
- 152. Hubert, F.-X. *et al.* Aire regulates the transfer of antigen from mTECs to dendritic cells for induction of thymic tolerance. *Blood* **118**, 2462–2472 (2011).
- 153. Dembić, Z. *et al.* Transfer of specificity by murine alpha and beta T-cell receptor genes.

 Nature **320**, 232–238 (1986).
- 154. Samelson, L. E., Patel, M. D., Weissman, A. M., Harford, J. B. & Klausner, R. D. Antigen activation of murine T cells induces tyrosine phosphorylation of a polypeptide associated with the T cell antigen receptor. *Cell* **46**, 1083–1090 (1986).
- 155. June, C. H., Ledbetter, J. A., Gillespie, M. M., Lindsten, T. & Thompson, C. B. T-cell proliferation involving the CD28 pathway is associated with cyclosporine-resistant interleukin 2 gene expression. *Mol. Cell. Biol.* **7**, 4472–4481 (1987).
- 156. Bachmann, M. F., Speiser, D. E., Mak, T. W. & Ohashi, P. S. Absence of co-stimulation and not the intensity of TCR signaling is critical for the induction of T cell unresponsiveness in vivo.

 Eur. J. Immunol. 29, 2156–2166 (1999).
- 157. Linsley, P. S. *et al.* Human B7-1 (CD80) and B7-2 (CD86) bind with similar avidities but distinct kinetics to CD28 and CTLA-4 receptors. *Immunity* **1**, 793–801 (1994).
- 158. Kurts, C., Robinson, B. W. S. & Knolle, P. A. Cross-priming in health and disease. *Nat. Rev. Immunol.* **10**, 403–414 (2010).
- 159. Smith, G. A., Taunton, J. & Weiss, A. IL-2Rβ abundance differentially tunes IL-2 signaling dynamics in CD4+ and CD8+ T cells. *Sci. Signal.* **10**, eaan4931 (2017).

- 160. Au-Yeung, B. B. *et al.* IL-2 Modulates the TCR Signaling Threshold for CD8 but Not CD4 T Cell Proliferation on a Single-Cell Level. *J. Immunol. Baltim. Md* 1950 **198**, 2445–2456 (2017).
- 161. Sakaguchi, S., Sakaguchi, N., Asano, M., Itoh, M. & Toda, M. Immunologic self-tolerance maintained by activated T cells expressing IL-2 receptor alpha-chains (CD25). Breakdown of a single mechanism of self-tolerance causes various autoimmune diseases. *J. Immunol. Baltim. Md* 1950 155, 1151–1164 (1995).
- 162. Kalia, V. *et al.* Prolonged Interleukin-2Rα Expression on Virus-Specific CD8+ T Cells Favors

 Terminal-Effector Differentiation In Vivo. *Immunity* **32**, 91–103 (2010).
- 163. Krummel, M. F. & Allison, J. P. CD28 and CTLA-4 have opposing effects on the response of T cells to stimulation. *J. Exp. Med.* **182**, 459–465 (1995).
- 164. Ishida, Y., Agata, Y., Shibahara, K. & Honjo, T. Induced expression of PD-1, a novel member of the immunoglobulin gene superfamily, upon programmed cell death. *EMBO J.* **11**, 3887–3895 (1992).
- 165. Latchman, Y. et al. PD-L2 is a second ligand for PD-1 and inhibits T cell activation. *Nat. Immunol.* **2**, 261–268 (2001).
- 166. Khantakova, J. N. & Sennikov, S. V. T-helper cells flexibility: the possibility of reprogramming T cells fate. *Front. Immunol.* **14**, (2023).
- 167. Romagnani, S. Th1/Th2 cells. Inflamm. Bowel Dis. 5, 285–294 (1999).
- 168. Annunziato, F., Cosmi, L., Liotta, F., Maggi, E. & Romagnani, S. Human Th1 dichotomy: origin, phenotype and biologic activities. *Immunology* **144**, 343–351 (2014).
- 169. Hwang, E. S., Hong, J.-H. & Glimcher, L. H. IL-2 production in developing Th1 cells is regulated by heterodimerization of RelA and T-bet and requires T-bet serine residue 508. *J. Exp. Med.* 202, 1289–1300 (2005).

- 170. Bonecchi, R. *et al.* Differential expression of chemokine receptors and chemotactic responsiveness of type 1 T helper cells (Th1s) and Th2s. *J. Exp. Med.* **187**, 129–134 (1998).
- 171. Wei, G. *et al.* Genome-wide analyses of transcription factor GATA3-mediated gene regulation in distinct T cell types. *Immunity* **35**, 299–311 (2011).
- 172. Walker, J. A. & McKenzie, A. N. J. TH2 cell development and function. *Nat. Rev. Immunol.* **18**, 121–133 (2018).
- 173. Fort, M. M. *et al.* IL-25 induces IL-4, IL-5, and IL-13 and Th2-associated pathologies in vivo. *Immunity* **15**, 985–995 (2001).
- 174. Dardalhon, V. *et al.* IL-4 inhibits TGF-beta-induced Foxp3+ T cells and, together with TGF-beta, generates IL-9+ IL-10+ Foxp3(-) effector T cells. *Nat. Immunol.* **9**, 1347–1355 (2008).
- 175. Chen, J. et al. T Helper 9 Cells: A New Player in Immune-Related Diseases. DNA Cell Biol. 38, 1040–1047 (2019).
- 176. Dong, C. TH17 cells in development: an updated view of their molecular identity and genetic programming. *Nat. Rev. Immunol.* **8**, 337–348 (2008).
- 177. Veldhoen, M., Hocking, R. J., Atkins, C. J., Locksley, R. M. & Stockinger, B. TGFβ in the Context of an Inflammatory Cytokine Milieu Supports De Novo Differentiation of IL-17-Producing T Cells. *Immunity* **24**, 179–189 (2006).
- 178. Ivanov, I. I. *et al.* The orphan nuclear receptor RORgammat directs the differentiation program of proinflammatory IL-17+ T helper cells. *Cell* **126**, 1121–1133 (2006).
- 179. Chung, Y. *et al.* Expression and regulation of IL-22 in the IL-17-producing CD4+ T lymphocytes. *Cell Res.* **16**, 902–907 (2006).
- 180. Duhen, T., Geiger, R., Jarrossay, D., Lanzavecchia, A. & Sallusto, F. Production of interleukin 22 but not interleukin 17 by a subset of human skin-homing memory T cells. *Nat. Immunol.* **10**, 857–863 (2009).

- 181. Jia, L. & Wu, C. The Biology and Functions of Th22 Cells. in *T Helper Cell Differentiation and Their Function* (ed. Sun, B.) 209–230 (Springer Netherlands, Dordrecht, 2014).

 doi:10.1007/978-94-017-9487-9_8.
- 182. Yang, X.-W. *et al.* Recruitment and significance of Th22 cells and Th17 cells in malignant ascites. *Oncol. Lett.* **16**, 5389–5397 (2018).
- 183. Trifari, S., Kaplan, C. D., Tran, E. H., Crellin, N. K. & Spits, H. Identification of a human helper T cell population that has abundant production of interleukin 22 and is distinct from TH-17, TH1 and TH2 cells. *Nat. Immunol.* **10**, 864–871 (2009).
- 184. Johnston, R. J. *et al.* Bcl6 and Blimp-1 are reciprocal and antagonistic regulators of T follicular helper cell differentiation. *Science* **325**, 1006–1010 (2009).
- 185. Nurieva, R. I. *et al.* Bcl6 mediates the development of T follicular helper cells. *Science* **325**, 1001–1005 (2009).
- 186. Yu, D. *et al.* The transcriptional repressor Bcl-6 directs T follicular helper cell lineage commitment. *Immunity* **31**, 457–468 (2009).
- 187. Lee, S. K. *et al.* B cell priming for extrafollicular antibody responses requires Bcl-6 expression by T cells. *J. Exp. Med.* **208**, 1377–1388 (2011).
- 188. Zhang, Y. *et al.* Plasma cell output from germinal centers is regulated by signals from Tfh and stromal cells. *J. Exp. Med.* **215**, 1227–1243 (2018).
- 189. Yusuf, I. *et al.* Germinal center T follicular helper cell IL-4 production is dependent on signaling lymphocytic activation molecule receptor (CD150). *J. Immunol. Baltim. Md* 1950 **185**, 190–202 (2010).
- 190. Caramalho, Í., Nunes-Cabaço, H., Foxall, R. B. & Sousa, A. E. Regulatory T-Cell Development in the Human Thymus. *Front. Immunol.* **6**, 395 (2015).

- 191. Yadav, M., Bluestone, J. A. & Stephan, S. Peripherally Induced Tregs Role in Immune Homeostasis and Autoimmunity. *Front. Immunol.* **4**, (2013).
- 192. Hori, S., Nomura, T. & Sakaguchi, S. Control of regulatory T cell development by the transcription factor Foxp3. *Science* **299**, 1057–1061 (2003).
- 193. Fu, S. et al. TGF-beta induces Foxp3 + T-regulatory cells from CD4 + CD25 precursors. Am. J.

 Transplant. Off. J. Am. Soc. Transplant. Am. Soc. Transpl. Surg. 4, 1614–1627 (2004).
- 194. Mucida, D. *et al.* Oral tolerance in the absence of naturally occurring Tregs. *J. Clin. Invest.*115, 1923–1933 (2005).
- 195. Rubtsov, Y. P. *et al.* Regulatory T cell-derived interleukin-10 limits inflammation at environmental interfaces. *Immunity* **28**, 546–558 (2008).
- 196. Chaudhry, A. *et al.* Interleukin-10 signaling in regulatory T cells is required for suppression of Th17 cell-mediated inflammation. *Immunity* **34**, 566–578 (2011).
- 197. Konkel, J. E. *et al.* Transforming Growth Factor-β Signaling in Regulatory T Cells Controls T Helper-17 Cells and Tissue-Specific Immune Responses. *Immunity* **46**, 660–674 (2017).
- 198. Konopacki, C., Pritykin, Y., Rubtsov, Y., Leslie, C. S. & Rudensky, A. Y. Transcription factor Foxp1 regulates Foxp3 chromatin binding and coordinates regulatory T cell function. *Nat. Immunol.* **20**, 232–242 (2019).
- 199. Barthlott, T. *et al.* CD25+ CD4+ T cells compete with naive CD4+ T cells for IL-2 and exploit it for the induction of IL-10 production. *Int. Immunol.* **17**, 279–288 (2005).
- 200. Wu, Y. *et al.* FOXP3 controls regulatory T cell function through cooperation with NFAT. *Cell* **126**, 375–387 (2006).
- 201. Ono, M. *et al.* Foxp3 controls regulatory T-cell function by interacting with AML1/Runx1. *Nature* **446**, 685–689 (2007).

- 202. Feighery, C. & Stastny, P. HLA-D region-associated determinants serve as targets for human cell-mediated lysis. *J. Exp. Med.* **149**, 485–494 (1979).
- 203. Yang, D. *et al.* NKG2D+CD4+ T Cells Kill Regulatory T Cells in a NKG2D-NKG2D Ligand-Dependent Manner in Systemic Lupus Erythematosus. *Sci. Rep.* **7**, 1288 (2017).
- 204. Appay, V. et al. Characterization of CD4(+) CTLs ex vivo. J. Immunol. Baltim. Md 1950 168, 5954–5958 (2002).
- 205. Cachot, A. *et al.* Tumor-specific cytolytic CD4 T cells mediate immunity against human cancer. *Sci. Adv.* **7**, eabe3348 (2021).
- 206. Arenas-Ramirez, N., Woytschak, J. & Boyman, O. Interleukin-2: Biology, Design and Application. *Trends Immunol.* **36**, 763–777 (2015).
- 207. Saillard, M., Cenerenti, M., Romero, P. & Jandus, C. Impact of Immunotherapy on CD4 T Cell Phenotypes and Function in Cancer. *Vaccines* **9**, 454 (2021).
- 208. Potsch, C., Vöhringer, D. & Pircher, H. Distinct migration patterns of naive and effector CD8 T cells in the spleen: correlation with CCR7 receptor expression and chemokine reactivity. *Eur. J. Immunol.* 29, 3562–3570 (1999).
- 209. Schlub, T. E., Badovinac, V. P., Sabel, J. T., Harty, J. T. & Davenport, M. P. Predicting CD62L expression during the CD8+ T cell response in vivo. *Immunol. Cell Biol.* **88**, 157–164 (2010).
- 210. Kohlmeier, J. E. *et al.* Inflammatory chemokine receptors regulate CD8(+) T cell contraction and memory generation following infection. *J. Exp. Med.* **208**, 1621–1634 (2011).
- 211. Braun, J., Fujiwara, K., Pollard, T. D. & Unanue, E. R. Two distinct mechanisms for redistribution of lymphocyte surface macromolecules. I. Relationship to cytoplasmic myosin.
 J. Cell Biol. 79, 409–418 (1978).
- 212. Zöphel, D. *et al.* Faster cytotoxicity with age: Increased perforin and granzyme levels in cytotoxic CD8+ T cells boost cancer cell elimination. *Aging Cell* **21**, e13668 (2022).

- 213. Brincks, E. L., Katewa, A., Kucaba, T. A., Griffith, T. S. & Legge, K. L. CD8 T cells utilize TNF-related apoptosis-inducing ligand (TRAIL) to control influenza virus infection. *J. Immunol. Baltim. Md* 1950 **181**, 4918–4925 (2008).
- 214. Fu, Q. *et al.* Structural Basis and Functional Role of Intramembrane Trimerization of the Fas/CD95 Death Receptor. *Mol. Cell* **61**, 602–613 (2016).
- 215. Feau, S., Arens, R., Togher, S. & Schoenberger, S. P. Autocrine IL-2 is required for secondary population expansion of CD8(+) memory T cells. *Nat. Immunol.* **12**, 908–913 (2011).
- 216. Sa, Q., Woodward, J. & Suzuki, Y. IL-2 Produced by CD8+ Immune T cells Can Augment Their IFN-γ Production Independently from Their Proliferation in the Secondary Response to an Intracellular Pathogen. *J. Immunol. Baltim. Md* 1950 **190**, 2199–2207 (2013).
- 217. Toumi, R. *et al.* Autocrine and paracrine IL-2 signals collaborate to regulate distinct phases of CD8 T cell memory. *Cell Rep.* **39**, (2022).
- 218. Wang, S. *et al.* Exogenous IL-2 delays memory precursors generation and is essential for enhancing memory cells effector functions. *iScience* **27**, 109411 (2024).
- 219. Janas, M. L., Groves, P., Kienzle, N. & Kelso, A. IL-2 regulates perforin and granzyme gene expression in CD8+ T cells independently of its effects on survival and proliferation. *J. Immunol. Baltim. Md* 1950 **175**, 8003–8010 (2005).
- 220. Stonier, S. W., Ma, L. J., Castillo, E. F. & Schluns, K. S. Dendritic cells drive memory CD8 T-cell homeostasis via IL-15 transpresentation. *Blood* **112**, 4546–4554 (2008).
- 221. Montironi, C., Muñoz-Pinedo, C. & Eldering, E. Hematopoietic versus Solid Cancers and T Cell Dysfunction: Looking for Similarities and Distinctions. *Cancers* **13**, 284 (2021).
- 222. Gebhardt, T., Park, S. L. & Parish, I. A. Stem-like exhausted and memory CD8+ T cells in cancer. *Nat. Rev. Cancer* **23**, 780–798 (2023).

- 223. Manjunath, N. *et al.* Effector differentiation is not prerequisite for generation of memory cytotoxic T lymphocytes. *J. Clin. Invest.* **108**, 871–878 (2001).
- 224. Weninger, W., Crowley, M. A., Manjunath, N. & von Andrian, U. H. Migratory properties of naive, effector, and memory CD8(+) T cells. *J. Exp. Med.* **194**, 953–966 (2001).
- 225. Ortiz-Miranda, Y. *et al.* Transcriptional reprogramming by IL-2 variant generates metabolically active stem-like T cells. 2023.05.24.541283 Preprint at https://doi.org/10.1101/2023.05.24.541283 (2023).
- 226. Gattinoni, L. *et al.* A human memory T cell subset with stem cell-like properties. *Nat. Med.* **17**, 1290–1297 (2011).
- 227. Lugli, E. *et al.* Identification, isolation and in vitro expansion of human and nonhuman primate T stem cell memory cells. *Nat. Protoc.* **8**, 33–42 (2013).
- 228. Wherry, E. J. *et al.* Lineage relationship and protective immunity of memory CD8 T cell subsets. *Nat. Immunol.* **4**, 225–234 (2003).
- 229. Gattinoni, L. *et al.* A human memory T cell subset with stem cell–like properties. *Nat. Med.* **17**, 1290–1297 (2011).
- 230. Kumar, B. V. *et al.* Human tissue-resident memory T cells are defined by core transcriptional and functional signatures in lymphoid and mucosal sites. *Cell Rep.* **20**, 2921–2934 (2017).
- 231. Harding, F. A., McArthur, J. G., Gross, J. A., Raulet, D. H. & Allison, J. P. CD28-mediated signalling co-stimulates murine T cells and prevents induction of anergy in T-cell clones.

 Nature 356, 607–609 (1992).
- 232. Powell, J. D., Lerner, C. G. & Schwartz, R. H. Inhibition of cell cycle progression by rapamycin induces T cell clonal anergy even in the presence of costimulation. *J. Immunol. Baltim. Md* 1950 162, 2775–2784 (1999).

- 233. Liu, Y. *et al.* IL-2 regulates tumor-reactive CD8+ T cell exhaustion by activating the aryl hydrocarbon receptor. *Nat. Immunol.* **22**, 358–369 (2021).
- 234. Kim, Y.-J., Park, S.-J. & Broxmeyer, H. E. Phagocytosis, a potential mechanism for myeloid-derived suppressor cell regulation of CD8+ T cell function mediated through programmed cell death-1 and programmed cell death-1 ligand interaction. *J. Immunol. Baltim. Md* 1950 **187**, 2291–2301 (2011).
- 235. Thomas, D. A. & Massagué, J. TGF-beta directly targets cytotoxic T cell functions during tumor evasion of immune surveillance. *Cancer Cell* **8**, 369–380 (2005).
- 236. Ando, S. *et al.* mTOR regulates T cell exhaustion and PD-1-targeted immunotherapy response during chronic viral infection. *J. Clin. Invest.* **133**, e160025 (2023).
- 237. Fuertes Marraco, S. A., Neubert, N. J., Verdeil, G. & Speiser, D. E. Inhibitory Receptors

 Beyond T Cell Exhaustion. *Front. Immunol.* **6**, 310 (2015).
- 238. Gebhardt, T., Park, S. L. & Parish, I. A. Stem-like exhausted and memory CD8+ T cells in cancer. *Nat. Rev. Cancer* **23**, 780–798 (2023).
- 239. Hou, Y.-H. *et al.* Identification of a human B-cell/myeloid common progenitor by the absence of CXCR4. *Blood* **105**, 3488–3492 (2005).
- 240. Alt, F., Rosenberg, N., Lewis, S., Thomas, E. & Baltimore, D. Organization and reorganization of immunoglobulin genes in A-MULV-transformed cells: rearrangement of heavy but not light chain genes. *Cell* **27**, 381–390 (1981).
- 241. Gu, H., Förster, I. & Rajewsky, K. Sequence homologies, N sequence insertion and JH gene utilization in VHDJH joining: implications for the joining mechanism and the ontogenetic timing of Ly1 B cell and B-CLL progenitor generation. *EMBO J.* **9**, 2133–2140 (1990).
- 242. Jung, D. & Alt, F. W. Unraveling V(D)J Recombination: Insights into Gene Regulation. *Cell* **116**, 299–311 (2004).

- 243. Shinnakasu, R. & Kurosaki, T. Regulation of memory B and plasma cell differentiation. *Curr. Opin. Immunol.* **45**, 126–131 (2017).
- 244. Mintz, M. A. & Cyster, J. G. T follicular helper cells in germinal center B cell selection and lymphomagenesis. *Immunol. Rev.* **296**, 48–61 (2020).
- 245. Han, S. *et al.* Cellular interaction in germinal centers. Roles of CD40 ligand and B7-2 in established germinal centers. *J. Immunol. Baltim. Md* 1950 **155**, 556–567 (1995).
- 246. Howard, M. *et al.* Identification of a T cell-derived b cell growth factor distinct from interleukin 2. *J. Exp. Med.* **155**, 914–923 (1982).
- 247. Muramatsu, M. *et al.* Class Switch Recombination and Hypermutation Require Activation-Induced Cytidine Deaminase (AID), a Potential RNA Editing Enzyme. *Cell* **102**, 553–563 (2000).
- 248. Davis, M. M., Kim, S. K. & Hood, L. E. DNA sequences mediating class switching in alphaimmunoglobulins. *Science* **209**, 1360–1365 (1980).
- 249. Edelman, G. M. & Gally, J. A. The nature of Bence-Jones proteins. Chemical similarities to polypetide chains of myeloma globulins and normal gamma-globulins. *J. Exp. Med.* **116**, 207–227 (1962).
- 250. Edelman, G. M. DISSOCIATION OF γ-GLOBULIN. J. Am. Chem. Soc. **81**, 3155–3156 (1959).
- 251. Hilschmann, N. & Craig, L. C. Amino acid sequence studies with Bence-Jones proteins. *Proc. Natl. Acad. Sci.* **53**, 1403–1409 (1965).
- 252. Wu, T. T. & Kabat, E. A. AN ANALYSIS OF THE SEQUENCES OF THE VARIABLE REGIONS OF BENCE JONES PROTEINS AND MYELOMA LIGHT CHAINS AND THEIR IMPLICATIONS FOR ANTIBODY COMPLEMENTARITY. *J. Exp. Med.* **132**, 211–250 (1970).
- 253. Xu, J. L. & Davis, M. M. Diversity in the CDR3 region of V(H) is sufficient for most antibody specificities. *Immunity* **13**, 37–45 (2000).

- 254. Araki, K. & Maeda, R. A Brief Chronicle of Antibody Research and Technological Advances. *Antibodies Basel Switz.* **13**, 90 (2024).
- 255. Bournazos, S., Gupta, A. & Ravetch, J. V. The role of IgG Fc receptors in antibody-dependent enhancement. *Nat. Rev. Immunol.* **20**, 633–643 (2020).
- 256. de Taeye, S. W. *et al.* FcγR Binding and ADCC Activity of Human IgG Allotypes. *Front. Immunol.* **11**, (2020).
- 257. Schroeder, H. W. & Cavacini, L. Structure and Function of Immunoglobulins. *J. Allergy Clin. Immunol.* **125**, S41–S52 (2010).
- 258. Vidarsson, G., Dekkers, G. & Rispens, T. IgG Subclasses and Allotypes: From Structure to Effector Functions. *Front. Immunol.* **5**, 520 (2014).
- 259. Figure 1: The three Es of cancer immunoediting. | Nature Immunology.
- 260. Alexander, C. A. & Yang, Y. Y. Harnessing the combined potential of cancer immunotherapy and nanomedicine: A new paradigm in cancer treatment. *Nanomedicine Nanotechnol. Biol. Med.* 40, 102492 (2022).
- 261. Reva, B., Antipin, Y. & Sander, C. Predicting the functional impact of protein mutations: application to cancer genomics. *Nucleic Acids Res.* **39**, e118 (2011).
- 262. Angell, T. E., Lechner, M. G., Jang, J. K., LoPresti, J. S. & Epstein, A. L. MHC class I loss is a frequent mechanism of immune escape in papillary thyroid cancer that is reversed by interferon and selumetinib treatment in vitro. *Clin. Cancer Res. Off. J. Am. Assoc. Cancer Res.* 20, 6034–6044 (2014).
- 263. Anfossi, N. *et al.* Human NK cell education by inhibitory receptors for MHC class I. *Immunity* **25**, 331–342 (2006).

- 264. Lynch, T. J. *et al.* Activating mutations in the epidermal growth factor receptor underlying responsiveness of non-small-cell lung cancer to gefitinib. *N. Engl. J. Med.* **350**, 2129–2139 (2004).
- 265. Carlsson, J. *et al.* HER2 expression in breast cancer primary tumours and corresponding metastases. Original data and literature review. *Br. J. Cancer* **90**, 2344–2348 (2004).
- 266. De Falco, V. et al. Overexpression of CCL-20 and CXCL-8 genes enhances tumor escape and resistance to cemiplimab, a programmed cell death protein-1 (PD-1) inhibitor, in patients with locally advanced and metastatic cutaneous squamous cell carcinoma. *Oncoimmunology* 13, 2388315.
- 267. Yu, W. *et al.* PD-L1 promotes tumor growth and progression by activating WIP and β-catenin signaling pathways and predicts poor prognosis in lung cancer. *Cell Death Dis.* **11**, 1–16 (2020).
- 268. Itakura, E. *et al.* IL-10 expression by primary tumor cells correlates with melanoma progression from radial to vertical growth phase and development of metastatic competence. *Mod. Pathol.* **24**, 801–809 (2011).
- 269. Roex, M. C. J. *et al.* A minority of T cells recognizing tumor-associated antigens presented in self-HLA can provoke antitumor reactivity. *Blood* **136**, 455–467 (2020).
- 270. Aleksic, M. *et al.* Different affinity windows for virus and cancer-specific T-cell receptors: implications for therapeutic strategies. *Eur. J. Immunol.* **42**, 3174–3179 (2012).
- 271. Schumacher, T. *et al.* A vaccine targeting mutant IDH1 induces antitumour immunity. *Nature* **512**, 324–327 (2014).
- 272. Poprach, A. *et al.* Impact of Immunotherapy on Real-World Survival Outcomes in Metastatic Renal Cell Carcinoma. *Target. Oncol.* **18**, 893–903 (2023).

- 273. Search Orphan Drug Designations and Approvals.https://www.accessdata.fda.gov/scripts/opdlisting/oopd/detailedIndex.cfm?cfgridkey=29088.
- 274. Kash, N. *et al.* Safety and Efficacy Data on Vaccines and Immunization to Human Papillomavirus. *J. Clin. Med.* **4**, 614–633 (2015).
- 275. Butts, C. *et al.* Tecemotide (L-BLP25) versus placebo after chemoradiotherapy for stage III non-small-cell lung cancer (START): a randomised, double-blind, phase 3 trial. *Lancet Oncol.* **15**, 59–68 (2014).
- 276. Makker, S., Galley, C. & Bennett, C. L. Cancer vaccines: from an immunology perspective. *Immunother. Adv.* **4**, Itad030 (2024).
- 277. Peng, L., Sferruzza, G., Yang, L., Zhou, L. & Chen, S. CAR-T and CAR-NK as cellular cancer immunotherapy for solid tumors. *Cell. Mol. Immunol.* **21**, 1089–1108 (2024).
- 278. Wachsmann, T. L. A. *et al.* Comparing CAR and TCR engineered T cell performance as a function of tumor cell exposure. *Oncoimmunology* **11**, 2033528 (2022).
- 279. Neelapu, S. S. *et al.* Axicabtagene Ciloleucel CAR T-Cell Therapy in Refractory Large B-Cell Lymphoma. *N. Engl. J. Med.* **377**, 2531–2544 (2017).
- 280. Marin, D. *et al.* Safety, efficacy and determinants of response of allogeneic CD19-specific CAR-NK cells in CD19+ B cell tumors: a phase 1/2 trial. *Nat. Med.* **30**, 772–784 (2024).
- 281. Krummel, M. F. & Allison, J. P. CD28 and CTLA-4 have opposing effects on the response of T cells to stimulation. *J. Exp. Med.* **182**, 459–465 (1995).
- 282. Peggs, K. S., Quezada, S. A., Chambers, C. A., Korman, A. J. & Allison, J. P. Blockade of CTLA-4 on both effector and regulatory T cell compartments contributes to the antitumor activity of anti-CTLA-4 antibodies. *J. Exp. Med.* **206**, 1717–1725 (2009).

- 283. Freeman, G. J. *et al.* Engagement of the PD-1 immunoinhibitory receptor by a novel B7 family member leads to negative regulation of lymphocyte activation. *J. Exp. Med.* **192**, 1027–1034 (2000).
- 284. Agata, Y. *et al.* Expression of the PD-1 antigen on the surface of stimulated mouse T and B lymphocytes. *Int. Immunol.* **8**, 765–772 (1996).
- 285. Ishida, Y., Agata, Y., Shibahara, K. & Honjo, T. Induced expression of PD-1, a novel member of the immunoglobulin gene superfamily, upon programmed cell death. *EMBO J.* **11**, 3887–3895 (1992).
- 286. Hodi, F. S. *et al.* Improved survival with ipilimumab in patients with metastatic melanoma. *N. Engl. J. Med.* **363**, 711–723 (2010).
- 287. Patnaik, A. *et al.* Phase I Study of Pembrolizumab (MK-3475; Anti-PD-1 Monoclonal Antibody) in Patients with Advanced Solid Tumors. *Clin. Cancer Res. Off. J. Am. Assoc. Cancer Res.* **21**, 4286–4293 (2015).
- 288. Felip, E. *et al.* Overall survival with adjuvant atezolizumab after chemotherapy in resected stage II-IIIA non-small-cell lung cancer (IMpower010): a randomised, multicentre, open-label, phase III trial. *Ann. Oncol. Off. J. Eur. Soc. Med. Oncol.* **34**, 907–919 (2023).
- 289. Socinski, M. A. *et al.* Atezolizumab for First-Line Treatment of Metastatic Nonsquamous NSCLC. *N. Engl. J. Med.* **378**, 2288–2301 (2018).
- 290. Reck, M. *et al.* Pembrolizumab versus Chemotherapy for PD-L1–Positive Non–Small-Cell Lung Cancer. *N. Engl. J. Med.* **375**, 1823–1833 (2016).
- 291. Yamaguchi, H., Hsu, J.-M., Sun, L., Wang, S.-C. & Hung, M.-C. Advances and prospects of biomarkers for immune checkpoint inhibitors. *Cell Rep. Med.* **5**, (2024).

- 292. Ozguroglu, M. *et al.* 971TiP Phase III trial of durvalumab combined with domvanalimab following concurrent chemoradiotherapy (cCRT) in patients with unresectable stage III NSCLC (PACIFIC-8). *Ann. Oncol.* **33**, S991 (2022).
- 293. Falchook, G. S. *et al.* Phase 1 trial of TIM-3 inhibitor cobolimab monotherapy and in combination with PD-1 inhibitors nivolumab or dostarlimab (AMBER). *J. Clin. Oncol.* **40**, 2504–2504 (2022).
- 294. Yoo, S.-K. *et al.* Prediction of checkpoint inhibitor immunotherapy efficacy for cancer using routine blood tests and clinical data. *Nat. Med.* 1–12 (2025) doi:10.1038/s41591-024-03398-5.
- 295. Gupta, R., Mehta, A. & Wajapeyee, N. Transcriptional determinants of cancer immunotherapy response and resistance. *Trends Cancer* **8**, 404–415 (2022).
- 296. Behring, N. & Kitasato, N. Ueber das Zustandekommen der Diphtherie-Immunität und der Tetanus-Immunität bei Thieren. *DMW Dtsch. Med. Wochenschr.* **16**, 1113–1114 (2009).
- 297. Shulman, M., Wilde, C. D. & Köhler, G. A better cell line for making hybridomas secreting specific antibodies. *Nature* **276**, 269–270 (1978).
- 298. Cotton, R. G. H. & Milstein, C. Fusion of Two Immunoglobulin-producing Myeloma Cells.

 Nature 244, 42–43 (1973).
- 299. Köhler, G. & Milstein, C. Continuous cultures of fused cells secreting antibody of predefined specificity. *Nature* **256**, 495–497 (1975).
- 300. Abramowicz, D., Crusiaux, A. & Goldman, M. Anaphylactic shock after retreatment with OKT3 monoclonal antibody [6]. *N. Engl. J. Med.* **327**, 736 (1992).
- 301. Jones, P. T., Dear, P. H., Foote, J., Neuberger, M. S. & Winter, G. Replacing the complementarity-determining regions in a human antibody with those from a mouse. *Nature* 321, 522–525 (1986).

- 302. Boulianne, G. L., Hozumi, N. & Shulman, M. J. Production of functional chimaeric mouse/human antibody. *Nature* **312**, 643–646 (1984).
- 303. Jespers, L. S., Roberts, A., Mahler, S. M., Winter, G. & Hoogenboom, H. R. Guiding the Selection of Human Antibodies from Phage Display Repertoires to a Single Epitope of an Antigen. *Bio/Technology* **12**, 899–903 (1994).
- 304. Smith, G. P. Filamentous Fusion Phage: Novel Expression Vectors That Display Cloned Antigens on the Virion Surface. *Science* **228**, 1315–1317 (1985).
- 305. Song, B. P. C., Ch'ng, A. C. W. & Lim, T. S. Review of phage display: A jack-of-all-trades and master of most biomolecule display. *Int. J. Biol. Macromol.* **256**, 128455 (2024).
- 306. Yang, C.-H., Li, H.-C. & Lo, S.-Y. Enhancing recombinant antibody yield in Chinese hamster ovary cells. *Tzu-Chi Med. J.* **36**, 240–250 (2024).
- 307. Liu, H. F., Ma, J., Winter, C. & Bayer, R. Recovery and purification process development for monoclonal antibody production. *mAbs* **2**, 480–499 (2010).
- 308. Slavny, P. *et al.* Advancements in mammalian display technology for therapeutic antibody development and beyond: current landscape, challenges, and future prospects. *Front. Immunol.* **15**, (2024).
- 309. Cheloff, A. Z. & Al-Samkari, H. Emapalumab for the treatment of hemophagocytic lymphohistiocytosis. *Drugs Today Barc. Spain 1998* **56**, 439–446 (2020).
- 310. Schiff, M. H. *et al.* Safety analyses of adalimumab (HUMIRA) in global clinical trials and US postmarketing surveillance of patients with rheumatoid arthritis. *Ann. Rheum. Dis.* **65**, 889–894 (2006).
- 311. Cheng, J., Liang, T., Xie, X.-Q., Feng, Z. & Meng, L. A new era of antibody discovery: an indepth review of Al-driven approaches. *Drug Discov. Today* **29**, 103984 (2024).

- 312. Brüggemann, M. *et al.* Comparison of the effector functions of human immunoglobulins using a matched set of chimeric antibodies. *J. Exp. Med.* **166**, 1351–1361 (1987).
- 313. Damelang, T. *et al.* The Influence of Human IgG Subclass and Allotype on Complement Activation. *J. Immunol. Author Choice* **211**, 1725–1735 (2023).
- 314. Gibson, T. B., Ranganathan, A. & Grothey, A. Randomized phase III trial results of panitumumab, a fully human anti-epidermal growth factor receptor monoclonal antibody, in metastatic colorectal cancer. *Clin. Colorectal Cancer* **6**, 29–31 (2006).
- 315. Saito, S., Namisaki, H., Hiraishi, K., Takahashi, N. & Iida, S. A stable engineered human IgG3 antibody with decreased aggregation during antibody expression and low pH stress. *Protein Sci. Publ. Protein Soc.* **28**, 900–909 (2019).
- 316. Labrijn, A. F., Aalberse, R. C. & Schuurman, J. When binding is enough: nonactivating antibody formats. *Curr. Opin. Immunol.* **20**, 479–485 (2008).
- 317. Burnet, F. M. *The Production of Antibodies; a Review and a Theoretical Discussion.*(Macmillan and Company Ltd., Melbourne, 1941).
- 318. Callahan, M. K. & Wolchok, J. D. At the Bedside: CTLA-4- and PD-1-blocking antibodies in cancer immunotherapy. *J. Leukoc. Biol.* **94**, 41–53 (2013).
- 319. Chin, S. M. *et al.* Structure of the 4-1BB/4-1BBL complex and distinct binding and functional properties of utomilumab and urelumab. *Nat. Commun.* **9**, 4679 (2018).
- 320. Chodorge, M. *et al.* A series of Fas receptor agonist antibodies that demonstrate an inverse correlation between affinity and potency. *Cell Death Differ.* **19**, 1187–1195 (2012).
- 321. Ho, M. Inaugural Editorial: Searching for Magic Bullets. Antib. Ther. 1, 1–5 (2018).
- 322. Shields, R. L. *et al.* High Resolution Mapping of the Binding Site on Human IgG1 for FcγRI, FcγRII, FcγRIII, and FcRn and Design of IgG1 Variants with Improved Binding to the FcγR *. *J. Biol. Chem.* **276**, 6591–6604 (2001).

- 323. Tien, J. *et al.* Modifying antibody-FcRn interactions to increase the transport of antibodies through the blood-brain barrier. *mAbs* **15**, 2229098.
- 324. Wilkinson, I. *et al.* Fc-engineered antibodies with immune effector functions completely abolished. *PLoS ONE* **16**, e0260954 (2021).
- 325. Lindley, C. *et al.* Perception of chemotherapy side effects cancer versus noncancer patients. *Cancer Pract.* **7**, 59–65 (1999).
- 326. Fu, Z., Li, S., Han, S., Shi, C. & Zhang, Y. Antibody drug conjugate: the "biological missile" for targeted cancer therapy. *Signal Transduct. Target. Ther.* **7**, 1–25 (2022).
- 327. Minckwitz, G. von *et al.* Trastuzumab Emtansine for Residual Invasive HER2-Positive Breast Cancer. *N. Engl. J. Med.* **380**, 617–628 (2019).
- 328. Schuurman, J. *et al.* Normal human immunoglobulin G4 is bispecific: it has two different antigen-combining sites. *Immunology* **97**, 693–698 (1999).
- 329. Milstein, C. & Cuello, A. C. Hybrid hybridomas and their use in immunohistochemistry.

 Nature **305**, 537–540 (1983).
- 330. Ridgway, J. B. B., Presta, L. G. & Carter, P. 'Knobs-into-holes' engineering of antibody CH3 domains for heavy chain heterodimerization. *Protein Eng. Des. Sel.* **9**, 617–621 (1996).
- 331. Gunasekaran, K. *et al.* Enhancing Antibody Fc Heterodimer Formation through Electrostatic Steering Effects. *J. Biol. Chem.* **285**, 19637–19646 (2010).
- 332. Schaefer, W. et al. Immunoglobulin domain crossover as a generic approach for the production of bispecific IgG antibodies. *Proc. Natl. Acad. Sci.* **108**, 11187–11192 (2011).
- 333. Fischer, N. *et al.* Exploiting light chains for the scalable generation and platform purification of native human bispecific IgG. *Nat. Commun.* **6**, 6113 (2015).
- 334. Mazor, Y. *et al.* Enhanced tumor-targeting selectivity by modulating bispecific antibody binding affinity and format valence. *Sci. Rep.* **7**, 40098 (2017).

- 335. Baines, A. C. *et al.* FDA Approval Summary: Teclistamab-A Bispecific CD3 T-Cell Engager for Patients with Relapsed or Refractory Multiple Myeloma. *Clin. Cancer Res. Off. J. Am. Assoc. Cancer Res.* **30**, 5515–5520 (2024).
- 336. Cho, B. C. *et al.* Amivantamab plus Lazertinib in Previously Untreated EGFR-Mutated Advanced NSCLC. *N. Engl. J. Med.* **391**, 1486–1498 (2024).
- 337. Wu, J. *et al.* A PD-1-targeted, receptor-masked IL-2 immunocytokine that engages IL-2Rα strengthens T cell-mediated anti-tumor therapies. *Cell Rep. Med.* **5**, (2024).
- 338. Wu, L. *et al.* Trispecific antibodies enhance the therapeutic efficacy of tumor-directed T cells through T cell receptor co-stimulation. *Nat. Cancer* **1**, 86–98 (2020).
- 339. Janas, M. L., Groves, P., Kienzle, N. & Kelso, A. IL-2 regulates perforin and granzyme gene expression in CD8+ T cells independently of its effects on survival and proliferation. *J. Immunol. Baltim. Md* 1950 **175**, 8003–8010 (2005).
- 340. Fyfe, G. *et al.* Results of treatment of 255 patients with metastatic renal cell carcinoma who received high-dose recombinant interleukin-2 therapy. *J. Clin. Oncol. Off. J. Am. Soc. Clin. Oncol.* **13**, 688–696 (1995).
- 341. Atkins, M. B. *et al.* High-dose recombinant interleukin 2 therapy for patients with metastatic melanoma: analysis of 270 patients treated between 1985 and 1993. *J. Clin. Oncol. Off. J. Am. Soc. Clin. Oncol.* **17**, 2105–2116 (1999).
- 342. Dutcher, J. P. *et al.* High dose interleukin-2 (Aldesleukin) expert consensus on best management practices-2014. *J. Immunother. Cancer* **2**, 26 (2014).
- 343. Zimmerman, R. J., Aukerman, S. L., Katre, N. V., Winkelhake, J. L. & Young, J. D. Schedule dependency of the antitumor activity and toxicity of polyethylene glycol-modified interleukin 2 in murine tumor models. *Cancer Res.* **49**, 6521–6528 (1989).

- 344. Yang, J. C. *et al.* The use of polyethylene glycol-modified interleukin-2 (PEG-IL-2) in the treatment of patients with metastatic renal cell carcinoma and melanoma. A phase I study and a randomized prospective study comparing IL-2 alone versus IL-2 combined with PEG-IL-2. *Cancer* **76**, 687–694 (1995).
- 345. Albertini, M. R. *et al.* Phase II trial of hu14.18-IL2 for patients with metastatic melanoma. *Cancer Immunol. Immunother. ClI* **61**, 2261–2271 (2012).
- 346. Shusterman, S. et al. Antitumor Activity and Tolerability of hu14.18-IL2 with GMCSF and Isotretinoin in Recurrent or Refractory Neuroblastoma: A Children's Oncology Group Phase II Study. Clin. Cancer Res. Off. J. Am. Assoc. Cancer Res. 25, 6044–6051 (2019).
- 347. Nirschl, C. J. *et al.* Discovery of a Conditionally Activated IL-2 that Promotes Antitumor Immunity and Induces Tumor Regression. *Cancer Immunol. Res.* **10**, 581–596 (2022).
- 348. Rodriguez-Rivera, I. I. *et al.* Abstract CT133: Trial in progress: a multicenter phase 1/1b dose escalation study of WTX-124 as a monotherapy and in combination with pembrolizumab in patients with selected advanced or metastatic solid tumors. *Cancer Res.* **83**, CT133 (2023).
- 349. Charych, D. H. *et al.* NKTR-214, an Engineered Cytokine with Biased IL2 Receptor Binding,
 Increased Tumor Exposure, and Marked Efficacy in Mouse Tumor Models. *Clin. Cancer Res. Off. J. Am. Assoc. Cancer Res.* **22**, 680–690 (2016).
- 350. Bentebibel, S.-E. *et al.* A First-in-Human Study and Biomarker Analysis of NKTR-214, a Novel IL2Rβγ-Biased Cytokine, in Patients with Advanced or Metastatic Solid Tumors. *Cancer Discov.* **9**, 711–721 (2019).
- 351. Zia, M. I., Siu, L. L., Pond, G. R. & Chen, E. X. Comparison of outcomes of phase II studies and subsequent randomized control studies using identical chemotherapeutic regimens. *J. Clin. Oncol. Off. J. Am. Soc. Clin. Oncol.* **23**, 6982–6991 (2005).

- 352. Lopes, J. E. *et al.* ALKS 4230: a novel engineered IL-2 fusion protein with an improved cellular selectivity profile for cancer immunotherapy. *J. Immunother. Cancer* **8**, e000673 (2020).
- 353. Vaishampayan, U. N. *et al.* Nemvaleukin alfa, a modified interleukin-2 cytokine, as monotherapy and with pembrolizumab in patients with advanced solid tumors (ARTISTRY-1). *J. Immunother. Cancer* **12**, e010143 (2024).
- 354. Herzog, T. J. *et al.* ARTISTRY-7: A phase 3, multicenter study of nemvaleukin alfa in combination with pembrolizumab versus chemotherapy in patients with platinum-resistant epithelial ovarian, fallopian tube, or primary peritoneal cancer (GOG-3063; ENGOT-OV68). *J. Clin. Oncol.* **41**, TPS5612–TPS5612 (2023).
- 355. Klein, C. *et al.* Cergutuzumab amunaleukin (CEA-IL2v), a CEA-targeted IL-2 variant-based immunocytokine for combination cancer immunotherapy: Overcoming limitations of aldesleukin and conventional IL-2-based immunocytokines. *Oncoimmunology* **6**, e1277306 (2017).
- 356. Simlukafusp alfa (FAP-IL2v) immunocytokine is a versatile combination partner for cancer immunotherapy PubMed. https://pubmed.ncbi.nlm.nih.gov/33974508/.
- 357. PD-1-cis IL-2R agonism yields better effectors from stem-like CD8+ T cells | Nature. https://www.nature.com/articles/s41586-022-05192-0.
- 358. Hoffmann-La Roche. *An Open-Label, Multicenter, Randomized, Dose-Escalation and Extension, Phase IA/IB Study to Evaluate Safety and Anti-Tumor Activity of RO7284755, A PD-1 Targeted IL-2 Variant (IL-2V) Immunocytokine, Alone or in Combination With Atezolizumab in Participants With Advanced and/or Metastatic Solid Tumors.*https://clinicaltrials.gov/study/NCT04303858 (2024).

- 359. Merchant, R. *et al.* Fine-tuned long-acting interleukin-2 superkine potentiates durable immune responses in mice and non-human primate. *J. Immunother. Cancer* **10**, e003155 (2022).
- 360. Atkinson, V. G. *et al.* Abstract CT259: Results from monotherapy dose escalation of MDNA11, a long-acting IL-2 superkine, in a phase 1/2 trial show evidence of single-agent activity in advanced solid tumors. *Cancer Res.* **84**, CT259 (2024).
- 361. Moynihan, K. D. *et al.* IL2 Targeted to CD8+ T Cells Promotes Robust Effector T-cell Responses and Potent Antitumor Immunity. *Cancer Discov.* **14**, 1206–1225 (2024).
- 362. Zhang, Q. *et al.* A human orthogonal IL-2 and IL-2Rβ system enhances CAR T cell expansion and antitumor activity in a murine model of leukemia. *Sci. Transl. Med.* **13**, eabg6986 (2021).
- 363. Synthekine. A Phase 1, Open-Label Study to Evaluate the Safety and Tolerability of a

 Combination Autologous CD19 CAR T Cell Therapy (SYNCAR-001 + STK-009) in Subjects with

 Severe, Refractory Systemic Lupus Erythematosus.

 https://clinicaltrials.gov/study/NCT06544330 (2024).
- 364. Chamie, K. *et al.* Final clinical results of pivotal trial of IL-15RαFc superagonist N-803 with BCG in BCG-unresponsive CIS and papillary nonmuscle-invasive bladder cancer (NMIBC). *J. Clin. Oncol.* **40**, 4508–4508 (2022).
- 365. Robinson, T. O. *et al.* NKTR-255 is a polymer-conjugated IL-15 with unique mechanisms of action on T and natural killer cells. *J. Clin. Invest.* **131**, e144365.
- 366. Srinagesh, H. *et al.* A phase 1 clinical trial of NKTR-255 with CD19-22 CAR T-cell therapy for refractory B-cell acute lymphoblastic leukemia. *Blood* **144**, 1689–1698 (2024).
- 367. Alizadeh, D. *et al.* IL15 Enhances CAR-T Cell Antitumor Activity by Reducing mTORC1 Activity and Preserving Their Stem Cell Memory Phenotype. *Cancer Immunol. Res.* **7**, 759–772 (2019).

- 368. Wang, X., Rickert, M. & Garcia, K. C. Structure of the Quaternary Complex of Interleukin-2 with Its a, b, and gc Receptors. **310**, (2005).
- 369. Yang, Y. & Lundqvist, A. Immunomodulatory Effects of IL-2 and IL-15; Implications for Cancer Immunotherapy. *Cancers* **12**, 3586 (2020).
- 370. Sznol, M. & Rizvi, N. Teaching an old dog new tricks: re-engineering IL-2 for immuno-oncology applications. *J. Immunother. Cancer* **11**, e006346 (2023).
- 371. Sprent, J. & Boyman, O. Optimising IL-2 for Cancer Immunotherapy. *Immune Netw.* **24**, e5 (2024).
- 372. Krieg, C., Létourneau, S., Pantaleo, G. & Boyman, O. Improved IL-2 immunotherapy by selective stimulation of IL-2 receptors on lymphocytes and endothelial cells. *Proc. Natl. Acad. Sci.* **107**, 11906–11911 (2010).
- 373. Peace, D. J. & Cheever, M. A. Toxicity and therapeutic efficacy of high-dose interleukin 2. In vivo infusion of antibody to NK-1.1 attenuates toxicity without compromising efficacy against murine leukemia. *J. Exp. Med.* **169**, 161–173 (1989).
- 374. Arenas-Ramirez, N. *et al.* Improved cancer immunotherapy by a CD25-mimobody conferring selectivity to human interleukin-2. *Sci. Transl. Med.* **8**, (2016).
- 375. Joerger, M. *et al.* Phase 1 first-in-human dose-escalation study of ANV419 in patients with relapsed/refractory advanced solid tumors. *J. Immunother. Cancer* **11**, e007784 (2023).
- 376. Lopes, J. E. et al. ALKS 4230: a novel engineered IL-2 fusion protein with an improved cellular selectivity profile for cancer immunotherapy. *J. Immunother. Cancer* **8**, e000673 (2020).
- 377. Merchant, R. *et al.* Fine-tuned long-acting interleukin-2 superkine potentiates durable immune responses in mice and non-human primate. *J. Immunother. Cancer* **10**, e003155 (2022).

- 378. Silva, D.-A. et al. De novo design of potent and selective mimics of IL-2 and IL-15. Nature **565**, 186–191 (2019).
- 379. Harris, K. E. *et al.* A bispecific antibody agonist of the IL-2 heterodimeric receptor preferentially promotes in vivo expansion of CD8 and NK cells. *Sci. Rep.* **11**, 10592 (2021).
- 380. Yen, M. et al. Facile discovery of surrogate cytokine agonists. Cell 185, 1414-1430.e19 (2022).
- 381. Margolin, K. *et al.* Phase I Trial of BAY 50-4798, an Interleukin-2–Specific Agonist in Advanced Melanoma and Renal Cancer. *Clin. Cancer Res.* **13**, 3312–3319 (2007).
- 382. Nirschl, C. J. *et al.* Discovery of a Conditionally Activated IL-2 that Promotes Antitumor Immunity and Induces Tumor Regression. *Cancer Immunol. Res.* **10**, 581–596 (2022).
- 383. Guzman, W. *et al.* 841 XTX202, a tumor-selective protein-engineered IL-2, exhibited enhanced anti-tumor activity in combination with checkpoint inhibition in mice. in *Regular and Young Investigator Award Abstracts* A877–A877 (BMJ Publishing Group Ltd, 2022). doi:10.1136/jitc-2022-SITC2022.0841.
- 384. Shi, W. *et al.* Next-generation anti-PD-L1/IL-15 immunocytokine elicits superior antitumor immunity in cold tumors with minimal toxicity. *Cell Rep. Med.* 101531 (2024) doi:10.1016/j.xcrm.2024.101531.
- 385. Klein, C. *et al.* Cergutuzumab amunaleukin (CEA-IL2v), a CEA-targeted IL-2 variant-based immunocytokine for combination cancer immunotherapy: Overcoming limitations of aldesleukin and conventional IL-2-based immunocytokines. *OncoImmunology* **6**, e1277306 (2017).
- 386. Ongaro, T. *et al.* A novel format for recombinant antibody-interleukin-2 fusion proteins exhibits superior tumor-targeting properties *in vivo*. *Oncotarget* **11**, 3698–3711 (2020).
- 387. Waldhauer, I. *et al.* Simlukafusp alfa (FAP-IL2v) immunocytokine is a versatile combination partner for cancer immunotherapy. *mAbs* **13**, 1913791 (2021).

- 388. Quijano-Rubio, A. *et al.* A split, conditionally active mimetic of IL-2 reduces the toxicity of systemic cytokine therapy. *Nat. Biotechnol.* **41**, 532–540 (2023).
- 389. Overwijk, W. W., Tagliaferri, M. A. & Zalevsky, J. Engineering IL-2 to Give New Life to T Cell Immunotherapy. *Annu. Rev. Med.* **72**, 281–311 (2021).
- 390. Smith, G. A., Taunton, J. & Weiss, A. IL-2Rβ abundance differentially tunes IL-2 signaling dynamics in CD4+ and CD8+ T cells. *Sci. Signal.* **10**, eaan4931 (2017).
- 391. Carmenate, T. *et al.* The antitumor effect induced by an IL-2 'no-alpha' mutein depends on changes in the CD8+ T lymphocyte/Treg cell balance. *Front. Immunol.* **13**, (2022).
- 392. Codarri Deak, L. *et al.* PD-1-cis IL-2R agonism yields better effectors from stem-like CD8+ T cells. *Nature* **610**, 161–172 (2022).
- 393. Piper, M. *et al.* Simultaneous targeting of PD-1 and IL-2Rβγ with radiation therapy inhibits pancreatic cancer growth and metastasis. *Cancer Cell* S1535610823001174 (2023) doi:10.1016/j.ccell.2023.04.001.
- 394. Hashimoto, M. *et al.* PD-1 combination therapy with IL-2 modifies CD8+ T cell exhaustion program. *Nature* **610**, 173–181 (2022).
- 395. Li, J. et al. Membrane-Proximal Epitope Facilitates Efficient T Cell Synapse Formation by Anti-FcRH5/CD3 and Is a Requirement for Myeloma Cell Killing. *Cancer Cell* **31**, 383–395 (2017).
- 396. Qi, J. *et al.* Potent and selective antitumor activity of a T cell-engaging bispecific antibody targeting a membrane-proximal epitope of ROR1. *Proc. Natl. Acad. Sci.* **115**, (2018).
- 397. Hatterer, E. *et al.* Targeting a membrane-proximal epitope on mesothelin increases the tumoricidal activity of a bispecific antibody blocking CD47 on mesothelin-positive tumors. *mAbs* **12**, 1739408 (2020).

- 398. Ortiz-Miranda, Y. *et al.* Transcriptional reprogramming by IL-2 variant generates metabolically active stem-like T cells. Preprint at https://doi.org/10.1101/2023.05.24.541283 (2023).
- 399. Andreata, F. *et al.* CD8 cis-targeted IL-2 drives potent antiviral activity against hepatitis B virus. *Sci. Transl. Med.* **16**, eadi1572 (2024).
- 400. Dautry-Varsat, A. Endocytosis of Interleukin 2 Receptors in Human T Lymphocytes: Distinct Intracellular Localization and Fate of the Receptor a,/3, and -yChains. (1995).
- 401. Diab, A. *et al.* Bempegaldesleukin Plus Nivolumab in Untreated Advanced Melanoma: The Open-Label, Phase III PIVOT IO 001 Trial Results. *J. Clin. Oncol.* **41**, 4756–4767 (2023).
- 402. Chamie, K. *et al.* N-803 Plus BCG Treatment for BCG-Naïve or -Unresponsive Non-Muscle Invasive Bladder Cancer: A Plain Language Review. *Future Oncol.* 1–11 (2024) doi:10.1080/14796694.2024.2363744.
- 403. Chamie, K. *et al.* IL-15 Superagonist NAI in BCG-Unresponsive Non–Muscle-Invasive Bladder Cancer. *NEJM Evid.* **2**, (2023).
- 404. Hassan, R. & Ho, M. Mesothelin targeted cancer immunotherapy. *Eur. J. Cancer* **44**, 46–53 (2008).
- 405. Rosen, D. B. *et al.* TransCon IL-2 β/γ : a novel long-acting prodrug with sustained release of an IL-2R β/γ -selective IL-2 variant with improved pharmacokinetics and potent activation of cytotoxic immune cells for the treatment of cancer. *J. Immunother. Cancer* **10**, e004991 (2022).
- 406. Akilesh, S. *et al.* Podocytes use FcRn to clear IgG from the glomerular basement membrane. *Proc. Natl. Acad. Sci. U. S. A.* **105**, 967–972 (2008).
- 407. Morphis, L. G. & Gitlin, D. Maturation of the maternofoetal transport system for human gamma-globulin in the mouse. *Nature* **228**, 573 (1970).

- 408. Toh, W. H. *et al.* FcRn mediates fast recycling of endocytosed albumin and IgG from early macropinosomes in primary macrophages. *J. Cell Sci.* **133**, jcs235416 (2019).
- 409. Klein, C. *et al.* Engineering therapeutic bispecific antibodies using CrossMab technology. *Methods* **154**, 21–31 (2019).
- 410. Dheilly, E. *et al.* Selective Blockade of the Ubiquitous Checkpoint Receptor CD47 Is Enabled by Dual-Targeting Bispecific Antibodies. *Mol. Ther.* **25**, 523–533 (2017).
- 411. Zervos, E., Agle, S., Freistaedter, A. G., Jones, G. J. B. & Roper, R. L. Murine mesothelin: characterization, expression, and inhibition of tumor growth in a murine model of pancreatic cancer. *J. Exp. Clin. Cancer Res. CR* **35**, 39 (2016).
- 412. Hassan, R. *et al.* Detection and Quantitation of Serum Mesothelin, a Tumor Marker for Patients with Mesothelioma and Ovarian Cancer. *Clin. Cancer Res.* **12**, 447–453 (2006).
- 413. Liu, X., Chan, A., Tai, C.-H., Andresson, T. & Pastan, I. Multiple proteases are involved in mesothelin shedding by cancer cells. *Commun. Biol.* **3**, 1–9 (2020).
- 414. Lichtenthaler, S. F., Lemberg, M. K. & Fluhrer, R. Proteolytic ectodomain shedding of membrane proteins in mammals-hardware, concepts, and recent developments. *EMBO J.* **37**, e99456 (2018).
- 415. Awuah, P., Bera, T. K., Folivi, M., Chertov, O. & Pastan, I. Reduced Shedding of Surface Mesothelin Improves Efficacy of Mesothelin Targeting Recombinant Immunotoxins. *Mol. Cancer Ther.* **15**, 1648–1655 (2016).
- 416. Stonier, S. W., Ma, L. J., Castillo, E. F. & Schluns, K. S. Dendritic cells drive memory CD8 T-cell homeostasis via IL-15 transpresentation. *Blood* **112**, 4546–4554 (2008).
- 417. Ross, S. H. *et al.* Phosphoproteomic Analyses of Interleukin 2 Signaling Reveal Integrated JAK Kinase-Dependent and -Independent Networks in CD8+ T Cells. *Immunity* **45**, 685–700 (2016).

- 418. Hémar, A. *et al.* Endocytosis of interleukin 2 receptors in human T lymphocytes: distinct intracellular localization and fate of the receptor alpha, beta, and gamma chains. *J. Cell Biol.* **129**, 55–64 (1995).
- 419. Hatterer, E. *et al.* Targeting a membrane-proximal epitope on mesothelin increases the tumoricidal activity of a bispecific antibody blocking CD47 on mesothelin-positive tumors. *mAbs* **12**, 1739408 (2020).
- 420. Nami, B., Maadi, H. & Wang, Z. The Effects of Pertuzumab and Its Combination with Trastuzumab on HER2 Homodimerization and Phosphorylation. *Cancers* **11**, 375 (2019).
- 421. Yu, X. *et al.* Reducing affinity as a strategy to boost immunomodulatory antibody agonism.

 Nature **614**, 539–547 (2023).
- 422. Jia, Z. *et al.* IL12 immune therapy clinical trial review: Novel strategies for avoiding CRS-associated cytokines. *Front. Immunol.* **13**, (2022).
- 423. Yen, M. et al. Facile discovery of surrogate cytokine agonists. Cell 185, 1414-1430.e19 (2022).
- 424. Tichet, M. *et al.* Bispecific PD1-IL2v and anti-PD-L1 break tumor immunity resistance by enhancing stem-like tumor-reactive CD8+ T cells and reprogramming macrophages. *Immunity* **56**, 162-179.e6 (2023).
- 425. Horn, L. A. *et al.* Vaccine Increases the Diversity and Activation of Intratumoral T Cells in the Context of Combination Immunotherapy. *Cancers* **13**, 968 (2021).
- 426. Peng, L., Sferruzza, G., Yang, L., Zhou, L. & Chen, S. CAR-T and CAR-NK as cellular cancer immunotherapy for solid tumors. *Cell. Mol. Immunol.* **21**, 1089–1108 (2024).
- 427. Rosenberg, S. A. *et al.* Durable complete responses in heavily pretreated patients with metastatic melanoma using T-cell transfer immunotherapy. *Clin. Cancer Res. Off. J. Am. Assoc. Cancer Res.* **17**, 4550–4557 (2011).

11 Appendices

11.1 Appendix 1:

Composition and methods for the selective activation of cytokine signaling pathways Patent filed internationally (PCT/EP2023/051721), January 2023

The patent protects the approach and illustrates the concept of paired bispecific antibodies. I was involved in most of the laboratory experiments presented here. While the final formatting and writing was done by attorneys, I was involved in the writing of the patent and presentation of the data.

COMPOSITION AND METHODS FOR THE SELECTIVE ACTIVATION OF CYTOKINE SIGNALING PATHWAYS

RELATED APPLICATIONS

[0001] This application claims priority to, and the benefit of, U.S. Application No. 63/302,514, filed on January 24, 2022. The contents of this application are incorporated herein by reference in its entirety.

INCORPORATION-BY-REFERENCE OF SEQUENCE LISTING

[0002] The Sequence Listing XML associated with this application is provided electronically in XML file format and is hereby incorporated by reference into the specification. The name of the XML file containing the Sequence Listing XML is NOVI_049_001WO_SeqList_ST26.xml. The XML file is 158,062 bytes in size, created on January 24, 2023.

BACKGROUND OF THE INVENTION

[0003] Interleukin-2 (IL-2) is a 15 kDa cytokine essential for the balance between activation and suppression of immune responses. Under normal conditions, CD4⁺ helper T cells are the main producers of the cytokine. Upon immune activation, both CD4⁺ and CD8⁺ T cells are induced to produce IL-2 and the induction is regulated through a negative feedback loop involving B lymphocyte-induced maturation protein 1 (BLIMP1)

[0004] IL-2 receptor (IL-2R) has three subunits, IL-2R α (CD25), IL-2R β (CD122) and IL-2R γ (CD132). Of the three IL-2R subunits, only IL-2R α is unique to IL-2R. IL-2R γ (also called the common γ chain) is common with IL-4, IL-7, IL-9, IL-15 and IL-21 receptor complexes. IL-2R β is common with the Interleukin-15 (IL-15) receptor complex. IL-15 is a cytokine for the development, proliferation, and activation of effector NK cells and CD8⁺ memory T cells. IL-15 binds to the IL-15 receptor α (IL-15R α) and is presented in trans to the IL-2R β -IL2R γ complex on effector cells. IL-15 and IL-2 share binding to the IL-2R β -IL2R γ complex, and signal through STAT3 and STATS pathways. However, unlike IL-2, IL-15 does not support maintenance of CD4⁺CD25⁺FoxP3⁺ regulatory T (Treg) cells or induce cell death of activated CD8⁺ T cells. Additionally, IL-15 is the only cytokine known to provide anti-apoptotic signaling to effector CD8⁺ T cells. IL-15 signaling exhibits

1

280919112 v1

11.2 Appendix 2:

IFN-γ-dependent tumor-antigen cross-presentation by lymphatic endothelial cells promotes their killing by T cells and inhibits metastasis

Published in Science Advances, June 2022

This paper publishes a study on which I have worked during my Master thesis. This study investigates the interaction between T cells and Lymphatic endothelial cells. This study illustrates the importance of IFN-γ for cytotoxic cell-mediated killing of lymphatic endothelial cells and the effect on metastasis development. In this study I was involved in the experiments performed and the discussions regarding the project while I was in the lab. During that time, we performed flow cytometry analysis of mouse tumors and lymphoid tissues, live cell imaging, and qPCR.

IMMUNOLOGY

IFN- γ -dependent tumor-antigen cross-presentation by lymphatic endothelial cells promotes their killing by T cells and inhibits metastasis

Laure Garnier¹*, Robert Pick¹†, Julien Montorfani¹†, Mengzhu Sun¹, Dale Brighouse¹, Nicolas Liaudet², Thomas Kammertoens^{3,4}, Thomas Blankenstein^{3,4,5}, Nicolas Page^{1,6}, Jeremiah Bernier-Latamani⁷, Ngoc Lan Tran¹, Tatiana V. Petrova⁷, Doron Merkler^{1,6,8}, Christoph Scheiermann^{1,8,9}, Stéphanie Hugues^{1,8}*

Tumor-associated lymphatic vessels promote metastasis and regulate antitumor immune responses. Here, we assessed the impact of cytotoxic T cells on the local lymphatic vasculature and concomitant tumor dissemination during an antitumor response. Interferon-\(\gamma\) (IFN-\(\gamma\)) released by effector T cells enhanced the expression of immunosuppressive markers by tumor-associated lymphatic endothelial cells (LECs). However, at higher effector T cell densities within the tumor, T cell-based immunotherapies induced LEC apoptosis and decreased tumor lymphatic vessel density. As a consequence, lymphatic flow was impaired, and lymph node metastasis was reduced. Mechanistically, T cell-mediated tumor cell death induced the release of tumor antigens and cross-presentation by tumor LECs, resulting in antigen-specific LEC killing by T cells. When LECs lacked the IFN-\(\gamma\) receptor expression, LEC killing was abrogated, indicating that IFN-\(\gamma\) is indispensable for reducing tumor-associated lymphatic vessel density and drainage. This study provides insight into how cytotoxic T cells modulate tumor lymphatic vessels and may help to improve immunotherapeutic protocols.

Copyright © 2022
The Authors, some rights reserved; exclusive licensee American Association for the Advancement of Science. No claim to original U.S. Government Works. Distributed under a Creative Commons Attribution NonCommercial License 4.0 (CC BY-NC).

INTRODUCTION

Metastasis is the principal cause of mortality in human cancers. Although cancer cells can disseminate through blood vessels (BVs), most solid cancers, such as breast cancer and melanoma, propagate through the lymphatic vessels (LVs) to first reach the sentinel lymph nodes (LNs) (1). Occurrence of tumor cells in LNs is associated with poor prognosis in multiple types of cancers (2). Studies have shown that metastatic tumor cells additionally migrate through LVs to settle adjacent LNs, where they invade local BVs to further colonize distant organs (3, 4). Tumor LVs are not simple passive conduits for metastatic dissemination. Mouse and human studies indicate that lymphatic endothelial cells (LECs) lining the lymphatic vasculature react to factors present in the tumor microenvironment (TME), promoting LV growth and remodeling in primary tumors and draining LNs (dLNs). This process is called lymphangiogenesis and correlates with metastasis and impaired disease-free survival (2, 5). Expression of the lymphangiogenic factor vascular endothelial growth factor-C (VEGF-C) in patient samples is associated with LN metastasis in several types of cancers (2, 6, 7). In murine models, alterations of VEGF-C and VEGF-D receptor signaling influence metastatic dissemination to LNs and/or distal organs (8–16). LV expansion within sentinel LNs induces the formation of a "premetastatic niche" that would favor metastatic cell colonization (10, 17, 18). LVs in distant metastatic regions further contribute to tumor progression by attracting chemotherapy-resistant cancer stem-like cells (19). Moreover, LVs promote lung metastasis and additional spreading to other organs in an inducible lung lymphangiogenesis mouse model (20). In patients with melanoma, lymphatic exudates are enriched in tumor-derived factors and exhibit distinct tumor protein profiles depending on the metastatic stage of the patients, suggesting that they might be used to predict disease progression and response to treatment (21).

Besides their critical role in tumor cell dissemination. LVs are key players in the initiation and the regulation of antitumor immune responses, including T cell activation and infiltration in tumors. While studies have indicated a possible local priming of naïve T cell infiltrating solid tumors (22-24), antigen transport by dendritic cells (DCs) through LVs to the dLNs is, nevertheless, crucial for the initiation of T cell responses in melanoma (25, 26). Consistent with a beneficial role of the lymphatic vasculature in antitumor immunity, the expression of genes associated to lymphatics or LV density (LVD) positively correlates with tumor-infiltrating inflammatory immune cell numbers in primary colorectal cancer and melanoma (27-29). Transgenic mice lacking or exhibiting disturbed local LVs demonstrate limited tumor drainage, reduced DC migration to dLNs, decreased tumor-infiltrating leucocyte numbers, and impaired antitumor adaptive immunity (25, 30). However, LVD and lymphatic score (attributed by the relative expression levels of LV-related genes) are also associated with enhanced infiltration of immunosuppressive cells and expression of immunoregulatory molecules (25, 27, 28). Therefore, although LVs are required for intratumoral T cell infiltration, they inhibit ongoing adaptive antitumor immunity. In mouse

Garnier et al., Sci. Adv. 8, eabl5162 (2022) 8 June 2022

¹Department of Pathology and Immunology, Geneva Medical School, Geneva, Switzerland. ²Bioimaging Core Facility, Faculty of Medicine, University of Geneva, Geneva, Switzerland. ³Institute of Immunology, Charité Campus Buch, 13125 Berlin, Germany. ⁴Max Delbrück Center for Molecular Medicine, 13125 Berlin, Germany. ⁵Berlin Institute of Health, 10117 Berlin, Germany. ⁵Department of Pathology and Immunology, Division of Clinical Pathology, University of Geneva and University Hospital of Geneva, Geneva, Switzerland. ⁷Department of Fundamental Oncology, Ludwig Institute for Cancer Research and Division of Experimental Pathology, University of Lusanne and University of Lusanne hospital, 1066 Lausanne, Switzerland. ⁸Geneva Centre for Inflammation Research, Geneva, Switzerland. ⁹Walter-Brendel-Centre of Experimental Medicine, BioMedical Centre, Ludwig Maximilians University Munich, Planega-Martinsried, Germany.

^{*}Corresponding author. Email: stephanie.hugues@unige.ch (S.H.); laure.garnier@unige.ch (L.G.)

[†]These authors contributed equally to this work.

melanoma, tumor dLN (TdLN) LECs cross-present tumor antigen to foster the apoptosis of tumor-specific CD8+ T cells (31). In colorectal cancer, VEGF-C signaling in tumor LECs enhances their immunosuppressive properties through a synergistic cooperation with tumor-associated macrophages (32). In multiple subcutaneous tumor mouse models, tumor LECs up-regulate the immunosuppressive molecule programmed death-ligand 1 (PD-L1) in response to interferon-γ (IFN-γ) produced by tumor-specific CD8⁺ T cells (33, 34), thereby reducing intratumoral CD8⁺ T cells (34). Recently, we demonstrated that IFN-γ signaling induces the up-regulation of major histocompatibility complex (MHC) class II molecules by tumor LECs, which locally promote the suppressive functions of regulatory T cells, leading to an inhibition of cytotoxic CD8+ T lymphocyte (CTL) effector functions and promoting tumor growth (35). VEGF-C-induced lymphangiogenesis combined with immunotherapy can potentiate antitumor T cell responses in murine melanoma and glioblastoma (28, 36). Furthermore, serum VEGF-C levels in patients with melanoma positively correlate with a response to immunotherapy and progression-free survival (28). In agreement, lymphangiogenic vaccines composed of irradiated tumor cells engineered to overexpress VEGF-C administered outside the tumor bed promote tumor-specific T cell immunity and potentiate antiprogrammed cell death protein 1 (PD-1) immunotherapy in mouse melanoma (37).

Although the dual role and the spatiotemporal effects of LVs in antitumor immunity need to be considered, targeting the lymphatic vasculature represents a promising therapeutic strategy to restrain cancer cell dissemination. A better understanding of the mechanisms implicated in solid tumor rejection and disruption of the tumor vasculature will help to optimize immunotherapeutic protocols. Effective antigen-dependent killing of stromal cells by transferred CTLs is crucial to indirectly eliminate antigen loss variants (ALVs) in established tumor (38, 39). Cancer cell death enhances the elimination of the tumor stroma through the release of tumor antigens that sensitize stromal cells for antigen-specific CTL killing (38-40). Tumor necrosis factor (TNF), Fas ligand (FasL), and IFN-γ expression by CTLs-together with the expression of their respective receptors TNFR, Fas, and IFN- γR by stromal cells—are required for the bystander eradication of ALVs (41-43). IFN-v produced by adoptively transferred CTLs inhibits tumorinduced angiogenesis (44). The selective expression of IFN-γR by endothelial cells is sufficient for IFN-y-induced BV destruction and tumor regression (45). IFN-γ secretion by T cells reduces LVD in both steady-state and inflamed LNs (46) and promotes LEC immunosuppressive function in tumors (34, 35). However, the impact of T cell-based immunotherapies on intratumor LVD has not been determined.

In this study, we show that therapies involving cytotoxic T cell responses targeting tumors induce LEC apoptosis and lead to a reduction of tumor LVD. As a consequence, lymphatic flow drainage and metastatic dissemination into LNs are diminished. These effects are abolished in the absence of IFN- γ R expression by LECs, indicating that T cells rely on the IFN- γ signaling pathway to restrain tumor LVs. Mechanistically, IFN- γ signaling in LECs potentiates their capacity to cross-present tumor antigens released after CTL-mediated tumor cell death and their subsequent killing by CTLs. This study provides important insights into how CTLs modulate LVs to optimize the design of protocols for immunotherapies in cancer.

RESULTS

Immunotherapy using tumor-specific CD8⁺ T cells induces tumor LEC apoptosis

We used several approaches to evaluate how T cell-based immunotherapies affect tumor LECs. First, we adoptively transferred 1×10^6 ovalbumin (OVA)-specific T cell receptor (TCR) transgenic OT-1 CD45.1+ CD8+ effector T cells into B16F10-OVA+VC+ tumor-bearing C57BL/6 mice (Fig. 1A). B16F10-OVA+VC+ is a melanoma cell line expressing the model antigen OVA and engineered to produce elevated levels of the lymphangiogenic factor VEGF-C (31). OT-1 effectors efficiently infiltrated OVA-expressing tumors, where they actively produced IFN-γ and granzyme-B (fig. S1A). OT-1 transfer induced efficient tumor regression (Fig. 1A), as well as a significant up-regulation of PD-L1 and MHCII molecules by tumor LECs (fig. S1, B and C), corroborating earlier findings that LECs exposed to IFN-γ up-regulated IFN-γ-target genes (34, 35). In addition, OT-1 effector cell transfer resulted in a significant decrease in the density of tumor LECs (Fig. 1B), as well as their increased expression of the proapoptotic marker activated caspase 3 (cleaved casp-3) (Fig. 1C). In contrast, we did not observe any effect of OT-1 transfer on LEC proliferation (fig. S1D), indicating that elevated intratumoral VEGF-C levels were maintained following OT-1-mediated tumor cell killing. In vitro generated OT-1 effectors adoptively transferred into tumor-bearing mice, representing 2% of CD8+T cells in TdLNs (fig. S1E), and failed at inducting cleaved casp-3 in LN LECs (fig. S1F).

Tumor LV reduction and tumor LEC apoptosis were also observed when OT-1 effector cells were adoptively transferred into mice bearing a mixed tumor, resulting from the injection of a 9:1 B16F10-VC+ and B16F10-OVA+VC+ cell ratio (fig. S1, G to I). Tumor rejection was not observed in this context (fig. S1G), ruling out the possibility that reduced LV densities in tumors following OT-1 effector cell transfer resulted from lower VEGF-C levels in smaller tumors. We further performed LEC (Lyve-1⁺) (31, 35) and OT-1 (CD45.1⁺) immunofluorescent staining on tumors from B16F10-OVA+VC+ bearing mice adoptively transferred with OT-1 effector cells (+OT-1) or not (-). OT-1 transfer induced a decrease in LV area (Lyve-1+) (Fig. 1D), with a more pronounced effect on LVs located at the center of the tumor compared to the periphery of the tumor (Fig. 1D). OT-1 transfer was further associated with a higher proportion of cleaved casp-3+ cells on tumor LECs (Fig. 1E). Transferred OT-1 cells were not randomly distributed in tumors but were preferentially localized in close proximity of tumor LVs (fig. S1J).

We next vaccinated B16F10-OVA+VC+ tumor-bearing mice with CpG-B + OVA, which led to increased density of IFN-γ- and granzyme-B-producing CD8⁺ T cell in the tumor (fig. S2A), tumor regression (Fig. 1F), as well as enhanced expression levels of PD-L1 and MHCII on tumor LECs (fig. S2, B and C). LEC proliferation was slightly decreased upon vaccination (fig. S2D). LVD was significantly reduced 7 days after vaccination (Fig. 1G), and cleaved casp-3 was increased in tumor LECs (Fig. 1H). To determine whether the pathway can be observed by vaccinating with an endogenous tumor antigen, B16F10-OVA⁺VC⁺ tumor-bearing mice were vaccinated with CpG-B + Gp100 peptide and transferred with Gp100specific TCR transgenic Pmel-1 CD8+ T cell effectors. Gp100 vaccination, Pmel-1 transfer, or a combination of the two all induced tumor regression and up-regulation of PD-L1 and MHCII by tumor LECs (fig. S3, A to C). However, only the combination of vaccination and T cell transfer reduced tumor LVD (fig. S3D) and enhanced LEC apoptosis (fig. S3E), confirming our observations by using an

Garnier et al., Sci. Adv. 8, eabl5162 (2022) 8 June 2022

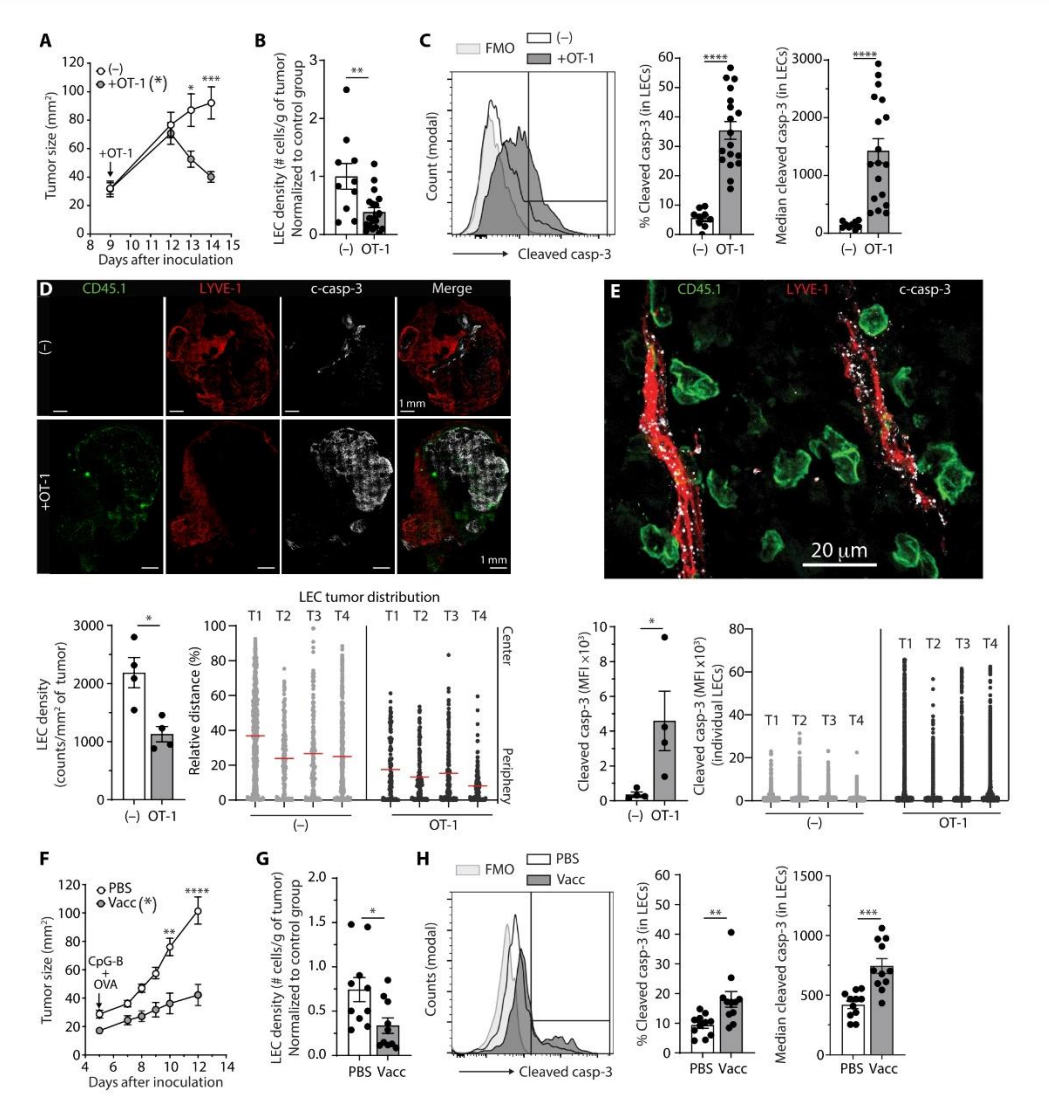


Fig. 1. Boosting tumor-specific T cell responses promotes tumor LEC apoptosis. (A to E) C57BL/6 mice were injected or not with in vitro activated CD8⁺ OT-1 CD45.1⁺ cells (1 × 10⁶ cells) 9 days after B16F10-OVA⁺VC⁺ inoculation. (A) Tumor growth. (B) LVD (number of LECs per grams of tumor, normalized to control group) and (C) frequency and median of cleaved casp-3⁺ (casp-3) LECs (CD45^{neg} CD31⁺ GP38⁺) in tumors at day 14 by flow cytometry. Graphs represent a pool of two experiments with 10 to 18 mice per group. (D and E) Representative immunofluorescent labeled tumor sections stained against OT-1 (CD45.1; green), LECs (Lyve-1; red), cleaved casp-3 (c-casp-3) (white), and merge without (–) or upon OT-1 transfer at day 4 after transfer. (D) LVD measured as Lyve-1⁺ cell counts per square millimeter of tumor and relative tumor LEC distribution in individual tumors (T1 to T4). (E) LEC cleaved casp-3 activity [mean fluorescence intensity (MFI)] per tumor and per individual tumor LECs. (F to H) C57BL/6 mice were vaccinated or not with CpG-8+ OVA at day 5 after B16F10-OVA⁺VC⁺ inoculation. (F) Tumor growth. (G) LVD and (H) frequency and median of cleaved casp-3⁺ LECs in tumors at day 12 by flow cytometry. Graphs represent a pool of two experiments with 10 to 11 mice per group. (A and F) Two-way analysis of variance (ANOVA) test; (B to E, G, and H) Mann-Whitney test. Error bars show means ± SEM. *P < 0.001, ***P < 0.001, ****P < 0.001.*****P < 0.0001.*****

endogenous tumor antigen. Last, B16F10-VC⁺ (OVA negative) tumor-bearing mice were vaccinated with irradiated B16F10-VC⁺ cells in the presence of CpG-B and adoptively transferred with CD8⁺ T cells preactivated in vitro with irradiated B16F10-VC⁺ cells loaded

DCs (Polyclonal-ATT). This treatment induced a potent tumor growth control (fig. S3F), induced the up-regulation of MHCII by tumor LECs (fig. S3G), and resulted in reduced tumor LEC density (fig. S3H) and increased frequencies of cleaved casp-3⁺ LECs (fig. S3I).

Garnier et al., Sci. Adv. 8, eabl5162 (2022) 8 June 2022

Therefore, tumor LEC killing and LV inhibition can be induced by boosting polyclonal tumor-specific CTLs. Together, our data indicate that immunotherapies aiming at increasing the numbers of tumor-specific T cell effectors in tumors locally induce LEC apoptosis and decrease LVD.

Tumor LEC apoptosis requires elevated CTL numbers

We hypothesized that a threshold of CTL density in tumors is necessary to overcome IFN-γ-mediated LV immunosuppression through the killing of tumor LECs. To determine whether LEC killing correlates with CTL density, we transferred two different amounts $(0.05 \times 10^6 \text{ and } 0.5 \times 10^6)$ of OT-1 effectors in B16F10-OVA+VC+ tumor-bearing mice. We observed a dose-dependent reduction of tumor growth 5 days after T cell transfer (Fig. 2A), which was correlated with the density of IFN-γ- and granzyme-B-producing OT-1 cell in tumors (fig. S4A). Whereas both doses induced PD-L1 up-regulation by tumor LECs as soon as 3 days after T cell transfer (fig. S4B), increased frequencies of cleaved casp-3+ LECs (Fig. 2B) and reduced LEC densities (Fig. 2C) happened to be T cell dose dependent. Densities of OT1 T cells within the tumor (Fig. 2D), producing IFN-γ (Fig. 2E) and granzyme-B (Fig. 2F), were positively correlated to the frequency of apoptotic tumor LECs, reinforcing a dose-dependent effect of OT-1 effectors on tumor LEC apoptosis. However, given the data distribution observed in Fig. 2 (D to F), additional factors present in the TME likely influence OT-1 effector location and functions.

We next investigated whether tumor LEC killing also occurs in the absence of immunotherapy in a more immunogenic tumor mouse model. We used MC38-OVA⁺ adenocarcinoma cells engineered to

overproduce VEGF-C (MC38-OVA+VC+ cells). In vitro, VEGF-C mRNA levels in MC38-OVA+VC+ cell cultures were increased around 60-fold compared with the MC38-OVA cell line and were 1.6-fold less than in B16F10-OVA+VC+ cells (fig. S4C). In vivo, VEGF-C levels in B16F10-OVA+VC+ and MC38-OVA+VC+ tumors were measured in the same range of concentrations (fig. S4D). We compared C57BL/6 inoculated with either B16F10-OVA+VC+ cells or MC38-OVA+VC+ cells. MC38-OVA+VC+ tumors exhibited a slower growth (fig. S4E). Granzyme-B CD8⁺ effector T cell densities were significantly enhanced in MC38-OVA+VC+ tumors compared to $B16F10\text{-}OVA^+VC^+$ tumors (fig. S4F). PD-L1 expression levels were increased in MC38-OVA+VC+ compared to B16F10-OVA+VC+ tumor LECs (fig. S4G). LV frequency and density were markedly lower (fig. S4H), and the frequency of cleaved casp-3 in tumor LECs was enhanced in MC38-OVA+VC+ tumors (fig. S4I). Although different molecular and/or cellular actors specific to a given TME may also influence LEC density, these data show that elevated CTL numbers in the tumor tissue correlate with tumor LVD inhibition. We next thought to determine whether LEC killing by infiltrating CTLs occurs in B16F10-OVA+ tumors, which do not overexpress VEGF-C. OT-1 effector transferred in B16F10-OVA+ and B16F10-OVA+VC+ tumorbearing mice controlled tumor growth (fig. S4J) and induced PD-L1 and MHCII up-regulation in tumor LECs (fig. S4, K and L). Frequencies of cleaved casp-3+ LECs were notably elevated in B16F10-OVA+ tumors compared to B16F10-OVA+VC+ tumors already in the absence of OT-1 transfer (fig. S4M). As expected, OT-1 transfer significantly increased cleaved casp-3⁺ LEC frequencies (fig. S4M) and reduced LEC densities (fig. S4N) in B16F10-OVA+VC+ tumors. In contrast, cleaved casp-3+ LEC frequencies remained similar in

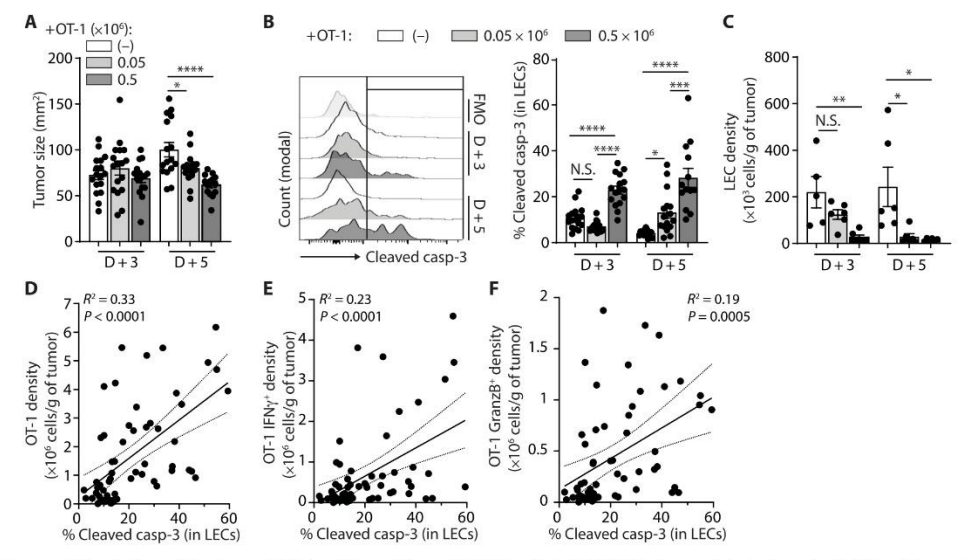


Fig. 2. Positive correlation between intratumoral CTL densities and tumor LEC killing. (A to C) C57BL/6 mice were injected or not with different doses of in vitro activated OT-1 cells $(0.05 \times 10^6 \text{ cells})$ 9 days after B16-OVA-VC inoculation and euthanized 3 or 5 days later. (A) Tumor size, (B) frequency of cleaved casp-3⁺ tumor LECs, and (C) LEC density 3 and 5 days after injection. Data represent a pool of three experiments (A and B) with N = 16 to 17 mice per group and one experiment (C) with 5 to 6 mice per group. (D to F) Correlations between (D) OT-1, (E) OT-1-producing IFN- γ , and (F) OT-1-producing granzyme-B densities and the frequency of cleaved casp-3⁺ tumor LECs 5 days after transfer of 0.5×10^6 activated OT-1 cells. Data represent a pool of six experiments, N = 59 mice. (A to C) One-way ANOVA test; (D to F) linear regression. Error bars show means $\pm 5 \text{EM}$. N.S., not significant. *P $\times 0.05$, **P $\times 0.01$, ***P $\times 0.001$, ***P $\times 0.0001$.

Garnier et al., Sci. Adv. 8, eabl5162 (2022) 8 June 2022

B16F10-OVA $^+$ tumors with and without OT-1 transfer (fig. S4M). The amount of LECs is extremely low in B16F10-OVA $^+$ compared to B16F10-OVA $^+$ VC $^+$ tumors (fig. S4N), supporting the idea that an elevated ratio CTL/LEC results in tumor LEC killing by infiltrating CTLs. Accordingly, whereas the density of CTL was 10-fold higher in B16F10-OVA $^+$ VC $^+$ tumors compared to B16F10-OVA $^+$ tumors (fig. S4O), the ratio CTL density/LEC density remained 50-fold higher in B16F10-OVA $^+$ tumors compared to B16F10-OVA $^+$ tumors (fig. S4P).

Adoptive transfer of tumor-specific T cells restricts lymphatic drainage

LVs are the primary route for cancer cell spreading and metastasis establishment in sentinel LNs and distal organs. Therefore, targeting the lymphatic vasculature represents a promising therapeutic strategy to restrain cancer cell dissemination. We next assessed whether LVD decrease upon tumor-specific CD8⁺ T effector transfer would result in impaired LV drainage functions.

in impaired LV drainage functions.

In B16F10-OVA 'VC' tumor-bearing mice injected intratumorally with fluorescein isothiocyanate (FITC) beads, the migration of FITC' DCs in TdLNs was reduced in mice adoptively transferred 5 days before with 0.5 × 10⁶ but not 0.05 × 10⁶ of OT-1 effectors (Fig. 3A). In contrast, the frequency of total DCs in the TdLNs was not altered in mice adoptively transferred with either of the two OT-1 doses (Fig. 3B). In addition, the transfer of 0.5 × 10⁶ OT-1 cells reduced metastasis in LNs proximal to the tumor, as quantified by the black color intensity in inguinal, axillary, and brachial LNs (fig. S5A). Whereas the number of cancer-positive inguinal LNs was not affected by OT-1 transfer, we observed an increased proportion of axillary and brachial LNs devoid of metastasis following adoptive T cell transfer (ATT) (fig. S5A). Gp100 staining of TdLN sections

further indicated that LN metastasis was significantly reduced 5 days after the transfer of 0.5×10^6 OT-1 effectors, in terms of both the number of metastatic foci per LNs and the number of metastasispositive LNs (fig. S5B). The size of primary tumors being significantly decreased upon OT-1 adoptive transfer, reduced LN metastasis can be a combination of lower tumor cell spreading and impaired LV drainage. Therefore, we next thought to determine whether LV disruption significantly contributes to reduced LN metastasis following ATT. We adoptively transferred OT-1 cells in B16F10-OVA+VC+ tumor-bearing mice and further injected peritumorally cell trace violet (CTV)-labeled B16F10-VC+ tumor cells at a time point primary tumor sizes were not decreased by the adoptive transfer of OT1. Adoptive transfer of OT-1 cells drastically inhibited the de novo migration of CTV-labeled B16F10-VC+ tumor cells toward primary and secondary TdLNs (Fig. 3C). In summary, these results demonstrate that elevated numbers of tumor-specific effector T cells induce LEC apoptosis in tumors, resulting in LV dismantling, altered drainage to TdLNs, and diminished LN metastasis.

IFN- γ has been shown to negatively affect LN-LV (46). As CTLs represent a substantial source of IFN- γ in tumors, we next sought to determine whether LV destruction by ATT relies on IFN- γ R signaling in tumor LECs. We generated conditional knockout (KO) mice in which LECs do not express IFN- γ R subunit 2. Prox-1 Cre^{ERT2} mice (47), which express the tamoxifen-inducible Cre recombinase under the promoter of the LEC-specific transcription factor Prox-1, were crossed with IFN- γ R2^{flox/flox} mice (IFN- γ R^{Δ prox-1} mice) (48). We validated by quantitative polymerase chain reaction (qPCR) the

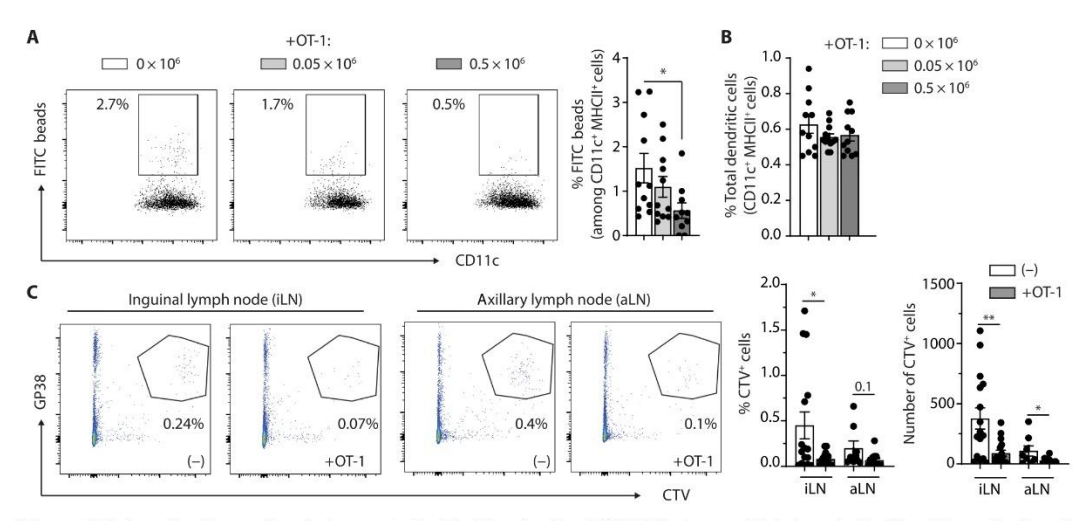


Fig. 3. Tumor LV drainage functions are impaired upon adoptive T cell transfer. (A and B) C57BL/6 mice were injected or not with different doses of in vitro activated OT-1 cells $(0.05 \times 10^6 \text{ col} \text{ S} \times 10^6 \text{ col} \text{ S})$ 9 days after B16F10-OVA $^+\text{VC}^+$ inoculation and euthanized 5 days later. FITC-labeled beads (0.5 mm) were injected intratumorally 24 hours before euthanasia. Frequencies of (A) FITC beads $^+$ DCs (CD11c $^+$ MHClI $^+$) and (B) total DCs in TdLNs (pool of inguinal and axillary LN) by flow cytometry. Data represent two pooled experiments, N = 10 to 11 mice per group. (C) C57BL/6 mice were inoculated with B16F10-OVA $^+$ VC $^+$ and were injected or not with 0.5×10^6 in vitro activated OT-1 cells 9 days later. CTV-labeled B16F10-VC $^+$ tumor cells were injected peritumorally at day 13, and mice were euthanized at day 14. Frequencies of GP38 $^+$ CTV $^+$ cells in the TdLNs (inguinal and axillary). Data represent a pool of three experiments, N = 14 to 15 mice per group. (A and B) One-way ANOVA; (C) Mann-Whitney statistical test. Error bars show means \pm SEM. $^+P < 0.05$, $^+P < 0.01$.

Garnier et al., Sci. Adv. 8, eabl5162 (2022) 8 June 2022

deletion of IFN- γ R2 in LECs sorted from B16F10-OVA $^+$ VC $^+$ tumors of IFN- γ R $^{\Delta prox-1}$ mice (fig. S6A). Lyve-1 staining of naïve LNs showed a modest but significant increase in LVD in steady-state IFN- γ R $^{\Delta prox-1}$ LNs compared to IFN- γ R WT control LNs (Fig. 4A), confirming previously published data that T cell–derived IFN- γ secretion inhibits LV-specific genes in LN LECs and consequently reduce in LN-LV (46). Whereas ATT did not modify IFN- γ R1 and Jak1 mRNA levels, it enhanced the expression of STAT-1 and different IFN- γ response genes, such as IFN regulatory factor 1 (IRF-1), CIITA (Class II Major Histocompatibility Complex Transactivator), MHCII, and PD-L1 genes in LECs from B16F10-OVA $^+$ VC $^+$ tumors in IFN- γ R WT control mice (fig. S6A). These effects were abolished in tumor LECs from IFN- γ R $^{\Delta prox-1}$ mice, highlighting an IFN- γ R signaling–dependent

mechanism (fig. S6A). PD-L1 and MHCII were also up-regulated at the protein level in tumor LECs following OT-1 transfer in IFN-γ R^{WT} controls, whereas it was abrogated in IFN-γ $R^{\Delta prox-1}$ mice (fig. S6, B and C). Notably, PD-L1 and MHCII up-regulation after OT-1 transfer was observed in tumor blood endothelial cells (BECs) from both IFN-γ R^{WT} and IFN-γ $R^{\Delta prox-1}$ mice (fig. S6, D and E), again validating the specific deletion of IFN-γR in LECs.

Although OT-1 transfer similarly induced B16F10-OVA ${}^{+}$ VC ${}^{+}$ tumor regression in IFN- $\gamma R^{\rm MT}$ and IFN- $\gamma R^{\rm Aprox-1}$ mice (Fig. 4B), both the reduction of tumor LVD (Fig. 4C) and the increase of LEC apoptosis (Fig. 4D) induced by ATT were abolished in IFN- $\gamma R^{\rm Aprox-1}$ mice, demonstrating that IFN- γ is crucial for LV killing. Whereas LVs were increased in steady-state LNs from IFN- $\gamma R^{\rm Aprox-1}$ mice

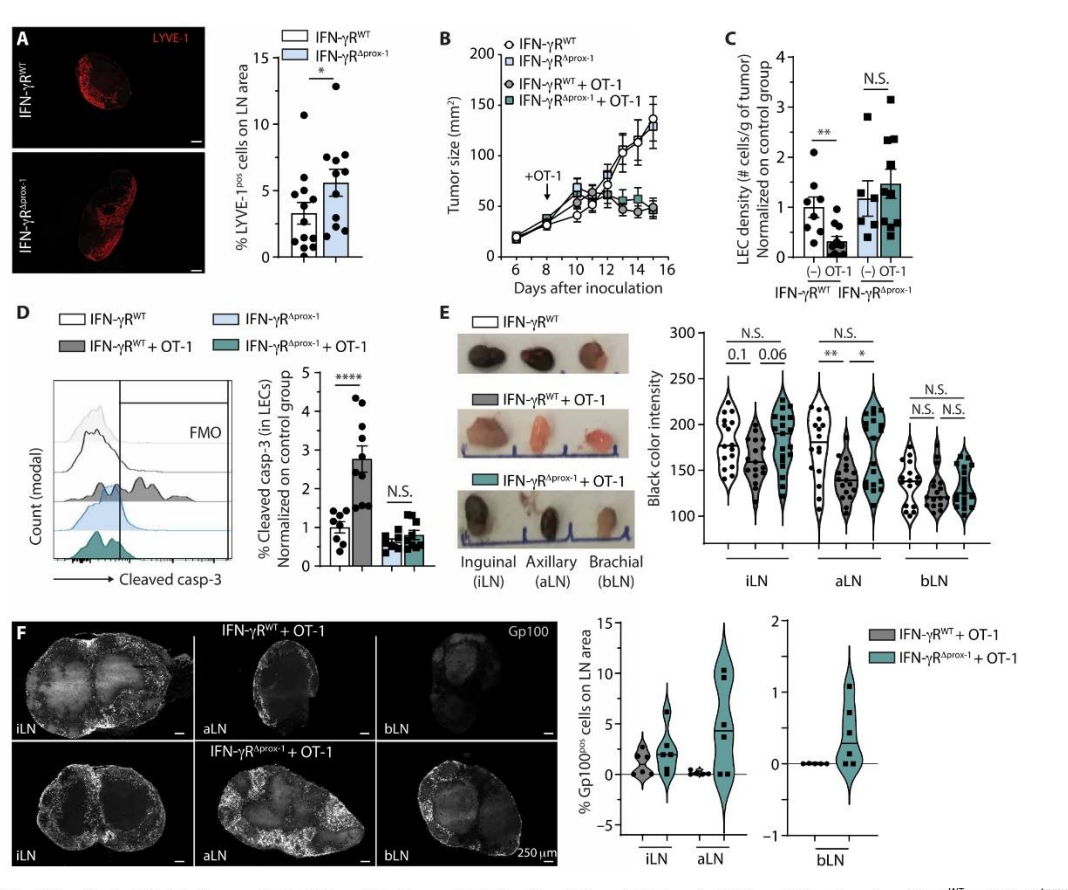


Fig. 4. IFN- γ R signaling in LECs is indispensable to ATT-mediated tumor LV destruction. (A) Lyve-1 staining of ndLN (non dLN) sections from IFN- γ R and IFN-

Garnier et al., Sci. Adv. 8, eabl5162 (2022) 8 June 2022

6 of 18

Downloaded from https://www.science.org on January 17, 2025

compared to IFN- γR^{WT} mice (Fig. 4A), tumor LVD and frequency of cleaved casp-3+ tumor LECs were not different between the two groups in the absence of OT-1 transfer (Fig. 4, C and D), suggesting that the IFN- γ produced by endogenous immune cells is not sufficient to induce B16F10-OVA+VC+ tumor LEC apoptosis. Notably, OT-1 effector transfer also reduced tumor BEC density (fig. S6F) and induced BEC apoptosis (fig. S6G) in both IFN- γR^{WT} and IFN- $\gamma R^{\Delta prox-1}$ mice.

We next investigated the impact of OT-1-induced LV dismantling, as well as the requirement of ÎFN-γ signaling, on metastasis establishment in TdLNs. In the absence of OT-1 transfer, TdLNs from B16F10-OVA⁺VC⁺ tumor-bearing IFN- γ R^{WT} and IFN- γ R^{Δ prox-1} mice exhibited similar levels of metastasis (fig. S6H), ruling out the possibility that increased LVD observed at steady state in IFN- $\gamma R^{\Delta p_i}$ LNs (Fig. 4A) would provide a better metastatic niche compared to IFN- γR^{WT} LNs. The adoptive transfer of OT-1 in B16F10-OVA $^{\dagger}VC^{\dagger}$ tumor-bearing IFN- γR^{WT} mice only modestly alters tumor metastasis in inguinal TdLNs, while it significantly reduced tumor metastasis in axillary TdLNs (Fig. 4E). In contrast, both inguinal and axillary TdLNs from adoptively transferred B16F10-OVA+VC tumor-bearing IFN- $\gamma R^{\Delta prox^{-1}}$ mice showed more metastasis compared to control IFN- γR^{WT} mice (Fig. 4E). Tumor regression induced by OT-1 effector transfer was identical in IFN- $\gamma R^{\Delta prox^{-1}}$ and IFN- γR^{WT} mice (Fig. 4B), ruling out the possibility that differences in primary tumor size would account for the modulation of TdLN metastasis. Gp100 immunofluorescent staining demonstrated that, upon OT-1 transfer, metastatic foci were increased in TdLNs from B16F10-OVA+VC+ tumor-bearing IFN-γR^{Δprox-1} mice compared to IFN-γR^{WT} mice (Fig. 4F). After OT-1 transfer, the number of metastatic positive LNs was generally higher in B16F10-OVA $^+$ VC $^+$ tumor-bearing IFN- $\gamma R^{\Delta prox-1}$ mice compared to IFN- γR^{WT} mice, with significant difference in black color intensity in inguinal and axillary TdLNs (fig. S6, I and J). In addition, OT-1 frequencies were found similar in TdLNs of IFN- γR^{prox1} and IFN- γR^{WT} mice (fig. S6K), dismissing a potential difference in the local control of metastasis by CTLs in LNs. Together, these data indicate that the reduction in tumor LV induced by tumor-specific effector CD8+ T cells inhibits metastasis in TdLNs in an IFN-γR-signaling dependent manner.

CTLs eliminate LECs through antigenic contact and killing

Manipulating CTL killing activity in tumors represents an attractive immunotherapeutic approach. CTLs kill target cells on the basis of antigenic peptide MHCI recognition through the release of cytotoxic molecules. IFN-γ enhances antigen processing and presentation in tumor cells, which, in turn, promotes their recognition and killing by T cells (49). Hence, promoting the production of IFN-γ by CTLs leads to enhanced antitumor responses in vivo in mouse models (50, 51). In vitro, LEC killing by OT-1 cells was found to be dependent on the number of T cells transferred and required preloading of LECs with OVA peptide (Fig. 5A). Soluble IFN-γ favored, as expected, PD-L1 and MHCII expression on LECs (fig. S7, A and B), testifying LEC responsiveness to the cytokine. However, IFN-γ signaling was not sufficient to promote LEC apoptosis (Fig. 5A), suggesting that antigen-dependent CTL-LEC interactions are necessary. In vivo, multiple intratumoral injections of high doses (1.5 μg twice a day for 4 days) of IFN-γ significantly reduced tumor growth (fig. S7C), likely due to the proapoptotic function of the cytokine on tumor cells. However, although this treatment efficiently induced the up-regulation of IFN-γ-responsive genes PD-L1 and

MHCII by tumor LECs (fig. S7, D and E), it did not induce cleaved casp-3 expression by tumor LECs (fig. S7F), confirming that IFN- γ is not sufficient to induce tumor LEC apoptosis. It has been previously published that IFN- γ negatively regulates LN LECs by inhibiting sprouting lymphangiogenesis and decreased markers of LEC fate, without, however, evidencing any direct effect on LEC apoptosis (46). Furthermore, LECs from steady-state skin and from B16F10-OVA+VC+ tumors expressed significantly lower levels of IFN- γ R compared to TdLN and non-dLN LECs (fig. S7G), suggesting that LECs from different organs may respond differently when exposed to similar cytokine milieu.

To firmly determine whether OT-1 selectively eliminates LECs presenting their cognate antigenic peptide, OT-1 effectors were incubated with WT (GFP $^{\rm h}$) and $\beta_2 {\rm m}^{\rm KO}$ (β2-microglobulin) (GFP $^{\rm neg}$) LEC cocultures, loaded or not with OVA peptide, and treated or not with IFN- γ blocking antibodies or granzyme-B inhibitor. Effector CD8 $^{\rm t}$ T cells induced cleaved casp-3 expression exclusively in OVA peptide–loaded WT LECs (Fig. 5B), resulting in a lower proportion of WT LECs compared to $\beta 2 {\rm m}^{\rm KO}$ LECs (fig. S7H). Those effects were abolished in the presence of granzyme-B inhibitor (Fig. 5B and fig. S7H). In contrast, IFN- γ blocking antibodies did not prevent LEC apoptosis, demonstrating that IFN- γ does not exert a direct proapoptotic effect (Fig. 5B and fig. S7H). Live imaging experiments also showed that OVA-loaded WT (GFP $^{\rm t}$) LECs, but not OVA-loaded $\beta_2 {\rm m}^{\rm KO}$ (GFP $^{\rm neg}$) LECs, expressed cleaved casp-3 and underwent apoptosis after establishing an antigenic synapse with OT-1 effector T cells (Fig. 5C and movie S1).

We next compared the ability of different doses of high–TCR affinity OT-1 and low–TCR affinity OT-3 effector T cells (52) to induce the expression of cleaved casp-3 in LECs in vitro. OT-3 cells were less efficient at inducing LEC apoptosis (fig. S7I). Therefore, in vitro LEC killing requires the establishment of cognate antigenspecific synapses with high-affinity TCR CTLs.

CTLs induce apoptosis in tumor-antigen cross-presenting tumor LECs, resulting in LN metastasis inhibition

We have shown that B16F10-OVA+VC+ tumor LECs exhibit the ability to capture and process exogenous antigens (35). Furthermore, LECs are capable of antigen cross-presentation in steady-state LNs (53), TdLNs, and tumors (31). To determine whether, as demonstrated in vitro, the killing of tumor LECs is also dependent on antigenspecific cognate interaction with CTLs in vivo, we first assessed the ability of tumor LECs to function as antigen cross-presenting cells. LECs (CD45⁻CD31⁺gp38⁺) and DCs (CD45⁺CD11c isolated from B16F10-OVA+VC+ tumors, and mRNA levels of genes implicated in the MHCI-restricted antigen (cross-)presentation pathways were evaluated. H-2K^b, B2m, Nlrc5, Tap-1, and Lmp2 mRNAs were significantly induced in tumor LECs from IFN-γR^V control mice 4 days after the transfer of OT-1 effectors (Fig. 6A). In notable contrast, tumor LECs from IFN-γR^{Δprox-1} mice expressed lower mRNA levels of all these genes with or without OT-1 transfer (Fig. 6A), demonstrating that IFN-y signaling in tumor LECs promotes their ability to function as bona fide antigen (cross-)presenting cells. The fold induction of the different mRNAs after OT-1 transfer was superior in tumor LECs from IFN- γR^{WT} mice compared to tumor DCs, which otherwise behaved similarly in IFN- γR^{WT} and IFN- γ R^{Δprox-1} mice (fig. S8).

On the basis of the observation that cancer cell apoptosis was induced in B16F10-OVA⁺VC⁺ tumors following OT-1 effector

Garnier et al., Sci. Adv. 8, eabl5162 (2022) 8 June 2022

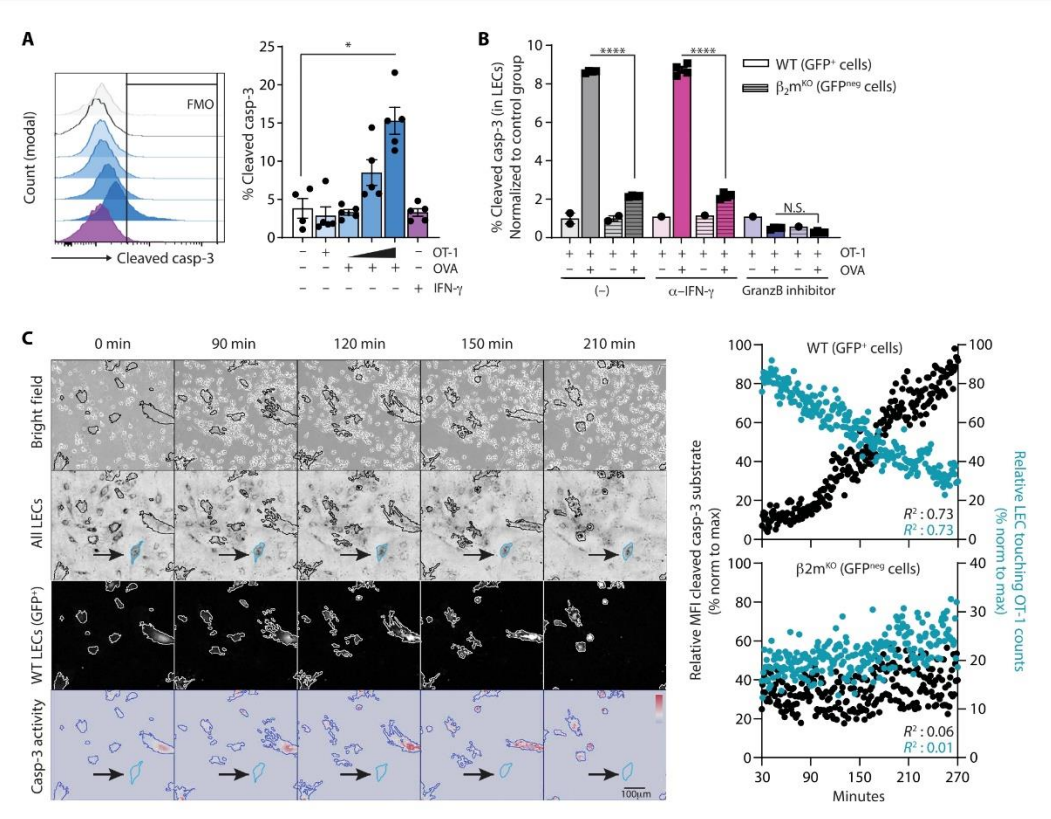


Fig. 5. CTLs induce LEC apoptosis through antigen-specific interactions. (A) LEC/FRC cultures were loaded or not with OVA peptide (OVA) and incubated with either different ratios of in vitro activated OT-1 cells (1:10, 1:3, and 3:1 OT1:LEC/FRC) or soluble IFN- γ . Frequencies of cleaved casp-3* LECs after 14 hours. Data are representative of two independent experiments. Each point represents a technical replicate. (B) WT (LC3-GFP⁺) or β_2 m^{KO} (GFP^{neg}) LEC/FRC cultures were loaded or not with OVA and incubated or not with anti-IFN- γ antibodies and granzyme-B inhibitor. In vitro activated OT-1 cells were added in the cultures and frequencies of cleaved casp-3* WT and β_2 m^{KO} LECs (gated on CD45^{neg}CD31⁺gp38⁺ cells) 14 hours later. Data are from one experiment. (C) Sorted WT (LC3-GFP⁺) and β_2 m^{KO} (GFP^{neg}) LEC cocultures (ratio of 1:1) were loaded with OVA and in vitro activated OT-1 cells were added (OT-1:LEC ratio of 10:1), and time-lapse imaging was performed (see movie S1). Representative images at indicated time points of bright field, all LECs, WT LC3-GFP⁺ LECs, and cleaved casp-3 activity. The arrows indicate one example of β_2 m^{KO} (GFP^{neg}) LECs. Graphs represent the relative MFI of cleaved casp-3 substrate (left y axis) and the relative frequency of OT-1 touching LECs (right y axis) in WT and β_2 m^{KO} LECs. Data are representative pooled from three experiments. (A) Mann-Whitney statistical test. Error bars show means \pm SEM. (C) Linear regression. *P < 0.05, ****P < 0.0001.

transfer (fig. SA), we hypothesized that, upon ATT, tumor LECs exposed to IFN- γ would acquire the ability to cross-present tumor antigens released by CTL-mediated tumor destruction. Therefore, we measured the expression levels of MHCI-OVA complexes at the surface of LECs in B16F10-OVA $^+$ VC $^+$ tumors from mice adoptively transferred with 0.05×10^6 or 0.5×10^6 OT-1 effectors. MHCI-OVA complexes were up-regulated by tumor LECs in a T cell dose-dependent manner, and more at day 5 compared to day 3 after ATT (Fig. 6B). In line with our hypothesis, we found that tumor LECs underwent apoptosis upon antigen-specific interaction with CTLs and that cleaved casp-3 was specifically up-regulated by MHCI-OVA $^+$ tumor LECs (Fig. 6C).

Supporting the notion that effector T cells promote the ability of tumor LECs to cross-present tumor antigens, OVA + CpG-B vaccination of B16F10-OVA*VC* tumor-bearing mice resulted in an increased expression of MHCI-OVA complexes by tumor LECs

(fig. S9B). Similarly, LECs from MC38-OVA⁺VC⁺ tumors, which contained elevated CTL numbers (fig. S4F), expressed increased levels of MHCI-OVA complexes compared to LECs from B16F10-OVA⁺VC⁺ tumors (fig. S9C). In addition, B16F10-OVA⁺VC⁺ tumor LECs expressed increased levels of MHCI-OVA complexes following the adoptive transfer of Pmel-1 effectors or after vaccination with Gp100 + CpG (fig. S8D), demonstrating that tumor cell killing by CTLs induces tumor antigen spreading for cross-presenting LECs.

The up-regulation of MHCI-OVA complexes by LECs derived from B16F10-OVA⁺VC⁺ tumors of IFN-γR^{WT} control mice was higher at day 8 compared to day 5 after injection of 0.5 × 10⁶ OT-1 effectors and decreased again at day 16, likely due to variations of CTL-dependent tumor destruction followed by the release of tumor antigens over time (Fig. 6D). In contrast, the expression of MHCI-OVA complexes was almost fully abrogated in tumor LECs from

Garnier et al., Sci. Adv. 8, eabl5162 (2022) 8 June 2022

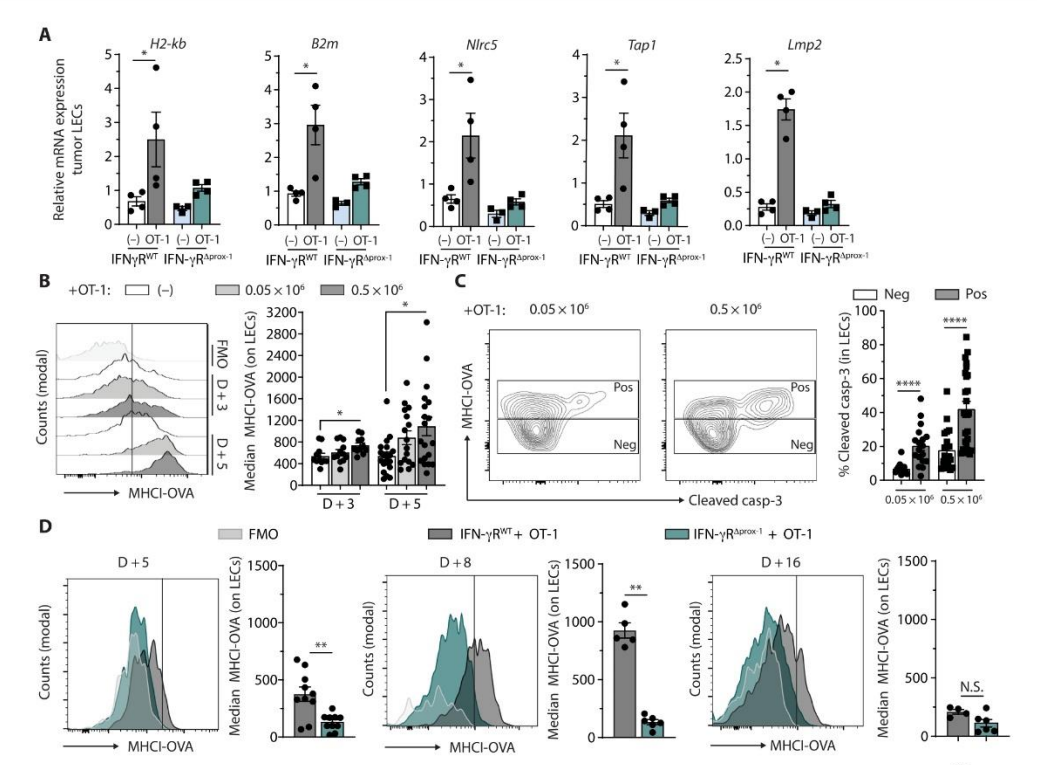


Fig. 6. CTLs induce the apoptosis of tumor-antigen cross-presenting tumor LECs in an IFN- γ -dependent manner. (A) Tamoxifen-treated IFN- γ R^{MT} and IFN- γ R^{Aprox-1} mice were injected or not with 0.5 × 10⁶ OT-1 cells 9 days after B16F10-OVA*VC* inoculation. mRNA levels of indicated genes in tumor LECs 4 days later. Data are from one experiment, N=3 to 4 mice per group. (B and C) C57BL/6 mice were injected or not with 0.05 × 10⁶ or 0.5 × 10⁶ OT-1 cells 9 days after B16F10-OVA*VC* inoculation. (B) MHCI-OVA complex levels in tumor LECs at days 3 and 5 after OT-1 transfer. (C) Frequencies of cleaved casp-3 among MHCI-OVA**eg (Neg) and MHCI-OVA**pos* (Pos) LECs 5 days after transfer. (D) Tamoxifen-treated IFN- γ R** and IFN- γ R**prox-1 mice were injected with 0.5 × 10⁶ OT-1 cells 9 days after B16F10-OVA*VC* inoculation. MHCI-OVA complex levels in tumor LECs at days 5, 8, and 16 after OT-1 transfer. Data are from one experiment, N=4 to 10 mice per group. (A, C, and D) Mann-Whitney statistical test; (B) one-way ANOVA test. Error bars show means \pm 5EM. *P<0.05, **P<0.01, ****P<0.001.

IFN- $\gamma R^{Aprox-1}$ mice (Fig. 6D), establishing a direct link between IFN- γ signaling and antigen cross-presentation in tumor LECs.

To prove that MHCI-restricted tumor antigen presentation is a prerequisite for LEC killing by CTLs, we adoptively transferred OT-1 effectors in B16F10-OVA $^{\rm t}$ VC $^{\rm t}$ tumor-bearing WT and $\beta_2 m^{\rm KO}$ mice, which lack MHCI expression. In the absence of OT-1, LVD was similar between WT and $\beta_2 m^{\rm KO}$ mice (fig. S10A). OT-1 transfer similarly reduced tumor growth in C57BL/6 and $\beta_2 m^{\rm KO}$ mice (Fig. 7A), and the density of IFN- $\gamma^{\rm t}$ and granzyme-B $^{\rm t}$ OT1 was identical in both groups (fig. S10B). PD-L1 and MHCII molecules were also up-regulated in a similar fashion by tumor LECs in both groups (fig. S10, C and D). In contrast, tumor LECs from $\beta_2 m^{\rm KO}$ mice did not express MHCI-OVA complexes (fig. S10E). The induction of cleaved casp-3 in tumor LECs by OT-1 transfer observed in WT mice was completely abolished in LECs from $\beta_2 m^{\rm KO}$ mice (Fig. 7B), demonstrating that MHCI expression by LECs is crucial for LV killing by OT1 cells. Last, we have generated mice in which the absence of β_2 -microglobulin ($\beta_2 m$) is restricted to LECs by crossing Prox-1Cre $^{\rm ERT2}$ mice with $\beta_2 m^{\rm flox/flox}$ mice ($\beta_2 m^{\rm Aprox-1}$). B16F10-OVA $^{\rm t}$ VC $^{\rm t}$ tumor-bearing control $\beta_2 m^{\rm WT}$ and $\beta_2 m^{\rm Aprox-1}$ mice

were adoptively transferred with OT-1 effectors. Tumor growths were similar in both groups (Fig. 7C), as well as the density of OT-1 effector infiltrating the tumors (fig. S10F). While PD-L1 and MHCII expression by LECs were identical in tumors isolated from $\beta_2 m^{WT}$ and $\beta_2 m^{\Delta prox-1}$ mice (fig. S10, G and H), LECs from $\beta_2 m^{\Delta prox-1}$ tumors do not express MHCI-OVA (fig. S10I). Tumor LEC apoptosis was reduced (Fig. 7D) in $\beta_2 m^{\Delta prox-1}$ mice compared to $\beta_2 m^{WT}$ mice, firmly demonstrating that MHCI expression by LEC is required for their killing by CTLs. Last, both the number of metastasis-positive LNs (Fig. 7E) and the number of metastatic foci per LNs (Fig. 7F) were augmented in $\beta_2 m^{\Delta prox-1}$ mice compared to $\beta_2 m^{WT}$ mice adoptively transferred with OT-1 effectors (Fig. 7F). These experiments firmly demonstrate that MHCI expression by LEC is required for their killing by CTLs, leading to the control of LN metastasis.

DISCUSSION

Immunotherapy has been the hallmark progress in the treatment of cancer over the last decade. Multiple immunotherapeutic approaches aiming at improving T cell responses, such as immune checkpoint

Garnier et al., Sci. Adv. 8, eabl5162 (2022) 8 June 2022

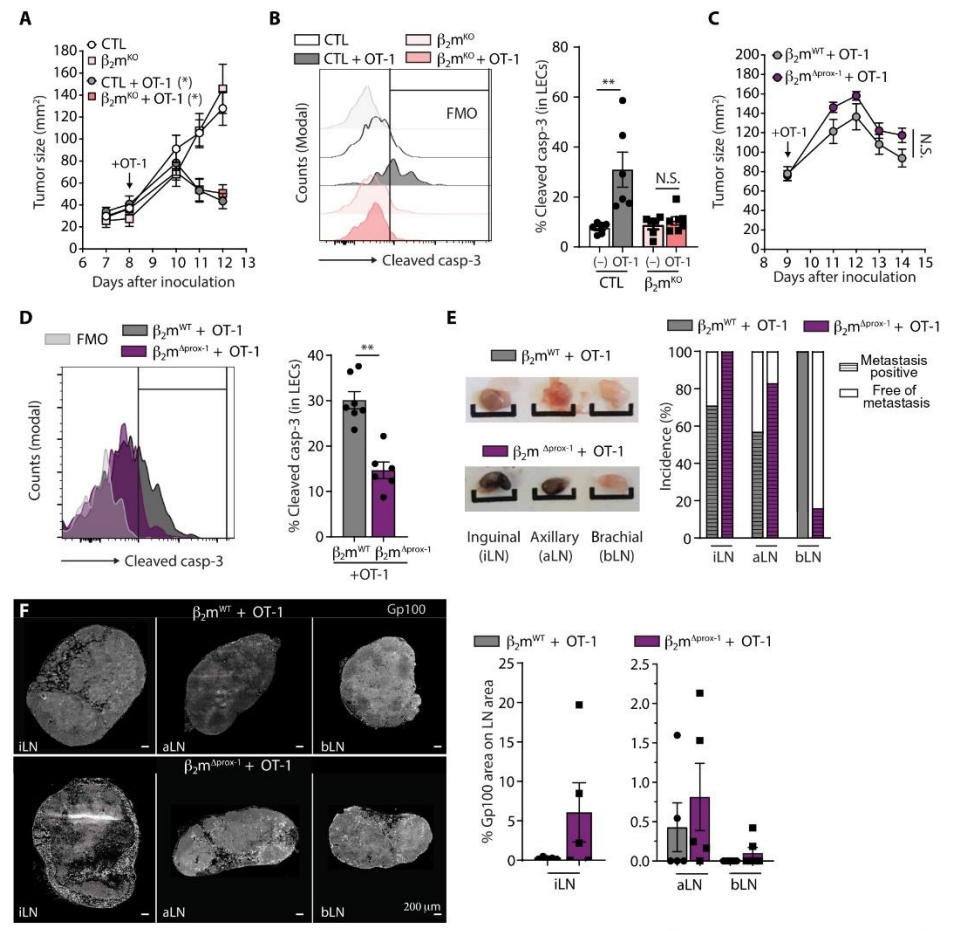


Fig. 7. T cell-mediated LEC apoptosis requires MHCl expression on tumor LECs. (A and B) C57BL/6 and $\beta_2 m^{KO}$ were injected or not with 0.5×10^6 OT-1 cells 8 days after B16F10-OVA * VC * inoculation. (A) Tumor growth and (B) frequencies of cleaved casp-3 * tumor LECs 4 days after OT-1 transfer. Data are from one experiment, N=6 to 7 mice per group. (C to F) Tamoxifen-treated $\beta_2 m^{WT}$ and $\beta_2 m^{Aprox-1}$ mice were injected with 0.5×10^6 OT-1 cells 9 days after B16F10-OVA * VC * inoculation. (C) Tumor growth and (D) frequencies of cleaved casp-3 * tumor LECs 5 days after OT-1 transfer. Data are from one experiment, N=6 to 7 mice per group. (E) The percentage of metastasis-positive and metastasis-negative (free of metastasis) LNs according to black color. Pictures show representative images. Scale bars, 0.5 cm. (F) Immunofluorescent Gp100 staining of inguinal, axillary, and brachial TdLNs (iLN, aLN, and bLN, respectively) 5 days after OT-1 transfer. Histograms represent the quantification of Gp100 * cells in LNs. (A and C) Two-way ANOVA test; (B, D, and E) Mann-Whitney statistical test. Error bars show means \pm SEM. *P < 0.05, **P < 0.05.

blockade, adoptive cellular therapies, and cancer vaccines, represent powerful tools in the fight against cancer. Although tumor-associated lymphangiogenesis has been shown to increase the responsiveness of the TME to immunotherapies (28), it simultaneously dampens the efficacy of antitumor cytotoxic T cell responses by enhancing immunosuppression (31, 34, 35, 54). In this study, we focused our research on LV alteration by therapies involving antitumor effector CD8⁺ T cell responses. As previously shown, we observed that the immunosuppressive phenotype of tumor LECs is stronger in immunogenic tumors (MC38-OVA-VC⁺) compared to less-immunogenic ones (B16-OVA-VC⁺) or following adoptive T cell and vaccination

strategies, therefore altering the efficacy of those approaches. However, when the scales are tipped toward potent T cell responses, boosting of antitumor cytotoxic T cell density not only promotes cancer cell death and tumor rejection but also triggers tumor LEC apoptosis and LV dismantling. Increasing effector CD8⁺ T cells in tumors enhances the expression of the proapoptotic marker cleaved casp-3 in tumor LECs, leading to reduced LV densities. The decrease in LVs was found more pronounced at the center of the tumor compared to the periphery of the tumor, which is reminiscent with the observation that T cells attack the tumor vasculature predominantly inside the tumor mass (55). CTL transfer also resulted in BEC

Garnier et al., Sci. Adv. 8, eabl5162 (2022) 8 June 2022

apoptosis and reduced densities in tumors, suggesting a broader mechanism of nonhematopoietic, or at least endothelial, cell death in the presence of potent cytotoxic T cell responses.

Using different tumor models and different T cell–based immunotherapeutic approaches, we show that enhanced infiltration of tumor-specific T effector positively correlated to the frequency of apoptotic tumor LECs. These results suggest that a certain threshold of CTL density in tumors is necessary to overcome IFN- γ -mediated LV immunosuppression by inducing tumor LEC apoptosis and concomitant LV destruction.

Cytotoxic T cells can kill target cells bearing specific cognate peptide-MHCI complexes via direct cell-cell contact, while ignoring healthy bystander cells lacking cognate peptide-MHCI complexes. As previously observed, after being adoptively transferred, OVAspecific CD8+ effector OT-1 cells infiltrate the stroma of OVAexpressing lymphangiogenic melanoma, localize, and cluster in close proximity to tumor LV (31). LECs were demonstrated to capture, process, and cross-present exogenous antigen, leading to CD8⁺ T cell clustering and suppression at steady state (31, 53, 56, 57) and in a tumor context (31). We show that molecules implicated in MHCIrestricted (cross-)presentation pathways (such as NLRC5 (NLR Family CARD Domain Containing 5), TAP1 (Transporter associated with antigen processing 1), LMP2 (Latent Membrane Protein 2), MHCI, and β₂m) are up-regulated by tumor LECs in mice that have received ATT. The expression level of these genes is higher in tumor LECs compared to total tumor CD11chiMHCII+ DCs. However, it is possible that specific DC subsets, or DCs in TdLNs, exhibit an increased ability to cross-present tumor antigens. LECs in OVAexpressing melanomas and their TdLNs express MHCI-SIINFEKL peptide (MHCI-OVA) complexes at their surface (31), suggesting that LECs in tumors can function as antigen cross-presenting cells. An alternative possibility is that preprocessed antigenic peptides released in the TME directly bind MHCI molecules expressed at the surface of tumor LECs.

Furthermore, we show that B16-OVA-VC+ tumor LECs upregulate MHCI-OVA complexes when treated with ATT or vaccination, suggesting that antigen-specific interactions with effector T cells induce apoptosis in tumor LECs. Accordingly, cleaved casp-3 expression is specifically enhanced in tumor LECs expressing MHCI-OVA complexes. In B16F10-OVA+ tumors that do not overexpress VEGF-C and contain very low LEC numbers, frequencies of cleaved casp-3 LECs were notably elevated compared to B16F10-OVA+VC+ tumors already in the absence of ATT, suggesting that elevated CTL/LEC ratio might enhance tumor LEC killing by infiltrating CTLs. VEGF-C has been described to exhibit cytoprotective effects on LECs (58). Therefore, it is likely that, in addition to direct killing by CTL, elevated amounts of VEGF-C in B16F10-OVA+VC tumors compared to B16F10-OVA+ tumors protect tumor LEC from apoptosis. Together, our data support the hypothesis that LEC apoptosis induced by CTLs is T cell dose dependent and TCR affinity/ avidity dependent.

Our in vitro and in vivo experiments demonstrate that LEC apoptosis induced by CTLs is abolished when LECs are deficient for $\beta_2 m$ molecules, demonstrating that ATT eliminates LECs through TCR-MHCI/tumor antigen interactions. It has been shown that the presentation of high-affinity ligands (peptide MHCI complexes) by cancer cells and/or the tumor stroma is required for cytokine production by T cell, stroma destruction, and relapse-free tumor regression (59). We provide evidence that the efficacy of LEC killing

by CTLs relies on direct TCR recognition most likely via high-affinity and/or high-avidity interactions. LEC apoptosis induced by CTLs is T cell dose dependent, indicating that the ratio between LECs and T cells is a critical parameter. In vivo, the transfer of effector Pmel-1 T cells, which express a TCR recognizing the low-affinity peptide Gp100 (59), is inefficient at inducing tumor LEC death and LV destruction and requires concomitant vaccination with Gp100 + CpG-B. Accordingly, OVA-specific low-TCR affinity OT-3 effector T cells are less efficient to promote LEC apoptosis compared to high-TCR affinity OT-1 T cells in vitro. Those findings imply that the selection of T cells with high TCR affinity for tumor-specific peptide-MHCI complexes for immunotherapies will not only promote the killing of cancer cells but also induce tumor LEC death. In addition, peptide-derived vaccine strategies aiming at enhancing T cell priming by DCs could also enhance peptide loading and presentation by tumor LECs and may help to disrupt the tumor-associated LV.

Our results indicate that tumor antigen release promotes the cross-presentation of tumor antigens by LECs, allowing their subsequent antigen-dependent killing by CTLs. Consistent with the hypothesis that CTL killing of tumor cells would increase the availability of tumor antigens for cross-presentation by LECs, we show that Pmel-1 effector transfer in B16F10-OVA⁺VC⁺ tumor-bearing mice enhances the expression of MHCI-OVA complexes by tumor LECs. This indicates that tumor antigen spreading for cross-presenting LECs occurs in the context of immunotherapy and will likely enlarge the breadth of CD8⁺ TCR repertoires and will amplify antigen-specific LEC killing by CTLs.

IFN-γ has been shown to play a dual and opposite role in cancer development. IFN- γ signaling not only enhances PD-L1 expression on tumor cells, inhibiting antitumor immunity (60), but also augments antigen processing and presentation, which, in turn, enhances their recognition and cytolysis by T cells (61). In developing tumors, the expression of PD-L1 and MHCII molecules by tumor LECs are dependent on IFN-yR signaling. We show that IFN-y produced intratumorally during ATT further enhances the expression of PD-L1 and MHCII by tumor LECs, which will likely promote their immunosuppressive functions (34, 35, 61). Following ATT, IFN-γ in LECs further increases their expression of the MHCI transactivator NLRC5- and MHCI-related genes, stimulating the antigen processing and presentation machinery in LECs, as was also shown for tumor cells (62). This mechanism could be useful to potentiate LEC killing by tumor-specific CTL through an antigen-dependent pathway. By using conditional KO mice in which LECs do not express IFN-γR, we observed that both the inhibition of tumor LVD and the induction of LEC apoptosis induced by ATT are abolished in the absence of IFN-yR signaling in LECs, demonstrating that IFN-y is crucial for their killing by CTLs. CTLs destroy their target cells through different pathways, triggering programmed intracellular events in target cells and leading to apoptotic cell death: the granule exocytosis (perforin/granzymes), the secretion of proinflammatory molecules (IFN-γ/TNF), and the expression of cell death ligand [FasL/TRAIL (tumor-necrosis-factor related apoptosis inducing ligand)] (63). In vitro, we observed that LEC killing by CTLs is abrogated by the addition of granzyme-B inhibitor, suggesting that involvement of this pathway in CTLs induced tumor LEC apoptosis. The addition of elevated doses of IFN-y alone does not favor the expression of cleaved casp-3 in LECs, confirming that LEC death is not a direct consequence of a proapoptotic effect of IFN-γ. Further investigations need to be performed to validate the implication of the granzyme pathway

Garnier et al., Sci. Adv. 8, eabl5162 (2022) 8 June 2022

in vivo. Together, our data show that LEC killing by CTLs is dependent on IFN- γ R signaling in LECs, which promotes their ability to cross-present tumor-derived antigenic peptides and to become CTL targets. However, we cannot rule out the possibility that IFN- γ further contributes to the pathway by directly modulating the expression of molecules implicated in tumor cell adhesion and transmigration through the lymphatic endothelium.

SCIENCE ADVANCES | RESEARCH ARTICLE

Tumor lymphangiogenesis and the remodeling of LVs are important steps in tumor cell dissemination. Cancer metastasis propagates through LVs to first reach the sentinel LNs and further colonize distant organs (3, 4). Our data show that T cells in tumors not only can support immunosuppressive functions of tumor LECs but also can induce their apoptosis. Which of the two opposite effects dominate depends on the number and affinity of CTLs attacking the tumor. Tumor LEC apoptosis and LV destruction by CTLs resulted in altered lymphatic drainage to TdLNs and reduced LN metastasis. Although we cannot firmly rule out a direct effect of CTL transfer on LN metastasis or the preexistence of undetectable micrometastasis in LNs at the time of CTL transfer, the reduced transport of injected tumor cells to TdLNs suggests that tumor LV disruption prevents tumor cell migration from primary tumors and subsequent transit to LNs. This is further supported by the fact that, upon OT-1 CTL adoptive transfer, TdLN metastasis are significantly increased in IFN-γR^{prox1} compared to IFN-γR^{WT} mice, and this is despite similar OT-1 CTL frequencies in TdLNs. It has been shown that lymphangiogenesis in TdLNs is part of the formation of the LN premetastatic niche and is associated with metastasis formation (10, 17, 18). However, metastatic scores in LNs from tumor-bearing conditional KO mice in which LECs do not express IFN-yR were not affected in the absence of CTL transfer, indicating that the disruption of tumor-associated LVs, and not alterations of LN premetastatic niches, is responsible for reduced LN metastasis after ATT. Last, we observed a significant reduction of LN metastasis in both primary (inguinal) and secondary (axillary and brachial) TdLNs. Further investigation will determine whether decreased metastasis in secondary TdLNs results from reduced inguinal LN burden or from a failure to sequentially colonize downstream LNs.

ATT and vaccination aiming at enhancing antitumor CTL responses and tumor cell killing represent up-and-coming strategies to fight cancers. Because LVs represent the main route for tumor cell spreading and dissemination to sentinel LNs and concomitant spreading to distal organs, our data reveal an unexpected mechanism by which tumor-associated LVs can be modulated by CTLs and metastasis can be reduced. Deciphering the mechanisms in LV destruction by antitumor CTLs, as well as determining the numbers of CTLs required to induce efficient LV destruction, is important to pave the way for the development of new therapeutic strategies to inhibit tumor dissemination.

METHODS

Mice

C57BL/6N (B6) mice were purchased from Charles River Laboratories, France. Mice with a disrupted $\beta_2 M$ gene (hereafter called $\beta_2 M^{KO}$) (64) were backcrossed onto the B6 background for at least 10 generations (from SwImMR, University of Zurich). To generate mice selectively lacking IFN-γR or $\beta_2 m$ in LECs (IFN-γR- h) or $\beta_2 m^{h}$ in IFN-γR- h) mice (48) or $\beta_2 m^{h}$ ($\beta_2 m^{WT}$) mice [purchased from Charles River Laboratories; B6(Cg)-B2mtm1c(EUCOMM)

Hmgu/J, strain #: 034858, RRID:IMSR_JAX:034858] were crossed with Prox1-Cre^{ERT2} mice (47). OVA₂₅₇₋₂₆₄-specific TCR transgenic OT-1 CD45.1 mice (purchased from Charles River Laboratories), OVA₂₅₇₋₂₆₄-specific TCR transgenic OT-3 CD45.1 mice (65), and Gp100₂₅₋₃₃-specific TCR transgenic Pmel-1 mice (66), as well as LC3-GFP mice (67), were bred in our animal facility. All mice (male and female) were used between the ages of 6 and 12 weeks and bred and maintained under specific-pathogen–free conditions at the animal facility of Geneva Medical School and under SPF (specific-pathogenfree) conditions at Charles River Laboratories, France. All procedures were approved and performed in accordance to the guidelines of the animal research committee of Geneva under the license number GE79/20.

Tamoxifen treatment

Prox-Cre^{ERT2} IFN- γ R2^{fl/fl} (IFN- γ R^{Δ prox-1}) mice and IFN- γ R2^{fl/fl} (IFN- γ R^{WT}) littermate control mice were treated intraperitoneally by injection with tamoxifen (T5648, Sigma-Aldrich), 1 mg per mouse twice a day for 4 days. Mice were used for experiments 2 weeks after the last injection.

Tumor cell lines

Mouse B16-F10 melanoma cells (American Type Culture Collection) were transfected with OVA (a gift from B. Huard) (B16F10-OVA⁺), and B16F10-OVA⁺ and B16F10 were engineered to overexpress VEGF-C (B16F10-OVA⁺VEGF-Chi or B16-VEGF-Chi) as previously published (31) and were maintained in RPMI supplemented with 10% heat-inactivated fetal bovine serum (FBS), 100 μ M penicillinstreptomycin, and 50 mM of β -mercaptoethanol. Geneticin was added after 1 day of culture to select OVA-expressing cells.

added after 1 day of culture to select OVA-expressing cells.

To obtain mouse MC38-VEGF-Chi cells, MC38 cells (a gift from W. Reith) were transduced with a third-generation lentivirus encoding full-length mouse vegfc (NM_009506.2) under the control of EF1A promoter (VectorBuilder) and selected using puromycin (4 μg/ml). To generate retroviral m(mouse)OVA vector particles, the MigR1-OVA-IRES-GFP retroviral vector was cotransfected with the package plasmids pMD-gag/pol and pMD-VSV-G (all plasmids gifted by P. Romero) into human embryonic kidney 293T cells. The medium was changed with fresh full medium after 8 hours. Forty-eight hours later, the supernatants were harvested and filtered with a 0.45-um filter and stored at -80°C (with the help of E. Cosset). MC38-VEGF-Chi cells were transfected with supernatants containing OVA-GFP retrovirus, and MC38-OVA+VEGF-Chi cells were sorted by flow cytometry on the basis of GFP expression. Cells were maintained in Dulbecco's modified Eagle's medium (Gibco), 10% heat-inactivated fetal calf serum, 100 µM penicillin-streptomycin, and 50 mM β-mercaptoethanol.

Cell lines were not authenticated, used at below passage 20, and tested negative for *Mycoplasma*. Mouse VEGF-C protein levels from B16F10-OVA⁺VEGF-C^{hi} and MC38-OVA⁺VEGF-C^{hi} tumors were measured by using a mouse VEGF-C enzyme-linked immunosorbent assay kit (Cusabio), according to the manufacturer's instructions.

Tumor cell inoculation and tumor measurement

Mice were anesthetized using isoflurane or a mix of 2% Rompun (Bayer)/10% ketamine (Vetoquinol), and their backs were shaved. A total of 0.5×10^6 B16F10-OVA $^{+}$ VEGF- C^{hi} cells, MC38-OVA $^{+}$ VEGF- C^{hi} cells, or a mixture of B16F10-VEGF- C^{hi} and B16F10-OVA $^{+}$ -VEGF- C^{hi} cells (ratio 9:1) were injected in 100 μ l of phosphate-buffered saline

Garnier et al., Sci. Adv. 8, eabl5162 (2022) 8 June 2022

(PBS) subcutaneously on the back dorsolateral side. Primary tumor inoculation was controlled by measuring the distance between the front leg, the back leg, and the vertebral column of the mice, and the injection was always performed at the same distances from these three locations, at equal distance from the vertebral column and the back leg, representing approximately one-third of the distance to the front leg. Tumor size was monitored blindly every 1 to 2 days using a caliper, and tumor size was calculated by length × width. Mouse exclusion criteria are the following: tumor necrosis, tumor size >15 mm (diameter), and/or signs of pain or anxiety.

Tissue processing for flow cytometry and in vitro culture LN cell isolation

For experiments involving the detection of fluorescent bead uptake by DCs or the presence of OT-1 in the TdLNs, LNs were cut into small pieces with scissors and digested in RPMI containing collagenase D (1 mg/ml; Roche) and deoxyribonuclease I (DNase I) (10 µg/ml; Roche) for 40 min at 37°C. After 20 min, solutions were mixed up and down and incubated for an additional 20 min at 37°C and filtered through a 70-µm cell strainer in fluorescence-activated cell sorting (FACS) buffer [PBS, 10% bovine serum albumin (BSA), and 5 mM EDTA], and single-cell suspensions were incubated with anti-CD16/CD32 antibody.

Stromal cell isolation

Tumors were cut into small pieces and digested in RPMI containing collagenase IV (1 mg/ml; Worthington Biochemical Corporation), DNase I (40 µg/ml; Roche), and 1% FBS for 30 min at 37°C. Samples were mixed up and down every 10 min. Tubes were centrifuged for a few seconds at 1500 rpm and supernatants were filtered through a 70-µm cell strainer in FACS buffer to stop the reaction. The remaining tissue was further digested in RPMI with collagenase D (1 mg/ml; Roche), DNase I (40 µg/ml; Roche), and 1% of FBS for 20 min at 37°C, with additional two cycles of repeated pipetting. The solution was filtered through a 70-µm cell strainer in FACS buffer and pooled into the first collected tubes.

OT-1, OT-3, Pmel-1, and polyclonal cell preparation

Spleens and LNs were smashed, filtered through a 70-μm mesh filter, and centrifuged at 1500 rpm for 5 min. Red blood cells were lysed with 1 ml of ammonium-chloride-potassium lysis buffer per spleen for 1 min. Following the addition of cell culture medium, splenocytes were washed and resuspended in complete medium (RPMI supplemented with 10% FBS, 1% penicillin-streptomycin, and 50 mM 2-β-mercaptoethanol).

LEC and fibroblastic reticular cell in vitro culture

A mixed LEC–fibroblastic reticular cell (FRC) culture was performed as previously described (68). Briefly, LNs from 6- to 8-week-old female mice (C57BL6N, LC3-GFP, or $\beta_2 m^{KO}$) were dissected and digested with a freshly prepared enzymatic solution containing RPMI 1640 (Gibco), dispase (0.8 mg/ml) (Gibco), collagenase P (0.2 mg/ml) (Roche), and DNase I (0.1 mg/ml) (Roche). Tubes containing the digestion mixture were incubated at 37°C in a water bath, and every 10 min, LNs were gently mixed using a 1-ml pipette and, thereafter, the supernatant was filtered through a 70- μ m cell strainer on 10 ml of cold FACS buffer containing 0.5% BSA (AppliChem) and 5 mM EDTA (AppliChem) in PBS. These steps were repeated every 10 min until all LNs were completely digested. Cells were washed and filtered through a 70- μ m cell strainer, quantified using a hemocytometer, and plated in a T75 flask [coated with human

fibronectin (10 µg/ml) (Millipore) and PureCol (10 µg/ml) (Advanced BioMatrix) for 30 min at $37^{\circ}C]$ at a concentration of 4×10^{7} to 6×10^{7} cells per well. The LEC-FRC cell culture medium was minimum essential medium— α (Gibco) supplemented with heatinactivated, 10% batch-tested, low immunoglobulin FBS (Gibco) and 1% penicillin/streptomycin (Gibco). Plates were washed and the culture medium was renewed every day to remove nonadherent cells. After 6 to 7 days, cultures primarily contained LECs and FRCs. Cells were detached with Accutase (Thermo Fisher Scientific) for 5 min at 37° C and plated on a 24-well plate (precoated with fibronectin and PureCol) at a concentration of 0.1×10^{6} to 0.2×10^{6} cells per well. In some experiments, cells were treated with IFN- γ (PeproTech; $10~\mu g/ml$) for 14 hours.

Vaccination

OVA + CpG-B vaccination

B16F10-OVA *VEGF-Chi tumor-bearing mice were injected subcutaneously at day 5 with OVA protein (50 µg per mouse; Invivogen) and CpG-B 1668 (30 µg per mouse; Invivogen).

Gp100 + CpG-B vaccination

B16F10-OVA⁺VEGF-C^{hi} tumor-bearing mice were injected subcutaneously at day 5 with human Gp100 peptide (KVPRNQDWL) (100 µg per mouse; Thermo Fisher Scientific) and CpG-B 1668 (30 µg per mouse; Invivogen).

Irradiated B16F10 VC+ + CpG-B vaccination

B16F10 VC⁺ tumor-bearing mice were injected subcutaneously at day 8 with irradiated B16F10-VC⁺ [100 gray (Gy)] and CpG-B 1668 (30 ug per mouse; Invivogen).

CTL activation, adoptive transfer, and coculture with LEC-FRC

Splenocytes and LNs from 6- to 8-week-old OT-1, OT-3, Pmel-1, and C57BL/6N female mice were prepared as mentioned above (see the "Tissue processing for flow cytometry and in vitro culture" section). OT-1 and OT-3 cells were stimulated with 1 nM of OVA peptide (SIINFEKL) (Sigma-Aldrich) in the presence of interleukin-2 (IL-2) (100 U/ml) (PeproTech) in complete medium for 3 days. For in vitro experiments, OT-1 and OT-3 were added to LEC-FRC cultures (loaded or not with 1 nM OVA peptide) at different T cell/LEC-FRC ratios (1:3, 1:1, and 3:1) for 14 hours, in the presence or absence of blocking IFN- γ antibodies (10 µg/ml; XMG1.2, Bio X Cell) or granzyme-B inhibitor (300 µM; Calbiochem). For in vivo experiments, 0.05 × 10^6 , 0.5 × 10^6 , or 1 × 10^6 OT-1 cells were injected intravenously into tumor-bearing mice (day 7 or 9 after tumor inoculation).

Pmel-1 cells were loaded with 1 nM hGp100 peptide (KVPRNQDWL) (Thermo Fisher Scientific) for 1 hour in complete medium and washed with complete medium. IL-2 (50 U/ml) was added to cultures at days 2 and 4, and cells were harvested after 5 days of culture. For in vivo experiment, 12×10^6 of *Pmel-1* effector cells were injected intravenously into tumor-bearing mice (day +9 after tumor inoculation).

Polyclonal CD8⁺ T cells were purified from spleen and LNs of C57BL/6 mice by using a CD8 α ⁺ T cell isolation kit according to the manufacturer's instructions (Miltenyi Biotec). CD8⁺ T cells were cultured with IL-2 (100 U/ml) and bone marrow–derived DCs (ratio 1:1). Before the coculture, DCs were preloaded with irradiated (100 Gy) B16F10 VC⁺ cells (ratio of 2:1) and preactivated with lipopolysaccharide (0.1 μ g/ml) for 18 hours. After 5 days of culture, CD8⁺ T cells were harvested and adoptively transferred into tumor-bearing mice (day 10 after tumor inoculation).

Garnier et al., Sci. Adv. 8, eabl5162 (2022) 8 June 2022

IFN-γ intratumoral injection

IFN- γ (1.5 µg; PeproTech) was injected or not intratumorally twice a day for 4 days into B16F10-OVA $^+$ VEGF-C hi tumor-bearing mice.

Lymphatic drainage function DC migration

Twenty microliters of 0.5-mm FITC-conjugated latex microspheres (Polysciences, diluted 1/50^e in PBS) was injected intratumorally. After 24 hours, flow cytometric analysis (CD11c+ MHCII+ FITC+) was performed on single-cell suspensions prepared from tumordraining inguinal and axillary LNs.

Tumor cell migration

B16F10-VEGF-C (B16-VC) melanoma cells (31) were stained with CTV for 20 min at 37°C in PBS, and 1×10^6 cells were injected peritumorally. Primary tumor inoculation was controlled by measuring the distance between the front leg, the back leg, and the vertebral column of the mice, and the injection was always performed at the same distances from these three locations. CTV+ B16-VC tumor cells were injected peritumorally at a time point primary tumor sizes were not decreased by the adoptive transfer of OT1, and the site of injection was at the limit border of the tumor mass, always in the same direction (30° related to the inguinal LN). A total of 30 µl of tumor cell suspension was injected with constant pressure (30 ul/3 s) by using a 0.3-ml syringe. After 36 hours, flow cytometric analysis (CD45 $^{\rm neg}$ CTV $^+$ GP38 $^+$) was performed on single-cell suspensions prepared from tumor-draining inguinal and axillary LNs.

Metastasis quantification Black color intensity quantification in TdLNs

The mean of black color intensity of inguinal, axillary, and brachial TdLN from pictures was calculated using ImageJ. The incidence was quantified as the percentage of black LNs among total LNs.

Gp100 staining

TdLNs (inguinal, axillary, and brachial) were mounted in OCT (Optimal cutting temperature) medium. Twenty-five-micrometerthick sections were cut and fixed with paraformaldehyde 4% for 15 min. Slides were washed and permeabilized [PBS + 0.2% Triton X-100 + 20% dimethyl sulfoxide (DMSO); 1 hour, room temperature], and incubated for 2 hours in DMSO:H2O2:PBS + 0.2% Triton X-100 (1:1:4) and 1 hour in PBS + 0.2% Triton X-100 + 20% DMSO and 0.3 M glycine. After washing (PBS + 0.2% Triton X-100) and blocking (PBS + 0.2% Triton X-100 + 10% DMSO + 10% FBS), sections were stained overnight at 4°C using Alexa Fluor 647-labeled Gp100 antibody (1/200°; clone; Abcam) in PBS + 5% DMSO + 5% FBS. Sections were mounted with 4',6-diamidino-2-phenylindole (DAPI) Fluoromount-G (SouthernBiotech). Tumor area within TdLNs was detected with QuPath 0.2.3 (69) using intensity thresholds. This area was then normalized with the ganglion area and expressed as a percentage. LNs were considered as "metastasis-free" when the percentage was less than 0.01%. The incidence was quantified as the percentage of Gp100-positive LNs among total LNs.

Antibodies, flow cytometry, and cell sorting

Monoclonal antibodies (mAbs) used for flow cytometry are listed in Table 1 below. For flow cytometric analysis, single-cell suspensions were incubated with Fc Block (anti-CD16/32 FcyRII-RIII) for 10 min at 4°C and stained with antibodies and fixable dye for 20 to 30 min in PBS at 4°C. Intracellular staining was performed using the Intracellular Fixation and Permeabilization Buffer Set (eBioscience). For

IFN-γ and granzyme-B, cells were first restimulated in complete RPMI containing phorbol 12-myristate 13-acetate (100 ng/ml; Sigma-Aldrich), ionomycin (1 µg/ml; Sigma-Aldrich), and GolgiStop solution (1/1000e; BD Biosciences) and incubated 4 hours at 37°C, 5% CO2. Data were acquired with a Fortessa analyzer (BD) and analyzed using FlowJo software (FlowJo company). For LEC sorting from LEC/FRC cultures, cells were stained with mAbs against CD45, GP38, and CD31 and sorted using MoFlo Astrios (Beckman Coulter).

For LEC sorting from tumors, single-cell suspensions were stained with mAbs against CD45, GP38, and CD31, and LECs were sorted using a MoFlo Astrios (Beckman Coulter) as CD45^{neg}, GP38⁺, and CD31⁺ cells. For DC sorting from tumors, single-cell suspensions were stained with mAbs against CD45, CD11c, and MHCII, and DCs were sorted using a MoFlo Astrios (Beckman Coulter) as CD45+, CD11c+, and MHCII+ cells. FMO (full stained minus one) was performed for cleaved casp-3, PD-L1, MHCII, and MHCI-OVA.

Immunohistochemistry on tumor sections

Mouse tumors were embedded for 4 hours in 4% paraformaldehyde overnight in 30% sucrose and mounted in OCT medium. Fiftymicrometer-thick sections were cut and fixed in 4% paraformaldehyde for 20 min. After washing and permeabilization [0.5% PBS/BSA + Triton X-100 (1/400e, AppliChem); 20 min, room temperature], sections were stained overnight at 4°C using a rat anti-Lyve-1 antibody (1/300e; Novus) and a rabbit anti-cleaved casp-3 (1/100e; Cell Signaling Technologies). Alexa Fluor 546-labeled goat anti-rat (1/1000e; Invitrogen) and donkey anti-rabbit AF647 (1/1000e; Jackson ImmunoResearch) and Alexa Fluor 488-labeled anti-CD45.1 (1/100e; BioLegend, clone A20) antibodies were incubated for 2 hours at room temperature. Sections were mounted with DAPI Fluoromount-G (SouthernBiotech).

Confocal imaging cytometry

Tumor lymphatic vascularization, apoptosis, and OT-1 (CD45.1) distribution in B16-OVA-VC tumors were analyzed as follows. Individual tumor slices were imaged using an upright spinning disk confocal microscope (Axio Examiner Z1 Advanced Microscope Base, Zeiss) equipped with a confocal scanner unit CSU-X1 A1 (Yokogawa Electric Corporation). Excitation of the fluorochromes was conducted via three lasers with the wavelengths of 488, 561, and 640 nm (LaserStack v4 Base, 3i). The fluorescence was detected using a 10×/0.3 numerical aperture (NA) or a 63×/1.0 NA water immersion objective (W Plan Apochromat, Zeiss), an appropriate band-pass emission filter (Semrock), and an electron-multiplying charge-coupled device camera (Evolve 512 10 MHz Back Illuminated, Photometrics). Three-dimensional image stacks were obtained by sequential acquisition of multiple field of views (FOVs) covering the whole individual section area along the complete z axis to screen through the complete tissue thickness using a motorized XY stage (ProScan, Prior). To ensure comparability between the samples, the same excitation light intensities and exposure times were adjusted, and the settings were chosen so that any over- or undersatured pixels were avoided. SlideBook software (6.0.17, 3i) was used for image acquisition and the creation of maximum projections. The subsequent generation of montage images from contiguous positions was performed using the Fiji "Grid/collection" stitching plugin (70). Before analysis, all images were processed using a "rolling ball" algorithm implemented into the Fiji plugin "Substract Background" to correct for uneven illuminated background (71).

Garnier et al., Sci. Adv. 8, eabl5162 (2022) 8 June 2022

Supplier name	Catalog number	RRID (Research Resource Identifiers)	Clone	Provider
Brilliant Violet 510 anti-mouse CD45 antibody	103138	AB_2563061	30-F11	BioLegend
Brilliant Violet 510 anti-mouse TER-119/erythroid cell antibody	116237	AB_2561661	TER-119	BioLegend
APC anti-mouse podoplanin antibody	127410	AB_10613649	8.1.1	BioLegend
PerCP/cyanine5.5 anti-mouse CD31 antibody	102522	AB_2566761	MEC13.3	BioLegend
Pacific Blue anti-human/mouse granzyme-B antibody	515408	AB_2562196	GB11	BioLegend
Fixable viability dye eFluor 780	65-0865-18	N/A	N/A	Thermo Fisher Scientific
CD274 (PD-L1, B7-H1) monoclonal antibody, super bright 780	78-5982-82	AB_2724081	MIH5	Thermo Fisher Scientific
Ki-67 monoclonal antibody, FITC	11-5698-82	AB_11151330	SoIA15	Thermo Fisher Scientific
OVA257–264 (SIINFEKL) peptide bound to H-2Kb monoclonal antibody, PE-cyanine7	25-5743-82	AB_10853347	25-D1.16	Thermo Fisher Scientific
CD45.1 monoclonal antibody (A20), PE-cyanine7	25-0453-82	AB_469629	A20	Thermo Fisher Scientific
CD11c monoclonal antibody, PE-cyanine7	25-0114-82	AB_469590	N418	Thermo Fisher Scientific
CD16/CD32 monoclonal antibody	14-0161-86	AB_467135	93	Thermo Fisher Scientific
BV421 rat anti-mouse I-A/I-E	743870	AB_2741821	2G9	BD Biosciences
PE rabbit anti-active caspase 3	550821	AB_393906	C92-605	BD Biosciences
BUV395 rat anti-mouse CD8a	563786	AB_2732919	53-6.7	BD Biosciences
Brilliant Violet 785 anti-mouse IFN-γ antibody	505838	AB_2629667	XMG1.2	BD Biosciences
BV605 rat anti-mouse CD119	745111	AB_2742716	GR20	BD Biosciences

LEC counts and cleaved casp-3 mean fluorescence intensity (MFI) in individual LEC were quantified automatically across whole tumor sections using ImageJ's (National Institutes of Health) implemented "Analyze Particles" tool upon prior intensity-based thresholding and image segmentation of individual fluorescent channels (561 nm, LEC; 640 nm, cleaved casp-3). LEC tumor distribution was calculated as the ratio of the shortest distance of individual LECs to the tumor edge divided by the sum of individual LEC distances toward the center and the edge of the tumor. Distance analysis between individual OT-1 and LEC and the verification of nonrandomized distribution pattern was performed using ImageJ's plugin DiAna (72).

Live cell imaging

LECs from WT (LC3-GFP) and $\beta_2 m^{KO}$ LEC/FRC cocultures were sorted by flow cytometry (see the "Antibodies, flow cytometry, and cell sorting" section), and 5×10^4 cells (ratio 1:1) were plated on fibronectin/PureCol-coated 35-mm by 10-mm petri dish. One day later, cells were loaded with OVA peptide (SIINFEKL) (1 nM;

Sigma-Aldrich) and stained with 0.5 μ M eF(eFluor)670-labeled cell proliferation dye (eBioscience) for 30 min at 37°C in PBS. Cells were washed three times in PBS and incubated for 30 min at 37°C with NucView 405 casp-3 substrate (5 μ M; Biotium). After washing, 1 × 10° in vitro activated OT-1 cells were added to the cultures. Time-lapse confocal spinning disk video microscopy was performed to measure cleaved casp-3 MFI in individual LEC as described above. To detect and to quantify LEC-touching OT-1 number, a mask around individual LECs was generated using the all-LEC channel. Last, this mask was applied to the bright-field channel to count temporal contacts between OT-1 and WT or $\beta_2 m^{KO}$ at a time-lapse interval of 1 min over 270 min.

RNA isolation and reverse transcription qPCR

Total RNA was isolated using the RNeasy Plus Micro Kit (QIAGEN) from sorted LEC and DC (see the "Antibodies, flow cytometry, and cell sorting" section). cDNA was synthesized using the PrimeScript RT Reagent Kit followed by a preamplification of the respective genes of interest using the TaqMan Preamp Master Mix (Applied

Garnier et al., Sci. Adv. 8, eabl5162 (2022) 8 June 2022

Biosystems). PCRs were performed with the ABI Prism 7900 HT detection system and the PowerUp SYBR Green Master Mix (Applied Biosystems). Results (two replicates) were normalized with glyceraldehyde phosphate dehydrogenase (gapdh), and l32 normalization factors and fold changes were calculated according to the GeNorm method

Primers were as follows: Ifngr2: GGCTGGAGCCATTTCAAC AC (forward) and AAAGGGCCTTCAACCTGTTC (reverse); Ifngr1: GCCTAAAGGGAAAGGTCGGG (forward) and CACTCCGGT TATGCTCCACA (reverse); Jak1: GTGCGTTTTTAGAGCGCAGG (forward) and CAGAGCTGATCACTTCCGTGT (reverse); Stat1: AAAGTCATGGCTGCCGAGAA (forward) and CATCGGTTCT-GGTGCTTCCT (reverse); Irf1: CCATTCACACAGGCCGATAC (forward) and ACAGCAGAGCTGCCCTTGTT (reverse); C2ta: CCCTGCGTGTGATGGATGTC (forward) and ATCTCAGACT-GATCCTGGCAT (reverse); H2-ab: CTGTGGTGG TGCTGATGG T (forward) and CGTTGGTGAAGTAGCACTCG (reverse); Cd274: CATCCCAGAACTGCCTGCAA (forward) and TGCCAATC-GACGATCAGAGG (reverse); H2kb: GTGATCTCTGGCTGT-GAAGT (forward) and GTCTCCACAAGCTCCATGTC (reverse); Nlrc5: CTTCCCGCCTCTCCTTCCACAAT (forward) and CTCCACCTGCCCACATCCTACCA (reverse); Tap1: GGACTTG-CCTTGTTCCGAGAG (forward) and GCTGCCACATAACTGA-TAGCGA (reverse); Lmp2: CATGAACCGAGATGGCTCTAGT (forward) and TCATCGTAGAATTTTGGCAGCTC (reverse); B2m: CCCCACTGAGACTGATACATACG (forward) and CGATCCCAG-TAGACGGTCTTG (reverse); Gapdh: CCCGTAGACAAAAT-GGTGAAG (forward) and AGGTCAATGAAGGGGTCGTTG (reverse); and L32: GAAACTGGCGGAAACCCA (forward) and GGATCTGGCCCTTGAACCTT (reverse). For VEGF-C qPCR, a RT2 qPCR primer assay was used (QIAGEN, catalog no 330001 PPM03061F; reference position: 449).

Statistical analysis

Statistical analysis was performed with Prism (version 9.0; GraphPad, San Diego, CA). Groups were first compared with F test to test the hypothesis of equal variances. In the presence of significantly different variances, datasets were compared using either a nonparametric test (specifically Mann-Whitney test for comparison of two groups). In the presence of equal variances, parametric tests were used, specifically one-way analysis of variance (ANOVA) with Tukey's multiple comparisons test for comparison of three or more groups and two-way ANOVA with Sidak's multiple comparisons test for comparison of the dataset containing repeated measurements. P values were reported as follows: *P < 0.05, **P < 0.01, ***P < 0.001, and ****P < 0.0001. Some data points were omitted from analysis by identifying outliers with the Prism software (ROUT method).

SUPPLEMENTARY MATERIALS

Supplementary material for this article is available at https://science.org/doi/10.1126/sciadv.abl5162

View/request a protocol for this paper from Bio-protocol.

REFERENCES AND NOTES

- S. P. Leong, E. K. Nakakura, R. Pollock, M. A. Choti, D. L. Morton, W. D. Henner, A. Lal, R. Pillai, O. H. Clark, B. Cady, Unique patterns of metastases in common and rare types of malignancy. *J. Surg. Oncol.* **103**, 607–614 (2011).
- of malignancy. *J. Surg. Oncol.* **103**, 607–614 (2011).

 2. S. A. Stacker, S. P. Williams, T. Karnezis, R. Shayan, S. B. Fox, M. G. Achen, Lymphangiogenesis and lymphatic vessel remodelling in cancer. *Nat. Rev. Cancer* **14**, 159–172 (2014).

Lymph node metastases can invade local blood vessels, exit the node, and colonize distant organs in mice. *Science* **359**, 1403–1407 (2018).

5. S. Dadras, T. Paul, J. Bertoncini, L. F. Brown, A. Muzikansky, D. G. Jackson, U. Ellwanger,

M. Brown, F. P. Assen, A. Leithner, J. Abe, H. Schachner, G. Asfour, Z. Bago-Horvath,

4. E. R. Pereira, D. Kedrin, G. Seano, O. Gautier, E. F. J. Meijer, D. Jones, S.-M. Chin, S. Kitah

E. M. Bouta, J. Chang, E. Beech, H.-S. Jeong, M. C. Carroll, A. G. Taghian, T. P. Padera,

J. V. Stein, P. Uhrin, M. Sixt, D. Kerjaschki, Lymph node blood vessels provide exit routes for metastatic tumor cell dissemination in mice. Science 359, 1408–1411 (2018).

- C. Garbe, M. C. Mihm, M. Detmar, Tumor lymphangiogenesis: A novel prognostic indicator for cutaneous melanoma metastasis and survival. *Am. J. Pathol.* 162, 1951–1960 (2003).
 6. M. Rinderknecht, M. Detmar, Tumor lymphangiogenesis and melanoma metastasis. *J. Cell. Physiol.* 216, 347–354 (2008).
- 7. W. Thiele, J. P. Sleeman, Tumor-induced lymphangiogenesis: A target for cancer therapy?

 L. Biotechnol. 12a. 274–241 (2006).
- J. B. Burton, S. J. Priceman, J. L. Sung, E. Brakenhielm, D. S. An, B. Pytowski, K. Alitalo, L. Wu, Suppression of prostate cancer nodal and systemic metastasis by blockade of the lymphangiogenic axis. *Cancer Res.* 68, 7828–7837 (2008).
- A. Gogineni, M. Caunt, A. Crow, C. V. Lee, G. Fuh, N. van Bruggen, W. Ye, R. M. Weimer, Inhibition of VEGF-C modulates distal lymphatic remodeling and secondary metastasis. *PLOS ONE* 8, e68755 (2013).
- S. Hirakawa, L. F. Brown, S. Kodama, K. Paavonen, K. Alitalo, M. Detmar, VEGF-C-induced lymphangiogenesis in sentinel lymph nodes promotes tumor metastasis to distant sites. *Blood* 109, 1010–1017 (2007).
- T. Hoshida, N. Isaka, J. Hagendoorn, E. di Tomaso, Y. L. Chen, B. Pytowski, D. Fukumura, T. P. Padera, R. K. Jain, Imaging steps of lymphatic metastasis reveals that vascular endothelial growth factor-C increases metastasis by increasing delivery of cancer cells to lymph nodes: Therapeutic implications. Cancer Res. 66, 8065–8075 (2006).
- J. Lin, A. S. Lalani, T. C. Harding, M. Gonzalez, W.-W. Wu, B. Luan, G. H. Tu, K. Koprivnikar, M. J. VanRoey, Y. He, K. Alitalo, K. Jooss, Inhibition of lymphogenous metastasis using adeno-associated virus-mediated gene transfer of a soluble VEGFR-3 decoy receptor. Cancer Res. 65, 6901–6909 (2005).
- S. J. Mandriota, L. Jussila, M. Jeltsch, A. Compagni, D. Baetens, R. Prevo, S. Banerji, J. Huarte, R. Montesano, D. G. Jackson, L. Orci, K. Alitalo, G. Christofori, M. S. Pepper, Vascular endothelial growth factor-C-mediated lymphangiogenesis promotes tumour metastasis. EMBO J. 20, 672–682 (2001).
- N. Roberts, B. Kloos, M. Cassella, S. Podgrabinska, K. Persaud, Y. Wu, B. Pytowski, M. Skobe, Inhibition of VEGFR-3 activation with the antagonistic antibody more potently suppresses lymph node and distant metastases than inactivation of VEGFR-2. Cancer Res. 66, 2650–2657 (2006).
- M. Skobe, T. Hawighorst, D. G. Jackson, R. Prevo, L. Janes, P. Velasco, L. Riccardi, K. Alitalo, K. Claffey, M. Detmar, Induction of tumor lymphangiogenesis by VEGF-C promotes breast cancer metastasis. *Nat. Med.* 7, 192–198 (2001).
- S. A. Stacker, C. Caesar, M. E. Baldwin, G. E. Thornton, R. A. Williams, R. Prevo,
 D. G. Jackson, S. I. Nishikawa, H. Kubo, M. G. Achen, VEGF-D promotes the metastatic spread of tumor cells via the lymphatics. *Nat. Med.* 7, 186–191 (2001).
- S. Hirakawa, S. Kodama, R. Kunstfeld, K. Kajiya, L. F. Brown, M. Detmar, VEGF-A induces tumor and sentinel lymph node lymphangiogenesis and promotes lymphatic metastasis. *J. Exp. Med.* 201, 1089–1099 (2005).
- C. N. Qian, B. Berghuis, G. Tsarfaty, M. Bruch, E. J. Kort, J. Ditlev, I. Tsarfaty, E. Hudson, D. G. Jackson, D. Petillo, J. Chen, J. H. Resau, B. T. Teh, Preparing the "soil": The primary tumor induces vasculature reorganization in the sentinel lymph node before the arrival of metastatic cancer cells. Cancer Res. 66, 10365–10376 (2006).
- M. Kim, Y. J. Koh, K. E. Kim, B. I. Koh, D. H. Nam, K. Alitalo, I. Kim, G. Y. Koh, CXCR4 signaling regulates metastasis of chemoresistant melanoma cells by a lymphatic metastatic niche. *Cancer Res.* 70, 10411–10421 (2010).
- Q. Ma, L. C. Dieterich, K. Ikenberg, S. B. Bachmann, J. Mangana, S. T. Proulx, V. C. Amann, M. P. Levesque, R. Dummer, P. Baluk, D. M. McDonald, M. Detmar, Unexpected contribution of lymphatic vessels to promotion of distant metastatic tumor spread. Sci. Adv. 4. eaat4758 (2018).
- M. A. S. Broggi, L. Maillat, C. C. Clement, N. Bordry, P. Corthésy, A. Auger, M. Matter, R. Hamelin, L. Potin, D. Demurtas, E. Romano, A. Harari, D. E. Speiser, L. Santambrogio, M. A. Swartz, Tumor-associated factors are enriched in lymphatic exudate compared to plasma in metastatic melanoma patients. J. Exp. Med. 216, 1091–1107 (2019).
- J. D. Peske, E. D. Thompson, L. Gemta, R. A. Baylis, Y. X. Fu, V. H. Engelhard, Effector lymphocyte-induced lymph node-like vasculature enables naive T-cell entry into tumours and enhanced anti-tumour immunity. *Nat. Commun.* 6, 7114 (2015).
- E. D. Thompson, H. L. Enriquez, Y. X. Fu, V. H. Engelhard, Tumor masses support naive T cell infiltration, activation, and differentiation into effectors. J. Exp. Med. 207, 1791–1804 (2010).
- P, Yu, Y, Lee, W. Liu, R. K. Chin, J. Wang, Y. Wang, A. Schietinger, M. Philip, H. Schreiber, Y. X. Fu, Priming of naive T cells inside tumors leads to eradication of established tumors Nat. Immunol. 5, 141–149 (2004).

Garnier et al., Sci. Adv. 8, eabl5162 (2022) 8 June 2022

- A. W. Lund, M. Wagner, M. Fankhauser, E. S. Steinskog, M. A. Broggi, S. Spranger, T. F. Gajewski, K. Alitalo, H. P. Eikesdal, H. Wiig, M. A. Swartz, Lymphatic vessels regulate immune microenvironments in human and murine melanoma. *J. Clin. Invest.* 126, 3389–3402 (2016).
- E. W. Roberts, M. L. Broz, M. Binnewies, M. B. Headley, A. E. Nelson, D. M. Wolf, T. Kaisho, D. Bogunovic, N. Bhardwaj, M. F. Krummel, Critical role for CD103 */CD141* dendritic cells bearing CCR7 for tumor antigen trafficking and priming of T cell immunity in melanoma. Cancer Cell 30, 324–336 (2016).
- N. Bordry, M. A. S. Broggi, K. de Jonge, K. Schaeuble, P. O. Gannon, P. G. Foukas,
 E. Danenberg, E. Romano, P. Baumgaertner, M. Fankhauser, N. Wald, L. Cagnon,
 S. Abed-Maillard, H. M. E. Hajjami, T. Murray, K. Ioannidou, I. Letovanec, P. Yan,
 O. Michielin, M. Matter, M. A. Swartz, D. E. Speiser, Lymphatic vessel density is associated
 with CD8⁺T cell infiltration and immunosuppressive factors in human melanoma.
 Onco. Targets. Ther. 7, e1462878 (2018).
- M. Fankhauser, M. A. S. Broggi, L. Potin, N. Bordry, L. Jeanbart, A. W. Lund, E. da Costa, S. Hauert, M. Rincon-Restrepo, C. Tremblay, E. Cabello, K. Homicsko, O. Michielin, D. Hanahan, D. E. Speiser, M. A. Swartz, Tumor lymphangiogenesis promotes T cell infiltration and potentiates immunotherapy in melanoma. Sci. Transl. Med. 9, eaal4712 (2017).
- B. Mlecnik, G. Bindea, A. Kirilovsky, H. K. Angell, A. C. Obenauf, M. Tosolini, S. E. Church, P. Maby, A. Vasaturo, M. Angelova, T. Fredriksen, S. Mauger, M. Waldner, A. Berger, M. R. Speicher, F. Pagès, V. Valge-Archer, J. Galon, The tumor microenvironment and Immunoscore are critical determinants of dissemination to distant metastasis. Sci. Transl. Med. 8, 327ra26 (2016).
- T. Kimura, M. Sugaya, T. Oka, A. Blauvelt, H. Okochi, S. Sato, Lymphatic dysfunction attenuates tumor immunity through impaired antigen presentation. Oncotarget 6, 18081–18093 (2015).
- A. W. Lund, F. V. Duraes, S. Hirosue, V. R. Raghavan, C. Nembrini, S. N. Thomas, A. Issa,
 S. Hugues, M. A. Swartz, VEGF-C promotes immune tolerance in B16 melanomas and cross-presentation of tumor antigen by lymph node lymphatics. *Cell Rep.* 1, 191–199 (2012).
- C. Tacconi, F. Ungaro, C. Correale, V. Arena, L. Massimino, M. Detmar, A. Spinelli, M. Carvello, M. Mazzone, A. I. Oliveira, F. Rubbino, V. Garlatti, S. Spanò, E. Lugli, F. S. Colombo, A. Malesci, L. Peyrin-Biroulet, S. Vetrano, S. Danese, S. D'Alessio, Activation of the VEGFC/VEGFR3 pathway induces tumor immune escape in colorectal cancer. Cancer Res. 79, 4196-4210 (2019).
- L. C. Dieterich, K. Ikenberg, T. Cetintas, K. Kapaklikaya, C. Hutmacher, M. Detmar, Tumor-associated lymphatic vessels upregulate PDL1 to inhibit T-cell activation. Front. Impunol. 8, 66 (2017).
- R. S. Lane, J. Femel, A. P. Breazeale, C. P. Loo, G. Thibault, A. Kaempf, M. Mori, T. Tsujikawa, Y. H. Chang, A. W. Lund, IFNy-activated dermal lymphatic vessels inhibit cytotoxic T cells in melanoma and inflamed skin. J. Exp. Med. 215, 3057–3074 (2018).
- A. O. Gkountidi, L. Garnier, J. Dubrot, J. Angelillo, G. Harlé, D. Brighouse, L. J. Wrobel, R. Pick, C. Scheiermann, M. A. Swartz, S. Hugues, MHC class II antigen presentation by lymphatic endothelial cells in tumors promotes intratumoral regulatory T cellsuppressive functions. Cancer Immunol. Res. 9, 748–764 (2021).
- E. Song, T. Mao, H. Dong, L. S. B. Boisserand, S. Antila, M. Bosenberg, K. Alitalo, J.-L. Thomas, A. Iwasaki, VEGF-C-driven lymphatic drainage enables immunosurveillance of brain tumours. *Nature* 577, 689–694 (2020).
- M. S. Sasso, N. Mitrousis, Y. Wang, P. S. Briquez, S. Hauert, J. Ishihara, J. A. Hubbell, M. A. Swartz, Lymphangiogenesis-inducing vaccines elicit potent and long-lasting T cell immunity against melanomas. Sci. Adv. 7, eabe4362 (2021).
- M. T. Spiotto, D. A. Rowley, H. Schreiber, Bystander elimination of antigen loss variants in established tumors. Nat. Med. 10, 294–298 (2004).
- M. T. Spiotto, H. Schreiber, Rapid destruction of the tumor microenvironment by CTLs recognizing cancer-specific antigens cross-presented by stromal cells. Cancer Immun. 5, 8/2005.
- B. Zhang, N. A. Bowerman, J. K. Salama, H. Schmidt, M. T. Spiotto, A. Schietinger, P. Yu, Y. X. Fu, R. R. Weichselbaum, D. A. Rowley, D. M. Kranz, H. Schreiber, Induced sensitization of tumor stroma leads to eradication of established cancer by T cells. J. Exp. Med. 204, 49–55 (2007).
- J. J. Listopad, T. Kammertoens, K. Anders, B. Silkenstedt, G. Willimsky, K. Schmidt, A. A. Kuehl, C. Loddenkemper, T. Blankenstein, Fas expression by tumor stroma is required for cancer eradication. Proc. Natl. Acad. Sci. U.S.A. 110, 2276–2281 (2013).
- T. Schuler, T. Blankenstein, Cutting edge: CD8+ effector T cells reject tumors by direct antigen recognition but indirect action on host cells. J. Immunol. 170, 4427–4431 (2003).
- B. Zhang, T. Karrison, D. A. Rowley, H. Schreiber, IFN-7— and TNF-dependent bystander eradication of antigen-loss variants in established mouse cancers. J. Clin. Invest. 118, 1398–1404 (2008).
- Z. Qin, J. Schwartzkopff, F. Pradera, T. Kammertoens, B. Seliger, H. Pircher, T. Blankenstein, A critical requirement of interferon gamma-mediated angiostasis for tumor rejection by CD8⁺T cells. Cancer Res. 63, 4095–4100 (2003).

- T. Kammertoens, C. Friese, A. Arina, C. Idel, D. Briesemeister, M. Rothe, A. Ivanov, A. Szymborska, G. Patone, S. Kunz, D. Sommermeyer, B. Engels, M. Leisegang, A. Textor, H. J. Fehling, M. Fruttiger, M. Lohoff, A. Herrmann, H. Yu, R. Weichselbaum, W. Uckert, N. Hübner, H. Gerhardt, D. Beule, H. Schreiber, T. Blankenstein, Tumour ischaemia by interferon-y resembles physiological blood vessel regression. *Nature* 545, 98–102 (2017).
- R. P. Kataru, H. Kim, C. Jang, D. K. Choi, B. I. Koh, M. Kim, S. Gollamudi, Y.-K. Kim, S.-H. Lee, G. Y. Koh, T lymphocytes negatively regulate lymph node lymphatic vessel formation. *Immunity* 34, 96–107 (2011).
- E. Bazigou, O. T. A. Lyons, A. Smith, G. E. Venn, C. Cope, N. A. Brown, T. Makinen, Genes regulating lymphangiogenesis control venous valve formation and maintenance in mice. *J. Clin. Invest.* 121, 2984–2992 (2011).
- H. M. Lee, A. Fleige, R. Forman, S. Cho, A. A. Khan, L.-L. Lin, D. T. Nguyen, A. O'Hara-Hall, Z. Yin, C. A. Hunter, W. Muller, L.-F. Lu, IFNy signaling endows DCs with the capacity to control type I inflammation during parasitic infection through promoting T-bet[†] regulatory T cells. *PLOS Pathog.* 11, e1004635 (2015).
- G. P. Dunn, C. M. Koebel, R. D. Schreiber, Interferons, immunity and cancer immunoediting. *Nat. Rev. Immunol.* 6, 836–848 (2006).
- A. J. Ligocki, J. R. Brown, J. Y. Niederkorn, Role of interferon-γ and cytotoxic T lymphocytes in intraocular tumor rejection. J. Leukoc. Biol. 99, 735–747 (2016).
- J. Zhou, P. Ma, J. Li, X. Cui, W. Song, Improvement of the cytotoxic T lymphocyte response against hepatocellular carcinoma by transduction of cancer cells with an adenoassociated virus carrying the interferon-y gene. *Mol. Med. Rep.* 13, 3197–3205 (2016).
- G. Segal, S. Prato, D. Zehn, J. D. Mintern, J. A. Villadangos, Target density, not affinity or avidity of antigen recognition, determines adoptive T cell therapy outcomes in a mouse lymphoma model. J. Immunol. 196, 3935–3942 (2016).
- S. Hirosue, E. Vokali, V. R. Raghavan, M. Rincon-Restrepo, A. W. Lund, P. Corthésy-Henrioud, F. Capotosti, C. Halin Winter, S. Hugues, M. A. Swartz, Steady-state antigen scavenging, cross-presentation, and CD8⁺ T cell priming: A new role for lymphatic endothelial cells. *J. Immunol.* 192, 5002–5011 (2014).
- N. Cousin, S. Cap, M. Dihr, C. Tacconi, M. Detmar, L. C. Dieterich, Lymphatic PD-L1 expression restricts tumor-specific CD8⁺T cell responses. *Cancer Res.* 81, 4133–4144 (2021).
- U. Blohm, D. Potthoff, A. J. van der Kogel, H. Pircher, Solid tumors "melt" from the inside after successful CD8 T cell attack. Eur. J. Immunol. 36, 468–477 (2006).
- A. Schurich, J. P. Böttcher, S. Burgdorf, P. Penzler, S. Hegenbarth, M. Kern, A. Dolf, E. Endl, J. Schultze, E. Wiertz, D. Stabenow, C. Kurts, P. Knolle, Distinct kinetics and dynamics of cross-presentation in liver sinusoidal endothelial cells compared to dendritic cells. *Hepatology* 50, 909–919 (2009).
- N. von Oppen, A. Schurich, S. Hegenbarth, D. Stabenow, R. Tolba, R. Weiskirchen, A. Geerts, W. Kolanus, P. Knolle, L. Diehl, Systemic antigen cross-presented by liver sinusoidal endothelial cells induces liver-specific CD8 T-cell retention and tolerization. Hepatology 49, 1664–1672 (2009).
- T. Makinen, T. Veikkola, S. Mustjoki, T. Karpanen, B. Catimel, E. C. Nice, L. Wise, A. Mercer, H. Kowalski, D. Kerjaschki, S. A. Stacker, M. G. Achen, K. Alitalo, Isolated lymphatic endothelial cells transduce growth, survival and migratory signals via the VEGF-C/D receptor VEGFR-3. EMBO J. 20, 4762–4773 (2001).
- B. Engels, V. H. Engelhard, J. Sidney, A. Sette, D. C. Binder, R. B. Liu, D. M. Kranz,
 C. Meredith, D. A. Rowley, H. Schreiber, Relapse or eradication of cancer is predicted by peptide-major histocompatibility complex affinity. Cancer Cell 23, 516–526 (2013).
- L. Ni, J. Lu, Interferon gamma in cancer immunotherapy. Cancer Med. 7, 4509–4516 (2018).
- S. J. Patel, N. E. Sanjana, R. J. Kishton, A. Eidizadeh, S. K. Vodnala, M. Cam, J. J. Gartner, L. Jia, S. M. Steinberg, T. N. Yamamoto, A. S. Merchant, G. U. Mehta, A. Chichura, O. Shalem, E. Tran, R. Eil, M. Sukumar, E. P. Guijarro, C.-P. Day, P. Robbins, S. Feldman, G. Merlino, F. Zhang, N. P. Restifo, Identification of essential genes for cancer immunotherapy. *Nature* **548**, 537–542 (2017).
- K. S. Kobayashi, P. J. van den Elsen, NLRC5: A key regulator of MHC class I-dependent immune responses. Nat. Rev. Immunol. 12, 813–820 (2012).
- L. Martinez-Lostao, A. Anel, J. Pardo, How do cytotoxic lymphocytes kill cancer cells? Clin. Cancer Res. 21, 5047–5056 (2015).
- B. H. Koller, P. Marrack, J. W. Kappler, O. Smithies, Normal development of mice deficient in β₂M, MCClass I proteins, and CD8⁺T cells. Science 248, 1227–1230 (1990).
- S. Enouz, L. Carrié, D. Merkler, M. J. Bevan, D. Zehn, Autoreactive T cells bypass negative selection and respond to self-antigen stimulation during infection. J. Exp. Med. 209, 1769–1779 (2012).
- 66. W. W. Overwijk, M. R. Theoret, S. E. Finkelstein, D. R. Surman, L. A. de Jong, F. A. Vyth-Dreese, T. A. Dellemijn, P. A. Antony, P. J. Spiess, D. C. Palmer, D. M. Heimann, C. A. Klebanoff, Z. Yu, L. N. Hwang, L. Feigenbaum, A. M. Kruisbeek, S. A. Rosenberg, N. P. Restifo, Tumor regression and autoimmunity after reversal of a functionally tolerant state of self-reactive CD8⁺T cells. J. Exp. Med. 198, 569–580 (2003).
- N. Mizushima, A. Yamamoto, M. Matsui, T. Yoshimori, Y. Ohsumi, In vivo analysis
 of autophagy in response to nutrient starvation using transgenic mice expressing
 a fluorescent autophagosome marker. Mol. Biol. Cell 15, 1101–1111 (2004).

- A. L. Fletcher, V. Lukacs-Kornek, E. D. Reynoso, S. E. Pinner, A. Bellemare-Pelletier, M. S. Curry, A. R. Collier, R. L. Boyd, S. J. Turley, Lymph node fibroblastic reticular cells directly present peripheral tissue antigen under steady-state and inflammatory conditions. J. Exp. Med. 207, 689–697 (2010).
- Conditions. J. Exp. Med. 207, 689–697 (2010).
 P. Bankhead, M. B. Loughrey, J. A. Fernández, Y. Dombrowski, D. G. McArt, P. D. Dunne,
 McQuaid, R. T. Gray, L. J. Murray, H. G. Coleman, J. A. James, M. Salto-Tellez,
 P. W. Hamilton, QuPath: Open source software for digital pathology image analysis. Sci. Rep. 7, 16878 (2017).
- S. Preiblisch, S. Saalfeld, P. Tomancak, Globally optimal stitching of tiled 3D microscopic image acquisitions. *Bioinformatics* 25, 1463–1465 (2009).
- 71. S. Sternberg, Biomedical image processing. Computer 16, 22–34 (1983).
- J. F. Gilles, M. Dos Santos, T. Boudier, S. Bolte, N. Heck, DiAna, an ImageJ tool for object-based 3D co-localization and distance analysis. Methods 115, 55–64 (2017).

Acknowledgments: We thank J. P. Aubry-Lachainaye, C. Gameiro, and G. Schneiter for excellent assistance in flow cytometry; N. Liaudet and F. Prodon for excellent assistance in imaging; D. Chollet for excellent assistance in qPCR experiments; E. Cosset for the generation of MC38-OVA-VEGF-C^{hi} cells; J. Angelillo for the color intensity quantification in TdLNs; B. Nizil

and I. Senoner for the setup of Gp100 immunofluorescent staining; D. Speiser and K. Schäuble for helpful discussion; W. Muller for providing IFN-y^{MI} mice; and P. Romero for providing OT-3 mice. **Funding:** This work was supported by the Geneva Cancer League to S.H., the Swiss Cancer League (NLS-4836-08-2019) to C.S., and the Swiss National Science Foundation (310030_16554 and 310030_185255 to S.H. and 310030_182417/1 to C.S.). **Author contributions:** Conceptualization: L.G. and S.H. Methodology; L.G., R.P., J.M., C.S., M.S., J.B.-L., N.L., and S.H. Investigation: L.G., R.P., J.M., M.S., D.B., T.K., T.B., N.P., N.L.T., T.V.P., D.M., C.S., and S.H. Visualization: L.G., R.P., J.M., M.S., D.B., V.P., T.V.P., D.M., C.S., and S.H. Writing—Original draft: L.G. and S.H. Writing—Review and editing: L.G., R.P., S.H., C.S., T.K., N.L.T., and T.B. Resources: C.S. and S.H. Competing interests: The authors declare that they have no competing interests. **Data and materials availability:** The data underlying this article are accessible at https://doi.org/10.26037/yaretaw7bz/Tvlhbfanbfgzmsifu3394. All data needed to evaluate the conclusions in the paper are present in the paper and/or the Supplementary Materials.

Submitted 19 July 2021 Accepted 22 April 2022 Published 8 June 2022 10.1126/sciady.abl5162

Garnier et al., Sci. Adv. 8, eabl5162 (2022) 8 June 2022

11.3 Appendix 3:

Lymphatic-derived oxysterols promote antitumor immunity and response to immunotherapy in melanoma

Published in Nature Communications, January 2025

This paper publishes a study on which I have worked during my Master thesis. This study investigates the importance of Lymphatic endothelial cells' derived 25-hydroxycholesterol and shows its involvement in promoting the pro-inflammatory phenotype of myeloid cells. In this study I helped with some of the *in vivo* experiments and participated in some of the discussions during the time I spent in Prof. Hugues' laboratory.



Article

https://doi.org/10.1038/s41467-025-55969-w

Lymphatic-derived oxysterols promote antitumor immunity and response to immunotherapy in melanoma

Received: 4 December 2023

Accepted: 7 January 2025

Published online: 31 January 2025

Check for updates

Mengzhu Sun¹, Laure Garnier¹, Romane Chevalier¹, Martin Roumain², Chen Wang ^{① 1.77}, Julien Angelillo¹, Julien Montorfani¹, Robert Pick ^{② 1}, Dale Brighouse¹, Nadine Fournier ^{② 3}, David Tarussio ^{4.5,6}, Stéphanie Tissot ^{② 4.5,6}, Jean-Marc Lobaccaro ^{② 7,8,9}, Tatiana V. Petrova ^{③ 6.10}, Camilla Jandus ^{③ 1,6,11,12}, Daniel E. Speiser ^{③ 10}, Manfred Kopf ¹³, Caroline Pot ^{⑤ 14}, Christoph Scheiermann ^{⑥ 1,11,12,15}, Krisztian Homicsko ¹⁰, Giulio G. Muccioli ^{⑥ 2}, Abhishek D. Garg ^{⑥ 16} & Stéphanie Hugues ^{1,11,12} ⋈

In melanoma, lymphangiogenesis correlates with metastasis and poor prognosis and promotes immunosuppression. However, it also potentiates immunotherapy by supporting immune cell trafficking. We show in a lymphangiogenic murine melanoma that lymphatic endothelial cells (LECs) upregulate the enzyme Ch25h, which catalyzes the formation of 25hydroxycholesterol (25-HC) from cholesterol and plays important roles in lipid metabolism, gene regulation, and immune activation. We identify a role for LECs as a source of extracellular 25-HC in tumors inhibiting PPAR-y in intratumoral macrophages and monocytes, preventing their immunosuppressive function and instead promoting their conversion into proinflammatory myeloid cells that support effector T cell functions. In human melanoma, LECs also upregulate Ch25h, and its expression correlates with the lymphatic vessel signature, infiltration of pro-inflammatory macrophages, better patient survival, and better response to immunotherapy. We identify here in mechanistic detail an important LEC function that supports anti-tumor immunity, which can be therapeutically exploited in combination with immunotherapy.

Lymphangiogenesis is a hallmark of many solid tumors. The expansion of tumor lymphatic vessels (LVs) is largely mediated by VEGF-C and its receptors VEGFR-2/3, and high VEGF-C levels in the tumor microenvironment (TME) increase lymph node (LN) metastasis¹. In preclinical tumor models, an increase in VEGF-C signaling enhances metastatic dissemination to LNs and/or distal organs (reviewed in ref. 2). In addition, increased lymphatic drainage from the primary solid tumor to the sentinel LNs induces intra-LN LV expansion, associated with the formation of a "premetastatic niche" that favors metastatic cell colonization^{3,4}. LVs further impact anti-tumor immunity. First, LVs drain antigens and

antigen-presenting dendritic cells (DCs) to LNs and are, therefore, essential for the initiation of anti-tumor T-cell responses. However, tumor lymphatic endothelial cells (LECs) upregulate immunoregulatory molecules such as PD-L1 and MHCII to limit T cell-mediated immunity (especially against self-antigens), and hence their high density in tumors is associated with immunosuppression⁵⁻⁷. Finally, VEGF-C-induced lymphangiogenesis combined with immunotherapy approaches, including vaccination or PD-1 blockade, promote tumor-specific T cell immunity in tumor mouse models⁸⁻¹⁰. These results suggest that LECs are sensitive to the TME and that their high level of plasticity allows

A full list of affiliations appears at the end of the paper. 🖾 e-mail: stephanie.hugues@unige.ch

them to adopt different phenotypes that can differentially impact tumor and immune cells.

Our RNA sequencing data indicates that, among other genes, LECs in murine melanoma upregulate the enzyme cholesterol 25-hydroxylase (Ch25h). *Ch25h* is an interferon-stimulated gene oxidizing cholesterol, and its primary product 25-hydroxycholesterol (25-HC) exhibits a broad-spectrum antiviral activity, by inducing membrane modifications blocking virus-cell interactions¹¹. Specifically, 25-HC inhibits the lipid-condensing effects of cholesterol, rendering the lipid bilayers less rigid. 25-HC further exhibits functions in modulating the inflammatory response. On one hand, it enhances the expression of IL-8, IL-6, CCL5, and CSF1, while on the other hand inhibits the production of IL-1β due to an effect on sterol regulatory element-binding proteins (SREBP)¹². In vitro, 25-HC regulates transcriptional responses in macrophages and acts as an amplifier of inflammation via AP-1. In vivo, Ch25h^{xO} mice exhibit dampened inflammatory responses in influenza-infected mice¹³.

In the context of tumor development, oxysterols can exert both pro- and anti-tumorigenic functions in vitro14. In patients, low expression of Ch25h has been correlated with poor disease outcomes in colorectal cancer15. Studies have described that tumor-derived extracellular vesicles (TEVs) dampen the expression of Ch25h in the TME and educate healthy cells to function as premetastatic niches and to promote metastasis 6. Furthermore, Ch25h expression in endothelial cells (ECs) dampens tumor-associated angiogenesis in melanoma and CRC mouse models¹⁵. In addition, Ch25h expression in tumorinfiltrating cytotoxic T lymphocytes (CTLs) prevents trogocytosis with cancer cells, and consequently inhibits CTL fratricide by other CTLs17. Finally, tumor-derived factors downregulate Ch25h in phagocytes, promoting phagolysosome fusion and dampening the crosspresentation of tumor antigens by the intratumoral DCs18. Altogether, these studies highlight a role for Ch25h expression and intracellular 25-HC in promoting CTL and DC functions, and inhibiting metastasis. However, whether and how the upregulation of Ch25h by LECs and the subsequent release of 25-HC in the TME will impact the tumorassociated lymphatic vasculature and anti-tumor immunity is

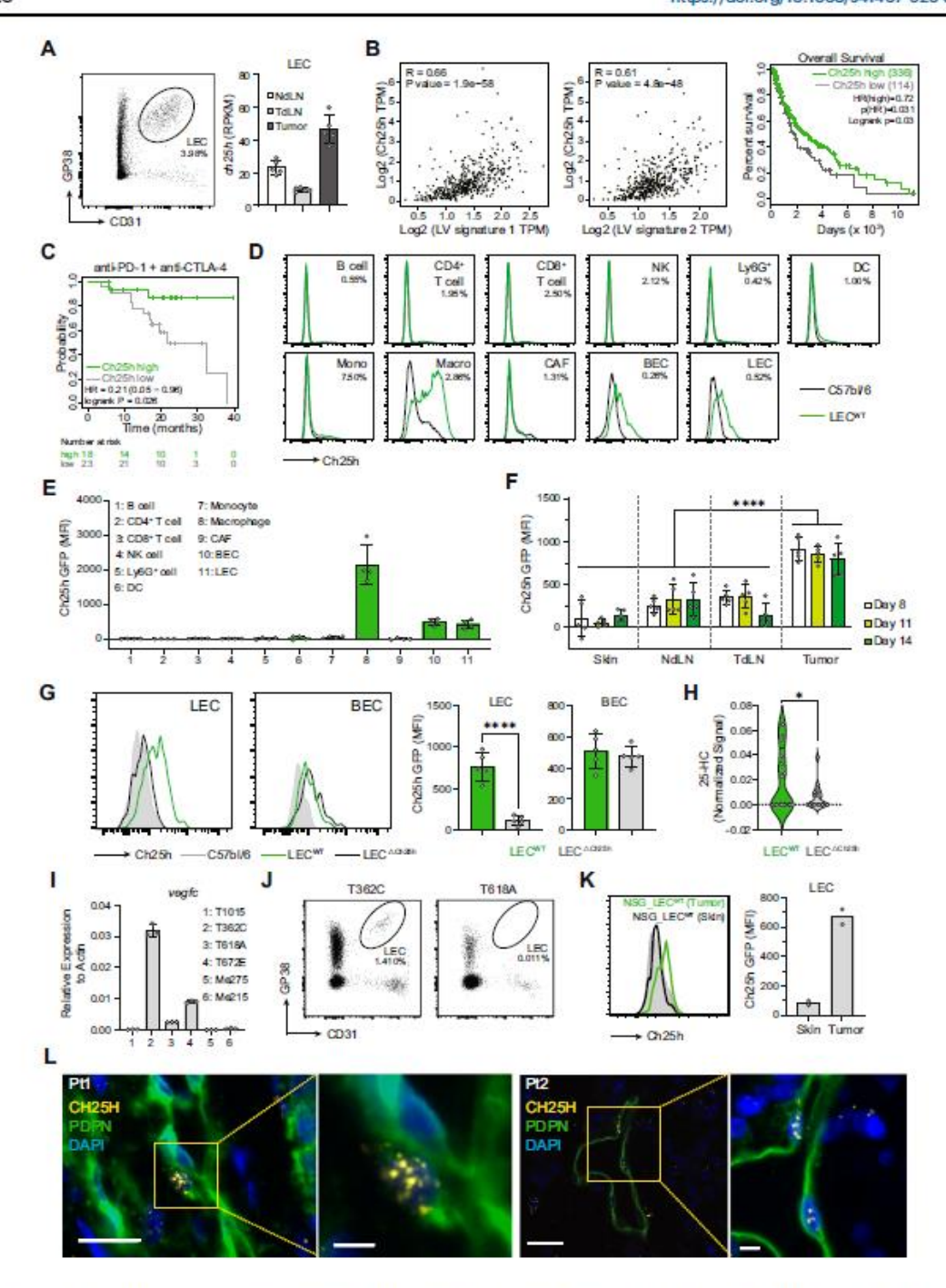
Here, we assess the impact of Ch25h expression by LECs in lymphangiogenic murine melanoma on tumor growth and anti-tumor immunity. In these settings, LECs represent a source of extracellular 25-HC in tumors, and the specific Ch25h abrogation in LECs induces a significant reduction of 25-HC levels. Subsequent 25-HC deprivation in the TME leads to a polarization of tumor-associated myeloid cells towards an immunosuppressive phenotype and prevents them from supporting effector T cells controlling tumor growth. Mechanistically, tumor LEC-derived 25-HC inhibits PPAR-y in macrophages and monocytes and allows them to differentiate into proinflammatory iNOS+ myeloid cells in the TME. Importantly, the whole pathway, from the upregulation of Ch25h expression in tumor LECs to the promotion of immunogenic myeloid cells, enhanced T cell responses, and better control of tumor growth, is amplified upon immunotherapy, i.e., vaccination or adoptive T cell transfer. This suggests that protocols aiming at reinvigorating anti-tumor immunity can also promote LECimmunogenic functions through the production of 25-HC. LECs in human melanoma express Ch25h, and levels of expression correlate with better response to ICB therapy. Our results highlight a role of extracellular oxysterols in strengthening and boosting anti-tumor immunity.

Results

Tumor LECs upregulate Ch25h and contribute to extracellular 25-hydroxy cholesterol levels in lymphangiogenic melanoma

To assess LEC immunomodulatory functions in lymphangiogenic melanoma, we have used B16F10-OVA tumors overexpressing VEGF-C (B16F10-OVA VEGF-C), which, upon inoculation in mice, exhibit increased density of tumoral LECs compared to parental B16F10-OVA tumors^{6,19}. Tumor cells were inoculated in C57BL/6 mice, and RNA sequencing was performed on LECs sorted from tumors, tumordraining LNs (TdLN) and non-draining LNs (NdLN) on day 11. Principal component analysis showed that LECs in different organs exhibited a tissue-specific signature, which was further affected by the TME (Supplementary Fig. 1A). Over 3000 genes were dysregulated in tumor LECs compared to TdLN or NdLN (Supplementary Fig. 1A). Cholesterol 25-hvdroxylase (Ch25h) mRNA was upregulated in tumor LECs compared to TdLN LECs and NdLN LECs (Fig. 1A). We have previously published that Ch25h expression in central nervous system (CNS) endothelial cells promotes neuroinflammation by inhibiting immunosuppressive myeloid cells20. In addition, studies have shown that Ch25h expression in the TME impacts anti-tumor immunity¹⁵⁻¹⁸ Importantly, TCGA datasets indicate that Ch25h mRNA expression in tumors positively correlates with LV signatures (LV signature 1: pdpn, vegfc, lyve1, and LV signature 2: prox1, flt4, lyve1, pdpn, vegfc) in melanoma patients (Fig. 1B). Overall survival (OS) was improved in melanoma patients with high tumoral Ch25h expression (top 25% cutoff) compared to relatively lower expression (bottom 75% cutoff) (Fig. 1B). Although standalone PD-1 or CTLA-4 blockade treatments did not have significant positive predictive activity related to Ch25h levels in melanoma patients (Supplementary Fig. 1B), Ch25h shows strong and significant effect in a large integrated dataset of melanoma patients that received PD-1+CTLA-4 co-blockade21,22 (Fig. 1C). This indicates that Ch25h expression correlates with a better response to the immune checkpoint blockade (ICB)-based combinatorial regimen.

Flow cytometry on B16F10-OVA VEGF-C tumors inoculated in Ch25h-GFP^{loxP} fluorescent reporter mice (Supplementary Fig. 1C)²⁰, revealed that whereas different cells in the TME (Supplementary Fig. 1D) were mostly GFP negative (Fig. 1D, E), macrophages were the main expressors, followed by blood endothelial cells (BECs) and LECs, which expressed significant and comparable levels of Ch25h (Fig. 1D, E). In addition, tumor cells expressed negligible levels of Ch25h mRNA ex vivo (Supplementary Fig. 1E). Immunofluorescent staining on B16F10-OVA VEGF-C tumor sections further confirmed that LECs, BECs, and macrophages express Ch25h protein (Supplementary Fig. 1F), Analysis of LECs from skin, tumors, TdLNs, and NdLNs at different time points after tumor inoculation confirmed that Ch25h protein expression was significantly upregulated in tumor LECs compared to the other sites (Fig. 1F), and further showed that tumor LECs not only expressed high Ch25h levels already at day 8 after tumor inoculation, but further maintained elevated levels over the course of tumor growth (Fig. 1F). Of note, Ch25h expression levels in BECs followed a pattern that was comparable to LECs (Supplementary Fig. 1G). To determine the role of Ch25h expression by LECs in tumors, Ch25h-GFPbxP mice were crossed with Prox-1Cre^{ERT2} mice²³ (LEC^{△Ch25h} mice). Ch25h-GFP^{hoxP} mice were used as controls (LECWT mice). Upon tamoxifen treatment, Ch25h protein expression was efficiently abrogated in tumor LECs from LEC∆Ch25h mice compared to LECWT mice (Fig. 1G), whereas its expression by tumor BECs was not affected (Fig. 1G). Flow cytometry analysis showed that LEC density was unaffected in LEC Ch25h and LECWT tumors (Supplementary Fig. 2A), and Lyve-1 staining on LEC△Ch25h and LECWT tumor sections did not indicate any alterations of the LV structure after Ch25h abrogation in LECs (Supplementary Fig. 2B). In addition, draining of Alexa Fluor 488-dextran from tumor to tumordraining LNs was unaffected in LEC AChash mice compared to LEC T mice (Supplementary Fig. 2C). Therefore, abrogation of Ch25h in LECs does not affect gross LV vasculature and drainage function, suggesting that 25HC has no major intracellular impact on LEC themselves, Accordingly, bulk RNA sequencing on LECs sorted from tumors in LEC^{△Ch,25h} and LEC^{WT} mice showed high sample similarity between the two groups (Supplementary Fig. 2D). Besides confirming an efficient deletion of Ch25h in LECs from LEC^{△C1025h}



(Supplementary Fig. 2E), data revealed very few differentially expressed genes (Supplementary Fig. 2F). None of these genes, except vcam1, are implicated in LV structure and functions. However, vcam1 expression levels were negligible in all samples compared to highly expressed genes such as ch25h, lyve1, prox1, icam1, and pecam1 (Supplementary Fig. 2G). These results are in agreement with the fact that vcam1 is not expressed by LV capillaries and plays a

functional role in LV collectors 24 , indicating that its differential expression between tumor LECs from LEC $^{\Delta \text{CD2Sh}}$ and LEC $^{\text{WT}}$ mice has no major effect on tumor LV functions.

Altogether, these results show that Ch25h abrogation in LECs does not affect their structure and drainage functions in tumors. In contrast, lipid spectrometry analysis on tumor interstitial fluid showed that 25-HC levels were significantly reduced in LEC^{\(\Delta\)}Class tumors compared to

Fig. 1 | LECs express Ch25h and control extracellular 25-hydroxycholesterol (25-HC) levels in lymphangiogenic B16F10-OVA tumors. A B16F10-OVA VEGF-C tumors were inoculated in C57BL/6 mice. LECs were sorted by flow cytometry (CD45^{reg}CD31^tGP38^t) from tumors, tumor-draining LNs (TdLN) and non-draining LNs (NdLN) after 11 days, Ch25h mRNA levels (RPKM) provided by RNA sequencing. n = 5 mice/group. Data were presented as mean values \pm SD. B Correlation between Ch25h expression and lymphatic vessel (LV) signature (LV signature 1: pdpn, vegfc, lyve1, and LV signature 2: prox1, flt4, lyve1, pdpn, vegfc) in SKCM (Skin cutaneous melanoma) patients (TPM transcript per million). SKCM patient overall survival (OS) of high and low Ch25h expression. Data extracted from TCGA. C Predictive activity (OS) of Ch25h high and Ch25h low-expressors SKCM patients treated with anti-PD-1 and anti-CTLA-4, from an integrated dataset of multiple clinical trial studies. Significance was determined by log-rank analysis. D-F B16F10-OVA VEGF-C tumor cells were injected into Ch25h-GFP and WT mice, D. E Ch25h expression by tumor infiltrated cells on day 14. (DC dendritic cells, CAF cancer-associated fibroblasts, BEC blood endothelial cells), Results are representative of two independent experiments, with n = 4 mice/group. F Ch25h expression by LECs in indicated

organs at different time points. Results are pooled from two independent experiments, with n = 2-3 mice/group each. Two-way ANOVA, P < 0.0001. G, H B16F10-OVA VEGF-C tumor cells were injected in LECNCH2th and LECWT mice. G Ch25h expression by LECs and BECs in tumors on day 11. Results are representative of two independent experiments, with n=5 mice/group, D-G Ch25h expression is represented as MFI Ch25h-GFP - MFI-WT mice. H 25-HC levels in tumor interstitial fluid measured by liquid chromatography-mass spectrometry. Results are pooled from two experiments, with n = 4-13 mice /group. G, H Two-tailed unpaired t-test. P< 0.05; P< 0.0001 IVEGF-C expression in human melanoma cell lines by Q-PCR. Histograms depict technical triplicates from one experiment. E-I Data were presented as mean values ± SD. J, K Human melanoma VEGF-Chiph T362C and VEGF-Clin T618A cells were injected in NSG (WT), NSG-LEC ACADA, and NSG-LEC MT mice. Ch25h expression (MFI Ch25h-GFP-MFI-WT mice) by LECs from tumors and skin was assessed by flow cytometry. Data were presented as mean values ± SD. Results are representative of two independent experiments. L Ch25h mRNA and PDPN staining on human melanoma sections (n = 3 patients). Representative images are shown for patients 1 (Pt1) and 2 (Pt2). Scale bar, 20 and 5 µm (zoomed).

LECWT tumors (Fig. 1H). This indicates that, although they are not the main Ch25h expression in the TME, LECs significantly contribute to extracellular 25-HC levels in B16F10-OVA VEGF-C tumors. Accordingly, primary cultured WT LECs exposed to B16F10-OVA VEGF-C tumor cell conditioned medium (TCM) potently released 25-HC in vitro compared to Ch25h knockout LECs (Supplementary Fig. 2H). This was not the case for WT BMDMs, which, similar to Ch25h knockout BMDMs. did not release detectable levels of 25-HC extracellularly when exposed to TCM (Supplementary Fig. 2H). In addition, 25-HC was detected in the culture supernatant of b.END3 mouse brain EC line exposed to TCM, suggesting that BECs can produce extracellular 25-HC (Supplementary Fig. 2H). These in vitro results suggest that 25-HC produced by LECs and BECs can be secreted, while macrophages likely maintain this metabolite intracellularly. Systemic levels of 25-HC in sera of B16-OVA VEGF-C tumor mice were not affected in LEC△Ch28h mice compared to controls (Supplementary Fig. 21) and were lower compared to local tumor levels (Fig. 1H). These results demonstrate that LEC-specific depletion of Ch25h controls 25-HC in the TME without inducing variation of systemic 25-HC levels (which are relatively low), Ch25h is also implicated in the production of 7-keto-25-hydroxycholesterol (7-keto-25-HC)25. 7-keto-25-HC was decreased in B16-OVA VEGF-C tumors from LEC^{△Ch25h} compared to LEC^{WT} mice (Supplementary Fig. 2J), however, its levels in the TME remained abundant compared to 25-HC (Fig. 1H).

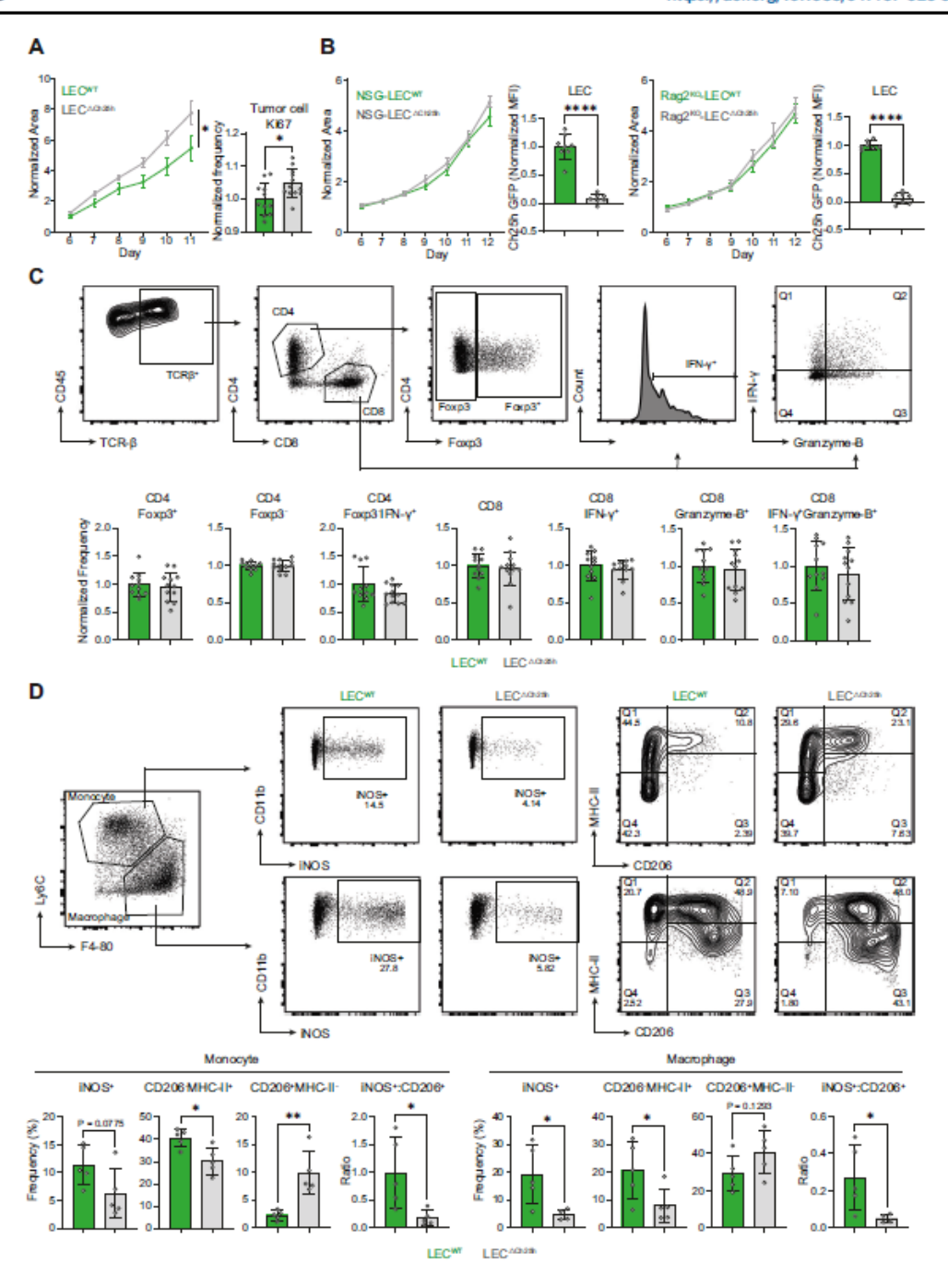
To determine whether our findings translate to human tumors. VEGF-C production was assessed by measuring VEGF-C mRNA levels in a panel of human melanoma cell lines (Fig. 11). Some of the cell lines did not express detectable vegfc (T1015, Me275, Me215) or only low levels (T618A), while others (T362C, T672E) showed significant expression of vegfc (Fig. 1I). To assess if the in vitro measured VEGF-C mRNA expression were biologically relevant in promoting LV formation in an in vivo tumor setting, VEGF-Chigh T362C and VEGF-Chow T618A human melanoma cells were implanted into immune-compromised NSG mice crossed with Ch25h-GFP^{loop} fluorescent reporter (NSG_LEC^{WT}). In contrast to VEGF-C^{loop} T618A cells, VEGF-C^{loop} T362C human melanoma induced detectable amounts of tumoral LECs (Fig. 1J). Strikingly, LECs upregulated Ch25h in T362C lymphangiogenic tumors compared to skin LECs (Fig. 1K). These results show that melanoma patient-derived cell lines produce VEGF-C that supports LV sprouting in the TME of mice in vivo, and the upregulation of Ch25h in mouse LECs. Importantly, we also detected Ch25h mRNA in LECs from human melanoma (Fig. 1L).

Ch25h expression by tumor LECs controls tumor growth by impacting anti-tumor immunity

We next tested the impact of Ch25h abrogation in LECs on B16F10-OVA VEGF-C tumor development. Tumor growth was significantly increased, and tumor cell proliferation enhanced, in LEC $^{\Delta \text{Ch25h}}$ mice

compared to LECWT mice (Fig. 2A). Increased tumor growth in LEC△Ch2Sh mice compared to LECWT mice was also observed in parental B16F10, and in models of colorectal adenocarcinoma (ectopic subcutaneous MC38 and MC38 VEGF-Chigh, orthotopic intrarectal MC38) and breast cancer (orthotopic mammary fat pad E0771) (Supplementary Fig. 3A). These results demonstrate that Ch25h expression by LECs controls the growth of other tumors and is not restricted to OVA expressing or to VEGF-C overexpressing tumors (% of LEC among CD45reg cells = 9.562 ± 5.963; % of LEC among live cells = 0.5275 ± 0.3225). In addition, Ch25h GFP* expression was detected in tumor LECs in parental B16F10 (% of LEC among CD45neg cells = 0.029 ± 0.053; % of LEC among live cells = 0.0043 ± 0.0049), orthotopic MC38 (LEC% among CD45^{neg} cells = 0.244 ± 0.140 ; % of LEC among live cells = $0.0166 \pm$ 0.0084) and ectopic MC38 VEGF-Chigh (% of LEC among CD45neg cells = 0.475 ± 0.250 ; % of LEC among live cells = 0.0081 ± 0.0059) tumors (Supplementary Fig. 3B). In these tumor models, macrophages are more or less abundant (%: 2.252 ±1.092 in B16F10, 10.823 ± 7.277 in MC38 and 0.980 ± 0.930 in MC38 VEGF-Chigh tumors) and are the main expression of Ch25h (Supplementary Fig. 3B). In ectopic MC38 and orthotopic E0771 tumors, however, LEC numbers were too low to be detected by flow cytometry.

Differences in B16F10-OVA VEGF-C tumor growth were abrogated when LEC Ch25h and LEC T mice were crossed on either NSG or Rag2^{KO} background (Fig. 2B). Ch25h was nevertheless expressed in tumoral LECs from NSG-LECWT and Rag2KO-LECWT mice and abrogated in NSG-LEC △Ch28h and Rag2KO-LEC △Ch28h mice (Fig. 2B). Therefore, the anti-tumorigenic effect of 25-HC is immune cell-dependent, although Ch25h expression can be induced in tumoral LECs in the absence of immune cells. Accordingly, B16F10-OVA VEGF-C tumor growth was not only increased in LEC^{△Ch25h} mice (Fig. 2A and Supplementary Fig. 4A), but the CD45*/tumor cell ratio was significantly decreased in tumors from LEC^{△Ch25h} compared to tumors from LEC^{WT} mice (Supplementary Fig. 4A). Therefore, our data indicates that Ch25h expression by LECs dampens B16F10-OVA VEGF-C tumor growth by impacting anti-tumor immunity. Furthermore, tumor growth difference being abrogated in a Rag 260 background, this phenotype likely requires B and/or T cell-mediated immunity. B-cell depletion did not abolish B16F10-OVA VEGF-C tumor growth difference in LECWT and LEC^{△Ch25h} mice (Supplementary Fig. 4B), suggesting that T-cell responses are essential. Ch25h-derived metabolite 25-HC can be further metabolized by the enzyme Cyp7b1 into 7α-25-HC, which is a ligand for the G-protein coupled receptor Epstein-Barr virus-induced gene 2 (EBI2)26 that induces chemotactic migration of a large variety of immune cells27-29. A negligible level of Cyp7b1 mRNA was found in tumoral LECs by RNAseq or by Q-PCR (Supplementary Fig. 4C). In addition, B16F10-OVA VEGF-C tumors transplanted in mixed bone marrow (BM) chimeric mice (50% WT CD45.1+ BM cells+50% EBI2KO



CD45.1°/2° BM cells) did not show any difference in the ratio of WT/ EBI2^{KO} infiltrating immune cells compared to blood circulating cells (Supplementary Fig. 4D), ruling out a role for EBI2-mediated immune cell recruitment in tumors in the impact of LEC-derived 25-HC on anti-tumor immunity.

In-depth analysis of B16F10-OVA VEGF-C tumor-infiltrating T cells did not show any significant difference in frequencies of

effector T cell populations in tumors from LEC^{WT} and LEC^{\triangle Ch25h} mice, such as CD4* T cells producing IFN- γ , Treg, and CD8* T cells or CD8* T cells producing IFN- γ and Granzyme-B (Fig. 2C). Whereas some OVA-specific effector CD8* T cells are detectable in tumors, no difference was observed in frequencies between LEC^{WT} and LEC $^{\triangle$ Ch25h} mice (Supplementary Fig. 4E). These results were surprising, since differences in tumor growth between LEC^{WT} and LEC $^{\triangle$ Ch25h} mice were

Fig. 2 | Loss of Ch25h expression by tumor LECs enhances tumor growth by dampening anti-tumor immunity. A – D Bi6F10-OVA VEGF-Ccells were injected in LECAGAZA and LECAGAZA and Rag2²⁰⁰-LECAGAZA and NSG-LECAGAZA and NSG-LECAGAZA and Rag2²⁰⁰-LECAGAZA and Rag2²⁰⁰-LECAGAZA

C CD4' and CD8' T cells were analyzed for their expression of indicated markers. Representative flow cytometry dot plots and histograms provide the frequency of positive cells among T cell subsets. Data are presented as mean values ± SD. Results are pooled from two independent experiments (n = 4-8 mice/ group each) and normalized to WT. D Myeloid cells (CD1Ib'CD68') were separated into monocytes (Ly6CF4/80') and were analyzed for their expression of indicated markers. Representative flow cytometry dot plots provide the frequency of positive cells among indicated cells. Data were presented as mean values ± SD. Results are representative of two independent experiments, n = 5-7 mice/group each. A-D For FACS analysis, two-tailed unpaired etest. 'P<0.05; "P<0.001" T < 0.0001.

abrogated in a Rag2^{KO} background (Fig. 2A, B). This indicates that T cells may be needed to support or amplify other immune cell functions

CD68*CD11b* myeloid cells, further separated based on Ly6C and F4/80 expression to discriminate between monocytes (Ly6C*F4/ 80') and macrophages (Ly6C'F4/80[†]), showed striking phenotypic differences between in tumors from LEC△Ch2Sh and LECWT mice. Both cell subsets demonstrated a significant shift toward an immunosuppressive state (CD206+) in LEC△Ch28h mice compared to LECWT mice for which tumors contained more pro-inflammatory monocytes and macrophages (CD206'MHCII', iNOS') (Fig. 2D). Therefore, in the absence of Ch25h expression by tumoral LECs, the phenotype of tumor-infiltrating monocytes and macrophages is biased towards an immunosuppressive phenotype. Supporting the hypothesis of T cells promoting anti-tumor monocyte and macrophage functions in LECWT mice, tumors in Rag2^{KO} mice exhibited an almost complete absence of iNOS+ monocytes or macrophages compared to WI tumors (Supplementary Fig. 4F), Consistent with an absence of contribution for B cells to the phenotype, the frequencies of iNOS+ monocytes and macrophages in tumors were not affected by the deletion of B cells (Supplementary Fig. 4G). Other innate leukocyte populations infiltrating tumors from LEC^{WT} and LEC^{\(\triangle \)}Cick bight. reduction in NK frequency, but did not reveal any further major difference, including DC and NK effector populations (Supplementary Fig. 4H). In contrast, although the frequency of total neutrophils (Ly6G+) was not affected, we observed a decrease in iNOS+ ones (Supplementary Fig. 4H).

Impaired response to immunotherapy in mice lacking Ch25h expression in LECs

B16F10 melanoma is often classified as an immunologically cold tumor30. Having in mind that the expression of Ch25h in human melanoma correlates with a better response to immunotherapy (Fig. 1C), we reasoned that by mitigating immunogenicity of B16F10-OVA VEGF-C tumors, we might observe a superior impact of Ch25h expression by LECs on anti-tumor immune responses. To this aim, B16F10-OVA VEGF-C tumor-bearing LEC △Ch28h and LECWT mice were vaccinated with OVA protein combined with CpG-B. First, we observed that upon vaccination, tumor LECs from LECWT mice upregulated even further Ch25h (Fig. 3A). Interestingly, the vaccination did not potentiate Ch25h expression in BECs (Fig. 3A). In addition, whereas both LEC^{△Ch28h} and LECWT mice efficiently controlled tumor growth the first 2 weeks of vaccination compared to unvaccinated controls (Fig. 3B), tumors relapsed in LEC^{\(\triangle Ch28\)} mice, whereas LEC^{WT} mice can maintain small tumor sizes for up to 24 days at least, afterwards they may relapse (Fig. 3B and Supplementary Fig. 5A) possibly due to immune cell exhaustion. Tumor cell analysis revealed that the CD45⁺/tumor cell ratio and CD45 frequency in the tumor were decreased, whereas tumor cell proliferation was increased in vaccinated LEC△Ch28h mice compared to controls (Fig. 3C). Apart from CD206 MHCII monocyte frequencies, alterations toward an immunosuppressive phenotype of tumorinfiltrating monocytes and macrophages in LEC^{△CI} mice were mostly recapitulated upon vaccination (Fig. 3D) as in unvaccinated mice (Fig. 2D), with significantly less iNOS+ in both monocytes and macrophages, and less CD206 MHCII cells in macrophages compared to LECWT mice. Consequently, the ratios iNOS+/CD206+ monocytes and macrophages were impaired in tumors of vaccinated LEC^{△Ch29h} mice, with a more drastic effect on monocytes compared to macrophages (Fig. 3D). Strikingly, whereas differences in T cells were absent without vaccination (Fig. 2C), tumor-infiltrating IFN-γ and TNF-α producing effector CD8⁺ T cell frequencies were impaired in LEC^{△C105h} mice, whereas PD-1*Tim-3* exhausted CD8* T cells were increased (Fig. 3E). Granzyme-B expression by CD8+T cells was however not affected by the abrogation of Ch25h in LECs (Fig. 3E). IFN-y producing CD4⁺ T cell (Th1) frequencies were significantly impaired in tumors in vaccinated 5h mice (Fig. 3E), while Treg frequencies were not altered (Fig. 3E). Although RNA sequencing data did not show any difference in the expression of genes related to antigen presentation between tumor LECs from LECWT and LEC△Ch25h mice (Supplementary Fig. 2F), it is possible that upon vaccination, LEC antigen-presentation functions were affected by the loss of Ch25h and contributed to the impact observed in T cell responses in tumors from LEC^{△Ch28h} mice. LECs are well known to express negligible levels of co-stimulatory molecules31. We nevertheless assessed the frequency of MHCII positive cells, the expression levels of SIINFEKL-MHC-I complexes and PD-L1 in tumor LECs from LECWT and LEC△Ch25h mice (Supplementary Fig. 5B) and could not observe any difference. These results suggest that Ch25h expression by LECs does not modulate their ability to present antigens and does not contribute to differences in T cell responses in tumors from LECWT and LEC△Ch2Sh mice.

NK frequencies and effector functions (production of IFN-y and Granzyme-B) appeared unaffected in tumors from vaccinated LEC $^{\Delta \text{Ch2Sh}}$ mice compared to their controls (Supplementary Fig. 5C). DC and neutrophil (Ly6G*) frequencies were respectively increased and decreased in tumors from LEC \(^{\text{Clesh}}\) mice, with however no difference in iNOS+ neutrophils (Ly6G+iNOS+) (Supplementary Fig. 5C), suggesting that some populations in the TME were affected by the loss of inflammatory myeloid cells and effector T cells in vaccinated LEC△C mice. In TdLNs, we could not find any difference in DC frequencies, SIINFEKL-MHC-I complexes expression levels by DCs, or effector T cell frequencies, and the frequencies of monocytes and macrophages expressing iNOS and CD206 were negligible (Supplementary Fig. 5D). Together with the fact that LECs express negligible levels of Ch25h in TdLNs, these data support a local modulation of tumor-infiltrating immune cells by Ch25h expressing LECs. Finally, LN metastasis was augmented in LEC^{△C1Q:Sh} mice (Supplementary Fig. 5E), probably due to primary tumor relapse, and not because of an alteration of the lymphatic vasculature associated with the tumor, which appears comparable in tumors from vaccinated LEC^{ΔCR2Sh} and LEC^{WT} mice (Supplementary Fig. 5F).

We tested a second approach of immunotherapy, the adoptive transfer of tumor-specific effector CD8* T cells. In this setting, the priming phase of anti-tumor CD8* T cells is bypassed, allowing a focus on the impact of Ch25h expression by LECs on effector T cells in tumors. Preactivated OT-1 cells injected intravenously into B16F10-OVA VEGF-C tumor-bearing mice were significantly

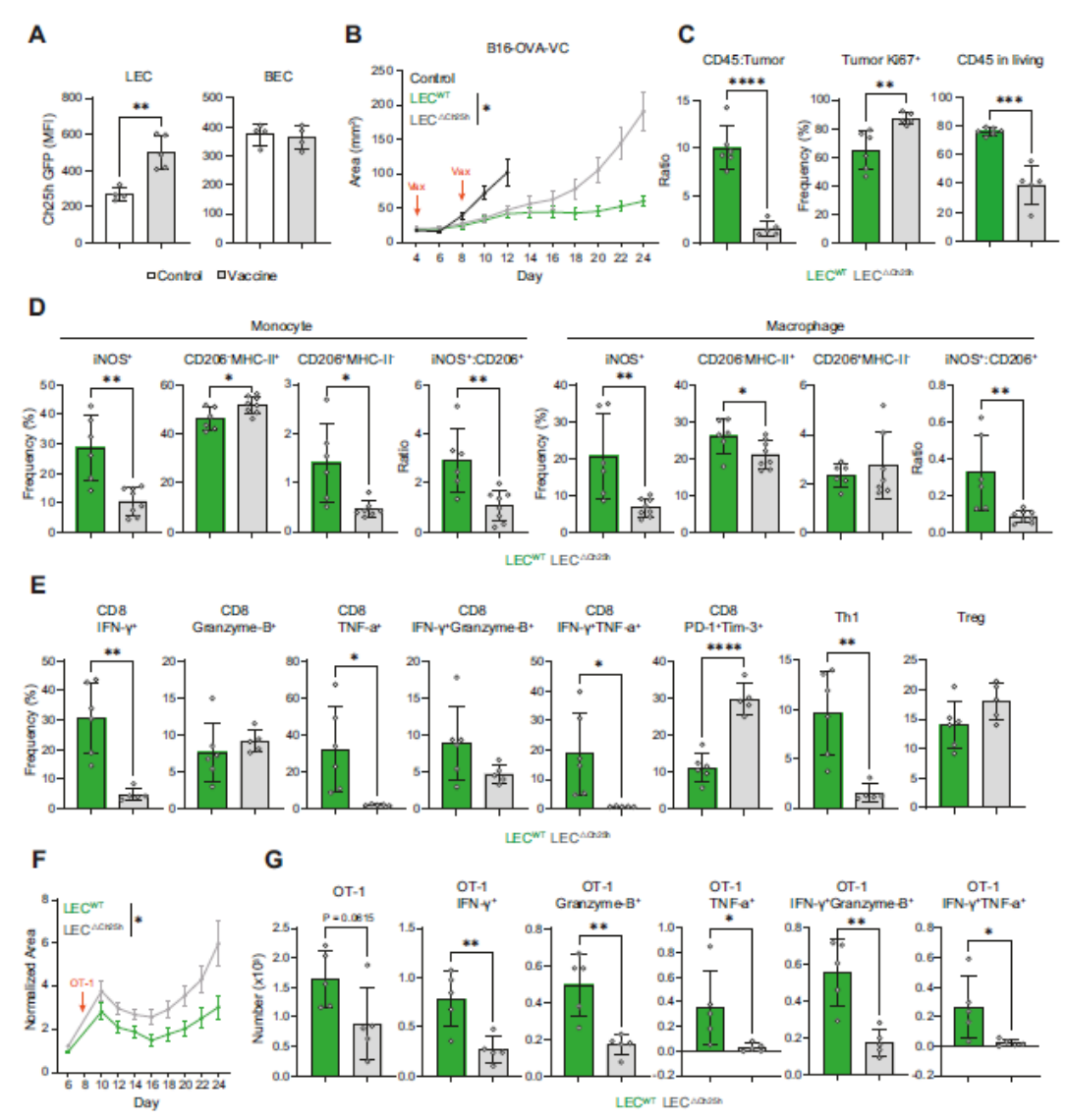
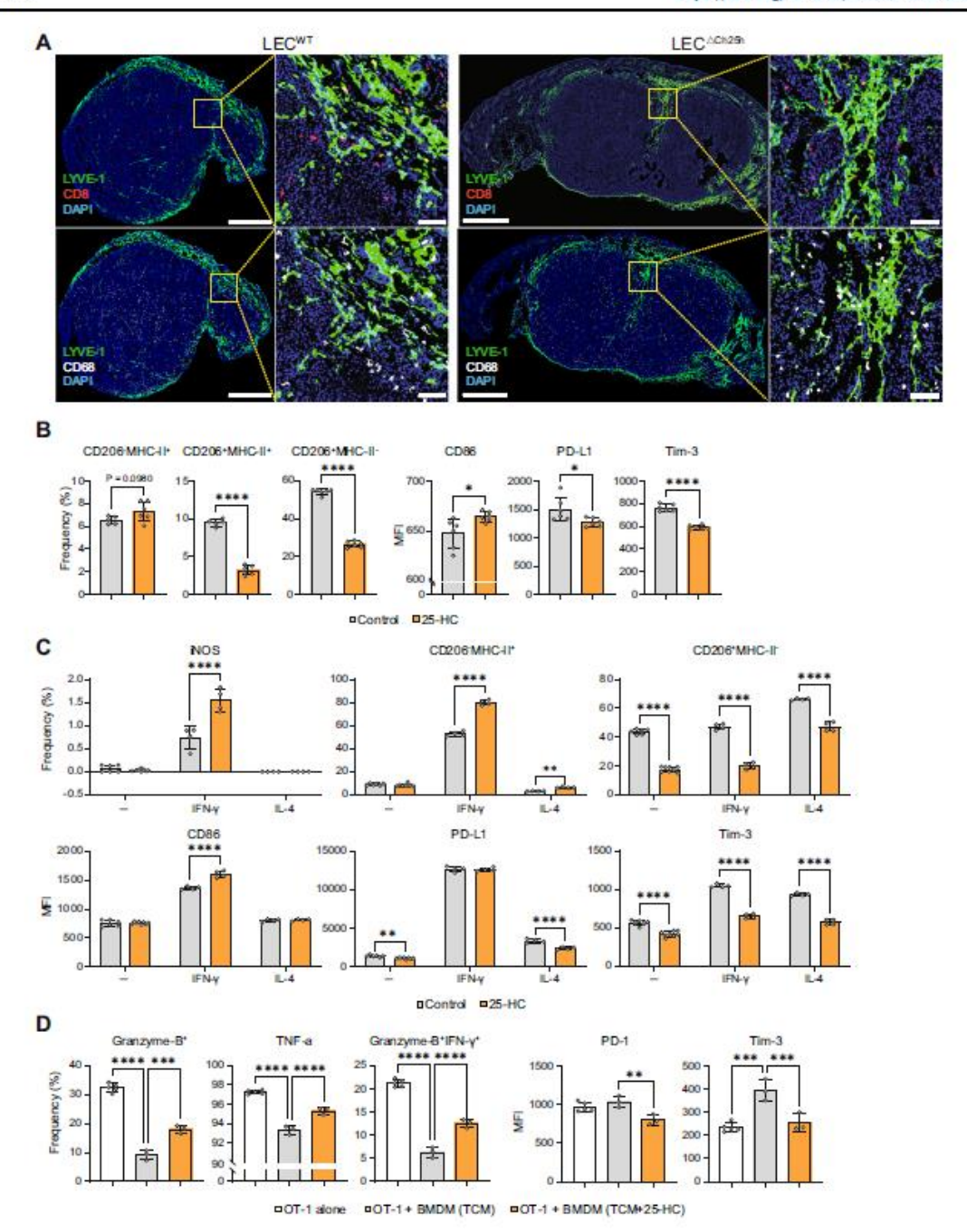


Fig. 3 | Loss of Ch25h in LECs dampens immunotherapy efficacy in lymphangiogenic melanoma. A-E LEC^{aCh25h} and LEC^{WT} mice were inoculated with B16F10-OVA VEGF-C (B16-OVA-VC) cells and vaccinated with OVA protein and CpG-B at day 5 (A) or at day 4 and day 8 (B-E). A Ch25h expression (GFP MFI) was measured by flow cytometry on day 11. n=5 mice/group. B Tumor growth was followed and compared to unvaccinated B16F10-OVA VEGF-C tumor-bearing WT mice. Representative of four independent experiments, n=5-6 mice/group each. C-E Tumor were harvested on day 24 and analyzed by flow cytometry. C CD45/tumor cell ratio and tumor cell proliferation (Ki67') and CD45' cell frequency in living cells. D Myeloid cells (CD10b'CD68') were separated into monocytes (Ly6CF4/80') and macrophages (Ly6CF4/80') and were analyzed for their

expression of indicated markers. **E** CD4' and CD8' T cells were analyzed for their expression of indicated markers. **C**-**E** Representative of two independent experiments, n=5-8 mice/group each. Data were presented as mean values \pm SD (**F**, **G**) LEC^{AD-2D} and LEC^{WT} mice were inoculated with B16F10-OVA VEGF-C cells and adoptively transferred 8 days later with OT-1 effector T cells. Tumor growth was followed and normalized to the size of WT at day 6 (**F**), and OT-1 cells were analyzed in tumors 2 days after transfer for indicated markers (**G**). Data were pooled from two independent experiments, n=2-5 mice/group each, and are presented as mean values \pm SEM (**F**) or as mean values \pm SD (**G**). **B**, **F** Two-way ANOVA, $^{\prime}P < 0$. 05. (**A**, **C**, **D**, **E**, **G**) Two-tailed unpaired rest. $^{\prime}P < 0$.05; $^{\prime}P < 0$.01; $^{\prime}P < 0$.0001.

less efficient at controlling tumor growth in LEC $^{\Delta Ch28h}$ mice compared to LEC WT controls (Fig. 3F). Already 2 days post-adoptive transfer, OT-1 cells infiltrating tumors exhibited reduced effector functions (lower numbers of IFN- γ^* , TNF- α^* , Granzyme- B^* cells) (Fig. 3G).

Altogether, our data suggest that upon vaccination or effector T cell transfer, the expression of Ch2Sh in tumor LECs induces the release of extracellular 25 HC in the TME and promotes anti-tumor activity of monocytes, macrophages, and effector T cells, resulting in a better response to immunotherapy.



25-HC alters the phenotype of tumor-associated myeloid cells in vitro

We next determined whether the expression of Ch25h by LECs in the TME has a direct effect on myeloid cells and/or T cells. Immunostaining on B16F10-OVA VEGF-C tumor sections revealed that both T cells and macrophages are positioned in proximity of LVs (Fig. 4A). Ch25h is responsible for the production of 25 HC and 7-keto-25-HC. Given that

extracellular 25-HC has been shown to impact macrophage phenotype in vitro³², whereas only an endogenous expression has been reported to alter T cell effectors^p, we first tested in vitro the impact of 25-HC on tumor-conditioned BM-derived macrophages (BMDM). Flow cytometry experiments revealed that BMDM cultures exposed to tumor-conditioned medium (TCM) mostly exhibited an M2-like phenotype, with more than 70% expressing CD206 (MHCII⁻ or MHCII) and

Fig. 4 | 25-HC treatment reverses tumor-associated macrophage immunosuppressive phenotype and functions in vitro. A LEC ALEC ALEC MIT mice were inoculated with B16F10-OVA VEGF-C cells and tumors were harvested at day 11. Montages of maximum projected 3D confocal images of representative sections (n = 3 mice/group) immunostained for lymphatic vessels (Lyve-1, green), T cells (CD8, red), myeloid cells (CD68, white), and nuclei (blue). Images were obtained using a 10x objective, including a 3x relative magnification. Selected regions of interest are indicated by dashed squares and denoted magnified areas are shownin images beside. Scale bars, 1mm, 100 µm (zoomed). B BMDMs were incubated with B16F10-OVA VEGF-C tumor-conditioned medium (TCM) and treated or not with 25-HC for 48 h. BMDM phenotype was analyzed by flow cytometry. Data were

contained very few MHCII*CD206 cells (Fig. 4B), among which iNOS* cells were undetectable in absence of further treatment (Fig. 4C). This is in line with the results obtained in Rag2^{KO} mice (Supplementary Fig. 4F), and probably due to the absence of inflammatory factors. 25-HC treatment significantly reduced the frequencies of CD206+ TCMexposed BMDM, increased their CD86 expression, and further decreased their expression levels of Tim-3 and PD-L1 (Fig. 4B), molecules that have been shown to participate in immunosuppression mediated by macrophages33,34. A modulation of TCM-exposed macrophages by 25-HC toward a less immunosuppressive phenotype as also confirmed by Q-PCR, with increased cd86, cd80, il1b, tnf, il6, il12 mRNA expression levels, and decreased myc, il10, tgfb1, mrc1, cd274, and haver2 mRNA levels (Supplementary Fig. 6A). Although it has been shown that intracellular 25-HC acts as an antagonist of SREBP in macrophages, resulting in decreased IL-1ß production, our data suggest that extracellular 25HC acts through a different mechanism and promotes IL-1β production. In agreement, similar results (upregulation of cd80, cd86, il1b, tnf, il6 and il12 expression, downregulation of mrc1, il10, and tgfb1) were observed when TCM-exposed Ch25h-/- BMDM were treated with 25-HC (Supplementary Fig. 6B).

The proportion of BMDM treated with the MI-polarizing cytokine IFN-y that differentiated into iNOS' cells, although represented at low frequency, was potentialized by the addition of 25-HC (Fig. 4C). Low iNOS+ cell frequencies might be explained by a lack of proinflammatory factors that need to synergize with IFN-y and 25-HC to promote its expression. Frequencies of MHCII+CD206 cells and the expression levels of CD86 (Fig. 4C), all hallmarks of pro-inflammatory, or immunogenic, macrophages were also enhanced, 25-HC did reduce Tim-3 expression by M1-polarized BMDM, without modulating PD-L1 levels, which directly respond to IFN-y and were very high (Fig. 4C). In contrast to IFN-y, pre-treatment of the M2-polarizing cytokine IL-4 increased the frequencies of CD206+ cells (Fig. 4C). The addition of 25-HC inhibited the polarization of immunosuppressive macrophages mediated by IL-4, with decreased CD206+, decreased PD-L1, and decreased Tim-3 (Fig. 4C). As previously shown35, IFN-y treatment induced upregulation of ch25h in BMDM (Supplementary Fig. 6C). However, Ch25h-F BMDM exhibited similar phenotypic modulation compared to WT BMDM (Fig. 4C) when exposed to polarizing cytokines IFN-y or IL-4 and treated with 25-HC (Supplementary Fig. 6D), demonstrating that endogenous Ch25h expression does not contribute to the modulation of BMDM polarization induced by extracellular 25-HC. To determine whether alterations of phenotypes translate into impaired functions of macrophages, we further assessed their ability to modulate T cell effector and exhausted phenotypes. As published36, tumor-conditioned BMDM significantly inhibited T cell effector functions (decreased frequencies of Granzyme-B⁺ and IFN-y⁺ OT-1 cells) and promoted a T cell exhausted phenotype (increased expression levels of Tim-3 and PD-1 by OT-1) (Fig. 4D). Strikingly, 25 HC pre-treatment of TCM-exposed BMDM significantly dampened their ability to inhibit effector T cells (Fig. 4D), which exhibited restored production of effector factors, and decreased expression of exhaustion markers, suggesting that in vivo, 25-HC might dampen the immunosuppressive functions of tumor-associated macrophages.

Although it remained elevated compared to 25-HC levels, 7-keto-25-HC was also reduced in the TME of LEC $^{\Delta \text{Ch2Sh}}$ mice (Supplementary Fig. 2J). Therefore, we tested whether it could impact macrophage phenotype and functions. 7-keto-25-HC treatment induced minor modulations of BMDM phenotype (Supplementary Fig. 6E), however, it did not affect their ability to suppress effector T cells (Supplementary Fig. 6F). Altogether, these data suggest that 25-HC produced by LECs in the TME is a main regulator of tumor-associated myeloid cells.

LEC-derived 25-HC controls tumor growth by regulating myeloid cell functions

To determine whether myeloid cells are the primary cellular targets of LEC-derived 25-HC in vivo in tumors, and subsequently impact antitumor T cell responses, we depleted myeloid cells by injecting anti-CSFIR (CD115) antibodies37 into B16F10-OVA VEGF-C tumor-bearing LEC^{△Ch25h} and LEC^{WT} mice vaccinated as before. This treatment resulted in the depletion of 73% of macrophages and 25% of monocytes in LECWT tumors and 65% of macrophages and 51% of monocytes in LEC COLOSIN tumors (Supplementary Fig. 7A) and was sufficient to abrogate the difference in tumor size between LEC\(^{\text{Ch2Sh}}\) and LEC\(^{\text{WT}}\) mice (Fig. 5A). Upon myeloid cell depletion, vaccinated LECWT mice could not control the growth of tumors as efficiently (Fig. 5A). This suggests that in vaccinated LECWT mice, the net-effect of antibody-mediated cell depletion in tumors resulted in the elimination of anti-tumoral proinflammatory monocytes and macrophages. The TME of LECWT unvaccinated mice contains a balanced mix of pro- and anti-tumoral myeloid cells (Fig. 2D). As such, anti-CSF1R (CD115) antibody treatment in unvaccinated WT mice did not impact tumor growth (Supplementary Fig. 7B), suggesting that the net-effect of myeloid cell depletion was zero, with the depletion of both immunogenic and immunosuppressive myeloid cells. Next, we have used a reductionist approach to assess directly if the impact of LEC-derived 25-HC on tumor myeloid cells is indeed responsible for controlling tumor growth, by excluding the contribution from other immune cells in the TME. Immunodeficient (NSG) mice in which LECs express (NSG-LECWT) or not (NSG-25h) Ch25h were transplanted with B16F10-OVA VEGF-C tumor cells mixed with BMDM or not. Tumor-bearing mice were next adoptively transferred with OT-1 effectors. NSG-LECWT and NSG-LEC△C mice transplanted with tumor cells alone and transferred with T cells exhibited an efficient and similar tumor growth regression, confirming that 25-HC released by LECs in the TME does not directly impact the ability of effector T cells to control tumor growth (Fig. 5B). In contrast, when co-transplanted with tumor cells and BMDM, compared to NSG-LECWT mice, NSG-LEC△Ch2Sh mice developed larger tumors (Fig. 5B).

These results, combined with our in vitro data (Fig. 4), demonstrate that myeloid cells represent the targets of 25-HC produced by LECs in the TME, resulting in a dampening of their immunosuppressive functions.

25-HC produced by LECs prevents the acquisition of an immunosuppressive phenotype by tumor-associated myeloid cells Transcriptomic analysis of monocytes (CD11b*Ly6C*F4/80^{eqs}) and macrophages (CD11b*Ly6C**§F4/80*) sorted from B16F10-OVA VEGF-C

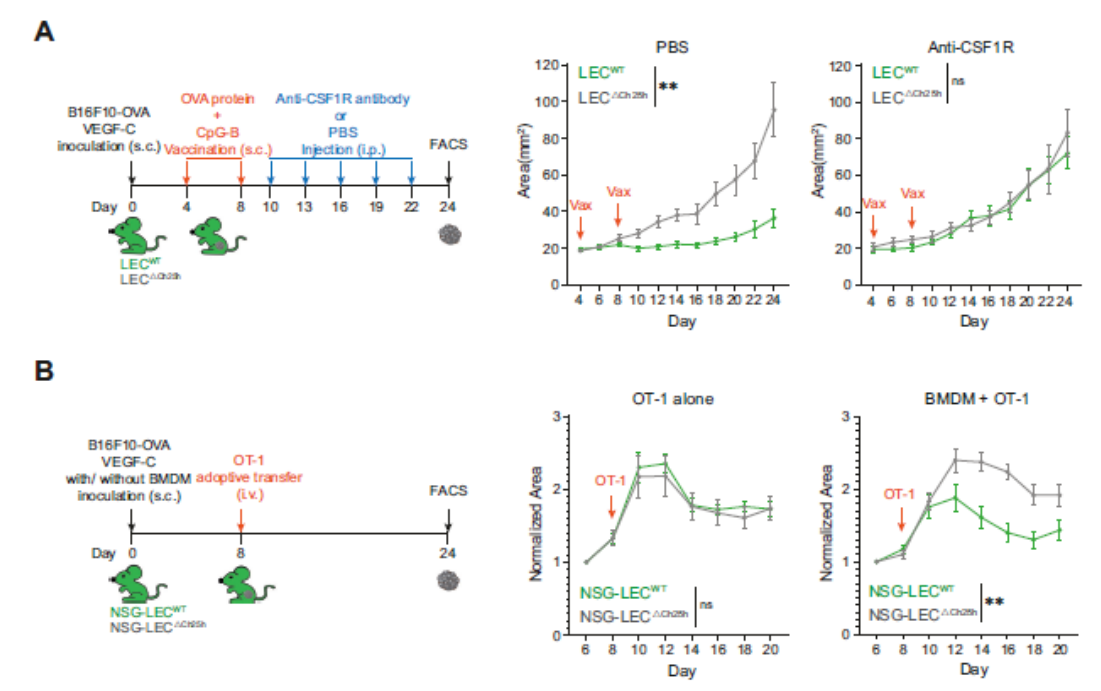
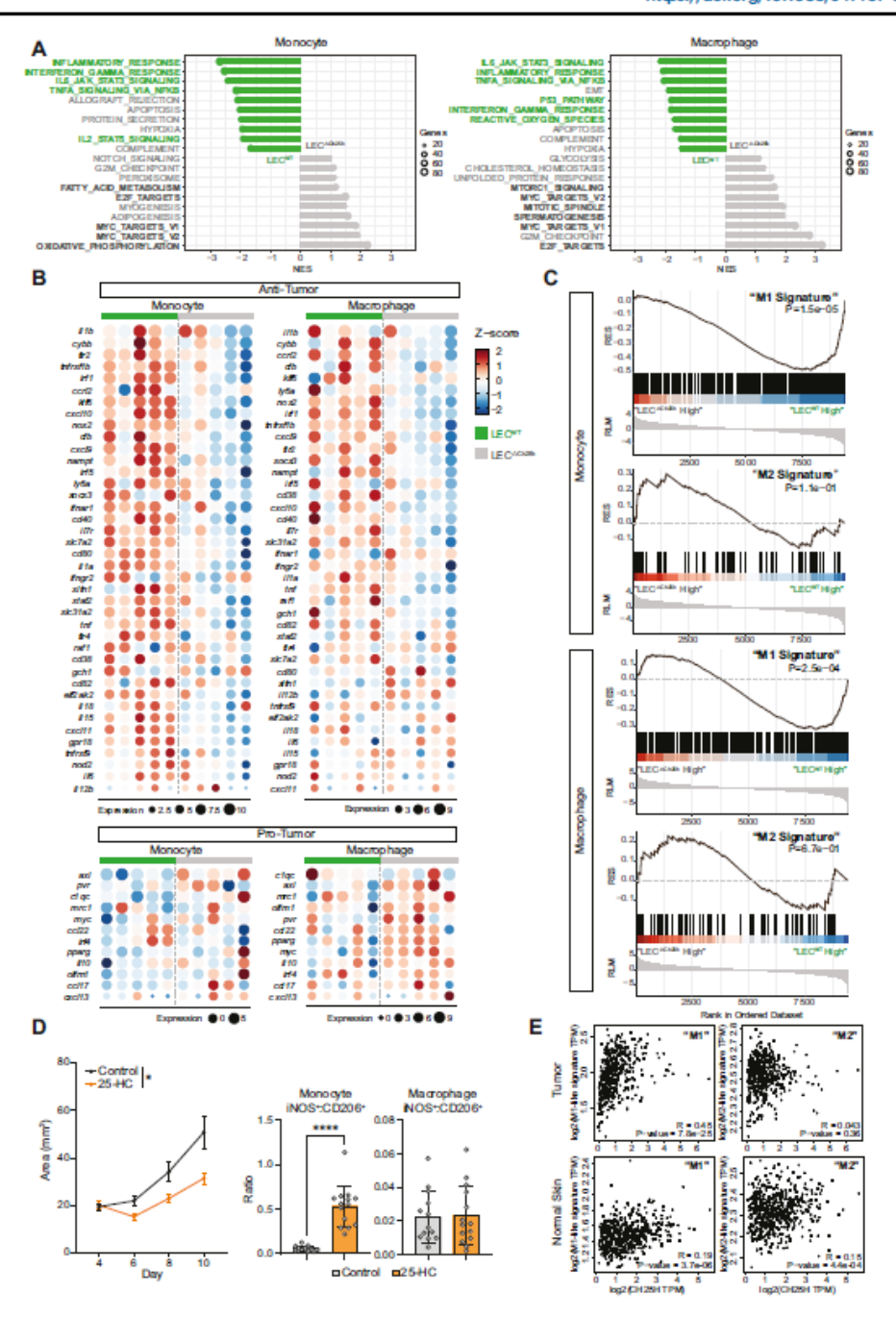


Fig. 5 | LEC-derived 25-HC modulates tumor growth by impacting tumorassociated macrophages and monocytes. A LEC* $^{ACh.Zh}$ and LEC* WT mice were inoculated with B16F10-OVA VEGF-C cells and vaccinated with OVA protein and CpG-B at day 4 and day 8. Mice were additionally injected with anti-CSF1R (1 mg / mouse at day 10, followed by $500\,\mu\text{g}$ /mouse every 3 days or PBS), as represented in the scheme. Tumor growth was followed. Two-way ANOVA, ** ** P-C 0,01. Data were representative of two independent experiments with n = 5-7 mice/group each.

B NSG-LEC ACRESS and NSG-LEC TIME were inoculated with B16F10-OVA VEGF-C cells mixed or not with BMDM. Tumor-bearing mice were further adoptively transferred with OT-1 effectors on day 8, as represented in the scheme. Tumor growth was followed and normalized to the size individually from day 6. Two-way ANOVA, **P < 0.01. Data were pooled from two independent experiments with n = 5-8 mice/group each. A, B Data were presented as mean values ± SEM.

tumors after OVA+CpG-B vaccination revealed that their phenotype was strongly altered by the absence of Ch25h expression in LECs. First, most of the top ten Hallmark pathways expressed by monocytes in LECWT tumors were related to inflammation, such as inflammatory responses, IFN-γ response, IL-6/Jak/STAT3 signaling, TNF-α signaling via NF-KB and IL-2/STATS signaling (Fig. 6A). Similarly in tumor-infiltrating macrophages from LEC^{WT} mice, the top ten Hallmark pathways were related to inflammation and MI-like TAM signature, such as IL-6/Jak/STAT3 signaling, inflammatory response, TNF-α signaling via NF-KB, IFN-y response, ROS pathway, P53 pathway (Fig. 6A). In contrast, the 10 top pathways expressed by LEC∆C tumor macrophages contained E2F targets that promote tumor cell metastasis39, Myc-targets that mediate early glycolysis and dampen proinflammatory responses in macrophages by inhibiting IRF440, mTORC1 signaling that regulates proinflammatory macrophage function and metabolism 41,42, mitotic spindles, which seem to be a mutually exclusive events of NLRP3 activation43, and spermatogenesis, a pathway containing known TAM receptors, such as Tyro3, Axl and MerTK, promoting M2 polarization and efferocytosis, two pro-tumoral processes⁴⁴⁻⁴⁷ (Fig. 6A). Interestingly, whereas in macrophages pathways related to metabolism were particularly expressed in LEC $^{\Delta G}$ tumors (normalized enrichment score of 1.3 and 1.3 for cholesterol homeostasis and glycolysis, respectively), oxidative phosphorylation was the highest pathway upregulated in monocytes in LEC△Ch28h tumors (Fig. 6A). The fatty acid oxidation pathway was also upregulated in monocytes from LEC LUCAN tumors (Fig. 6A), Knowing that M2like myeloid cells undergo a metabolic reprogramming toward oxidative metabolism for bioenergetic purposes (OXPHOS)42,48, and that

mitochondrial fatty acid oxidation has been associated with an immunosuppressive myeloid cell phenotype49, it is tempting to speculate that the modulation of the "M2-like" phenotype by LEC-derived 25-HC might reprogram pro-resolving and pro-tumoral cells into more inflammatory anti-tumoral myeloid cells. Accordingly, by looking more precisely at the heatmaps generated with genes classified as "anti-tumor", monocytes and macrophages present in tumors isolated from LECWT mice expressed a far more anti-tumor immune signature compared to LEC^{△ChgSh} mice (Fig. 6B), with higher gene expression such as #1b, cxcl9, cxcl10, nos2, and others. Other pro-inflammatory genes were also more expressed in monocytes and macrophages in LECWT compared to LEC^{\(\triangle \)} tumors, such as, for example, *nlrp3* or (Supplementary Fig. 8A), although their role in tumor context remains unclear. In contrast, monocytes and macrophages in tumors from LEC^{△Ch25h} mice upregulated genes clearly related to pro-tumoral immune functions, such as Axl, Il10, and pparg (Fig. 6B), with a more pronounced effect in macrophages compared to monocytes. Finally, monocytes and macrophages in LECWT tumors exhibited enrichment in genes described as "M1" signature by Pan W. et al., whereas monocytes and macrophages in LEC^{\triangle Chash} tumors showed an association with the "M2" signature 50 (Fig. 6C). No clear difference was observed in genes implicated in other myeloid cell functions, such as phagocytosis, or SERBP targets, between monocytes and macrophages isolated from LECWT and LEC△Ch25h tumors (Supplementary Fig. 8B). In order to determine whether 25-HC could be considered as a therapy to redirect the myeloid cells in vivo, we treated B16F10-OVA VEGF-C tumor-bearing mice intratumorally with 25-HC. We observed a better control of tumor growth in treated



animals compared to untreated controls (Fig. 6D). In addition, a shift toward more pro-inflammatory tumor-infiltrating myeloid cells was observed, as indicated by an increased ratio of iNOS $^{\prime}$ CD206 $^{\circ}$ monocytes (Fig. 6D). We did not observe a significant change in macrophages, for which the ratio was very low.

Supporting a role for 25-HC in promoting anti-tumor macrophages in melanoma patients, we found that Ch25h showed a significant positive correlation with an MI-like macrophage signature but no clear correlation with M2-like macrophage signature in the skin cutaneous melanoma (SKCM) TCGA dataset (Fig. 6E). In addition, although correlation of Ch25h with M2-signature was weak in both normal skin and tumor melanoma (R = 0.15 and R = 0.043, respectively), the correlation of Ch25h with MI-signature was much stronger in melanoma (R = 0.45) compared to normal skin (R = 0.19) (Fig. 6E),

Fig. 6 | Altered monocyte and macrophage transcriptomes in the absence of Ch25h expression by LECs in lymphangiogenic melanoma. A - C LECACASTA and LECWT mice were inoculated with B16F10-OVA VEGF-C cells and vaccinated with OVA protein and CpG-B on day 4 and day 8. Tumors were harvested on day 24, and monocytes and macrophages were sorted by flow cytometry (see Fig. 2D for gating strategy). RNA sequencing was performed (Illumina). A Top 10 Hallmark pathways expressed in monocytes and macrophages in tumors from LECACASTA and LECWT mice. B Heatmap showing expression levels of genes implicated in "anti-tumor" or "pro-tumor" immune signatures in monocytes and macrophages and in tumors from LECACASTA and LECWT mice. C GSEA enrichment of M1 and M2 signatures in

monocytes and macrophages from tumor in LEC^{ACDSh} and LEC^{WT} mice using gene set from ref. 50. D B16F10-OVA VEGF-C tumor-bearing CS7BL/6 mice were treated with 25-HC every 2 days, starting at day 4. Tumor growth was followed. Two-way ANOVA, "P < 0.05. Data were a pool of three independent experiments with n = 4-6 mice/group each. On day 11, tumors were harvested, and the CD68°CD11b' myeloid cell (macrophage, F4/80'Ly6C' and monocytes, F4/80'Ly6C') phenotype was assessed by flow cytometry. Ratio iNOS'/CD206' cells are provided. Two-tailed unpaired t-test, "t-P < 0.001. E Correlation between Ch25h expression and MI/M2 signatures in normal skin and in SKCM patients. Data were extracted from the TCGA database.

indicating that Ch25h is not generally associated with MI macrophages but rather only in tumoral or tumor-associated context.

LEC-derived 25-HC decreases PPAR-y levels in tumor-associated macrophages to dampen their immunosuppressive functions

25-HC has been shown to mediate both LXR-dependent and -independent effects⁵¹. Therefore, we investigated whether this pathway is implicated in the ability of extracellular 25-HC to modulate macrophage phenotype and functions. In vitro, LXR deficient and WT BMDM pre-exposed to TCM and treated with 25-HC exhibited similar regulation of their phenotype, with decreased CD206*MHCII* frequencies and decreased Tim-3 expression levels (Supplementary Fig. 9A) indicating that the impact of 25-HC on macrophages in tumoral context is LXR independent. In vivo, when co-inoculated with B16F10-OVA VEGF-C tumor cells into NSG mice, LXR deficient BMDM supported the control of tumor growth mediated by the transfer of OT-1 effectors as efficiently as WT BMDM (Supplementary Fig. 9B), confirming that 25-HC present in the TME promotes the ability of macrophages to control tumor growth independently of LXR.

Macrophages strongly upregulated PPAR-y in B16F10-OVA VEGF-C tumors from LEC^{△C10:Sh} mice (Fig. 6B), which is well-known to exert an anti-inflammatory effect on macrophages by inhibiting AP-1/ NF-KB/ STAT1 pathways, COX-2, MPO, Caspase 3, and ROS production, and in contrast promoting OXPHOS and the production of anti-inflammatory cytokines 42,52. All these pathways being also modulated in myeloid cells infiltrating tumors from LEC\(\triangle C \triangle D HC having been shown to decrease PPAR-y levels in vitro in THP-1 macrophages53, we wondered whether this pathway could be implicated in the ability of 25-HC to prevent macrophage immunosuppressive phenotype and function. Accordingly, TCM-exposed BMDM treated with 25-HC downregulated PPAR-y mRNA (Fig. 7A). As shown before, the addition of 25-HC inhibited the "M2-like" phenotype of TCM-exposed BMDM, inducing downregulation of CD206 (MHCII⁺ or MHCII') and Tim-3 (Fig. 4B). Supporting the hypothesis of an implication for PPAR-y, treatment with the PPAR-y antagonist T0070907 had a similar effect (Supplementary Fig. 9C). In addition, BMDM treated with the PPAR-y agonist Troglitazone significantly inhibited 25-HC ability to prevent the induction of "M2-like" BMDM by the TCM (Fig. 7B), establishing a direct link between the mode of action of 25-HC and PPAR-y in TCM-exposed macrophages. More importantly, TCMexposed, 25-HC treated, BMDM pretreated with Troglitazone maintained their ability to inhibit effector T cell functions and to promote T cell exhaustion when incubated with 25-HC (Fig. 7C). In vivo. LECWT mice transplanted with B16F10-OVA VEGF-C tumor cells mixed with WT BMDM controlled significantly better the growth of tumors upon OVA+CpG-B vaccination compared to LEC^{\(\Delta\)} mice (Fig. 7D). In contrast, both LEC^{\(\mathbb{MT}\)} and LEC^{\(\Delta\)} mice efficiently controlled tumor growth after vaccination when tumor cells were mixed with PPAR-y deficient macrophages (Fig. 7D), indicating that the lack of LECderived 25-HC can be compensated by the absence of PPAR-y expression by tumor-associated myeloid cells.

Altogether, these experiments demonstrate that 25-HC produced by LECs in B16F10-OVA VEGF-C tumors prevents the induction of immunosuppressive functions in macrophages by the TME by inhibiting their expression of PPAR-y, consequently allowing effector T cells to maintain their effector phenotype in tumors and to provide better control of tumor growth.

Discussion

During tumor development, malignant cells take advantage of multiple mechanisms to evade immune-mediated recognition and killing his why approaches aiming at reinvigorating anti-tumor immunity currently represent the most promising treatment against cancer. The link between tumor-associated lymphangiogenesis and cancer cell spreading, and metastasis is well-established. However, the growth and the remodeling of LVs at the primary tumor, draining LNs and distant premetastatic niches, has been shown to not only support metastasis but also impact anti-tumor immunity complex interactions between tumor cells, immune cells, and stromal cells make it hard to precisely decipher the contribution of LECs in shaping immune cell phenotype and functions in tumors. In addition, the plasticity of LECs and their response to molecular cues from the TME are still unclear.

Here we show that in comparison to LECs in steady-state skin or LNs, LECs in murine lymphangiogenic melanoma upregulate the oxysterol-producing enzyme Ch25h, which has been shown to play important roles in regulating lipid metabolism, gene expression, and immune activation. We further translated our findings to human tumors, showing that VEGF-Chiệth human melanoma cells promote LV expansion in immune-compromised mice, and induce the upregulation of Ch25h in the TME compared to skin LECs, suggesting that LECs in tumors from melanoma patients will likely upregulate Ch25h and produce 25-HC in the TME. In agreement, LECs express Ch25h mRNA in melanoma tumors.

Specific genetic abrogation of Ch25h in murine LECs demonstrates that in lymphangiogenic melanoma, LECs significantly contribute to the levels of extracellular 25-HC, the main product of the enzyme, which is beneficial for the control of tumor growth, by promoting anti-tumor immunity and response to immunotherapy. We further showed an impaired control of tumor growth of poorly lymphangiogenic tumors, and of different cancer types, in mice in which Ch25h was abrogated in LECs, indicating that beneficial Ch25h expression by LECs is not restricted to melanoma or to VEGF-C overexpressing tumors. The role of oxysterols in tumor settings is controversial. Some oxysterols (22-HC and 24-HC) can recruit pro-tumoral CXCR2⁺ neutrophils, promoting an immunosuppressive TME⁵⁵, Intracellular cholesterol and derivatives, including exysterols, are directly sensed by LXRa/B nuclear receptors, leading to the transcription of genes implicated in reverse cholesterol transport. LXRs activation correlates with the generation of anti-inflammatory macrophages and DCs56,57. In contrast, therapeutic GW3965 agonist-mediated LXR activation has been shown to promote anti-tumoral immune response, decreasing MDSC numbers while enhancing the activation of CTLs in both murine models and in cancer patients88. However, we do not foresee LXRs activation as a pathway being involved in the ability of LEC-derived 25-HC to promote anti-tumor immunity. Indeed, LXRs sense intracellular cholesterol derivatives, whereas we show that tumor LECs do not exhibit any significant transcriptomic changes in the absence of Ch25h expression. In agreement, our in vitro and in vivo

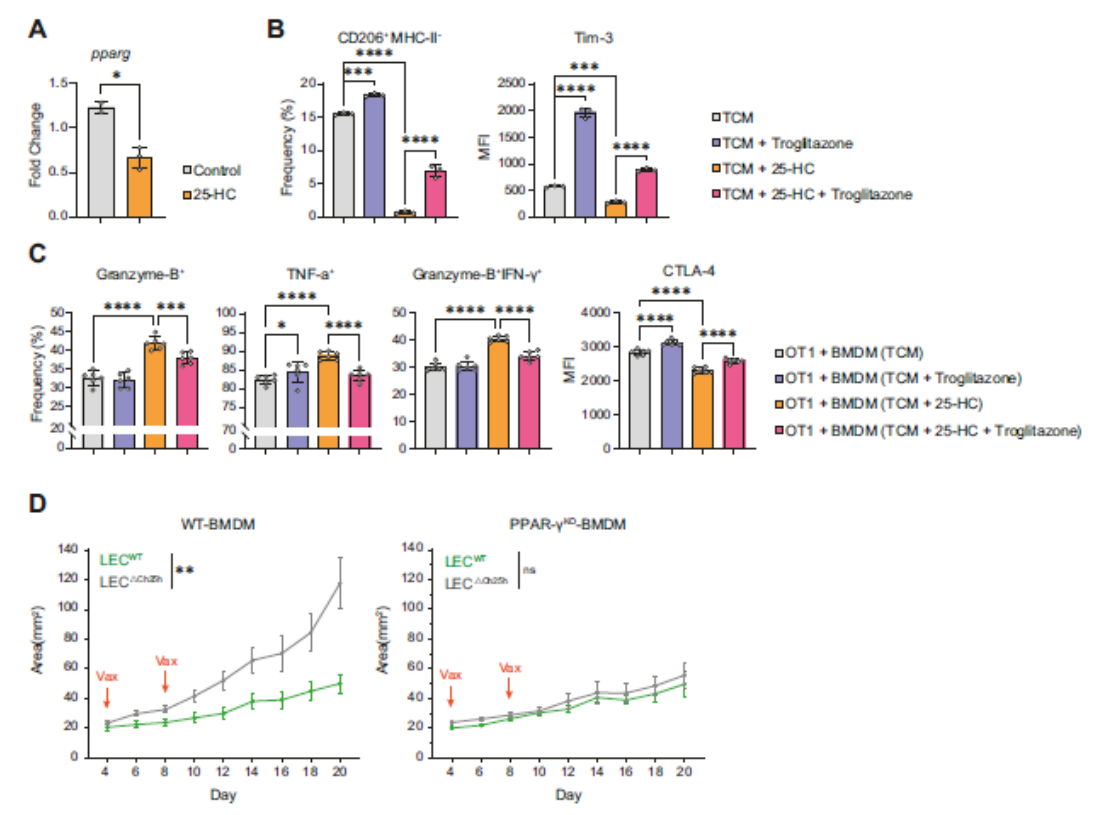


Fig. 7 | LEC-derived 25-HC dampens the Immunosuppressive functions of tumor-associated macrophages by inhibiting PPAR-γ expression. A BMDM were incubated with Bi 6F10-OVA VEGF-C tumor-conditioned medium (TCM), treated or not with 25-HC for 48 h, and analyzed by Q-PCR for PPAR-γ mRNA levels. Data were representative of two experiments with n = 2-3 replicates each. Data were presented as mean values ± 5D. Two-tailed unpaired rtest. *P < 0.05.

B BMDMs were incubated with tumor-conditioned medium (TCM), treated or not with 25-HC, Troglitazone, or the combination of 25-HC and Troglitazone for 48 h. BMDM phenotype was analyzed by flow cytometry. Data were representative of two independent experiments with n = 3 replicates each. Data were presented as mean values ± 5D. One-way ANOVA. **P < 0.001; ****P < 0.0001. C TCM-exposed BMDM

were treated or not with 25-HC, Troglitazone, or the combination of 25-HC and Troglitazone for 48 h, washed, and incubated with OT-1 effector cells for 48 h. T-cell phenotype was analyzed by flow cytometry. Data were representative of two independent experiments with n=6 replicates each. Data were presented as mean values \pm 5D. One-way ANOVA. * $^{*}P < 0.05$; * $^{*}P < 0.001$; * $^{*}P < 0.0001$. D LEC * $^{*}D$ and LEC * $^{*}T$ mice were inoculated with B16F10-OVA VEGF-C cells mixed with either WT or PPAR- $^{*}Y$ deficient (IP AR- $^{*}Y$) BMDM and vaccinated with OVA protein and CpG-B on day 4 and day 8. Tumor growth was followed. Data are presented as mean values \pm 5EM. Two-way ANOVA, * $^{*}P < 0.01$. Data were representative of two independent experiments with n=4-5 mice/group each.

data show that 25-HC in the TME enhances the ability of macrophages to control tumor growth independently of the LXR pathway.

Whereas Ch25h has been described to be expressed by CTL and DCs in mouse tumors, including B16F10 melanoma 18,46, we could not detect it in lymphangiogenic B16F10-OVA VEGF-C tumors. This could be explained by the fact that the production of tumor-derived factors 18,46, which seem to inhibit Ch25h expression in both CTLs and DCs, might be increased in our model. Although we detected high levels of Ch25h expression in tumor-associated macrophages, it is likely that they do not dominantly contribute to extracellular 25HC levels, as, at least in vitro, they do not release 25-HC in the extracellular medium, whereas LECs and BECs can do so. Although we did not decipher the mechanisms, it is likely that ECs exhibit particular features, which are not shared by macrophages, involved in the ability to secrete 25-HC. In addition, Ch25h abrogation in LECs leads to a significant decrease in extra cellular 25-HC levels in tumors. It was recently shown that 25-HC produced by macrophages promotes their immunosuppressive phenotype in mouse colorectal cancer99. Although this seems to be in contradiction with our data, it is possible that

extracellular and intracellular 25-HC differentially impact tumorassociated macrophage (TAM) phenotype and function. In their study, in vitro treatment of macrophages with 25-HC surprisingly promotes their immunosuppression. However, macrophages were pretreated with 25-HC before being exposed to IL-4 and IL-13, which might affect the data. It is however difficult to explain why the authors observed a better control of tumor growth in mice fully deficient for Ch25h, and why they reported a negative impact of high Ch25h expression in human colorectal cancer on prognosis, as we and others show the opposite ¹⁵⁻¹⁷.

We observed that Ch25h is also expressed by tumor BECs, likely, as previously described, dampening their expansion and subsequent angiogenesis, and inhibiting metastasis¹⁵. However, as LECs seem to significantly contribute to extracellular 25-HC levels in lymphangiogenic melanoma, our data argue for an intracellular role of Ch25h expression and 25-HC in BECs in regulating the tumor-associated blood vasculature, whereas LEC-derived 25-HC certainly exerts extracellular functions. It was shown that in tumor-associated BECs, intracellular 25-HC prevents their uptake of TEVs, leading to their activation

and enhancing their ability to promote metastasis¹⁵. However, it is unlikely that this process occurs in tumor LECs, as the transcriptome of Ch2Sh deficient LECs exhibits high similarity with control LECs.

Our data show that in the absence of 25-HC production by LECs in tumors, infiltrating monocytes and macrophages adopt a completely different phenotype, with profound transcriptomic alterations, including a dampening of pro-inflammatory gene signature and an upregulation of genes implicated in immunosuppression. These modulations result from an unbalance of pathways that are important for myeloid cell functions, with impaired inflammatory response, TNFα and IFN-y response, or ROS production, and in contrast enhanced immun oregulation, M2-like responses, oxidative metabolism, and fatty acid oxidation. Interestingly, among the genes that are downregulated in monocytes and macrophages when 25-HC production by LECs has been abrogated, we identified IL-1B. This can be surprising, since 25 HC has been shown to downregulate IL-1β in macrophages12. The study indicates that intracellular 25-HC acts as an antagonist of SREBP in the cytoplasm of macrophages, and therefore dampens their production of IL-1B. However, our data show that 25-HC is produced by LECs extracellularly in the TME and promotes anti-tumoral macrophages and monocytes, including upregulation of IL-1\beta. The role of IL-1\beta in tumors is controversial. It has been described as a protumoral factor in most cancers 60-63, promoting M2-like macrophages and pro-tumoral neutrophil recruitment. However, and supporting our data indicating that 25-HC exposed macrophages promote anti-tumor effector T cell functions, it has been shown that IL-1β enhanced the ability of tumorspecific T cells to eradicate established B16 melanoma64. In the breast cancer model as well, IL-1β promotes the infiltration of anti-tumor immune cells and controls primary tumor growth65.

We further demonstrate that tumor-infiltrating myeloid cells are the primary targets of LEC-derived 25-HC. Indeed, myeloid cell depletion abolished the impact on effector T cell responses observed in the absence of Ch25h expression by LECs, indicating that T cells are not directly impacted by 25-HC released by LECs in the TME. A study has described that IL-27-induced Ch25h in CD4* T cells acts as an immunoregulatory enzyme, through the production of 25-HC, interfering with cholesterol metabolism and leading to bystander CD4* T cell inhibition. However, in the TME of the different models used, we could not detect Ch25h expression in T cells, suggesting that this pathway is not involved.

We provide additional in vitro and in vivo evidence that 25-HC can inhibit CD206+ immunosuppressive monocytes and macrophages. However, this effect is not sufficient to induce pro-inflammatory iNOS+ myeloid cells. In vitro, iNOS induction in macrophages requires proinflammatory polarizing cytokines (IFN-y) and is potentiated by the addition of 25-HC. In vivo, iNOS expression by tumor macrophages and monocytes also requires T-cell derived cytokines (likely IFN-y as well), as demonstrated by an almost total absence of iNOS+ myeloid cells in tumors in Rag2KO mice, and is further potentialized by LEC-derived 25-HC. Therefore, 25-HC produced by LECs in the TME dampens myeloid cell immunosuppressive properties and further synergizes with other factors to promote pro-inflammatory myeloid cells and support antitumor effector T cells. These effects are amplified when the immunogenicity of the TME is boosted through immunotherapy protocols, such as vaccination or adoptive T cell transfer, and correlate with enhanced Ch25h expression by LECs in the TME. Our findings are in line with a study showing a role for 25-HC acting as an amplifier of inflammatory signaling in macrophages in the context of viral infection13. Although the molecular mechanism promoting the upregulation of Ch25h by LECs was not deciphered here, our data argue for a primary role of non-immune cells, either tumor cells themselves or stromal cells, and show that it is further promoted by vaccine-induced inflammation. Therefore, protocols aiming at strengthening tumorspecific immunity might boost the production of 25HC by LECs in tumors and function as a loop to further enhance anti-tumor immunity. Accordingly, we observed that melanoma patients with high Ch25h expression exhibit better survival and improved response to immunotherapy. This suggests that Ch25h expression might be a prognostic biomarker in melanoma patients and their response to immunotherapy. Further reinforcing the translational aspects of our findings, intratumoral injection of 25-HC redirects myeloid cells toward a less immunosuppressive phenotype, allowing a better control of tumor growth. However, the hydrophobic features of 25-HC may limit its direct use as a therapeutical compound.

Among the mRNA transcripts differentially regulated in macrophages and monocytes in the absence of ch25h expression by LECs, one particularly caught our attention, pparg. PPAR-y belongs to the family of Peroxisome proliferator-activated receptors (PPARs), which are ligand-regulated transcription factors influencing several cellular pathways52. It has been known for decades that PPAR-v agonists suppress the production of inflammatory cytokines by monocytes in vitro⁶⁷. Furthermore, PPAR-y activation has been shown to modulate macrophage polarization in vitro, by suppressing their immunogenic state with downregulation of nos2, tnf, il6, il1b, and mcp168 while promoting their expression of immunosuppressive markers such as il10, arg1, mrc1, and others69. In lymphangiogenic melanoma, we observed that both monocytes and macrophages upregulate ppag when LECs do not express Ch25h, likely promoting their immunosuppressive phenotype. In vitro, pparg is downmodulated by 25-HC in macrophages, supporting a direct implication of this pathway in controlling their immunoregulatory functions in tumors. The pathway is also implicated in vivo, with a restored control of B16F10-OVA VEGF-C tumor growth in LEC∆C125h mice vaccinated with OVA+CpG-B when macrophages do not express PPAR-y. Altogether, our data argue for a key role of LEC-derived extracellular 25-HC in dampening PPAR-v expression and the immunosuppressive phenotype of monocytes and macrophages in the TME.

Because tumor LEC exhibits timely-related pro- and antitumorigenic effects, it is becoming clearer that it will be very difficult to target the whole lymphatic vasculature in tumors as a therapeutic approach. On the one hand, we and others have shown that LECs in primary tumors and in TdLNs can specifically inhibit tumorspecific T cells by functioning as MHCI and MHCII-restricted antigenpresenting cells to induce CD8+T cell deletion and Treg generation, respectively^{67,19}. As such, it appears relevant to delete them, either through depleting antibodies or AAVs87071, or through immunotherapeutic approaches, such as their antigen-specific killing mediated by high-density tumor-infiltrating CTLs72. However, tumor LVs are needed for the drainage of tumor antigens and the migration of DCs to the TdLNs, and, therefore, are essential in the initiation of anti-tumor adaptive immunity⁷³⁻⁷⁵. In addition, tumoral LVs increase the overall recruitment of immune cells in tumors8 and are therefore beneficial for immunotherapy protocols that either boost or reinvigorate immune cells8-10. Therefore, the targeting of specific LEC functions, and not of the whole lymphatic vasculature, seems more pertinent, especially if it can be achieved through established immunotherapeutic protocols. Here we show that Ch25h upregulation by LECs in murine melanoma leads to the production of 25-HC in the TME and inhibits PPAR-y in myeloid cells, allowing their conversion into pro-immunogenic cells that support T cell effector functions and prevent their exhaustion. Interestingly, this mechanism is amplified upon vaccination with a tumor antigen or after the adoptive transfer of anti-tumor effector T cells, with increased Ch25h expression in tumor LECs, increased pro-immunogenic myeloid cell generation, improved anti-tumor effector T cell responses and better control of tumor growth. Hence, besides their purpose of promoting anti-tumor immunity, immunotherapy protocols can further act on multiple LEC immunomodulatory facets, by favoring either their immunosuppressive6.7, or their immunogenic functions, such as the upregulation of Ch25h. Altogether, these studies revealed the

incredible complexity of LEC-mediated immunomodulation, and indicate that the immunogenicity of the TME, which also depends on the course of tumor growth, greatly influences LEC phenotype and functions.

In our study, 25-HC produced by LECs in the TME has a beneficial effect on murine melanoma growth and response to immunotherapy, revealing an important role of extracellular oxysterols in preventing the polarization of tumor-associated monocytes and macrophages into immunosuppressive cells by inhibiting PPAR-y. Therefore, an angle of attack, in combination with immunotherapy, would be to provide sufficient levels of tumoral extracellular 25-HC or to locally inhibit PPAR-y.

Methods

Mice

C57BL/6N wild-type (WT) mice (Mus musculus, mixed sexes, 7-12 weeks old) were purchased from Charles River. Ch25h-eGFP^{f/f} mice were generated by Cyagen as published20. Briefly, a constitutive Knock-In (KI) with conditional knockout (KO), using a floxed-reporter Ch25h knock-in, with eGFP was used as a reporter protein fused to the 3' end of Ch25h. The entire gene was further flanked with LoxP sites, avoiding promoter disruption. Linker-eGFP reporter was inserted in the targeting cassette and is thus not expressed as a fusion protein before cre-recombination. To generate mice selectively lacking Ch25h in lymphatic endothelial cells (LEC\(\triangle \text{Ch28h}\), Ch25h-eGFP^{0/0} mice were crossed with Prox1-CreERT2 mice23. Ch25h-eGFPfff mice were used as controls (LECWT). For some experiments, LEC△Ch28h and LECWT mice were crossed on NSG or Rag2ko mice (both obtained from Charles River). EBi2KO mice were obtained from Prof. C. Pot. OVA257-264-specific TCR transgenic OT-1 CD45.1 mice, CD45.1(Lv5), and C57BL/6 mice (obtained from Charles River), were bred in our animal facility, LXR-KO mice76 and Vav-Cre PPAR-y101 mice77 were described before. Ch25h full knockout mice were purchased from Jackson Laboratories. All mice were used between 6-12 weeks of age, randomized among groups, and maintained under SPF conditions at the animal facility of Geneva Medical School. Mice were housed under a 12 h:12 h light:dark schedule, with temperature maintained between 20 and 22 °C and a humidity level of around 50%. Mice had access to food and water ad libitum. No statistical methods were applied a priori to calculate group sample size, all experiments were performed at least twice with a minimum of three animals per group. All procedures were approved and performed in accordance with the guidelines of the animal research committee of Geneva (Commission Cantonale pour les Expériences sur les Animaux (CCEA) and the Office fédéral de la santé alimentaire et des affaires vétérinaires (OSAV)) under the licence numbers GE/149/19 and GE167.

Tamoxifen treatment

 $LEC^{\Delta Ch25h}$ mice and LEC^{WT} littermate control mice were injected intraperitoneally with tamoxifen (T5648, Sigma-Aldrich), $1\,\text{mg/mouse}$ twice a day for 4 continuous days. Mice were used for experiments two weeks after the last injection.

Cell lines

Mouse B16F10 melanoma cells (ATCC) were transfected with ovalbumin (gift of B. Huard) (B16F10-OVA), and B16F10-OVA were engineered to overexpress VEGF-C (B16F10-OVA VEGF-C) as published¹⁹, and B16F10 and B16F10-OVA VEGF-C were maintained in RPMI supplemented with 10% heat-inactivated FBS, 100μM penicillinstreptomycin. Geneticin was added after 1 day of culture to select OVA-expressing cells. MC38 cells, MC38 VEGF-C cells⁷², E0771 cells, were maintained in DMEM (Gibco), 10% heat-inactivated FCS, 100 μM penicillin-streptomycin. Cell lines were not authenticated, used at below passage 20, and tested negative for Mycoplasma. Human melanoma cell lines T1015, T362C, T618A, Me215, Me275⁷⁸, and T672E⁷⁹

were maintained in RPMI supplemented with 10% heat-inactivated FBS, $100\,\mu\text{M}$ penicillin-streptomycin. b.End3 mouse endothelial cells were a gift from B. Kwak.

Human melanoma samples

Patients signed the informed consent form for the translational clinical trial PEMSYS (NCT03534635) and agreed to the re-use of their biological material and clinical data. The study was approved by the competent local ethics committee (https://www.cer-vd.ch/, CER-VD, Switzerland) under the identification of BASEC ID 2017-01107.

Tumor cell inoculation and tumor measurement

Mice were anesthetized using isoflurane or a mix of Rompun 2% (Bayer)/Ketamine 10% (Vetoquinol) and their backs were shaved. Unless specified, 0.5 × 106 B16F10, B16F10-OVA VEGF-C, MC38, MC38 VEGF-C cells, and 2 × 106 human melanoma cell lines T362C and T618A cells, were injected in 100 µl of PBS subcutaneously on the back dorsolateral side. For BMDMs and tumor cells co-injection experiment. 0.5 × 106 B16F10-OVA VEGF-C tumor cells were co-injected with 0.1 × 106 BMDMs from C57BL/6 mice or LXR-KO mice (OT-1 adoptive transfer experiment in NSG) or 0.25 × 106 BMDMs from WT/PPAR-γ^{KO} mice (vaccination experiment) in 100 µl of PBS subcutaneously on the back dorsolateral side. Primary tumor inoculation was controlled by measuring the distance between the front leg, the back leg, and the vertebral column of the mice, and the injection was always performed at the same distances from these three locations, at equal distance from the vertebral column and the back leg, representing -1/3 of the distance to the front leg. For orthotopic tumor models, 0.5×106 E0771 cells were injected into the fourth mammary fat pad, and 0.5 × 106 MC38 cells were injected into the rectum. Tumor size was monitored blindly every 1-2 days using a caliper, and tumor size was calculated by length × width or measured at the ending point (weight). For some experiments, tumor growth has been normalized in order to pool data from different experiments. Tumor size for each day was normalized to the size of controls or to the size for each group from measurement at the first timepoint (details are indicated in the figure legends accordingly). Mouse exclusion criteria permitted by our ethics committee are tumor size >15 mm (diameter) and/or signs of pain or anxiety. We confirm that the exclusion criteria were not exceeded.

Tissue digestion and single-cell preparation

Stromal cell isolation. Tissues were cut into small pieces and digested in RPMI containing collagenase IV (1 mg/ml; Worthington Biochemical Corporation), DNase I (40 µg/ml; Roche), and 1% FBS for 30 min at 37 °C. Samples were mixed up and down every 10 min. Tubes were centrifuged for a few seconds at 400 vg, and supernatants were filtered through a 70 µm cell strainer in FACS buffer to stop the reaction. The remaining tissue was further digested in RPMI with collagenase D (1 mg/ml; Roche), DNase I (40 μg/ml; Roche), and 1% of FBS for 20 min at 37°C, with an additional two cycles of repeated pipetting. The solution was filtered through a 70 µm cell strainer in FACS buffer and pooled into the first collected tubes. For tumors, digestion was followed by debris removal using Lympholyte®-M (CEDARLANE) according to the manufacturer's instructions. For LNs, stromal cells were further enriched by CD45 negative selection using MACS® Column (Miltenyi Biotec). For skin, the remaining tissues after digestion were gently scratched on 70 µm cell strainers and filtered for the following staining.

Leukocyte isolation. Tissues were cut into small pieces and digested in RPMI containing collagenase D (1 mg/ml; Worthington Biochemical Corporation), DNase I (40 μ g/ml; Roche), and 1% FBS for 40 min at 37 °C. Samples were mixed up and down every 10 min. The solution was filtered through a 70 μ m cell strainer in FACS buffer to stop the reaction. For tumors, digestion was followed by debris removal using

Lympholyte®-M (CEDARLANE) according to the manufacturer's instructions.

Mouse OT-1 T cell isolation, activation, and purification

Spleens and LNs from OT-1 CD45.1 mice were smashed, filtered through a 70-μm mesh filter, and centrifuged at 400×g for 5 min. Red blood cells were lysed with ammonium-chloride-potassium lysis buffer. Following the addition of the cell culture medium, splenocytes were washed and resuspended in complete RPMI (supplemented with 10% FBS, 1% penicillin-streptomycin, and 50 mM 2-β-mercaptoethanol). OT-1 cells were activated with 1nM OVA-I peptide (SIINFEKL) (Sigma-Aldrich) in the presence of 100 U/ml interleukin-2 (IL-2) (PeproTech) in vitro for 3 days. Activated OT-1 T cells were purified by using a CD8° T cell isolation kit (Miltenyi Biotec) according to the manufacturer's instructions.

Generation of naïve bone marrow-derived macrophages (BMDMs)

Bone marrow cells were collected from femurs obtained from 8 to 10week-old mice. After red blood cell lysis, bone marrow cells were seeded at a density of 10⁷ cells/100 × 15-mm Petri dish and cultured at 37 °C in DMEM containing 20 ng/ml CSF1 (PeproTech). BMDMs were ready for use on day 7 following a fresh medium change on day 4.

Vaccination

B16F10-OVA VEGFC tumor-bearing mice were injected subcutaneously at days 4 and 8 post tumor inoculation with OVA protein ($50 \mu g/mice$; Invivogen) and CpG-B 1826 ($30 \mu g/mice$; Invivogen).

Activated OT-1 T cell adoptive transfer

OT-1 CD45.1 cells were activated and purified as described above. In the experiments with LEC $^{\rm WT}$ and LEC $^{\Delta {\rm Ch25h}}$ mice, B16F10-OVA VEGF-C tumor-bearing mice received 1.5 × 106 activated OT-1 cells per mouse intravenously at day 8 post tumor inoculation. In the experiments with NSG, NSG-LEC $^{\rm WT}$, and NSG-LEC $^{\Delta {\rm Ch25h}}$ mice, 0.5 × 106 activated OT-1 cells were injected intravenously at day 8 post tumor inoculation. Tumor growth was measured every 2 days using a caliper.

25-HC intratumoral injection

25-HC was resuspended into a solution of 50% Ethanol (Fluka Analytical) and 50% Poly (ethylene glycol) methacrylate-500 (Sigma) via sonication. 25-HC or control solution was injected intratumorally at 200 μg in 20 $\mu l/mouse$ every two days starting at day 4 post tumor injection.

Bone marrow (BM) chimeric mice construction

Bone marrow (BM) chimeric mice were generated as described ⁸⁰. Briefly, BM cells were recovered from the tibia and femurs of WT CD45.1' and EBI2^{KO} CD45.1'/.2' donor mice and mixed in a 1:1 ratio. About 5-7×10⁶ cells were injected intravenously into sub-lethally irradiated recipient LEC^{WT} and LEC^{ΔCD,SSh} mice (two consecutive doses of 500 cGy with 4-h intervals). Experiments were performed at least 6 weeks after reconstruction.

In vitro BMDM polarization and treatment with 25-HC or 7-keto-25-HC

BMDMs from WT or Ch25h $^{-/-}$ mice were stimulated for 48 h with IFN- γ (20 ng/ml, PeproTech) or with IL-4 (50 ng/ml, PeproTech) to polarize toward an M1-like or M2-like phenotype, respectively, and treated or not with 1 μ g/ml of either 25-HC (MedChemExpress) or 7-keto-25-HC (Cayman Chemical Company)

Ex vivo LEC cultures

LNs were harvested and digested in MEM Alpha Medium (Gibco) with Dispase ($800 \, \mu g/ml$, Sigma), Collagenase P ($200 \, \mu g/ml$, Roche), DNase I

 $(100\,\mu g/ml; Roche)$ at $37\,^{\circ}C$, resuspended every $10\,min$, 2/3 of the digestion mix was transferred to collecting tubes and replaced by fresh digestion mix. The operation was repeated until full digestion. Culture plates precoated with PureCol $(10\,\mu g/ml, Advanced BioMatrix)$ and human fibronectin $(10\,\mu g/ml, Gibco)$ were seeded with the cell suspension for 7 days. The medium, containing cells in suspension, was removed at day 1 and day 3, to keep adherent cells that are mainly a mixture of (CD45 negative) LECs and FRCs. LECs were sorted with a FACS Aria Fusion sorter (BD) based on CD45 $^{\circ\circ}8(P38\,^{\circ}CD31\,^{\circ}$ expression and put back in culture on precoated culture plates.

In vitro 25-HC release experiments

LECs and BMDMs were generated from WT and Ch2Sh knockout mice. 10,000 cells/well of LECs, BMDMs, and b.END3 cells were put in culture in 96-well plates precoated with PureCol (10 μ g/ml, Advanced BioMatrix) and human fibronectin (10 μ g/ml, Gibco) for LECs, and L.S% gelatin for b.END3 cells. Cells were treated with B16-OVA VEGF-C cell culture supernatants for 3 days, and supernatants were harvested for 25-HC dosage.

In vitro BMDMs treatment with tumor conditional medium (TCM), 25-HC, 7-keto-25-HC, PPAR-y inhibitor, and PPAR-y agonist

BMDMs from WT, Ch2Sh⁺⁻ or LXR-KO mice were harvested and preseeded into a Petri dish or six-well non-treated cell culture plates (Corning Inc.) overnight and treated with different compounds used either alone or incombination: 1 μg/m125-HC (MedChemExpress), 1 μg/ ml 7-keto-25-HC (Cayman Chemical Company), 20 nM PPAR-γ inhibitor T0070907 (Cayman Chemical Company), 50 μM PPAR-γ agonist Troglitazone (MedChemExpress) and TCM (prepared from 2 days B16F10-OVA VEGF-C cells in vitro culture medium). After 48 h, BMDMs were harvested for flow cytometry, Q-PCR, or co-culture experiments with T cells.

For in vitro co-culture of BMDMs and OT-1 cells, OT-1 cells and BMDMs were preactivated or pretreated as described above. Activated OT-1 cells and pretreated BMDMs were co-cultured at a ratio of 1:5 in flat-bottom 96-well plates in a complete RPMI medium. After 48 h, OT-1 cells were harvested for flow cytometry.

Lymphatic vessel drainage

Dextran–Alexa Fluor 488 (40 kD) was injected intratumorally (3 μ l at 100 mg/ml). 20 min later, inguinal and axillary tumor dLNs and their contralateral control LNs were harvested and dissociated in 200 μ l of PBS, centrifuged at 400×g and 100 μ l of supernatant from each sample was transferred to a new plate. A fluoro spectrometer (Spectamax Paradigm; Molecular Devices) was used to determine Alexa Fluor 488 fluorescence intensity in dLNs. The background of fluorescence in the contralateral side was removed to the intensity of the dextran–Alexa Fluor 488 tumor side.

Flow cytometry analysis

Monoclonal antibodies (mAbs) used for flow cytometry are listed in Supplementary Table 1. Unless specified, antibodies were used at 1:200 working dilution. For flow cytometry, single-cell suspensions were incubated with FcBlock (anti-CD16/32 FcyRII-RIII; Invitrogen) for 10 min, at 4 °C and stained for extracellular markers with antibodies and fixable viability dye (Dye eFluor TM 780, Thermo Fisher) for 20 min in PBS at 4 °C. To assess Ch25h-GFP expression, cells were stained for extracellular markers, and live-cell impermeant DNA DRAQ7 dye (Biolegend) was used for viability evaluation on unfixed cells. Antimouse antibodies used for stain cell surface markers: anti-GP38 (8.1.1), anti-CD31(390), anti-I-A/I-E (M5/114.15.2), anti-B220 (RA3-6B2), anti-CD11b (M1/70), anti-CDI1c (HL3 or N48), anti-CD19 (6D5), anti-CD3 (REA641), anti-CD4 (GK1.5 or RM4-5), anti-CD45 (GL1), anti-CD45.1 (A20), anti-CD45.2 (104), anti-CD8 (53-6.7), anti-CD86 (GL1), anti-F4/80

(BM8), anti-I-a/I-E (M5/I14.15.2 or 2G9), anti-Iy6C (HK1.4), anti-Iy6G (1A8), anti-NK1.1 (PK136), anti-PD-1 (RMPI-30), anti-PD-L1 (10 F.9G2), anti-TCRβ (H57-597), anti-Ter119 (TER-119), anti-Tim-3 (RMT3-23), H-2K(b) chicken ova 257-264 SIINFEKL tetramer (NIH tetramer core facility). Intracellular staining was performed using the Intracellular Fixation & Permeabilization buffer set (eBioscience). Antibodies to intracellular markers: anti-CD206 (CO68C2), anti-CD68 (FA-11), anti-Foxp3 (FJK-16s), anti-Granzyme-B (GB11), anti-IFN-γ (XMG1.2), anti-INS (CXNFT), anti-Ki67 (SolAL5), and anti-TNF-α (MP6-XT22).

For IFN- γ , Granzyme-B, and TNF- α , cells were first re-stimulated in complete RPMI containing PMA (100 ng/ml; Sigma-Aldrich), Ionomycin (1 μ g/ml, Sigma-Aldrich), and Golgi Plug solution (1/1000; BD Biosciences), and incubated 4 h at 37 °C. 5% CO₂.

Data were acquired with a Fortessa analyzer (BD) and analyzed using FlowJo software (FlowJo).

Hematoxylin & Eosin (H&E) and immunofluorescence (IF) staining

Tumors and dLNs were embedded either into OCT (Optimal cutting temperature) medium and kept at $-80\,^{\circ}\text{C}$ or fixed with 4% paraformaldehyde (PFA) and embedded into paraffin. Frozen samples were sectioned into 7 μ m, a ir-dried, and postfixed with 4% PFA for 10 min at room temperature (RT), washed with PBS three times, and followed with permeabilization with 0.1% Triton-100 for 10 min. Paraffin samples were sectioned into 4–7 μ m, di-paraffined, and performed antigen retrieval with the Tintoretriever pressure cooker (Bio SB) using the high-pressure setting for 10 minutes in Tris-EDTA buffer (pH 9) before the following steps.

H&E staining was performed with H&E staining kit (Vector Laboratories) for LN-metastasis analysis. Images were obtained by Axio Scan.ZI (Zeiss), processed and analyzed with QuPath. Metastasis fraction was calculated as the percentage of melanoma area among total LN area.

IF staining was performed for lymphatic vessel density, and macrophage/monocyte proximity analysis. Following the blocking with 10% FBS for 1 h at RT. The sections were stained overnight with primary antibodies diluted in 10% BSA at 4 °C overnight. The following primary anti-mouse antibodies were used according to the experiments; anti-Lyve-1 (1:1000, ab14917, Abcam; 1:200, 14-0443-82, Invitrogen), anti-CD8 (1:100, 14-0808-82, Thermo), anti-CD68 (1:2000, 137002, Biolegend), anti-CD31 (1: 100, AF3628, R&D Systems), anti-Ch25h (1:100, ABIN1387938, ANTIBODIES). Sections were washed and stained with unconjugated secondary fluorochromecoupled antibodies for 1h at room temperature. The following secondary antibodies from Thermo were used: Alexa Fluor™546 goat anti-rat (LOT: 2146039), Alexa Fluor™488 goat anti-rabbit (LOT: 1386400), Alexa Fluor™647 donkey anti-rabbit (LOT: 2420695). Prior to mounting with Fluoromount™ Aqueous Mounting Medium (Sigma), sections were stained with DAPI (1:1000 dilution of 1 mg/ml stock) for nuclei staining. Images were obtained by spinning disk confocal microscope (Axio Examiner Z1 Advanced Microscope Base, Zeiss) equipped with a confocal scanner unit CSU-XLA1 (Yokogawa Electric Corporation). The fluorescence was detected using three laser-excitation wavelengths (488 nm, 561 nm, and 640 nm; Laser-Stack v4 Base, 3i) in combination with appropriate band-passemission filters (Semrock), an electron-multiplying charge-coupled device camera (EMCCD, Evolve 512 10 MHz Back Illuminated, Photometrics) and a 10x /0.3 NA water immersion objective (W Plan Apochromat, Zeiss). 3D image stacks were obtained by sequential acquisition of multiple fields of views along the z-axis using a motorized XY-stage (ProScan, Prior). SlideBook software (6.0.17, 3i) was used for image acquisition and the creation of maximum projections. The subsequent generation of montage images from contiguous positions was performed using the Fiji grid/collection stitching plugin81.

RNA in situ hybridization combined with immunofluorescence

For the combined RNA-ISH-IF (RNAscope®) analysis, samples were fixed in 4% NBF at 4°C for 24 h and 5-µm thick sections from FFPE blocks were cut. In situ hybridization (ISH) with co-immunostaining (IF) was performed following the manufacturer's recommendation of the RNAscope Multiplex Fluorescent Reagent Kit v2 assay (Cat# 323100, Advanced Cell Diagnostics). Standard conditions were used: 15 min, incubation for the Antigen retrieval step and 8 min, for Protease Plus treatment. Combined ISH and antibody staining with Opal dyes (Akoya Biosciences) was performed manually for ISH and employing an automated Ventana Discovery Ultra Staining module (Ventana, Roche) for IF. For the individual experiments, the following combinations of RNAscope® probes (all from Biotechne) and antibodies were employed. All opal dyes were purchased from Akoya Biosciences inc: Probe-Hs-CH25H probe (Cat# 533811) with opal570 (Cat# FP1488001KT), anti-Podoplanin Ab (Cat# 916605, Biolegend, diluted 1/250) with opal690 (Cat# FP1497001KT). Nuclei were visualized by final incubation with Spectral DAPI (1/10, Cat# FP1490, Akoya Biosciences). The slides were mounted with fluorescence mounting medium (Cat# S3023, Dako) and stored in the dark at 4°C until scanned within 48 h. Images were acquired on the Vectra Polaris automated imaging system at 40X (Akoya Biosciences, Marlborough, USA), allowing the unmixing of spectrally overlapping fluorophores and tissue autofluorescence of whole slide scans using Phenochart (Akova Biosciences).

RNA isolation and quantitative RT-PCR (Q-PCR)

Total RNA was isolated using Trizol Reagent (Thermo) or miRNeasy Mini Kit (Qiagen) depending on cell numbers. RNA quantity and quality were analyzed using a Nanodrop 2000 (Thermo Fisher) or Bio analyzer (Agilent Technologies). Reverse transcription was performed using PrimeScript^M RT Reagent Kit (Takara) followed by a pre-amplification of the respective genes of interest using the TaqMan Preamp Master Mix (Applied Biosystems) or M-MLV (Promega). Q-PCR analyses were performed with the ABI Prism 7900 HT detection system and the PowerUp SYBR Green Master Mix (Applied Biosystems). Primer sequences are provided in Supplementary Table 2. Quantification of the transcript was performed using the $2-\Delta\Delta Ct$ method with glyceraldehyde phosphate dehydrogenase (gapdh), actb, or together with rpl32 as internal reference genes.

Bulk RNA sequencing and data analysis

Single cell suspensions from tumors, LNs, and skin, were obtained as described above. Cells were stained with cell surface markers and live/dead dye DRAQ7 (Biolegend), and then sorted directly into RNA Protector Reagent (Qiagen) with a FACS Aria Fusion sorter (BD). For LECs from C57BL/6 NdLNs, TdLNs, and tumors, cells were sorted as CD45CD31'GP38' population from B16F10-OVA VEGF-C tumorbearing mice sacrificed at day 11. For tumor LECs from LEC^{WT} and LEC^{ΔCD,25h} mice, cells were sorted from tumors as CD45CD31'GP38' cells from B16F10-OVA VEGF-C tumor-bearing mice sacrificed on day 11. For macrophages and monocytes from LEC^{WT} and LEC^{ΔCD,25h} mice, cells were sorted from tumors of OVA+CpG-B vaccinated B16F10-OVA VEGF-C tumor-bearing mice sacrificed at day 24. Sorting was based on common markers CD45'Lin (CD19/CD3)'Ly6G'CD11b' with exclusion of DCs (CD11c)^{Is} F4/80'), and further separated as macrophages (F4/80'Ly6C') and monocytes (F4/80Ly6C').

Total RNA was quantified with a Qubit (fluorimeter from Life Technologies) and RNA integrity was assessed with a Bioanalyzer (Agilent Technologies). The SMART-Seq v4 kit from Clonetech was used for the reverse transcription and cDNA amplification according to the manufacturer's specifications, starting with 1ng (for LEGs and Macrophages) or 10 ng (for monocytes) of total RNA as input. 200 pg of cDNA were used for library preparation using the Nextera XT kit from Illumina. Library molarity and quality were assessed with Qubit

and Tapestation using a DNA High-sensitivity chip (Agilent Technologies). Libraries were sequenced on a HiSeq 4000 (for LECs)/NovaSeq 6000 (for macrophages and monocytes) Illumina sequencer for SR50(for LECs) or SR100 (for macrophages and monocytes) reads.

Analysis for LECs from C57BL/6 NdLNs, TdLNs, and tumors (GSE242026). FastQ reads were mapped to the ENSEMBL reference genome (GRCm38.80) using STAR version 2.4.0j[®] with standard settings, except that any reads mapping to more than one location in the genome (ambiguous reads) were discarded (m=1). A unique gene model was used to quantify reads per gene. Briefly, the model considers all annotated exons of all annotated protein-coding isoforms of a gene to create a unique gene where the genomic region of all exons is considered coming from the same RNA molecule and merged. All reads overlapping the exons of each unique gene model were reported using featureCounts version 1.4.6-p183. Gene expressions were reported as raw counts and, in parallel, normalized in RPKM to filter out genes with low expression values (1 RPKM) before calling for differentially expressed genes, Library size normalizations and differential gene expression calculations were performed using the package edgeR84 designed for the R software. Only genes having a significant fold-change (Benjamini-Hochberg corrected p value <0.001) were considered. Sample similarity was analyzed as follows: Euclidean distance between samples was calculated from the log transformed gene expression counts matrix with the dist function (vectors), 0 = identity (same sample). The color key indicates the values given by the Euclidean distance calculation.

Analysis for TA-LECs from LEC^{wt} and LEC^{△Chesh} mice (GSE242150). Mapping was done with the STAR v.2.7.0 software to the UCSC mm10 Mus musculus reference. Biological quality control and summarization were done with PicardTools (v.1.141). The number of reads was prepared with HTSeq v0.9.1 (htseq-count). The differential expression analysis was performed with R/Bioconductor package EdgeR (v.3.26.8). The genes having a count above 1 count per million reads (cpm) in at least 3 samples were kept for the analysis. The poorly or not expressed genes were filtered out. The filtered dataset consists of 13,454 genes. The differentially expressed gene tests were done with a GLM (general linear model) with a negative binomial distribution. The differentially expressed genes are corrected for multiple testing errors with a 5% FDR (false discovery rate). The correction used is Benjamnini-Hochberg (BH). The likelihood test was used for the statistical test of differential expression.

Analysis for macrophages and monocytes from LEC^{WT} and LEC^{\(\text{LEC}\)} mioc (GSE239972). Mapping and quantification using STAR and Salmon: nf-core/maseq pipelin (v.3.9) on mm10. Counts were normalized for library size using the TMM method from EdgeR (v.3.32.1) and voom from limma (v.3.46.0). Differential expression was computed with limma, after filtering out low expressed genes (with average FPKM <2 or average reads counts <5) and not characterized, non-coding or pseudo genes; the filtered set of genes contains n = 9392 genes. Gene set enrichment analysis was performed with clusterProfiler (v3.18.1) applying GSEA (Gene Set Enrichment Analysis) on the Hallmark collection of genesets. The gene lists used for M1 and M2 signature enrichment were used as described in ref. 50. Gene lists for heatmaps are listed in Supplementary Table 3.

Generation of anti-CSF1R(CD115) depleting antibody

Monoclonal anti-mouse CSF1R(CD115) depletion antibody was generated with AFS98 hybridoma. Briefly, AFS98 hybridoma cells were cultured with the CELLine 1000 system (Wheaton) in PFHM-II medium supplementing with 1% penicillin and streptomycin. Cell culture content was harvested on day 14 and day 21. Hybridoma cells were spined down by centrifuging at 400×g for 5 min. The supernatant was

harvested, filtered, and concentrated (using AMICON concentrators) for purification (performed by our Protein Core Facility). Antibodies were purified with Superdex200 10/300 Size Exclusion Chromatography (SEC) system. The purity of the antibodies was analyzed by acrylamide gel electrophoresis.

In vivo myeloid cell depletion

To deplete myeloid cells in the vaccination experiment, 1 mg/ mouse anti-CSFIR depletion antibody or PBS control was injected intraperitoneally at day 10 (2 days after second dose of vaccination) after tumor inoculation. In the non-vaccinated experiment, 1 mg/ mouse anti-CSFIR depletion antibody or PBS was injected intraperitoneally on day 4 after tumor inoculation. The following injections were done every 3 days at 500 $\mu g/mouse$ until the day of sacrifice for all experiments.

In vivo B-cell depletion

To deplete B cells in the BI6FI0-OVA VEGFC model, one dose of 250 ug/mouse anti-CD20 depletion antibody was injected intraperitoneally 3 days before tumor inoculation.

Correlation analysis in TCGA melanoma dataset

A Spearman's correlation analysis was carried out between CH25H gene expression and a signature of lymphatic vessels (LV signature 1: pdpn, vegfc, lyve1; LV signature 2: prox1, flt4, lyve1, pdpn, vegfc) or MI/M2 macrophage (Blueprint 2) signatures in The Cancer Genome Atlas' (TCGA) skin cutaneous melanoma (SKCM) patients' dataset (n = 458 patients), accessed via the UCSC Xena project (http://xena.ucsc.edu). Correlation between CH25H and MI/M2-signature in normal skin samples was performed in TCGA normal skin and normal skin from the GTEx dataset, both sun-exposed and non-exposed. Different datasets and analysis workflows were used as described 1.15. All tests were two-sided and without adjustments for multiple comparisons.

Survival analyses in the TCGA melanoma dataset

Survival analysis was carried out using CH25H gene expression in the TCGA melanoma dataset. We accessed patient OS or PFS durations and tumor gene expression profiles for SKCM patients' dataset (n=458) based on the UCSC Xena project (http://xena.ucsc.edu)²¹. Briefly, OS/PFS analysis was based on a log-rank hypothesis test (the Mantel–Cox statistical test) that also estimated the Cox-proportional hazard ratio (HR) and the 95% confidence intervals accompanied by a Kaplan–Meier (KM) plot. Herein, the expression threshold cut-off at 25% (top) vs. 75% (rest) gene expression level was used for splitting the patients into high-expression and low-expression sub-cohorts. All tests were two-sided and without adjustments for multiple comparisons.

Survival analysis of immuno-oncology clinical trials

Patient survival analysis in immuno-oncology clinical trials was carried out using ch25h gene expression. We accessed tumor transcriptomic data from melanoma patients profiled before anti-PD-1 immunotherapy alone, anti-CTLA-4 immunotherapy alone, or a combination of anti-PD-1/CTLA-4 immunotherapy. These data and subsequent OS estimates were accessed from an integrated dataset of multiple clinical trial studies consisting of 570 melanoma patients 21,22,86. Briefly, OS analysis was based on a log-rank hypothesis test (the Mantel-Cox statistical test) that also estimated the Coxproportional hazard ratio (HR) and the 95% confidence intervals accompanied by a Kaplan-Meier (KM) plot. Herein, the expression threshold cut-offwas based on a statistical auto-cutoff criterion^{21,85,87} Thresholds (overall expression ranges lowest-highest) for each treatment condition: PD1: 8 (1-1571); CTLA-4: 29 (2-283); PD1 + CTLA-4: 29 (2-80). All tests were two-sided and without adjustments for multiple comparisons.

Ex vivo and in vitro 25-HC and 7-keto-25-HC dosage

25-hydroxycholesterol was analyzed using a validated HPLC-MS method584. For tumor interstitial fluid: harvested tumors were placed on 70 µm filters at the top of 5-ml-tubes, and centrifuged at 300×g for 20 min, interstitial fluid was collected. For serum samples: fresh blood was collected and centrifuged at 500×g for 5 min, and serum was collected. For in vitro samples: LECs, BMDMs, and b.End3 blood endothelial cells were treated with tumor cell supernatants for 3 days. supernatant were harvested and centrifuged at 500×g for 5 min to remove the debris. Tumor interstitial fluids and sera were collected and placed in glass vials containing d₇-4β-hydroxycholesterol and d₇-24-hydroxycholesterol as deuterated internal standards and dichloromethane (8 ml), methanol (4 ml, containing 10 µg of butylated hydroxytoluene), and water (2 ml, containing 20 ng ethylenediaminetetraacetic acid). The samples were then mixed and sonicated. After that, they were centrifuged, and the organic phase was recovered and dried under nitrogen steam. Finally, samples were purified by solidphase extraction using columns made of normal silica. Cholesterol was removed from the samples using hexane-isopropanol (99:1, v/v). 25 HC (from tumor interstitial fluid and sera) and 7-keto-25-HC (from tumor interstitial) were then eluted using hexane-isopropanol (73, v/v) and analyzed by HPLC-MS using an LTQ-Orbitrap XL mass spectrometer (Thermo Fisher Scientific) coupled to an Accela HPLC system (Thermo Fisher Scientific). Chromatographic separation was performed using an Ascentis Express C18 column (2.7 µm, 150 × 4.6 mm, Sigma), kept at 15 °C. The mobile phase was a gradient of methanol and water containing acetic acid. Values have been normalized to the sample volume.

Statistical analysis

Data were analyzed using Prism 9 software (GraphPad). Unless specified, analysis for significance was performed by one-way or two-way ANOVA when more than two groups were compared and by two-tailed Student t-test when only two groups were compared. p < 0.05 was considered statistically significant (*p < 0.05, **p < 0.01, ***p < 0.001).

Reporting summary

Further information on research design is available in the Nature Portfolio Reporting Summary linked to this article.

Data availability

The data underlying this article are accessible at https://doi.org/10. 26037/yareta:aoweiaahjvcmjmfx23mdtefvyu. All data needed to evaluate the conclusions in the paper are present in the paper and/or the Supplementary Materials. The RNA sequencing data generated in this study has been deposited in the Gene Expression Omnibus (GEO) database with public accessibility, the link to each dataset is listed below: Bulk RNA sequencing on LECs from C57BL/6 NdLNs, TdLNs, and tumors (GSE242026): https://www.ncbi.nlm.nih.gov/geo/query/acc.cgi. Bulk RNA sequencing on TA-LECs from LEC^{WT} and LEC^{\(\Delta\)} mice (GSE242150): https://www.ncbi.nlm.nih.gov/geo/query/acc.cgi. Bulk RNA sequencing on macrophages and monocytes from LEC^{WT} and LEC^{\(\Delta\)} mice (GSE239972): https://www.ncbi.nlm.nih.gov/geo/query/acc.cgi Source data are provided with this paper.

References

- Jones, D., Pereira, E. R. & Padera, T. P. Growth and immune evasion of lymph node metastasis. Front. Oncol. 8, 36 (2018).
- Stacker, S. A. et al. Lymphangiogenesis and lymphatic vessel remodelling in cancer. Nat. Rev. Cancer 14, 159–172 (2014).
- Hirakawa, S. et al. VEGF-A induces tumor and sentinel lymph node lymphangiogenesis and promotes lymphatic metastasis. J. Exp. Med. 201, 1089–1099 (2005).
- Qian, C. N. et al. Preparing the "soil": the primary tumor induces vasculature reorganization in the sentinel lymph node before the

- arrival of metastatic cancer cells. Cancer Res. 66, 10365-10376 (2006).
- Gamier, L., Gkountidi, A. O. & Hugues, S. Tumor-associated lymphatic vessel features and immunomodulatory functions. Front. Immunol. 10, 720 (2019).
- Gkountidi, A. O. et al. MHC class II antigen presentation by lymphatic endothelial cells in tumors promotes intratumoral regulatory T cell-suppressive functions. Cancer Immunol. Res. 9, 748–764 (2021).
- Lane, R. S. et al. IFNgamma-activated dermal lymphatic vessels inhibit cytotoxic T cells in melanoma and inflamed skin. J. Exp. Med. 215, 3057–3074 (2018).
- Fankhauser, M. et al. Tumor lymphangiogenesis promotes T cell infiltration and potentiates immunotherapy in melanoma. Sci. Transl. Med. https://doi.org/10.1126/scitranslmed.aal4712 (2017).
- Sasso, M. S. et al. Lymphangiogenesis-inducing vaccines elicit potent and long-lasting T cell immunity against melanomas. Sci. Adv. https://doi.org/10.1126/sciadv.abe4362 (2021).
- Song, E. et al. VEGF-C-driven lymphatic drainage enables immunosurveillance of brain tumours. Nature 577, 689–694 (2020).
- Mao, S. et al. Studies in the antiviral molecular mechanisms of 25hydroxycholesterol: disturbing cholesterol homeostasis and posttranslational modification of proteins. Eur. J. Pharm. 926, 175033 (2022).
- de Freitas, F. A. et al. Effects of oxysterols on immune cells and related diseases. Cells https://doi.org/10.3390/cells11081251 (2022).
- Gold, E. S. et al. 25-Hydroxycholesterol acts as an amplifier of inflammatory signaling. Proc. Natl Acad. Sci. USA 111, 10666–10671 (2014).
- Kloudova, A., Guengerich, F. P. & Soucek, P. The role of oxysterols in human cancer. *Trends Endocrinol. Metab.* 28, 485–496 (2017).
- Lu, Z. et al. Regulation of intercellular biomolecule transfer-driven tumor angiogenesis and responses to anticancer therapies. J. Clin. Invest. https://doi.org/10.1172/JCf144225 (2021).
- Ortiz, A. et al. An interferon-driven oxysterol-based defense against tumor-derived extracellular vesicles. Cancer Cell 35, 33–45.e36 (2019).
- Lu, Z. et al. ATF3 and CH25H regulate effector trogocytosis and antitumor activities of end ogenous and immunothera peutic cytotoxic T lymphocytes. Cell Metab. 34, 1342–1358.e1347 (2022).
- Lu, Z. et al. Tumor factors stimulate lysosomal degradation of tumor antigens and undermine their cross-presentation in lung cancer. Nat. Commun. 13, 6623 (2022).
- Lund, A. W. et al. VEGF-C promotes immune tolerance in B16 melanomas and cross-presentation of tumor antigen by lymph node lymphatics. Cell Rep. 1, 191–199 (2012).
- Ruiz, F. et al. Endothelial cell-derived oxysterol ablation attenuates experimental autoimmune encephalomyelitis. EMBO Rep. 24, e55328 (2023).
- Naulaerts, S. et al. Multiomics and spatial mapping characterizes human CD8(+) T cell states in cancer. Sci. Transl. Med. 15, eadd1016 (2023).
- Vanmeerbeek, I. et al. Early memory differentiation and cell death resistance in T cells predicts melanoma response to sequential anti-CTLA4 and anti-PD1 immunotherapy. Genes Immun. 22, 108–119 (2021).
- Bazigou, E. et al. Genes regulating lymphangiogenesis control venous valve formation and maintenance in mice. J. Clin. Investig. 121, 2984–2992 (2011).
- Arasa, J. et al. Upregulation of VCAM-1 in lymphatic collectors supports dendritic cell entry and rapid migration to lymph nodes in inflammation. J. Exp. Med. https://doi.org/10.1084/jem. 20201413 (2021).

- Beck, K. R. et al. Enzymatic interconversion of the oxysterols 7beta, 25-dihydroxycholesterol and 7-keto, 25-hydroxycholesterol by 11beta-hydroxysteroid dehydrogenase type 1 and 2. J. Steroid Biochem. Mol. Biol. 190, 19–28 (2019).
- Liu, C. et al. Oxysterols direct B-cell migration through EBI2. Nature 475, 519–523 (2011).
- Hannedouche, S. et al. Oxysterols direct immune cell migration via EBI2. Nature 475. 524–527 (2011).
- Lu, E., Dang, E. V., McDonald, J. G. & Cyster, J. G. Distinct oxysterol requirements for positioning naive and activated dendritic cells in the spleen. Sci. Immunol. https://doi.org/10.1126/sciimmunol. aal5237 (2017).
- Sun, S. & Liu, C. 7alpha, 25-dihydroxycholesterol-mediated activation of EBI2 in immune regulation and diseases. Front. Pharm. 6, 60 (2015)
- Kamensek, U. et al. Mutational burden, MHC-I expression and immune infiltration as limiting factors for in situ vaccination by TNFalpha and IL-12 gene electrotransfer. *Bioelectrochemistry* 140, 107831 (2021).
- Tewalt, E. F., Cohen, J. N., Rouhani, S. J. & Engelhard, V. H. Lymphatic endothelial cells - key players in regulation of tolerance and immunity. Front. Immunol. 3, 305 (2012).
- Pokharel, S. M. et al. Integrin activation by the lipid molecule 25hydroxycholesterol induces a proinflammatory response. Nat. Commun. 10, 1482 (2019).
- Li, W. et al. Correlation between PD-1/PD-L1 expression and polarization in tumor-associated macrophages: A key player in tumor immunotherapy. Cytokine Growth Factor Rev. 67, 49–57 (2022).
- Tian, T. & Li, Z. Targeting Tim-3 in cancer with resistance to PD-1/PD-L1 blockade. Front. Oncol. 11, 731175 (2021).
- Liu, S. Y. et al. Interferon-inducible cholesterol-25-hydroxylase broadly inhibits viral entry by production of 25-hydroxycholesterol. Immunity 38, 92-105 (2013).
- Benner, B. et al. Generation of monocyte-derived tumor-associated macrophages using tumor-conditioned media provides a novel method to study tumor-associated macrophages in vitro. J. Immunother. Cancer 7, 140 (2019).
- Ries, C. H. et al. Targeting tumor-associated macrophages with anti-CSF-1R antibody reveals a strategy for cancer therapy. Cancer Cell 25, 846–859 (2014).
- Ghosh, A. et al. Increased p53 expression induced by APR-246 reprograms tumor-associated macrophages to augment immune checkpoint blockade. J. Clin. Invest. https://doi.org/10.1172/ JCI148141 (2022).
- Trikha, P. et al. E2f3 in tumor macrophages promotes lung metastasis. Oncogene 35, 3636–3646 (2016).
- Bae, S. et al. MYC-mediated early glycolysis negatively regulates proinflammatory responses by controlling IRF4 in inflammatory macrophages. Cell Rep. 35, 109264 (2021).
- Collins, S. L. et al. mTORC1 signaling regulates proinflammatory macrophage function and metabolism. J. Immunol. 207, 913–922 (2021).
- Marelli, G. et al. Lipid-loaded macrophages as new therapeutic target in cancer. J Immunother Cancer https://doi.org/10.1136/jitc-2022-004584 (2022).
- Shi, H. et al. NLRP3 activation and mitosis are mutually exclusive events coordinated by NEK7, a new inflammasome component. Nat. Immunol. 17, 250–258 (2016).
- Deng, J. & Fleming, J. B. Inflammation and myeloid cells in cancer progression and metastasis. Front. Cell Dev. Biol. 9, 759691 (2021).
- Holland, S. J. et al. R428, a selective small molecule inhibitor of Axl kinase, blocks tumor spread and prolongs survival in models of metastatic breast cancer. Cancer Res. 70, 1544–1554 (2010).
- Lu, Q. et al. Tyro-3 family receptors are essential regulators of mammalian spermatogenesis. Nature 398, 723–728 (1999).

- Myers, K. V., Amend, S. R. & Pienta, K. J. Targeting Tyro3, Axl and MerTK (TAM receptors): implications for macrophages in the tumor microenvironment. Mol. Cancer 18, 94 (2019).
- Larionova, I., Kazakova, E., Patysheva, M. & Kzhyshkowska, J. Transcriptional, epigenetic and metabolic programming of tumor-associated macrophages. Cancers https://doi.org/10.3390/cancers12061411 (2020).
- Siddiqui, S. & Glauben, R. Fatty acid metabolism in myeloid-derived suppressor cells and tumor-associated macrophages: key factor in cancer immune evasion. Cancers https://doi.org/10.3390/ cancers14010250 (2022).
- Pan, W. et al. The DNA methylcytosine dioxygenase Tet2 sustains immunosuppressive function of tumor-infiltrating myeloid cells to promote melanoma progression. *Immunity* 47, 284–297 e285 (2017).
- Cyster, J. G., Dang, E. V., Reboldi, A. & Yi, T. 25-Hydroxycholesterols in innate and adaptive immunity. Nat. Rev. Immunol. 14, 731–743 (2014).
- Toobian, D., Ghosh, P. & Katkar, G. D. Parsing the role of PPARs in macrophage processes. Front. Immunol. 12, 783780 (2021).
- Xu, L. et al. 25-Hydroxycholesterol-3-sulfate attenuates inflammatory response via PPARgamma signaling in human THP-1 macrophages. Am. J. Physiol. Endocrinol. Metab. 302, E788–E799 (2012).
- Pitas, G. et al. Regulatory T cells exhibit distinct features in human breast cancer. *Immunity* 45, 1122–1134 (2016).
- Raccosta, L. et al. The oxysterol-CXCR2 axis plays a key role in the recruitment of tumor-promoting neutrophils. J. Exp. Med. 210, 1711–1728 (2013).
- Bensinger, S. J. & Tontonoz, P. Integration of metabolism and inflammation by lipid-activated nuclear receptors. *Nature* 454, 470–477 (2008).
- Villablanca, E. J. et al. Tumor-mediated liver X receptor-alpha activation inhibits CC chemokine receptor-7 expression on dendritic cells and dampens antitumor responses. Nat. Med. 16, 98–105 (2010).
- Tavazoie, M. F. et al. LXR/ApoE activation restricts innate immune suppression in cancer. Cell 172, 825–840.e818 (2018).
- Xiao, J. et al. 25-Hydroxycholesterol regulates lysosome AMPkinase activation and metabolic reprogramming to educate immunosuppressive macrophages. *Immunity* 57, 1087–1104.e1087 (2024).
- Caronni, N. et al. IL-1beta(+) macrophages fuel pathogenic inflammation in pancreatic cancer. Nature 623, 415–422 (2023).
- Chittezhath, M. et al. Molecular profiling reveals a tumor-promoting phenotype of monocytes and macrophages in human cancer progression. *Immunity* 41, 815–829 (2014).
- Kaplanov, I. et al. Blocking IL-1beta reverses the immunosuppression in mouse breast cancer and synergizes with anti-PD-1 for tumor abrogation. Proc. Natl Acad. Sci. USA 116, 1361–1369 (2019).
- Rebe, C. & Ghiringhelli, F. Interleukin-1beta and cancer. Cancers https://doi.org/10.3390/cancers12071791 (2020).
- Lee, P. H. et al. Host conditioning with IL-1beta improves the antitumor function of adoptively transferred T cells. J. Exp. Med. 216, 2619–2634 (2019).
- Tulotta, C. et al. IL-1B drives opposing responses in primary tumours and bone metastases; harmessing combination therapies to improve outcome in breast cancer. NPJ Breast Cancer 7, 95 (2021).
- Takahashi, H. et al. Cholesterol 25-hydroxylase is a metabolic switch to constrain T cell-mediated inflammation in the skin. Sci. Immunol. 6, eabb 6444 (2021).
- Jiang, C., Ting, A. T. & Seed, B. PPAR-gamma agonists inhibit production of monocyte inflammatory cytokines. *Nature* 391, 82–86 (1998).
- Su, M. et al. The in vitro and in vivo anti-inflammatory effects of a phthalimide PPAR-gamma agonist. Mar. Drugs https://doi.org/10. 3390/md15010007 (2017).

- Nelson, V. L. et al. PPARgamma is a nexus controlling alternative activation of macrophages via glutamine metabolism. Genes Dev. 32, 1035–1044 (2018).
- Antila, S. et al. Development and plasticity of meningeal lymphatic vessels. J. Exp. Med. 214, 3645–3667 (2017).
- Li, Z. et al. Blockade of VEGFR3 signaling leads to functional impairment of dural lymphatic vessels without affecting autoimmune neuroinflammation. Sci. Immunol. 8, eabq 0375 (2023).
- Gamier, L. et al. IFN-gamma-dependent tumor-antigen cross-presentation by lymphatic endothelial cells promotes their killing by T cells and inhibits metastasis. Sci. Adv. 8, eabl5162 (2022).
- Broggi, M. A. S. et al. Tumor-associated factors are enriched in lymphatic exudate compared to plasma in metastatic melanoma patients. J. Exp. Med. 216, 1091–1107 (2019).
- Randolph, G. J., Angeli, V. & Swartz, M. A. Dendritic-cell trafficking to lymph nodes through lymphatic vessels. *Nat. Rev. Immunol.* 5, 617–628 (2005).
- Swartz, M. A. & Lund, A. W. OPINION lymphatic and interstitial flow in the tumour microenvironment: linking mechanobiology with immunity. Nat. Rev. Cancer 12, 210–219 (2012).
- El-Hajjaji, F. Z. et al. Liver X receptors, lipids and their reproductive secrets in the male. Biochim. Biophys. Acta 1812, 974–981 (2011).
- Schneider, C. et al. Induction of the nuclear receptor PPAR-gamma by the cytokine GM-CSF is critical for the differentiation of fetal monocytes into alveolar macrophages. Nat. Immunol. 15, 1026–1037 (2014).
- Neubert, N. J. et al. Broad and conserved immune regulation by genetically heterogeneous melanoma cells. Cancer Res. 77, 1623–1636 (2017).
- Voelter, V. et al. An unusual case of metastatic melanoma sensitive to chemotherapy and immunotherapy, with late immune escape in the brain. Cancer Immun. 8, 6 (2008).
- Hinshaw, D. C. & Shevde, L. A. The tumor microenvironment innately modulates cancer progression. Cancer Res. 79, 4557–4566 (2019).
- Preibisch, S., Saalfeld, S. & Tomancak, P. Globally optimal stitching of tiled 3D microscopic image acquisitions. *Bioinformatics* 25, 1463–1465 (2009).
- Dobin, A. et al. STAR: ultrafast universal RNA-seq aligner. Bioinformatics 29, 15–21 (2013).
- Quinlan, A. R. & Hall, I. M. BEDTools: a flexible suite of utilities for comparing genomic features. Bioinformatics 26, 841–842 (2010).
- Robinson, M. D., McCarthy, D. J. & Smyth, G. K. edgeR: a Bioconductor package for differential expression analysis of digital gene expression data. *Bioinformatics* 26, 139–140 (2010).
- Sprooten, J. et al. Lymph node and tumor-associated PD-L1(+) macrophages antagonize dendritic cell vaccines by suppressing CD8(+) T cells. Cell Rep. Med. 5, 101377 (2024).
- Kovacs, S. A. & Gyorffy, B. Transcriptomic datasets of cancer patients treated with immune-checkpoint inhibitors: a systematic review. J. Transl. Med. 20, 249 (2022).
- Lanczky, A. & Gyorffy, B. Web-based survival analysis tool tailored for medical research (KMplot): development and implementation. J. Med. Internet Res. 23, e27633 (2021).

Acknowledgements

We thank C. Gameiro, G. Schneiter, and L. Tran for excellent assistance in flow cytometry, D. Chollet and M. Docquier for excellent assistance in Q-PCR and sequencing experiments, S. Lemeille for analysing some of

our RNA sequencing data, and O. Vadas from the Protein Core Facility for antibody purification. Anti-CSFR1 antibodies producing hybridoma were generated by M. Merad and obtained from M. Ingersoll. EO771 cells were obtained from M. De Palma. Research in SHlab is supported by the Swiss Cancer League (KFS-5108-08-2020-R), the SNSF (310030_185255, 310030_215017), the Geneva Cancer League, and the Leenaards Foundation. Research in AD Garg lab is supported by Research Foundation Flanders (FWO) (Fundamental Research Grant, G0B4620N; FWO SBO grant for "ANTIBODY" consortium), KU Leuven (C3 grants, C3/21/037, and C3/22/022), VLIR-UOS (iBOF grant, iBOF/21/048, for "MIMICRY" consortium), and Olivia Hendrickx Research Fund (OHRF Immunbiomarkers).

Author contributions

Conceptualization and methodology: M.S., T.V.P., C.J., D.E.S., C.P., C.S., K.H., G.G.M., A.D.G., and S.H. Investigation: M.S., L.G., R.C., M.R., C.W., J.A., J.M., R.P., D.B., N.F., D.T., S.T., J-M.L., and M.K. Data validation and analysis: M.S., N.F., A.D.G., and S.H. Writing and editing: M.S., L.G., T.V.P., C.J., D.E.S., C.S., A.D.G., and S.H. Correspondence to Stéphanie Hugues.

Competing interests

The authors declare no competing interests.

Additional information

Supplementary information The online version contains supplementary material available at https://doi.org/10.1038/s41467-025-55969-w.

Correspondence and requests for materials should be addressed to Stéphanie Hugues.

Peer review information Nature Communications thanks the anonymous reviewer(s) for their contribution to the peer review of this work. A peer review file is available.

Reprints and permissions information is available at http://www.nature.com/reprints

Publisher's note Springer Nature remains neutral with regard to jurisdictional claims in published maps and institutional affiliations.

Open Access This article is licensed under a Creative Commons Attribution-NonCommercial-NoDerivatives 4.0 International License, which permits any non-commercial use, sharing, distribution and reproduction in any medium or format, as long as you give appropriate credit to the original author(s) and the source, provide a link to the Creative Commons licence, and indicate if you modified the licensed material. You do not have permission under this licence to share adapted material derived from this article or parts of it. The images or other third party material in this article are included in the article's Creative Commons licence, unless indicated otherwise in a credit line to the material. If material is not included in the article's Creative Commons licence and your intended use is not permitted by statutory regulation or exceeds the permitted use, you will need to obtain permission directly from the copyright holder. To view a copy of this licence, visit http://creativecommons.org/licenses/by-nc-nd/4.0/.

© The Author(s) 2025

¹Department of Pathology and Immunology; Geneva Medical School, Geneva, Switzerland. ²Metabolism and Nutrition Research Group, Walloon Excellence in Life sciences and BlOtechnology (WELBIO), Louvain Drug Research Institute, Université catholique de Louvain, Brussels, Belgium. ³Translational Data Science (TDS), Swiss Institute of Bioinformatics (SIB), Lausanne, Switzerland. ⁴Swiss Cancer Center Leman, Lausanne, Switzerland. ⁵Department of Oncology, Center for Experimental Therapeutics, Lausanne University Hospital (CHUV), Lausanne, Switzerland. ⁶Ludwig Institute for Cancer Research, Lausanne, Switzerland. ⁷Université Clermont Auvergne, iGReD, CNRS UMR 6293, INSERM U1103, 28, place Henri Dunant, BP38, 63001 Clermont-Ferrand, France. ⁸Groupe Cancer Clermont Auvergne, 28, place Henri Dunant, BP38, 63001 Clermont-Ferrand, France. ⁸Groupe Cancer Clermont Auvergne, 28, place Henri Dunant, BP38, 63001 Clermont-Ferrand, France. ⁸Groupe Cancer Clermont Auvergne, 28, place Henri Dunant, BP38, 63001 Clermont-Ferrand, France. ⁸Groupe Cancer Clermont Auvergne, 28, place Henri Dunant, BP38, 63001 Clermont-Ferrand, France. ⁸Groupe Cancer Clermont Auvergne, 28, place Henri Dunant, BP38, 63001 Clermont-Ferrand, France. ⁸Groupe Cancer Clermont Auvergne, 28, place Henri Dunant, BP38, 63001 Clermont-Ferrand, France. ⁸Groupe Cancer Clermont Auvergne, 28, place Henri Dunant, BP38, 63001 Clermont-Ferrand, France. ⁸Groupe Cancer Clermont Auvergne, 28, place Henri Dunant, BP38, 63001 Clermont-Ferrand, France. ⁸Groupe Cancer Clermont Auvergne, 28, place Henri Dunant, BP38, 63001 Clermont-Ferrand, France. ⁸Groupe Cancer Clermont Auvergne, 28, place Henri Dunant, BP38, 63001 Clermont-Ferrand, France. ⁸Groupe Cancer Clermont Auvergne, 28, place Henri Dunant, BP38, 63001 Clermont-Ferrand, France. ⁸Groupe Cancer Clermont-Ferrand, Franc